OTTO VON GUERICKE UNIVERSITÄT MAGDEBURG

NAT FAKULTÄT FÜR NATURWISSENSCHAFTEN

Ultra-high resolution imaging of the functional anatomy and plasticity of the human hippocampal-entorhinal circuitry

Dissertation

zur Erlangung des akademischen Grades

doctor rerum naturalium

(Dr. rer. nat.)

genehmigt durch die Fakultät für Naturwissenschaften der Otto-von-Guericke-Universität Magdeburg

von M.Sc. Anne Maaß

geboren am 19.07.1985 in Gardelegen

Gutachter: Prof. Dr. med. Emrah Düzel

Prof. Dr. Magdalena Sauvage

eingereicht am 22.05.2015

verteidigt am 03.09.2015

Acknowledgements

First, I gratefully thank my supervisor Emrah Düzel, who always supported and encouraged me to go further in four challenging years of research on a completely novel field. He gave me the opportunity to get in touch and establish cooperations with great researchers from all over the world.

Moreover, I thank my colleagues from the IKND, especially Hartmut Schütze, who did always know how to revive a dying MAC, Selim for his expertise in editing figures and videos and Nicole, who was always ready to help me through a jungle of applications, reports and officialism. My deep thanks goes to David Berron, the best office mate and travelling companion I can imagine. I am grateful about the productive teamwork and about the mutual support and comprehension.

I also have to thank all MRI physicists and the technical assistants, especially Claus Tempelmann, Renate Blobel and Denise Scheermann, for their persistent work on and patience with the first but also oldest European 7T scanner

I am grateful to all the members of the DZNE who managed to successfully complete the first longitudinal, multimodal training study in Magdeburg. Here I want to thank especially Anica Weber for her perseverance in segmenting hundreds of hippocampi.

I also thank all collaborators from the Karolinska Institute (Martin Lövden, Lars Bäckman), the ETH Zurich (Klaas Enno Stephan and Kay Brodersen), the Max-Planck Institute in Berlin (Sandra Düzel and Ulmann Lindenberger) and the University California Davis (Laura Libby and Charan Ranganath) for the fruitful collaborative work.

Last but not least, I thank my family and friends and especially Chris for their understanding and social support during the last four years.

Abstract

The ability to encode novel daily experiences into long-term memory critically relies on the hippocampus (HC) and the adjacent entorhinal cortex (EC). These brain regions form a neural circuitry within the medial temporal lobe that is composed of anatomically distinct subregions and layers. Evidence from animal studies, neurocomputational models and postmortem data from humans suggests that these substructures play distinct roles in memory and moreover, are early and differentially affected in aging and age-related diseases. However, studying layer- and subfield-specific memory functions in humans remains challenging, as standard imaging techniques lack sufficient anatomical precision.

In the current work, ultra-high resolution structural and functional magnetic resonance imaging (MRI) at 7 Tesla was used to investigate the functional anatomy of the human hippocampal-entorhinal memory circuitry and its plasticity in old age. In Experiment 1, functional MRI data were acquired with 0.8 mm^3 isotropic resolution while young subjects performed an incidental learning task on novel and familiarized images of scenes. Whereas processing of novel information more strongly engaged the input regions of the HC-EC circuitry (superficial EC and DG/CA2–3), subsequent recognition memory was best predicted by activation of output regions (deep EC and pyramidal CA1). This study made the first step towards tracking memory formation at the level of hippocampal and entorhinal layers and thus provides the basis for a pathway-specific research agenda in humans. In Experiment 2, high-resolution fMRI was used to further determine how entorhinal connectivity is topographically organized in humans. Intrinsic connectivity analyses revealed a functional parcellation of the EC into anterior-lateral and posterior-medial subregions, which differentially connect with the perirhinal vs. parahippocampal cortex and proximal vs. distal subiculum. Together these approaches enable the possibility for future studies to test specific hypotheses relating to progression of neurodegeneration in old age and dementia.

Whilst vulnerable to aging and disease, the hippocampus is also highly plastic and responsive to exercise. Mouse models and data from young adults suggested that increased hippocampal perfusion is a key factor in the beneficial effects of exercise on memory. However, it remained unclear whether the aged human hippocampus also shows such plasticity. In Experiment 3, 7T imaging in combination with 3T perfusion imaging was used to study aerobic exercise-related vascular and structural plasticity of the hippocampus in healthy elderly adults. A 3-month intervention trial revealed first evidence for a preserved capacity of the aged human hippocampus for vascular plasticity that benefits episodic memory function. These findings further support the notion that aerobic training may be a promising treatment to prevent or slow age-related memory decline.

Zusammenfassung

Der Hippocampus (HC) und der angrenzende Entorhinale Cortex (EC) sind Strukturen im medialen Schläfenlappen unseres Gehirns, die für die Speicherung neuer Erlebnisse in unser Langzeitgedächtnis eine entscheidende Rolle spielen. Hier fließen Informationen aus verschiedensten sensorischen Hirnarealen zusammen, werden verknüpft und dann an den Cortex zur dauerhaften Speicherung zurückgesandt. Das hippocampale-entorhinale System ist aus verschiedenen neuronalen Schichten und Subfeldern aufgebaut, die früh und differenziell in altersbedingten Krankheiten wie der Alzheimer Demenz betroffen sind. Unser Wissen über die spezifischen Funktionen dieser Substrukuren in der Gedächtnisbildung basiert vor allem auf Tierstudien und neurobiologischen Modellen, da Standard-Bildgebungsmethoden meist nicht genügend Präzision liefern, um diese feinen Strukturen im Menschen anatomisch und funktionell zu differenzieren. In der vorliegenden Arbeit wurde 7 Tesla (7T) Hochfeld-Magnetresonanztomographie (MRT) genutzt, um die funktionelle Anatomie des hippocampalen-entorhinalen Gedächtnisnetzwerkes und deren Plastizität im Alter mit bislang unerreichter anatomischer Genauigkeit im Menschen zu untersuchen.

In Experiment 1 wurden hippocampale und entorhinale Aktivitätsmuster bei der Verarbeitung und erfolgreichen Enkodierung neuer Informationen mittels hochauflösender funktioneller MRT Bildgebung (fMRI) gemessen. Während der Lernphase wurden jungen Probanden neue sowie bereits bekannte Innen- und Außenaufnahmen von Szenen präsentiert, deren Wiedererkennung später außerhalb des Scanners getestet wurde. Die sehr hohe funktionelle Auflösung (0.8 mm^3 isotrope Voxel) der fMRI Daten ermöglichte es erstmals, Neuheitssignale und Korrelate erfolgreichen episodischen Enkodierens den spezifischen Schichten des ECs und HCs zuzuordnen. Dabei zeigte sich, dass bei der Verarbeitung neuer Informationen vor allem die Eingangsregionen von EC und HC aktiviert wurden (oberflächliche EC Schichten und gyrus dentatus [DG], CA2, CA3), während das spätere erfolgreiche Wiedererkennen der neuen Bilder besser von Aktivitätsmustern in den Ausgangsregionen des HC-EC Systems hervorgesagt werden konnte (tiefe EC Schichten und pyramidale Schichten von CA1). Mit Hilfe von 7 Tesla Hochfeld-fMRI konnte somit erstmals der „Informationsfluss“ bei der Gedächtnisbildung im Hippocampus beobachtet werden. Diese Methode könnte

neue Erkenntnisse über die Entstehung und den Verlauf von altersbedingten Gedächtnisstörungen und neurodegenerativen Erkrankungen wie der Alzheimer Demenz liefern, bei der vor allem oberflächliche EC Schichten frühe pathologische Veränderungen aufweisen.

In einem zweiten Experiment wurde mit Hilfe der hochaufgelösten fMRI Bildgebung untersucht, wie die funktionelle Konnektivität des ECs, der primären Schnittstelle für hippocampale-neocorticale Kommunikation, im Menschen organisiert ist. Aus anatomischen Studien in Ratten ist bekannt, dass vor allem laterale Bereiche des ECs („LEC“) reziproke Projektionen mit dem Perirhinalen Cortex („PRC“) eingehen, der für die Verarbeitung nicht-räumlicher Gedächtnisinhalte wie Objekten eine wichtige Rolle spielt. Im Gegensatz dazu sind mediale Teile des ECs („MEC“) vor allem mit dem Parahippocampalen Cortex („PHC“) verbunden, der den räumlich-zeitlichen Kontext von Gedächtnisinhalten prozessiert. In Affen zeigt sich eine ähnliche Dissoziation, wobei hier Unterschiede zwischen anterioren und posterioren Bereichen des ECs dominant sind. Um homologe Subregionen von LEC und MEC im Menschen zu bestimmen, wurden intrinsische (aufgabenunabhängige) Aktivitätsverläufe sowohl aus PRC als auch PHC extrahiert und Korrelationen mit dem EC analysiert. Während der PRC höhere intrinsische Konnektivität mit anterior-lateralen Bereichen des ECs zeigte („al-EC“), war die intrinsische Aktivität des PHCs stärker mit posterior-medial gelegenen Bereichen des ECs korreliert („pm-EC“). Darüber hinaus wiesen al-EC und pm-EC unterschiedliche funktionelle Konnektivität mit dem proximalen versus distalen Subiculum auf. Diese Ergebnisse deuten auf eine funktionelle Architektur des menschlichen ECs hin, die der Anatomie in Ratten und nicht-humanen Primaten sehr ähnlich ist.

In einer 3. Studie wurde untersucht, wie sich Ausdauertraining in älteren Menschen auf die Durchblutung und Struktur des Hippocampus auswirkt und wie fitnessbedingte hippocampale Plastizität mit Veränderungen in der Gedächtnisleistung zusammenhängt. Eine Studie in jungen Probanden hat bereits gezeigt, dass Ausdauertraining zu einer Erhöhung der hippocampalen Perfusion im DG führen kann und damit einhergehend zu einer verbesserten Abrufleistung einer kürzlich gelernten Wortliste.

Mausmodelle deuten darauf hin, dass die verbesserte Durchblutung mit Neubildung von Nervenzellen im DG assoziiert ist. Um zu bestimmen, ob das Potential für vaskuläre hippocampale Plastizität auch im Alter erhalten bleibt, wurde eine 3-monatige Interventionsstudie durchgeführt, bei der Teilnehmer im Alter zwischen 60 und 77 Jahren entweder regelmäßig auf einem Laufband trainierten (Trainingsgruppe) oder Dehnungs- und Entspannungsübungen absolvierten (Kontrollgruppe). Veränderungen in der Durchblutung des Hippocampus wurden mit Hilfe kontrastmittlelbasierter Perfusionsmessungen im 3T MRT erfasst. Darüberhinaus wurden Volumen hippocampaler Substrukturen mittels 7T MRT bestimmt. Gesteigerte Fitness in Folge der Intervention war mit verbesserter Durchblutung des Hippocampus verbunden, ein Effekt, der jedoch auf die jüngeren Versuchsteilnehmer beschränkt war (60-65 Jahre). Außerdem war die verbesserte hippocampale Durchblutung mit höherem anterioren Hippocampusvolumen sowie verbessertem visuellen Gedächtnis für komplexe, abstrakte Figuren assoziiert. Diese Ergebnisse deuten darauf hin, dass Ausdauertraining auch im Alter die Durchblutung des Hippocampus verbessern kann und dabei einer altersbedingten Abnahme der Gedächtnisleistung entgegenwirken könnte.

Contents

Abstract I

Zusammenfassung II

Contents V

List of Figures IX

List of Tables XI

List of Abbreviations XII

1 General Introduction 1

1.1 Aim of the thesis 1

1.2 Anatomical organization of the hippocampal-parahippocampal network 2

1.2.1 General overview of the medial temporal lobe memory circuitry 2

1.2.2 Topographical organization of entorhinal connectivity 3

1.2.3 Direct connectivity of PRC and PHC with the hippocampus 5

1.2.4 Laminar organization of entorhinal in- and output pathways 6

1.3 Functional implications of anatomical organization 8

1.3.1 Memory 8

1.3.2 Alterations in aging 13

1.3.3 Vulnerability to Alzheimer's disease 15

1.3.4 Exercise-related plasticity 16

1.4 High-resolution magnetic resonance imaging of the MTL 19

2 General Methods 22

2.1 Subjects 22

2.2 7 Tesla imaging protocol 22

2.3 Cross-participant alignment on group-specific template 24

2.4 Segmentation of subregions for region-specific analyses 26

2.4.1 Hippocampal subfields and layers 27

2.4.2 Entorhinal subregions 29

2.4.3 Perirhinal and Parahippocampal Cortex 30

3 Experiment 1

(Laminar activity in the EC-HC circuitry during novel scene encoding)..... 31

3.1 Introduction 31

3.2 Methods 33

3.2.1 Participants 33

3.2.2 Task and design 33

3.2.3 Recognition performance indices 34

3.2.4 FMRI data acquisition and preprocessing 35

3.2.5 First-level analyses 35

3.2.6 Segmentation of regions of interest 36

3.2.7 Second-level analyses 37

3.3 Results 42

3.3.1 Univariate group activation in HC and EC subregions 42

3.3.2 Region-specific Multivariate Bayesian decoding 44

3.3.3 Region-specific univariate differences in activation 46

3.3.4 Correlations of encoding activity with later memory performance 49

3.3.5 Layer-specific functional connectivity of the EC 49

3.3.6 Comparison between BOLD characteristics of HC and EC 51

3.4 Discussion 51

4 Experiment 2 (Functional subregions of the human EC) 54

4.1 Introduction 54

4.2 Methods 55

4.2.1 Participants 55

4.2.2 Tasks 55

4.2.3 7T fMRI data acquisition and preprocessing 56

4.2.4 Segmentation of regions of interest 57

4.2.5 First-level functional connectivity analyses 57

4.2.6 Second Level analyses 58

4.3 Results 60

4.3.1 Entorhinal connectivity topography related to PRC and PHC seeds 60
4.3.2 Subicular connectivity related to al-EC/pm-EC and PRC/PHC.....65
4.4 Discussion 70
5 Experiment 3
(Vascular hippocampal plasticity after aerobic exercise in older adults) 73
5.1 Introduction..... 73
5.2 Methods..... 75
5.2.1 Experimental Design 75
5.2.2 Participants' recruitment 76
5.2.3 Determination of fitness level and metabolic rates.....77
5.2.4 Measurement of cortisol and growth factors 78
5.2.5 Intervention 79
5.2.6 Cognitive functioning 80
5.2.7 3 Tesla MRI and perfusion imaging 82
5.2.8 7 Tesla MRI and volume measures 83
5.2.9 Statistical Analysis.....84
5.3 Results 87
5.3.1 Effects of exercise on fitness-related variables 87
5.3.2 Fitness-related changes in perfusion, volume and memory 88
5.3.3 Structural equation modeling 98
5.3.4 Analyses controlling for non-specific grey-matter changes 101
5.4 Discussion 102
6 General Discussion 104
6.1 Summary of findings..... 104
6.2 The functional organization of the human entorhinal-hippocampal memory circuitry..... 104
6.2.1 Laminar dissociation of novelty processing and successful encoding 104
6.2.2 CA1 encoding activation predicts recollection.....106
6.2.3 Functional connectivity structure of the human entorhinal cortex.....107

6.2.4 Implications of EC connectivity for differential memory processing 108
6.2.5 Dissociations along the longitudinal axis of the hippocampus 109
6.2.6 Implications for aging and disease 112
6.3 Vascular plasticity of the aged hippocampus 113
6.3.1 Age-dependence 113
6.3.2 Effects on memory 115
6.3.3 Underlying mechanisms 116
6.4 The potential and challenge of 7T high-field imaging 118
6.5 Future directions and Outlook 121
7 References 125
8 Appendix i
8.1 Supplementary Figures ii
8.2 Supplementary Tables ix
Curriculum Vitae .....
Eigenständigkeitserklärung .....

List of Figures

Figure 1. Anatomical organization of the parahippocampal-hippocampal memory system. 5

Figure 2. Laminar organization of entorhinal in- and output pathways. 7

Figure 3. T1-group template with overlaid MTL landmarks of one sample subject after label-guided diffeomorphic registration with ANTS..... 26

Figure 4. Segmentation scheme of entorhinal and hippocampal subregions. 28

Figure 5. Visual incidental encoding task on images of scenes..... 34

Figure 6. Processing stream for normalization-based univariate analyses..... 38

Figure 7. Processing stream for region-specific decoding analyses..... 40

Figure 8. Novelty processing and successful memory encoding elicit a distinct activity pattern in hippocampal and parahippocampal subregions. 43

Figure 9. Bayesian model comparisons for decoding of novelty and subsequent memory in entorhinal and hippocampal layers/subregions..... 45

Figure 10. Univariate analyses of entorhinal and hippocampal subregion/layer-specific activation during novelty processing and successful encoding..... 48

Figure 11. Successful encoding activity in pyramidal layers of CA1 predicts later memory and is correlated with activation in deep EC regions. 50

Figure 12. Functional connectivity profiles of PHC and PRC seeds with the EC.. 61

Figure 13. Differential connectivity topography of PRC vs. PHC seeds with the EC. 63

Figure 14. Anterior-posterior and lateral-medial gradients of entorhinal connectivity with PRC vs. PHC seeds..... 65

Figure 15. Functional connectivity gradients in the subiculum related to EC subregions and PRC/PHC seeds. 68

Figure 16. Changes in fitness levels after the 3-month intervention. 88

Figure 17. Relationship between changes in perfusion and age. 91

Figure 18. Relationships of changes in fitness, hippocampal perfusion and volume to memory. 93

Figure 19. Relationship of changes in IGF-1 levels, hippocampal volume and verbal recall 98

Figure 20. Estimated path models predicting the relationships of changes in fitness, hippocampal perfusion, and volume to recognition memory. 99

Figure 21. Schematic summary of functional connectivity gradients in the subiculum related to PRC/PHC seeds and EC subdivisions..... 111

List of Tables

Table 1. 7 Tesla imaging protocol. 24

Table 2. Summary of main parameters assessed in the training study 75

Table 3. Characteristics of the training and control group. 76

Table 4. Group means (SD) for fitness, perfusion, volume and memory pre and post intervention. 89

Table 5. Correlation coefficents (r) for the relationships of changes in fitness, perfusion and volume to memory across all participants. 95

List of Abbreviations

AD Alzheimer's disease
AIF arterial input function
al-EC anterior-lateral entorhinal cortex
BDNF brain-derived neurotrophic factor
BMI body-mass-index
BMS Bayesian model selection
BOLD blood oxygenation level-dependent
BP binding protein
CF Complex Figure Test
CFI Comparative Fit Index
CSF cerebral spinal fluid
DA dopamine
DG dentate gyrus
DM due to memory
EC entorhinal cortex
EPI echo planar imaging
FIML Full Information Maximum Likelihood
fMRI functional magnetic resonance imaging
FWHM full-width half-maximum
GLM general linear model
GM grey matter
HC hippocampus
HRF hemodynamic response function
IGF insulin-like growth factor
IPAQ International Physical Activity Questionnaire
ICC intra-class correlation coefficient
LFP local field potential
MCI Mild Cognitive Impairment
MRA magnetic resonance angiography
MET Metabolic Equivalent of Task
MMSE Mini-Mental State Examination
MPRAGE Magnetization Prepared Rapid Gradient Echo
MRI magnetic resonance imaging
MTL medial temporal lobe

MVB Multivariate Bayes
PET positron emission tomography
PHC parahippocampal cortex
PHG parahippocampal gyrus
pm-EC posterior-medial entorhinal cortex
POR postrhinal cortex
PPI psychophysiological interaction
PRC perirhinal cortex
PSF point spread function
rCBF regional cerebral blood flow
rCBV regional cerebral blood flow
RMSEA Root Mean Square Error of Approximation
ROC receiver operating characteristics
ROI region of interest
SEM structural equation modeling
SLM stratum lacunosum-moleculare
SN substantia nigra
SNR signal-to-noise ratio
SPM Statistical Parametric Mapping
SR stratum radiatum
SVM support vector machine
T Tesla
TE echo time
TI inversion time
TR repetition time
VEGF vascular endothelial growth factor
VLMT Verbal Learning and Memory Test
$VO_{2\,VAT}$ oxygen consumption at ventilatory anaerobic threshold
VTA ventral tegmental area
WM white matter

1 General Introduction

1.1 Aim of the thesis

The hippocampus (HC) and the entorhinal cortex (EC) build a neural circuitry within the medial temporal lobe (MTL) that is critical for the formation of long-term memory (for reviews see Eichenbaum et al., 2007; Squire et al., 2004).

The HC-EC circuitry is composed of different subfields and layers that are supposed to play distinct roles in memory based on their differential connectivity and cytoarchitecture. Moreover, dysfunction of specific hippocampal and entorhinal subregions has been implicated in cognitive aging and early stages of Alzheimer's disease (e.g. Small et al., 2011). While there is emerging neuroanatomical and neurophysiological evidence from animal studies and computational neurobiological models for subregional differences in mnemonic function and vulnerability to aging and disease (e.g. Leutgeb et al., 2007, 2004; O'Reilly et al., 2014; Wilson et al., 2006), little is known about the functional architecture of the human hippocampal-entorhinal network. This is because tract-tracing studies are not feasible in humans and MTL lesion studies lack the spatial resolution to examine subfield contributions to long-term memory. One promising tool for studying the functional organization of MTL subregions non-invasively in humans is ultra-high field magnetic resonance imaging (MRI). This method allows to assign memory function to small subregions and layers due to its very high anatomical and functional resolution. Although previous human imaging studies at 3 Tesla have demonstrated the involvement of HC subfields and the EC in memory encoding (see Carr et al., 2010 for a review), an understanding of circuit-level mechanisms underlying memory formation has been not possible so far. This lack of knowledge is a serious limitation for neurobiological theories of memory and aging and for our understanding of localized damage in the early stages of AD.

The current work aimed to investigate the functional anatomy and plasticity of the human hippocampal-entorhinal circuitry by means of 7 Tesla (7T) ultra-high field functional and structural MRI. In a first experiment, layer- and subfield-specific activation during memory encoding of novel events was measured by very high-resolution functional MRI (fMRI) in young adults (Experiment 1; Maass et al.,

2014a). Specifically, it was tested how novelty responses are distributed within input and output regions of the HC-EC circuitry and moreover, how these are related to later memory performance. In a subsequent experiment, the 7T high-resolution fMRI data were used to determine how hippocampal and neocortical connectivity with the EC is functionally organized in humans (Experiment 2; Maass et al., 2015). Finally, the potential of the hippocampus for exercise-related vascular plasticity in old age was investigated in a third experiment (Experiment 3; Maass et al., 2014b). Studies in young adults have suggested that a hallmark effect of aerobic exercise is to increase blood flow in the hippocampus, which is associated with improved episodic memory (Pereira et al., 2007). However, whether older adults also show such plasticity has not been studied so far. In a 3-month intervention trial it was tested how exercise-related benefits in fitness are related to changes in hippocampal perfusion and structure how this affects different hippocampus-dependent memory functions in healthy elderly adults.

1.2 Anatomical organization of the hippocampal-parahippocampal network

1.2.1 General overview of the medial temporal lobe memory circuitry

The medial temporal lobe forms a system of anatomically related structures that are essential for episodic memory, the ability to store and retrieve our personal daily experiences (Squire and Zola-Morgan, 1991; Squire et al., 2004; Eichenbaum et al., 2007). The MTL memory circuitry consists of the hippocampal region and the adjacent parahippocampal regions, comprising perirhinal, parahippocampal and entorhinal cortices. The HC consists of the hippocampus proper with subfields CA3, CA2 and CA1, the dentate gyrus (DG) and the subiculum. The hippocampus receives input from virtually every neocortical association area via the EC, its major source of cortical projections. Most of the cortical input to the EC originates in the adjacent perirhinal cortex (PRC) and parahippocampal cortex (PHC), regions which receive widespread projections from unimodal and polymodal association areas (for reviews see, e.g. Burwell, 2000; Furtak et al., 2007; Ranganath and Ritchey, 2012). Whereas the PRC is primarily interconnected with anterior-temporal regions (including amygdala, ventral temporopolar cortex and lateral orbitofrontal cortex), the PHC has more extensive connectivity with components of a posterior-medial network (e.g. retrosplenial cortex, mammillary bodies, anterior

thalamic nuclei, and components of the default mode network). These two neocortical processing streams, which are thought to support different types of memory, remain partially segregated within the EC until they converge in the hippocampus (Eichenbaum et al., 2012; Ranganath and Ritchey, 2012; van Strien et al., 2009).

1.2.2 Topographical organization of entorhinal connectivity

The EC constitutes the major interface for hippocampal-neocortical communication (Buzsáki, 1996; Lavenex and Amaral, 2000). Neuroanatomical evidence from studies in rodents suggests a functional distinction between the “lateral EC” (LEC) and the “medial EC” (MEC), based on their differential connectivity with PRC vs. PHC and with hippocampal subfields (for reviews see, e.g. Kerr et al., 2007; van Strien et al., 2009; Witter et al., 2000a). While the postrhinal cortex ([POR], which is the homologue of the primate PHC) primarily targets the MEC, the PRC shows preferential connectivity with LEC (Witter et al., 1989, 2000a). LEC and MEC, in turn, are differentially connected with hippocampal subfields (i.e. subiculum and CA1) along the proximo-distal (transverse) axis. More specifically, projections of the LEC preferentially target the region close to the border between CA1 and subiculum (distal CA1 and proximal subiculum), whereas the MEC preferentially projects to proximal CA1 (towards CA2) and distal subiculum (towards the presubiculum) (Witter et al., 2000a). Finally, pathways originating from LEC and MEC converge on the same cells in DG/CA3, although there is dissociation along the radial axis (Witter et al., 2000a). A schematic overview of this parahippocampal-hippocampal connectivity topography is given in Figure 1. Notably, although the terminology for EC subdivisions in the rat emphasizes the lateral to medial axis, these areas do not differ solely with respect to their position in relation to the hippocampal formation and the rhinal fissure. In actuality, LEC occupies the rostrolateral portion of the EC, whereas MEC occupies the caudomedial portion of the EC (Witter et al., 2000a). The two partially segregated pathways related to LEC and MEC have been differentially associated with the processing of non-spatial/item and spatial/context information (e.g. Hunsaker et al., 2007; see 1.3.1 for further details).

LEC/MEC–subicular connections along the longitudinal hippocampal axis are considered to be relatively widespread (Naber et al., 1999, 2001; O’Reilly et al.,

2013; Witter, 2006). However, a dorsoventral gradient of hippocampal-cortical connectivity in rodents exists, which maps on a dorsolateral-to-ventromedial gradient of origin in the EC (Canto et al., 2008; Strange et al., 2014). For instance, interconnected portions of both LEC and MEC close to the rhinal fissure (referred to as the dorsolateral band of the EC in rats), are connected to the dorsal (i.e. posterior in primates) part of the hippocampus, whereas increasingly more ventral and medial bands of the EC show stronger connectivity with more ventral parts of the hippocampus (Canto et al., 2008; Strange et al., 2014).

In primates, ventral hippocampus and the adjacent EC are situated in a relatively more rostral position in the anterior temporal lobe. Although the position of the EC on the cortical surface and the orientation of anatomical axes differ across species, the relative topography of EC connectivity seems to be highly preserved (e.g. Burwell, 2000; Strange et al., 2014; Suzuki and Amaral, 1994). Anatomical studies in non-human primates suggest that the PRC is predominantly interconnected with the anterior third of the EC, whereas the PHC is predominantly interconnected with approximately the posterior two-thirds (Suzuki and Amaral, 1994). In addition, PRC/PHC connectivity with EC differs between lateral and medial domains (Suzuki and Amaral, 1994). Similar to the rodent LEC and MEC, anterior and posterior EC are also differentially connected with the subiculum and CA1 along the transverse hippocampal axis (Witter and Amaral, 1991). Whereas more anterior levels of the EC most heavily project to the border of CA1 and the subiculum, more posterior levels of the EC projected to more distal portions of the subiculum and more proximal portions of CA1.

Because anatomical tracing studies cannot be performed in humans, almost nothing is known about the anatomical connectivity topography of the human EC. Recent work on resting state fMRI data has demonstrated that spatially contiguous but anatomically distinct brain regions can be reliably differentiated based on functional intrinsic connectivity profiles (see Fox and Raichle, 2007 for a review). While previous resting-state fMRI studies at 3T have analysed functional connectivity patterns between the PRC, PHC, and hippocampal subfields (Lacy and Stark, 2012; Libby et al., 2012), these studies were unable to assess functional connectivity with the EC due to limitations in signal-to-noise ratio (SNR) and spatial resolution.

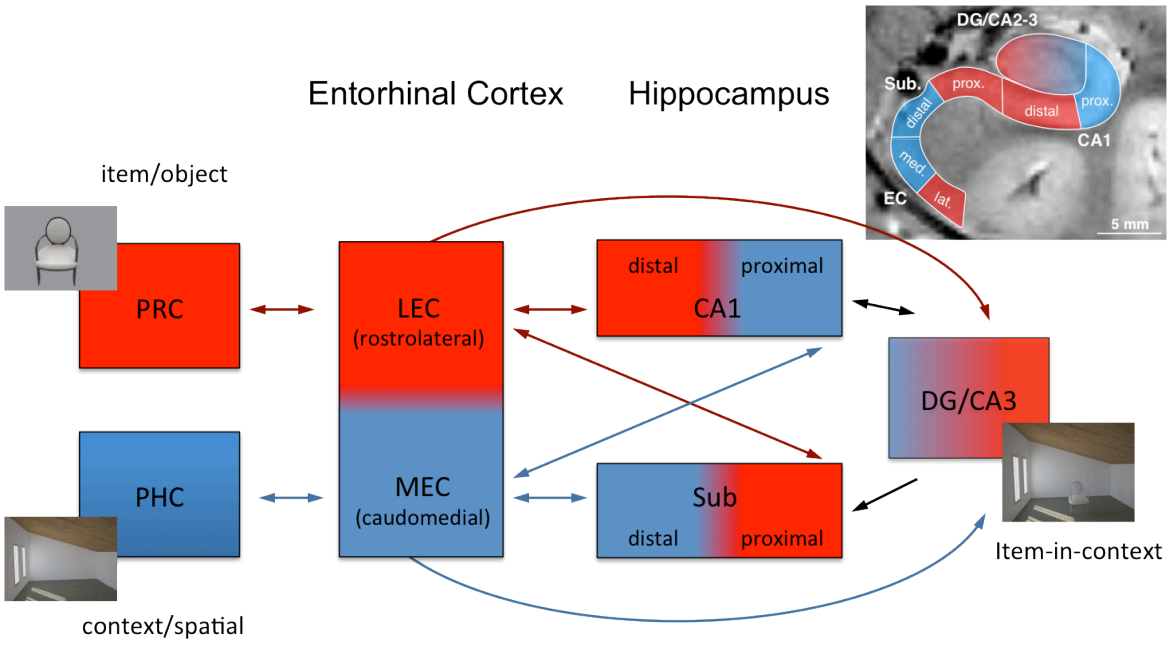

Figure 1. Anatomical organization of the parahippocampal-hippocampal memory system.
Neuroanatomical evidence from studies in rodents suggests that there are two parallel input pathways conveying item or object (red) versus contextual or spatial (blue) information into the hippocampus via the EC. While the postrhinal cortex (POR, homologous to the PHC in primates) preferentially connects with the "medial EC" (MEC), the PRC primarily connects with the "lateral EC" (LEC). Furthermore, projections of the LEC preferentially target the region close to the border between CA1 and subiculum (distal CA1 and proximal subiculum), whereas the MEC preferentially projects to proximal CA1 and distal subiculum. These partially segregated pathways finally converge in DG/CA3, where item and context are assumed to be associated. Non-human primates show a very similar connectivity topography with a functional distinction between anterolateral and posteromedial EC. This figure is partially adapted from Ranganath and Ritchey, 2012.

1.2.3 Direct connectivity of PRC and PHC with the hippocampus

Although the EC is a major gateway for the hippocampus, neocortical regions such as PRC and PHC are also directly reciprocally connected with the hippocampus (Agster and Burwell, 2013; Naber et al., 1999, 2001; Witter et al., 2000b). Studies in rodents indicate that these direct and indirect connectivity profiles show commonalities as well as differences. While the EC projects strongly to all components of the hippocampal formation, PRC and POR project weakly and only to CA1 and the subiculum. Direct projections of PRC and POR with CA1 and subiculum also dissociate along the proximo-distal (transverse) axis, converging on the same CA1/subiculum subregions as LEC vs. MEC (Naber et al., 1999, 2001; O'Reilly et al., 2013; Witter, 2006). In contrast to the relatively widespread extend of indirect PRC/PHC connections via LEC/MEC, direct projections to the subiculum and CA1 target a more limited extent along the longitudinal axis (Agster and Burwell, 2013; Naber et al., 1999, 2001).

While PRC is preferentially interconnected with ventral parts of CA1 and subiculum (analogous to anterior HC in primates), POR connects to more dorsal parts of CA1 and subiculum (analogous to posterior HC in primates).

In line with the anatomical evidence from animal models, human resting-state fMRI studies (Kahn et al., 2008; Libby et al., 2012) also found a dissociation of parahippocampal-hippocampal functional connectivity along the anterior-posterior axis of the hippocampus. While the PRC showed higher functional connectivity with the anterior hippocampus, the PHC showed stronger connectivity with the posterior hippocampus, a dissociation that was most evident for subiculum and CA1 subfields (Libby et al., 2012). However, a dissociation of parahippocampal-hippocampal functional connectivity along the proximal-distal axis of CA1 or subiculum has not been reported yet.

1.2.4 Laminar organization of entorhinal in- and output pathways

Entorhinal-hippocampal connectivity is not only organized along lateral-medial and transverse axes due to differential input from PRC and PHC. Input and output pathways of the HC-EC circuitry are also quantitatively segregated into different layers of the EC and HC subfields (for a review see van Strien et al., 2009; for a schematic overview see Figure 2). While input to the hippocampus is primarily sent from superficial EC (layers II and III) via the perforant pathway, HC output primarily targets the deep EC layers (layers V and VI). More specifically, EC neurons in layer II mainly project to DG and CA3 (Steward and Scoville, 1976; Tamamaki and Nojyo, 1993; Witter, 2007a), whereas EC neurons in layer III target CA1 apical layers (stratum lacunosum-moleculare: CA1-SLM) and the subiculum (Witter and Amaral, 1991). In addition, EC input reaches CA1 indirectly via the “trisynaptic hippocampal loop” (EC → DG → CA3 → CA1), in which CA3 projections finally target the stratum radiatum (SR) and stratum oriens (SO) of the CA1 region via the Schaffer collaterals (indirect pathway; see, e.g. Ishizuka et al., 1990; Kajiwara et al., 2008; Witter, 2007b). The HC output to EC originates from CA1 pyramidal layers and from the deepest layer of CA1, stratum oriens (containing a mixture of the axons of the pyramidal cells, afferent fibres and interneurons) as well as from the subiculum (van Haeften et al., 1995; Köhler, 1985; Sørensen and Shipley, 1979; Swanson and Cowan, 1977).

Although this layer-specific organization of HC inputs and outputs within EC is not exclusive, e.g. deep EC layers also contribute to input into the HC and subicular output can also reach the superficial layers of the EC (Deller et al., 1996; Kloosterman et al., 2003; Koganezawa et al., 2008), in quantitative terms this pattern is dominant (van Strien et al., 2009).

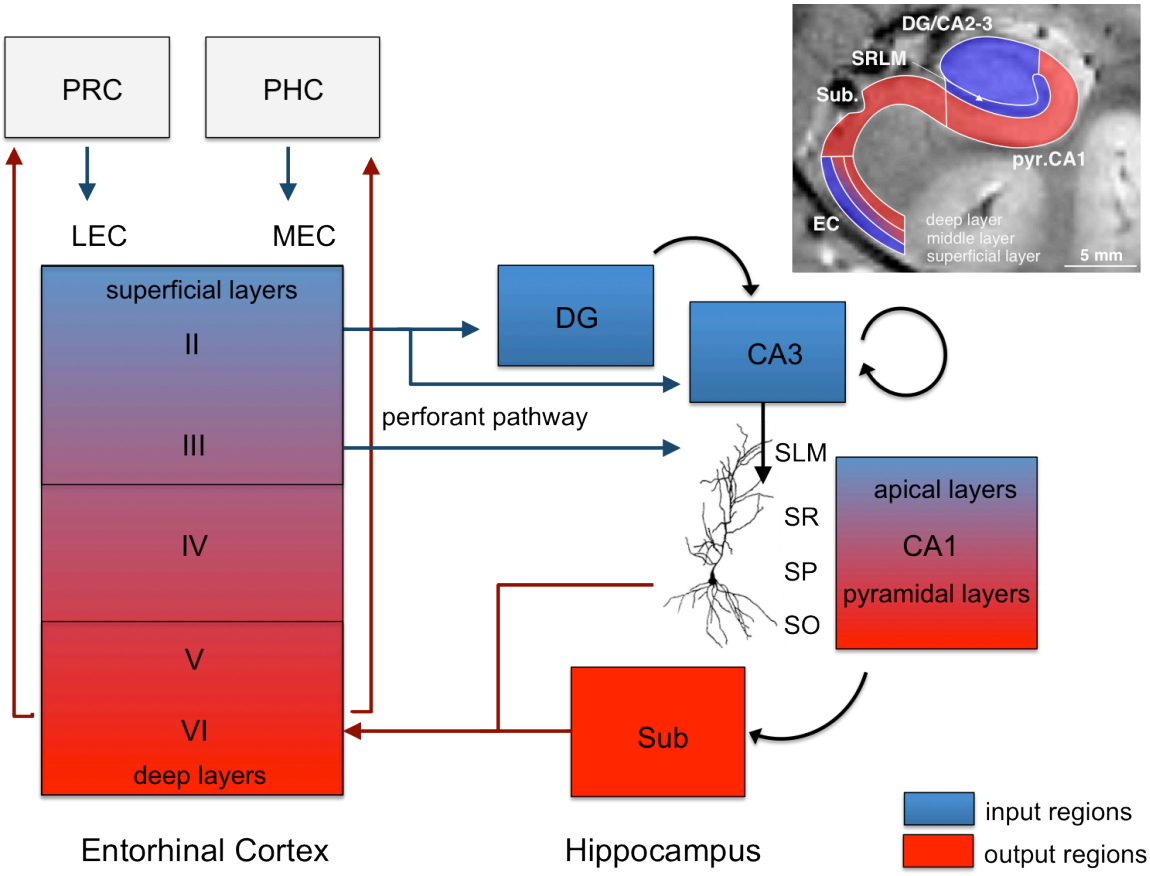

Figure 2. Laminar organization of entorhinal in- and output pathways.

Input (blue) and output (red) pathways of the entorhinal-hippocampal memory circuitry show a laminar segregation. While input from the EC is predominantly sent from superficial layers II and III to DG/CA3 and apical layers of CA1 (SR = stratum radiatum), respectively, output from the hippocampus mostly originates in pyramidal layers of CA1 (SP) and subiculum targeting deep EC layers V and VI. CA1 also receives indirect (processed) EC input via DG/CA3 that reaches the stratum lacunosum-moleculare (SLM). The integration of and comparison between direct EC input ("sensory reality") and indirect input ("predictions") has been proposed to allow match-mismatch or novelty detection in CA1 (Lisman and Grace, 2005).

1.3 Functional implications of anatomical organization

1.3.1 Memory

1.3.1.1 Object/item versus scene/context processing

The partially anatomically segregated pathways related to PRC-LEC and PHC-MEC are thought to play distinct roles in the processing of and memory for different types of information (for recent reviews see Eichenbaum et al., 2012; Knierim et al., 2014; Ranganath and Ritchey, 2012; Sauvage et al., 2013). Based on neuroanatomical and neurophysiological studies in rodents it has been proposed that information about object features or *items* („what“) is conveyed from unimodal and polymodal sensory areas PRC and then to LEC, whereas details about the location of objects or the spatial *context* („where“) is conveyed from parietal and retrosplenial cortex to POR (PHC in primates) and then to MEC (see, e.g. Eichenbaum et al., 2007, 2012). A recent model has further revised and refined this spatial-non-spatial dichotomy view (Hunsaker et al., 2007; Knierim et al., 2014; also see Sauvage et al., 2013). While LEC is proposed to process information about individual items and locations based on a local frame of reference providing the hippocampus with information about the *content* of an experience, MEC is thought to encode a global spatial framework providing the hippocampus with the spatial *context* of an experience. In non-human primates, a functional distinction between anterior and posterior EC with regard to spatial processing has been substantiated by a single-unit recording study that provided evidence for grid-cell-like neurons in the posterior EC (Killian et al., 2012).

FMRI studies have revealed a similar dissociation between PRC and PHC in humans, with PRC being preferentially engaged in memory tasks that involve object or item information and PHC being preferentially engaged in memory tasks that involve scenes, spatial or contextual information (see Ranganath and Ritchey, 2012 for a review). Limited evidence for a domain selective functional dissociation between lateral and medial EC in humans has been provided recently by task-related fMRI studies (Reagh and Yassa, 2014; Schultz et al., 2012). Schultz and colleagues found working-memory related activation in medial and lateral EC regions during scene and face processing, respectively. Furthermore, a study by Reagh and Yassa showed differential engagement of medial and lateral EC portions (obtained by equal-sized division of the EC) in a task that selectively taxed

mnemonic discrimination of spatial location and object identity. Based on the known anatomical segregation of pathways, object/item and spatial/context representations are thought to remain segregated in CA1/subiculum and probably also in CA3 (see, e.g. Nakamura et al., 2013; Sauvage et al., 2013) until they might converge to object-in-space or item-in-context representations in the DG (Eichenbaum et al., 2007; Knierim et al., 2014).

In humans, nothing is known so far about the functional connectivity topography of the EC or HC subfields related to PRC and PHC. This also seriously limits neurobiological theories of memory about object/item vs. scene/contextual processing streams within the human MTL. In order to determine how the human EC is functionally organized in humans, intrinsic functional connectivity analyses were performed on high-resolution fMRI data in Experiment 2.

1.3.1.2 Recollection versus familiarity

Furthermore, the parallel processing streams related to PRC and PHC that converge in the hippocampus have been proposed to implement distinct functions in the service of recollection and familiarity-based recognition memory (Aggleton and Brown, 1999; Eichenbaum et al., 2007, 2012; Yonelinas, 2001). *Recollection* involves retrieval of associative information about the spatiotemporal context in which an event was encountered. *Familiarity* is a relatively fast and automatic, item-based process that mediates a feeling of „knowing“ that the event was previously experienced, without retrieval of specific contextual details. According to dual-process theories, both processes independently contribute to successful recognition of studied material as old (for a review see Yonelinas, 2002).

One tool that has been extensively used to estimate contributions of recollection and familiarity to recognition memory in humans but also in animals is the analysis of receiver operating characteristics (ROCs; Fortin et al., 2004; Yonelinas, 1994; Yonelinas and Parks, 2007). An ROC is the function that relates the proportion of correctly recognized target items (i.e. the hit rate) to the proportion of incorrectly recognized lure items (i.e. the false alarm rate) across variations in response criterion (manipulated, e.g. by using a confidence rating scale).

Evidence from neuropsychological, neuroimaging, and neurophysiological studies of humans, monkeys, and rats suggest that the hippocampus is critical for recollection, whereas familiarity-based recognition can be preserved even after

bilateral hippocampal lesions (Bowles et al., 2010; Düzel et al., 2001; Guderian et al., 2011; Horner et al., 2012; Sauvage et al., 2008; Yonelinas et al., 2002). In contrast, an alternative view suggests that familiarity also depends on the HC (Smith et al., 2011; Squire et al., 2004; Wixted and Squire, 2010), if the accuracy and confidence (memory strength) of recollected and familiar items are matched.

The PHC is also thought to contribute to recollection, possibly via the representation and retrieval of contextual (especially spatial) information. Furthermore, data from rodents provide evidence that caudal MEC damage selectively eliminates the contribution of recollection in an odour-cued recognition memory task (Sauvage et al., 2010). In contrast, the PRC is supposed to contribute to and be necessary for familiarity-based recognition.

Whether recollection or familiarity is predicted by activation in specific HC or EC subregions/layers in humans has not been studied so far. Thus it is also unknown how recollection or familiarity are related to input or output regions in the EC/HC-circuitry. In Experiment 1 recollection and familiarity were estimated based on ROC curves and these questions were addressed.

1.3.1.3 Dissociations along the longitudinal axis of the hippocampus

There is also growing evidence for a functional hippocampal specialization along its long axis arising from differences in large-scale network connectivity (including different connectivity with PRC vs. PHC; see also 1.2.3), the organization of entorhinal grid cells, and subfield composition between the anterior and posterior HC (for recent reviews see Poppenk et al., 2013; Strange et al., 2014). Animal studies have supported distinct roles of the dorsal and ventral hippocampus in spatial memory and cognition vs. anxiety-related behaviours, respectively (for reviews see Bannerman et al., 2004; Fanselow and Dong, 2010). In humans, findings about an anterior-posterior functional dissociation have been much more controversial. In summary, the anterior HC has been more strongly related to motivational processing (including novelty), encoding and more global/coarse representations, whereas the posterior HC has been more strongly implicated in cognition, retrieval and local/detailed representations, respectively (Poppenk et al., 2013).

A functional dissociation between anterior and posterior HC in humans would be also proposed by the aforementioned findings by Libby and colleagues in 2012

(see 1.2.3), who found that PRC vs. PHC show preferential intrinsic connectivity with anterior vs. posterior CA1 and subiculum, respectively. Unfortunately, the authors were not able to assess differences of subicular or CA1 connectivity with EC subregions (e.g. with lateral vs. medial EC portions) due to insufficient resolution and SNR. In Experiment 2 of the current thesis, functional EC subregions were determined based on their preferential intrinsic connectivity with PRC vs. PHC and moreover, dissociations of EC connectivity along the longitudinal axis of the subiculum were assessed.

1.3.1.4 Pattern separation and pattern completion

The laminar and subfield functional organization of input and output operations within HC-EC circuitry has inspired computational theories of memory, such as the complementary systems learning (CSL) model (McClelland et al., 1995; Norman and O'Reilly, 2003; O'Reilly et al., 2014).

Input from the EC is sent to DG, which is composed of roughly four times as many projection cells as the EC or CA3 (Boss et al., 1985) and which shows a sparse firing level activity (Jung and McNaughton, 1993). These anatomical and physiological features have pointed towards a role of the DG in *pattern separation* that is the reduction of the similarity between input patterns during encoding while avoiding interference with existing memories (Marr, 1971). In contrast, the auto-associative network of recurrent collaterals in CA3 has been proposed to facilitate the completion of partial input patterns (*pattern completion*) and thereby enable memory retrieval. Animal studies (e.g .Leutgeb et al., 2007, 2004) and human high-resolution fMRI studies (e.g. Bakker et al., 2008; Lacy et al., 2011; see Deuker et al., 2014 for a review) have supported these neurocomputational predictions. CA1 has been postulated to be critical for developing a sparse, invertible mapping such that pattern-separated CA3 representations can be decoded into a format that can be fed back to the cortex (Kumaran and McClelland, 2012; McClelland and Goddard, 1996; Norman and O'Reilly, 2003).

Pattern separation and completion processes were not explicitly studied here. However, in Experiment 3 fitness-related changes in hippocampal perfusion and volume in older adults were measured and it was tested, whether hippocampal plasticity benefited memory performance in a configural object test that taxes hippocampal pattern separation.

1.3.1.5 Novelty detection

Furthermore, the anatomical organization of the hippocampal-entorhinal circuitry has inspired physiological models for the detection of novel information (Hasselmo et al., 1996; Lisman and Grace, 2005; Lisman et al., 2011).

An influential pathway-specific model suggests that CA1 is the region where novelty is computed (Lisman and Grace, 2005). According to this model a sensory cue triggers recall of stored memory sequences in DG/CA3, which in turn send predictions about what likely happens next via the Schaffer collaterals to CA1. CA1 compares these predictions to direct EC input ("the sensory reality") and a mismatch or novelty signal computed in CA1, is conveyed via subiculum, nucleus accumbens, and ventral pallidum to the dopaminergic midbrain cells in the substantia nigra/ventral tegmental area (SN/VTA). Finally, dopamine (DA) release in the hippocampus, particularly in the SRLM of CA1, which has been proposed to arise from SN/VTA fibres (Gasbarri et al., 1997; Lisman and Grace, 2005; but see also Smith and Greene, 2012 for discussion) enhances LTP and thus learning of novel or unpredicted information (Li et al., 2003). Supporting evidence for a role of SN/VTA-CA1 connectivity in successful long-term memory formation in humans has been provided recently by a high-resolution fMRI study showing that functional connectivity between CA1 and SN/VTA was predictive for subsequent retrieval (after 24h) of associative long-term memory (Duncan et al., 2014).

Novelty detection refers to a diversity of phenomena (for reviews see Kumaran and Maguire, 2007; Nyberg, 2005; Ranganath and Rainer, 2003), including the discrimination of stimuli (*stimulus novelty*) or new configurations of familiar stimuli (*associative novelty*) that have never experienced before but also events that are unexpected in a given context (*contextual novelty*). While the detection of associative or contextual novelty that involves recall of previous experiences critically depends on the hippocampus, converging evidence suggest that stimulus novelty can be detected already further upstream in the PRC (Aggleton and Brown, 2005; Brown and Aggleton, 2001).

Although previous 3T fMRI studies have already measured novelty-related activation in the MTL, layer-specific processing of novel information and related subsequent memory effects have not been studied in humans so far. In Experiment 1 ultra-high resolution fMRI was used to assess the distribution of novelty

responses in the EC-HC circuitry at the level of layers and subfields, and whether activation in the same regions also predicted the ability to subsequently recollect the novel scenes.

1.3.2 Alterations in aging

Aging is often associated with cognitive decline that comprises various cognitive domains, including working memory, processing speed and episodic memory (Grady, 2012; Jagust, 2013). Intriguingly, old people show specific impairments in the ability to encode novel events into long-term memory (Burke and Mackay, 1997; Wilson et al., 2006), while memories for older events and semantic memories are relatively preserved in old age (Park et al., 2002). This dysfunction has been related to structural and functional changes in the MTL memory system, in particular to deterioration of the hippocampus (see, e.g. Small et al., 2011 for a review).

Animal models propose that age-related changes in the MTL most prominently involve loss of synaptic input to DG and CA3 via the perforant pathway (i.e. EC layer II), whereas subsequent intrinsic connections in CA3 and synaptic inputs to CA1-SR (CA3 inputs) and CA1-LM (EC inputs) are relatively spared (Geinisman et al., 1992; Smith et al., 2000; Wilson et al., 2006). The input from EC layer II to DG and CA3 is crucial for the formation of distinctive representations of events that share overlapping elements with prior memories. Thus, it has been suggested that the synaptic loss of EC input might strengthen the auto-associative network of CA3 (facilitating pattern completion and recall of prior memories) at the cost of successfully separating and encoding novel input patterns sent from the EC (Gallagher and Koh, 2011; Wilson et al., 2006). Supporting data for an age-related decrease in human perforant path integrity have been provided by microstructural diffusion tensor imaging (Yassa et al., 2010a), with perforant pathway “degradation” being correlated with decreased performance on a word-list learning task. Furthermore, Yassa et al. (2011) found greater CA3/DG activity in healthy older adults than young adults during a task that stresses pattern separation and this increased BOLD activity was correlated with a behavioural bias towards “pattern completion”. Specifically, Yassa and colleagues found increased activation in CA3/DG during the correct rejection of lure items compared to lure false alarms, which they explained by hyperactivity in CA3 (in line with findings in rodents; e.g.

Wilson et al., 2005). Although synaptic alterations might predominate neuronal loss in normal aging, age has been also associated with loss of neurons in the hilus of DG and the subiculum (West et al., 1994), while notably sparing CA1–CA3 and EC. Finally, diminished neurogenesis in DG as early as middle age may also contribute to age-related learning and memory impairments (Drapeau and Nora Abrous, 2008; Kempermann et al., 1998; Kuhn et al., 1996)

With regard to parahippocampal networks, aging has been related to deficits in complex object discrimination and object recognition in rodents, monkeys and humans (Burke et al., 2011; Ryan et al., 2012), impairments that are similar to those observed after lesions to the PRC in young animals (Bartko et al., 2007; Bussey et al., 2003) and humans (Barense et al., 2012). For instance, Ryan and colleagues (2012) have shown that older adults have specific deficits in discriminating between objects when these objects share multiple common features but not when object discrimination can be resolved on the basis of a single feature (e.g. size or colour). Moreover, this deficit in performance was related to altered PRC activation in the old adults. Together these data indicate that aging may result in a loss of functional integrity of the PRC that results in a decreased ability to disambiguate between objects with multiple similar features (Ryan et al., 2012).

Moreover, hippocampal and parahippocampal regions are also particularly vulnerable to age-related neurodegenerative diseases, such as Alzheimer's disease (AD) and vascular disease (more details, see next chapter 1.3.3). Although studies of “normal” or “healthy” aging attempt to exclude individuals with significant cognitive impairments and vascular, metabolic or neurodegenerative disease, subtle neurodegenerative changes might occur early before symptoms onset and thus also reflect some alterations that have been related to normal aging (Jagust, 2013). Recent studies on aging have thus also considered Abeta deposition, a pathological hallmark of AD, by means of positron emission tomography (PET). Even older people without evidence of fibrillar Abeta show episodic memory decline and brain atrophy in AD-vulnerable MTL regions, suggesting that presymptomatic AD cannot explain all age-related changes in medial temporal memory function (Fjell et al., 2014; Oh et al., 2012). In addition, dissociations in patterns of hippocampal dysfunction between normal aging and AD have been observed. While neuronal loss in the DG has been related to age and not disease,

probably reflecting loss of synaptic input via the perforant pathway, CA1 – a region that shows considerable AD-related neuronal loss and high vulnerability to vascular disease – is relatively spared in normal aging (Price et al., 2001; West et al., 1994). Evidence from studies in rodents and non-human primates that do normally not suffer from AD or vascular disease has also highlighted the DG as the hippocampal subregion most sensitive to the effects of advancing age (Gazzaley et al., 1996; Moreno H et al., 2007; Small et al., 2004).

1.3.3 Vulnerability to Alzheimer's disease

The MTL is among the earliest regions affected in Alzheimer's disease. In contrast to normal aging, AD is characterized by prominent neuronal loss that specifically affects EC, CA1 and subiculum, whereas DG and CA3 are relatively preserved (Braak et al., 2006; West et al., 1994). AD is pathologically defined by the presence of senile plaques (amyloid [Abeta] aggregations) and neurofibrillary tangles (aggregates of hyperphosphorylated tau protein) (see, e.g. Hyman et al., 2012 for neuropathological AD criteria).

CSF (cerebral spinal fluid) markers and postmortem data from the EC indicate that tau aggregation begins already in mid-life, years before Abeta deposits in the neocortex (e.g. Braak and Braak, 1997; Fagan et al., 2009). Tau pathology emerges in superficial EC layers (Braak and Braak, 1991; Gómez-Isla et al., 1996), most prominently in the transentorhinal region (Braak and Braak, 1985) that is located in the medial wall of the collateral sulcus (Taylor and Probst, 2008) corresponding to the transition from EC to PRC. Evidence for an early metabolic dysfunction in the lateral EC, the transentorhinal cortex and PRC in preclinical AD patients has been provided by Gadolinium-based perfusion imaging (Khan et al., 2014). The authors found decreased cerebral blood volume (CBV) in the EC of those adults that progressed to mild AD later and parallel mouse models showed that APP (Amyloid-Precursor-Protein) expression potentiated tau toxicity in driving LEC dysfunction.

In the course of AD, tau pathology propagates to the hippocampus probably via transsynaptic spread along anatomically connected networks (de Calignon et al., 2012; Liu et al., 2012). The apical dendrites of hippocampal CA1 pyramidal neurons (in the SRLM) are among the first targets of hippocampal pathology. Synaptic loss in CA1 apical layers has been shown to occur much earlier than

neuronal loss and might be implicated in the cognitive decline during early stages of AD (Scheff et al., 2007; Selkoe, 2002). Atrophy of the CA1-SRLM is apparent in postmortem tissue from patients with mild AD (Braak and Braak, 1997a; Thal et al., 2000) and CA1-SRLM thinning has been demonstrated *in vivo* by means of ultra-high field 7T MRI (Kerchner et al., 2010). Moreover, the CA1-SRLM thickness measured by 7T MRI has been shown to correlate with episodic memory performance (delayed recall) among patients with mild AD (Kerchner et al., 2012).

Perforant path input from superficial EC layers to the HC (apical CA1 and DG/CA3), which is essential for pattern separation and distinct encoding, and which is weakened in aging, comprises also a significant early lesion in AD (Gallagher and Koh, 2011). In comparison to age-matched controls, individuals with amnestic Mild Cognitive Impairment (MCI) have been shown to be progressively impaired in a continuous recognition task designed to emphasize pattern separation (Yassa et al., 2010b). Moreover, this impairment was coupled to increased DG/CA3 activity ("hyperactive BOLD") during encoding and retrieval of correctly identified lures compared to normal age-matched controls, whereas the EC showed decreased activation in the same contrast (Yassa et al., 2010b).

The topology of Abeta plaque deposition has been well defined in later stages of AD, but the earliest sites of deposition are not as clearly known. PET imaging data suggest that amyloid accumulation begins in medial frontal cortex and posterior cortical regions including the precuneus extending to posterior cingulate and retrosplenial cortex (Buckner et al., 2005; Villeneuve et al., 2014). These areas are key regions of the default mode network and show prominent atrophy and metabolic abnormalities early in the disease progression (Buckner et al., 2005; Pengas et al., 2010a). Furthermore, these posterior regions are densely interconnected with the MTL via the cingulum bundle, particularly with PHC and MEC (Burwell and Amaral, 1998; Jones and Witter, 2007; Kobayashi and Amaral, 2007; Suzuki and Amaral, 1994). As neocortical Abeta deposition starts, tau spreads outside the MTL and hippocampal/neocortical connectivity is affected resulting in further episodic memory decline.

1.3.4 Exercise-related plasticity

The hippocampus is not only especially susceptible to aging and neurodegenerative disease-related atrophy, but also highly plastic (Thomas et al.,

2012; Voss et al., 2013a). The DG subfield of the hippocampus is unique in its ability of adult neurogenesis (Eriksson et al., 1998), which can be more than doubled by aerobic exercise in rodents (van Praag et al., 1999). This exercise-mediated neurogenesis is associated with improved hippocampus-dependent memory, in particular with enhanced discrimination between highly similar patterns (Creer et al., 2010), which is thought to rely on the reduction of interference between overlapping memories due to improved pattern separation (Clelland et al., 2009; Yassa and Stark, 2011). However, these exercise-induced increases in neurogenesis seem to be reduced in old (van Praag et al., 2005) and absent in very old mice (Creer et al., 2010), which also show impaired spatial discrimination and low basal neurogenesis rates. Furthermore, exercise-related neurogenesis is associated with specific functional circuits that may influence pattern separation for certain types of information (Vivar and Van Praag, 2013; Vivar et al., 2012). Newly born granular cells in the DG receive predominantly input from PRC and LEC, rather than MEC, which convey novel object information to the hippocampus and are required for discrimination of and memory for complex objects (see also 1.3.1 and 1.3.2). These findings suggest that effects of aerobic exercise might specifically benefit performance in complex object-recognition tests that pose high demands on pattern separation.

In humans, comparable findings regarding the effect of exercise on cognition have been observed in preadolescent children and young adults, where cardiovascular fitness and exercise training were associated with benefits in relational mnemonic functions (Chaddock et al., 2011; Monti et al., 2012) and improved performance in an object memory test that taxes pattern separation (Dery et al., 2013). If these exercise-induced benefits in pattern separation-related memory tasks are due to increased neurogenesis in humans is unclear because direct *in vivo* imaging of newly born neurons in the DG in humans has not yet been established. However, a study in young/middle-aged humans (21–45 years old, no control group) that measured hippocampal perfusion by means of MRI found selective increases in dentate gyrus CBV after three months of exercise, and these CBV changes were also positively related to post-exercise performance in an early verbal recall test (Pereira et al., 2007). In a different experiment with mice, Pereira et al. (2007) showed that exercise-induced increases in DG CBV were correlated with postmortem measurements of neurogenesis, proposing that perfusion in DG is an

indirect measure of neurogenesis. The increase in DG perfusion is thought to be mediated by exercise-induced angiogenesis, which is tightly coupled to neurogenesis (Louissaint et al., 2002; Palmer et al., 2000). An effect of aerobic exercise on hippocampal perfusion in old individuals has not yet been demonstrated, although a preliminary observation, using only post-intervention measures (of arterial spin labelling) in a small group of six individuals, provided encouraging results in this direction (Burdette et al., 2010). However, it has been shown that aerobic exercise in old age is effective in preventing the human hippocampus from atrophy over a period of one year (Erickson et al., 2011). It remains unclear through which physiological mechanisms exercise may improve hippocampal function in older individuals.

Extensive neurobiological studies in animals have identified several neurochemicals that mediate downstream effects of exercise on the brain and cognition, including brain-derived neurotrophic factor (BDNF), insulin-like growth factor-1 (IGF-1), and vascular endothelial growth factor (VEGF) (see Cotman and Berchtold, 2007; Cotman et al., 2007; Voss et al., 2013a for reviews). BDNF, which supports neural survival, growth, and synaptic plasticity, is enhanced by exercise (e.g. Neeper et al., 1996). Decreased levels have been associated with age-related hippocampal dysfunction and memory impairment (for a review see Erickson et al., 2012). VEGF is a hypoxia-inducible protein that promotes angiogenesis and neurogenesis and is associated with improved cognition (Adams and Alitalo, 2007; During and Cao, 2006). The interactive effects of IGF-1 with VEGF, which are both increased in the periphery after exercise and cross the blood–brain barrier, are thought to mediate neurogenesis and angiogenesis (for a review see Cotman et al., 2007). Enhanced IGF-1 is also thought to mediate the induction of hippocampal BDNF, and together they are thought to be the key factors in the effects of exercise on learning and memory (Cotman et al., 2007).

Although converging evidence from animal models highlights the importance of exercise-induced increases of neurotrophic factors in modulating memory, the role of these molecules in exercise-related changes of human brain function are not fully resolved. One year moderate aerobic exercise training (walking) in healthy older adults did not reveal significant effects on serum levels of BDNF, IGF-1 or VEGF compared to a stretching control intervention (Erickson et al., 2011; Voss et al., 2013b; see Vital et al., 2014 for a review on VEGF). However, increases in

growth factors have been found to correlate with increases in functional connectivity between the bilateral parahippocampal and bilateral middle temporal gyrus (Voss et al., 2013b). Furthermore increases in serum BDNF after 1-year aerobic training were correlated with increases in hippocampal volume (exercise group only) and these volume changes were related to improvements in spatial memory performance (Erickson et al., 2011).

In the current thesis, effects of 3-month exercise on fitness, hippocampal perfusion, hippocampal volume and hippocampal-dependent memory were investigated in a longitudinal intervention study with older adults (Exp. 3). Here, it was specifically tested how perfusion or volume changes in the hippocampus were related to changes in configural object memory or verbal memory and whether effects were specific to early recall, late recall or recognition. Moreover, it was studied how vascular or structural hippocampal plasticity and memory changes were related to changes in angiogenic or neurotrophic growth factors.

1.4 High-resolution magnetic resonance imaging of the MTL

Functional and structural high-resolution MRI is a promising method to study the functional organization of MTL subregions non-invasively in humans.

MRI or nuclear magnetic resonance imaging enables to create 3-dimensional images of the human brain by using the interaction between a static magnetic field that aligns hydrogen atoms (from tissues containing water molecules) and radio frequency pulses that cause the atoms to absorb the energy (resonate), thus altering their alignment relative to the field (for general overview see, e.g. Huettel et al., 2008). The retransmitted energy emits a radio frequency signal that can be measured by a receiver coil.

Functional MRI (fMRI) has become one of the most prominent methods to investigate human brain function by detecting activity-associated changes in blood flow. The method relies on the blood oxygenation level-dependent (BOLD) contrast (Ogawa et al., 1993) – an indirect measure of neuronal activity that is based upon changes in deoxyhemoglobin concentration in response to neuronal dynamics at the cellular and micro-circuitry level (Friston, 2008; Goense and Logothetis, 2008). The physiological basis of the fMRI signal is still not fully resolved (Ekstrom, 2010). Simultaneous imaging and neuronal recording in the visual cortex of anaesthetized and awake monkeys has suggested that the BOLD signal strongly correlates with

local field potentials (LFPs) and thus reflects presynaptic activity (input) rather than action potentials (output) of neurons (Goense and Logothetis, 2008; Logothetis and Wandell, 2004). In contrast, other studies have shown that the BOLD response correlates with neuronal firing (Lee et al., 2010). Whether this relationship is a direct metabolic consequence of neuronal firing or rather related to activation of local horizontal microcircuits (Logothetis, 2010) remains controversial.

The term “high-resolution fMRI” is generally used to refer to functional imaging of a specific brain region at higher spatial resolution than typically acquired (e.g. ≤ 1 mm^3 in visual cortex; Grill-Spector et al., 2006). In functional studies of the human MTL, an in-plane resolution lower than ≤ 2 × 2 mm^2 is typically referred as high resolution (Carr et al., 2010), because standard-resolution fMRI data are often acquired at in-plane resolutions of ≥ 3 × 3 mm^2. So far, high-resolution fMRI studies of the human MTL have been largely conducted at field strengths of 3 Tesla (3T), which permit a resolution of up to 1.5 mm x 1.5 mm x 1.5 mm (corresponding to a volume of 3.375 mm^3). This resolution enables already to assign activation to distinct hippocampal subfields and the EC (e.g. Bakker et al., 2008; Bonnici et al., 2013; Duncan et al., 2014; Ekstrom et al., 2009; Kirwan et al., 2007; see Carr et al., 2010 for a review).

The high field strength of 7 Tesla MRI scanners and thus enhanced SNR enables to acquire structural and functional (BOLD) MRI data with strikingly enhanced resolution (≤ 1 mm^3) compared to imaging at 3T. This high resolution allows to assign activation even to distinct anatomical layers. Layer-specific BOLD activation in the visual cortex has been demonstrated already in several studies with cats, monkeys and humans (e.g. Harel et al., 2006; Goense and Logothetis, 2006; Koopmans et al., 2010; Goense et al., 2012). Furthermore, laminar differences in BOLD, CBV and CBF responses between stimulated and unstimulated cortical regions have been reported, indicating layer-specific differences in the neurovascular coupling (Goense et al., 2012). Although the underlying hemodynamic processes are not fully resolved, laminar differences in the fMRI response open up the possibility to study cortical processing and pathway-related hypotheses at the level of layers. While ultra-high field MRI at 7T has been already used to study structural changes in hippocampal layers (Kerchner et al., 2010, 2012), functional differences (in BOLD activation) between HC or EC layers have not been measured so far. The feasibility of ultra-high field fMRI in the

hippocampus has been demonstrated recently in a study that compared memory-related MTL activation at 3T and 7T (Theysohn et al., 2013). Theyson et al. found significantly stronger memory-related HC activation at 7T than 3T, suggesting higher BOLD sensitivity at 7T.

In the current thesis fMRI data of EC and HC regions were acquired with a resolution of 0.8 x 0.8 x 0.8 mm^3 (corresponding to a volume of 0.51 mm^3) that is more than 6.6 times higher than previous high-resolution studies at 3 Tesla (Exp.1/2). Furthermore, 7T high-field imaging was utilized to assess exercise-associated structural changes of hippocampal subregions in old age (Exp.3).

2 General Methods

2.1 Subjects

While Experiment 1 and 2 were conducted in healthy young individuals (18 to 32 years), participants in Experiment 3 were healthy older participants (60 to 77 years). All subjects gave written informed consent prior to participation and received monetary compensation for participation. Exclusion criteria for 7T MRI were metallic implants (other than standard dental implants), tinnitus, known metabolic disorders or a history of neurological or psychiatric disorders. All studies were approved by the ethics committee of the University of Magdeburg.

2.2 7 Tesla imaging protocol

In order to study the functional anatomy and plasticity of the entorhinal-hippocampal circuitry at the level of layers and subfields, functional and structural data were acquired by means of ultra-high field functional and structural MRI. Data were collected in Magdeburg using a 7T MR system (Siemens, Erlangen, Germany) and a 32-channel head coil (Nova Medical, Willmington, M).

Scanning protocols of all experiments started by acquisition of a whole-head **MPRAGE** volume (Magnetization Prepared Rapid Gradient Echo, TE = 2.8 ms, TR = 2500 ms, TI = 1050 ms, flip angle = 5°, duration ca. 14 min; see Table 1) with 0.6 mm^3 isotropic resolution. In contrast to T2*-weighted images, the T1-weighted MPRAGE images are less prone to motion and susceptibility artefacts close to the ear canals, which allows good delineation of parahippocampal regions (EC, PHC, PRC) and the hippocampus (including subfields) along the full longitudinal axis. The MPRAGE images were subsequently bias-corrected (SPM8, “New Segment”; Wellcome Department of Cognitive Neuroscience, University College, London, UK) and intensity-adjusted to increase contrast for segmentation homogenously across subjects.

To differentiate between hippocampal layers (Exp.1), a very high resolution **T2*-weighted partial structural volume** with 0.33 mm x 0.33 mm in-plane resolution and a slice alignment orthogonal to the hippocampus main axis was acquired (TE = 18.5 ms, TR = 680 ms, 45 slices, slice thickness 1.5 mm + 25% gap, FOV 212 mm x 179 mm, matrix 640 x 540, duration ca. 12 min; see Table 1). T2*-weighted

images enable to distinguish the apical dendritic layer (SRLM) of the CA1 region (Kerchner et al., 2010, 2012) from the rest of CA1 (stratum pyramidale, stratum oriens, see Figure 4a). In contrast to the MPRAGE images, they exhibit a higher in-plane resolution, which improves discriminability of hippocampal subfields, especially in the body. However, the T2* volumes also comprise a lower number of coronal slices and are more vulnerable to motion and dropouts in the anterior MTL, which makes them less suitable for volume measures of hippocampal and parahippocampal regions. Thus, for reliable volumetric measures of hippocampal volume the high-resolution MPRAGEs might be favoured (as used in Exp. 3).

In order to assess layer- and subfield-specific activity patterns along the hippocampal-parahippocampal circuitry (Exp.1) and determine functional subdivisions of the EC (Exp.2), **fMRI data** sensitive to BOLD were acquired with an isotropic resolution of 0.8 mm^3 (see Table 1). Each subject's functional MRI scan consisted of 370 volumes, each comprising 28 T2*-weighted echo planar slices (TE = 22 ms, TR = 2000 ms, FOV 205 mm, matrix 256 x 256, partial Fourier 5/8, parallel imaging with grappa factor 4, bandwidth 1028 Hz/Px, echo spacing 1.1 ms, echo train length 40, flip angle 90°) in a single session, summing to a session length of ca. 13 min. The slices were acquired in an odd–even interleaved fashion oriented parallel to the hippocampus long axis (see Figure 4b and Supplementary Fig. 4 for mean EPI images). EPIs were distortion corrected using a point spread function (PSF) mapping method (In and Speck, 2012) and motion corrected during the online reconstruction.

Table 1. 7 Tesla imaging protocol.

Volume (Sequence)	Target	Resolution (mm^3)	Alignment
MPRAGE (T1-weighted)	whole-head	0.6 isotropic	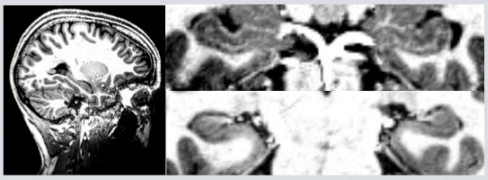
EPIs (T2*-weighted)	hippocampus and parahippopcampal subregions	0.8 isotropic (28 axial slices)	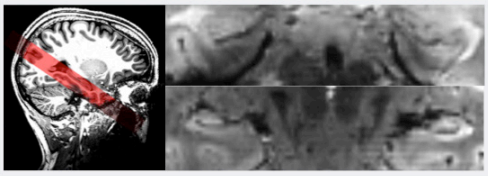
Structural T2*	hippocampus and parahippopcampal subregions	0.33 x 0.33 x 1.5 (45 coronal slices)	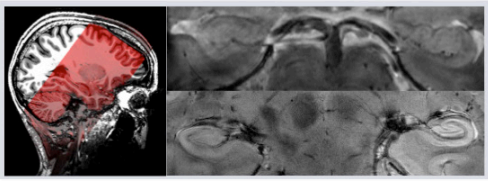

All scanning protocols started by acquisition of a high-resolution whole-head MPRAGE volume, a T1-weighted image that allows good delineation of hippocampal and parahippocampal regions. For mapping of laminar and subfield activation in the hippocampus and entorhinal cortex (Exp.1/2), BOLD sensitive fMRI data were measured with 0.8 mm^3 isotropic resolution. These partial images were aligned parallel to the hippocampal long axis. Furthermore, for laminar and subfield delineation, very high-resolution T2*-weighted images were acquired, with slice alignment orthogonal to the hippocampal main axis (Exp.1).

2.3 Cross-participant alignment on group-specific template

In order to perform group analyses on fMRI data (e.g. identify regions that show significant activation or functional connectivity across subjects), the standard fMRI preprocessing routine involves spatial normalization into a standard space. Therefore, most studies map each single brain to the space defined by the Montreal Neurological Institute (MNI; used e.g. by SPM). Normalization allows signal averaging across subjects and makes results from different studies comparable. Nevertheless, the commonly used standard templates have an insufficient resolution to delineate subregions of the hippocampus accurately (e.g. MNI template resolution: 2 mm^3 isotropic). In addition, the complex anatomy of the hippocampus and inter-subject variability raises difficulties for image-based computational morphometry techniques (Yushkevich et al., 2009).

Thus, in order to enable precise cross-participant alignment for hippocampal and parahippocampal regions, and to subsequently perform univariate group statistics in Experiments 1 and 2, *Region of Interest-Advanced Normalization Tools* (ROI-ANTS; Avants et al., 2011) was used. This nonlinear diffeomorphic mapping

procedure optimizes regional alignment (based on anatomically defined ROIs (Avants et al., 2011; Klein et al., 2009; Yassa and Stark, 2009) across subjects. Therefore, a study-specific template was created based on the high-resolution MPRAGE images of Experiment 1. Additionally, landmarks were added on each individual T1 image and the template to improve alignment for the regions of interest (Exp. 1/2).

First, the *Oxford Centre for Functional MRI of the Brain* (FMRIB) software library (FSL 5.0.6; Smith et al., 2004) was used to register (and reslice) the individual MPRAGE images to the individual mean functional images (EPIs). This was done with “epi_reg”, a command-line program that belongs to the FMRIB's linear registration tool (FLIRT v6.0; Jenkinson and Smith, 2001) and which was specifically written to register EPI images to structural images. Second, a study specific T1-template was created (same resolution as EPIs) in ANTS using the buildparalleltemplate.sh command-line script (Cross-Correlation similarity matrix; Avants et al., 2010). As a result, the study template together with the transformation matrices (from each subject to template space) were obtained. Generally, these alignment parameters allow already for a good registration to the template. Nevertheless, in order to further improve normalization for the MTL regions landmarks were added to the template. Therefore, the hippocampal head (on the first slice on which it appears), EC, hippocampal body and PHC (same slices as hippocampal body) were labelled on the T1-template as landmarks for the subsequent label-guided alignment. Similarly, subject-specific ROIs were adjusted to match the template priors. Third, the expectation-based point set registration (“pse”; step size: SyN[0.5]) was applied to register the individual MPRAGEs on the template based on the labelled points sets (= MTL masks).

The resulting transformation matrix of each subject was then applied to the corresponding subject’s MTL masks in order to verify alignment precision (see Figure 3). In one subject from Experiment 1 EC regions were improperly registered to the template. Thus, this subject was excluded from univariate group analyses that required normalization.

Finally, the individual contrast-images of all remaining subjects in Experiment 1 and 2 were normalized to template space and subsequently submitted to second-level group analyses in SPM (e.g. one-sample t-test).

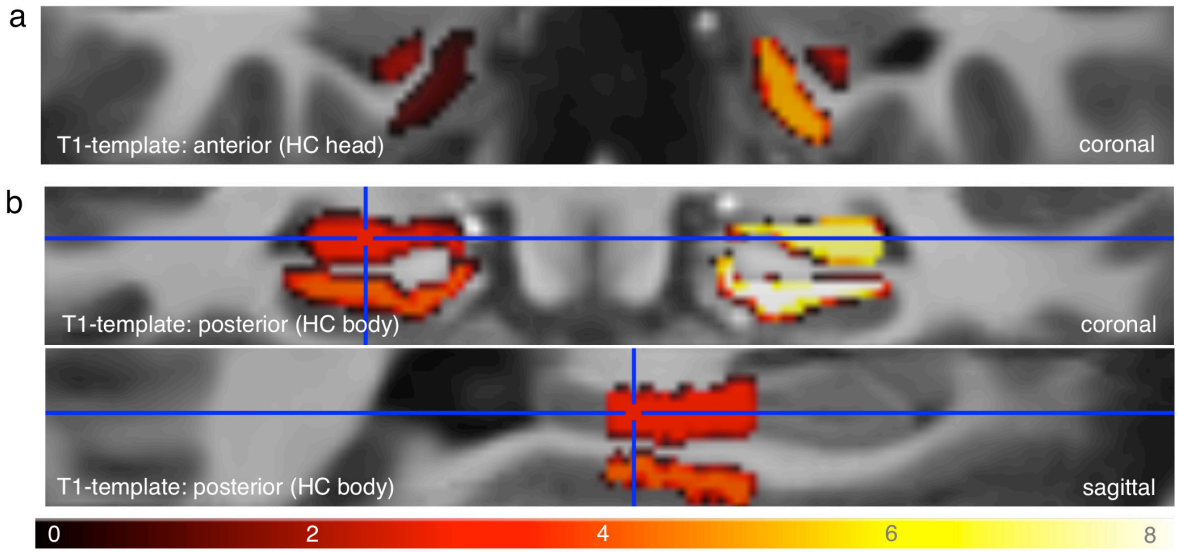

Figure 3. T1-group template with overlaid MTL landmarks of one sample subject after label-guided diffeomorphic registration with ANTS.

The high-resolution (0.6 mm^3 isotropic) MPRAGE images (Exp.1) were used to create a study-specific group template with ANTS (*Advanced Normalization Tools*). MTL landmarks were further used to improve registration by means of label-guided alignment. Therefore, MTL maps were created for all subjects and the template, in which each region was coded by a numeric value (from 1 to 8; e.g. left EC = 1, left HC head = 2, …, right PHC = 8; see different colors). To verify alignment precision, the transformation parameters were applied to the subject-specific MTL maps and checked their overlay on the template. Registered anterior MTL regions (EC and HC head) and posterior MTL regions (HC body and PHC) of one sample subject overlaid on the group template. Different colours denote probabilities; edges appear dark after registration due to low probability values. For one subject, alignment of EC regions failed and thus, this subject had to be excluded from all normalization-based analyses. This figure is adapted from Maass et al., 2014a.

2.4 Segmentation of subregions for region-specific analyses

The performance of group-level analyses in a common template space requires smoothing and normalization of the functional data, with the former aiming to reduce random noise and increase the probability of overlap across subjects. However, spatial smoothing also reduces the resolution in each image, and the width of the smoothing kernel should not exceed the size of the activated region.

To compare activation patterns across different layers/subregions in the EC-HC circuitry, activation measure should be extracted from the individual unnormalized (and unsmoothed) data to allow maximum spatial precision. Therefore, the ROIs need to be manually defined in each subject. Similarly, volumetric comparisons between hippocampal subregions require manual segmentation.

In order to compare encoding activations between EC/HC in- and output regions (Exp.1), extract time courses from subregions to test for intrinsic connectivity, i.e. correlated activity between regions (Exp.2) and finally, in order to measure exercise-related changes in hippocampal volume (Exp.3), ROIs were manually

segmented on the T2*-weighted (Exp.1) or T1-weighted (Exp.2/3) high-resolution structural images using the segmentation protocol described below.

Hippocampal and parahippocampal regions were traced on consecutive coronal slices using *MRIcron* (Chris Rorden, Version 4, April 2011). The detailed landmarks in the Atlas of the Human Brain (Mai et al., 2007) served as additional guideline for segmentation.

2.4.1 Hippocampal subfields and layers

The hippocampus was subdivided into head, body, and tail sections. Delineation of the hippocampal head (HH) started anteriorly on the first slice where the hippocampus was visible and was continued until the uncus disappeared (Wisse et al., 2012). The first slice where the HH was no longer visible was the starting point for the hippocampal body (HB), which was further subdivided into subfields (Exp.1 and Exp.3) and layers (Exp.1). Subfield labelling was continued caudally, ending on the last slice where the inferior and superior colliculi were jointly visible. This was the starting point of the hippocampal tail (HT), which was labelled without subregions, until the hippocampus disappeared.

Delineation of HB subfields comprised subiculum (Sub), CA1 and the remaining portion comprising CA2, CA3 and DG (DG/CA2-3). The CA1/subiculum border was determined by drawing a line perpendicular to the edge of the subiculum touching the medial border of the hippocampus (Mueller et al., 2007; Wisse et al., 2012). Although this marking scheme can result in a small part of the prosubiculum and subiculum proper being counted towards the CA1 subregion, this border was chosen because it could be reliably identified and replicated (Mueller et al., 2007). Furthermore, this problem of counting portions of subiculum towards CA1 might be especially prominent in the head but is less pronounced in the body (thus the proportion of subiculum being counted towards CA1 is relatively small in comparison to the size of the CA1 ROI). Finally, CA2, CA3, and DG were marked as one region (DG/CA2-3) because discrimination between these structures is very difficult (but note that 7T protocols exist for separation; e.g. Wisse et al., 2012). The most lateral point of DG (visible due to the SRLM, which appears dark) formed the border between CA1 and DG/CA2-3 and was constructed by drawing a straight, vertical line to the superior border of the hippocampus (Wisse et al., 2012).

In Experiment 1, the CA1 subfield was further subdivided into CA1-stratum pyramidale (pyr. CA1; probably also containing portions of the stratum oriens) and CA1-stratum radiatum/ stratum lacunosum moleculare (SRLM). The CA1-SRLM could be distinguished as the hypointense band lying between the more intense DG and CA1-pyramidal cell layers (Kerchner et al., 2010). Voxels overlapping with other ROIs (pyr. CA1, DG/CA2-3) were later deleted from these ROIs and preserved in the SRLM. Although the SRLM is slightly thinner than the present voxel size (ca. 0.68 mm; see Kerchner et al., 2010, 2012), its segmentation allows to make a first step towards separating laminar activity in pyramidal from apical CA1 regions (and also from activity in DG/CA3) and thus, to analyse activation related to hippocampal output pathways. Since these layers are difficult to visually identify in the DG, this region as well as CA3 and subiculum were manually segmented as subfields without layer-specific compartmentalization. Furthermore, segmentation of HC layers and subfields was only performed in the body, where borders could be precisely identified and not in the hippocampal head.

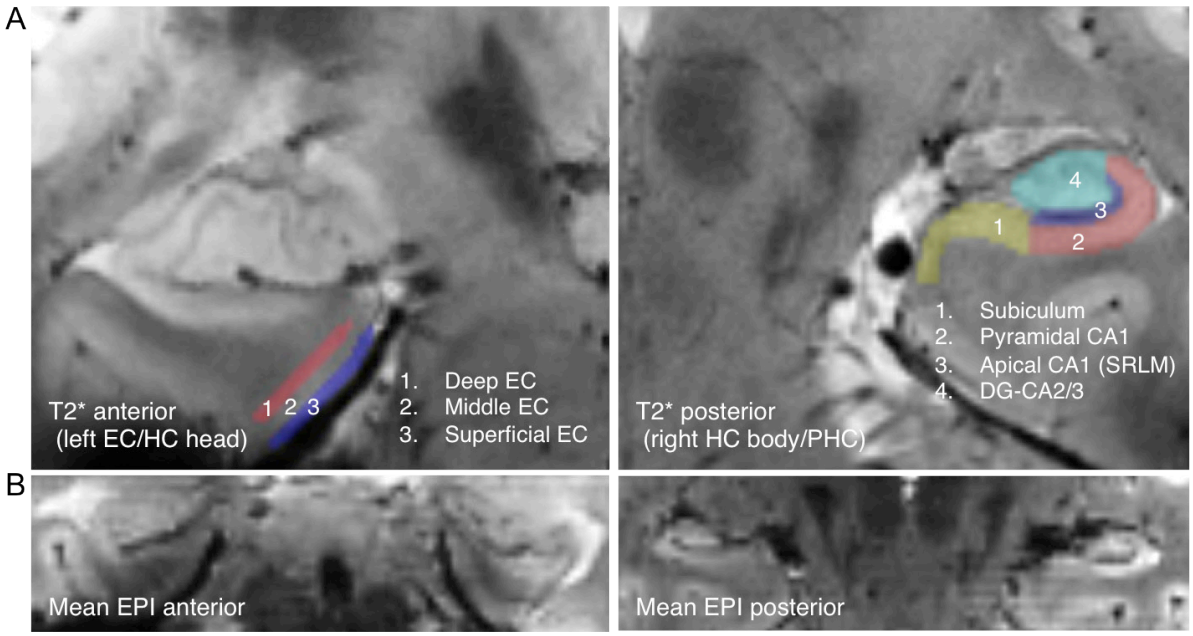

Figure 4. Segmentation scheme of entorhinal and hippocampal subregions.

A. Single-subject high-resolution T2* image (resolution: 0.33 mm^2 in-plane, 1.5 mm slice thickness) with overlaid entorhinal (EC; left) and hippocampal (HC; right) regions of interest (ROIs) on two coronal slices. ROIs were manually segmented on the individual T2* images and co-registered to the mean EPIs. The EC was equally divided into 3 regions: superficial, middle and deep. The CA1 region in the hippocampal body was subdivided into apical (Nr. 3) and pyramidal regions (Nr. 2). Note that the apical dendritic layer of CA1 ("SRLM") is well visible as a dark band on T2*-weighted images. **B.** Individual mean functional MR image (EPI, resolution: 0.8 mm^3) showing anterior MTL regions (EC, PRC and hippocampal head; left panel) and more posterior MTL regions (PHC and hippocampal body; right panel). This figure is adapted from Maass et al., 2014a.

2.4.2 Entorhinal subregions

Tracing of the EC started anteriorly at the level of the amygdala (if it was not covered by artefacts), moving caudally along the parahippocampal gyrus (PHG). As the collateral sulcus ends posteriorly, the posterior EC is winding down as well (Fischl et al., 2009), merging into the PHC. At anterior levels, the EC borders the amygdala nuclei medially (Fischl et al., 2009). When the gyrus ambiens disappears and the hippocampal fissure opens, the EC borders the parasubiculum medially. Laterally, the EC borders the PRC. The opening of the collateral sulcus typically coincides with the lateral border of the EC (Fischl et al., 2009), and was therefore chosen as lateral limit. Contrary to other markings schemes for the EC and PRC (Insausti et al., 1998), the part of the EC within medial banks of the collateral sulcus that depends on the depth of the collateral sulcus was not marked, since this border shows remarkable within and between subject variability and is also sometimes difficult to identify due to partially occurring susceptibility artefacts. Overall the EC covered approximately 25 functional (EPI) slices (Exp. 1/2). Distortion artefacts were most frequent in very anterior slices (at the level of the amygdala). Furthermore, dropouts occurred close to the ear canals, primarily affecting the PRC and partially spreading into the lateral EC (ca. 8.5% of EC slices). However, each subject also provided clean EC data. Overall, approximately 70% of slices covering the EC were usable for the final analysis. Sample EPI slices with and without dropout and are illustrated in the Figure S 1.

In order to assess differences in activity between entorhinal input and output regions (Exp.1), the EC was further divided into three equally sized portions: superficial, middle and deep. Therefore the superficial and deep layers were manually segmented. Although the microscopic anatomical EC layers could not be seen on the T2* images, previous 7T MR imaging studies of the human EC (Augustinack et al., 2005; Fischl et al., 2009) have shown that the cytoarchitectural features of EC layers can be distinguished with ultra-high resolution *ex vivo*. The cell-dense entorhinal layer II islands as well as the hypointense lamina dissecans can be robustly observed on MR images with 100 μm^3 isotropic resolution. These studies also show that the superficial third of the human EC mainly covers EC layer II, which gives primarily rise to input into DG and CA3, and probably also includes parts of entorhinal layer III, which projects mainly to the apical dendrites of CA1. In contrast, the deep third of the EC is mostly covered by the deep pyramidal layers

V, VI, and is the main target of output from the hippocampus. The middle EC portion, in turn, appears to mainly comprise the cell-free layer lamina dissecans (layer IV following Cajal's nomenclature) and parts of entorhinal layer III. Furthermore, dendrites of the deep pyramidal neurons might extend into the middle layer and contribute to activation. Regarding this anatomical layering of the EC, the current hypotheses focus on the superficial and deep EC regions, which can be relatively clearly assigned to input and output layers, respectively. Functional interpretations about the middle EC section, on the other hand, are uncertain. Kerchner et al. (2010, 2012) reported the thickness of the human EC to be 2.7 mm, while in Feczko et al. (2009) the mean thickness was 3.1 mm. With an isotropic voxel size of 0.8 mm^3, and after segmenting the EC into three sections, EC subregions with approximately 1 mm thickness were obtained, which allows to measure activity selectively in superficial and deep regions of the EC (see Figure 4a and Supplementary Figure S 2 for layer-specific activation).

2.4.3 Perirhinal and Parahippocampal Cortex

The PRC was defined as the region between the medial and lateral edges of the collateral sulcus (covering medial and lateral banks) on the same coronal slices as EC. Of note, this segmentation scheme also implies that the transentorhinal region and subportions of the lateral EC might be included in the PRC ROI (Insausti et al., 1998; Taylor and Probst, 2008). PRC and PHC ROIs in Experiment 1 were initially segmented on the T2*-weighted images but finally checked and corrected on the T1-weighted images which turned out to be much more suitable especially for PRC segmentation (less prone to artefacts, better contrast, lower slice thickness). Furthermore, in Experiment 2, in which PRC was used as seed region for functional connectivity analyses, voxels neighboured to lateral EC (1-2 voxels) were deleted from the PRC masks (see 4.2.4 and Figure 14) to avoid autocorrelations with neighboured EC voxels.

Segmentation of the PHC started one slice after the disappearance of the collateral sulcus, directly posterior to PRC and EC (when the uncus had disappeared). Labelling was continued posteriorly, ending on the last slice where the inferior and superior colliculi were jointly visible. The PHC was delineated as the region between subiculum (medial border) and the deepest point of the collateral sulcus (Zeineh et al., 2001; see Figure 14).

3 Experiment 1 (Laminar activity in the EC-HC circuitry during novel scene encoding)

3.1 Introduction

The ability to encode novel events into long-term memory critically depends on information processing within the hippocampus and the entorhinal cortex. The HC-EC circuitry shows a quantitative segregation of anatomical directionality into different neuronal layers (for a detailed description, see 1.2.4). Whereas superficial EC layers mainly project to DG, CA3 and apical CA1 layers, HC output is primarily sent from pyramidal CA1 layers and subiculum to deep EC layers.

The HC-EC circuitry is at the top of a visual processing hierarchy (Eichenbaum et al., 2007; Felleman and Van Essen, 1991) and receives inputs about object or item representations from PRC and spatial or contextual representations from PHC (see also 1.3.1 and Figure 1). These inputs are likely to remain segregated in EC until they are thought to converge to object-in-space scene representations in the hippocampus (Cashdollar et al., 2009; Eichenbaum et al., 2007; Nakamura et al., 2013; Saksida and Bussey, 2010). FMRI studies of scene processing have consistently observed “novelty responses” (stronger fMRI activation for novel as compared to familiar stimuli) or “repetition suppression” (reduced activation after repetition of a novel stimuli) in these regions (Howard et al., 2011; Yassa and Stark, 2008). However, layer-specific processing of novel information and related subsequent memory effects have not been studied in humans so far.

Using subfield and layer-specific fMRI at 7 Tesla, the current experiment aimed to assess the distribution of novelty responses for scenes, and how these are related to later recognition memory, within input and output regions of the HC-EC circuitry. Novelty responses could dominate in superficial EC layers because these receive afferent novelty signals from object and space processing pathways. Based on previous human fMRI data showing higher activation for novel than repeated objects (Bakker et al., 2008), one would also expect novelty responses in DG/CA3, which probably rest on an automatic representational orthogonalisation process (pattern separation, see also 1.3.1) in the DG. Previous studies in rodents (Karlsson and Frank, 2008; Nitz and McNaughton, 2004) and fMRI studies in

humans (Bakker et al., 2008) have also shown activation of CA1 during novel experiences. These novelty responses are predicted, for instance, by comparator models, which posit that comparison of input from the EC to CA1 with input that CA1 receives from CA3 aids the assessment of novelty (Lisman and Grace, 2005; see 1.3.1). According to these models, novelty detection should be associated with correlated activity of the superficial EC layers with DG/CA3 and the apical layers of CA1 (SRLM), compatible with input via the perforant path.

In addition to investigating which regions show novelty responses, it was assessed whether activation in the same regions also predicted the ability to subsequently recollect the novel scenes. An anatomical overlap between novelty and subsequent recollection would indicate that the functional strength of stimulus novelty in a given region is related to successful memory. For instance, when exposed to a series of novel scene images, effective pattern separation in DG/CA3 would prevent that incidental similarities between different scenes reduce novelty responses and at the same time improve subsequent memory (see, e.g. Bakker et al., 2008). Furthermore, the alternative possibility was tested that the ability to later remember information is influenced by hippocampal mechanisms that do not depend on the strength of the stimulus-novelty response. For instance, the aforementioned CA1 comparator process has also been hypothesized to incorporate predictions about the sequence of stimuli (e.g. if several successive stimuli belong to one of two categories, a category-change may be predicted), a process which could generate match/mismatch output signals in CA1 that influence memory independent of stimulus novelty (see also 1.3.1.5). Furthermore, CSL models (see 1.3.1.4) postulate that cooperation between CA1 and the output (deep) layer of EC is important for recollection because it allows pattern-separated CA3 representations to be decoded and fed back to the cortex and the success of this decoding could potentially also be independent of novelty. According to this possibility, and in contrast to stimulus novelty, activity predicting successful memory would therefore be dominant in the output structures of the HC-EC circuitry.

In order to address these hypotheses, it is necessary to measure activity of the entire HC-EC network with a spatial resolution that is high enough to segregate activity at a laminar level. Therefore, fMRI data were recorded with very high resolution (0.8 mm^3 isotropic voxels, see also Table 1) while healthy young adults

engaged in an incidental encoding task with novel and prefamiliarized images of scenes (see Figure 5). Recognition memory for the novel scenes was later tested outside of the scanner via memory confidence judgments that allowed to quantify recollection- and familiarity-based memory (see, e.g. Düzel et al., 2011; Yonelinas, 1994 and 1.3.1.2).

3.2 Methods

3.2.1 Participants

Twenty-two young subjects (students of the University of Magdeburg, mean age 26 ± 3.6 yrs, 12 males) participated in the study. Two subjects had to be excluded from further analyses due to strong dropouts in the EC and strong movement artefacts.

3.2.2 Task and design

During the fMRI session, subjects performed an incidental visual encoding task on images of scenes (see Figure 5). Subjects were instructed to discriminate between indoor/outdoor scenes by button press. The task ensures that subjects pay similar attention to every image. Moreover, we did not choose an explicit memory task in order to avoid that subjects recall other information to associate them with the images or try to associate images with each other (processes which might also vary from trial to trial). Instead the goal was to study incidental encoding activation in the HC-EC circuitry. The images comprised 120 new scenes (60 indoor and 60 outdoor), 60 ‘noise’ images and 60 repetitions of one familiar scene that were presented randomly. The familiar image and the ‘noise’ images were prefamiliarized directly before the functional MR scan with 10 presentations. This also served to familiarize subjects with the task. After a delay interval of about 85 minutes after starting the fMRI session, subjects performed a recognition memory task outside of the scanner. Therefore, the 120 target scenes (presented during the fMRI session) were intermixed with 60 novel distracter images (30 indoor / 30 outdoor). Subjects had to rate their confidence of recognition memory on a scale ranging from 1 - 5 (1: “sure new”; 2: “may be new”; 3: “I don’t know whether old or new”; 4: “may be old”; 5: “sure old”). These confidence ratings were later used as bases for contrast weights in the analysis of the fMRI data and for the calculation of receiver operating characteristics (ROCs) of recognition memory (Yonelinas,

1994). We showed twice as many novel scenes as familiar scenes (i.e. repetitions of one image) during the fMRI session in order to have a sufficient number of trials in every condition (remembered vs. forgotten) since memory for the novel scenes was tested afterwards.

The stimuli consisted of 120 digital photographic images with a size of 500 x 300 pixels and 8-bit grey scales (mean grey value 127 ± 75). Scrambled "noise" pictures were generated by using an 8-bit 50 x 30 pixel random grey value image (same mean and SD), which was upsampled to a resolution of 500 x 300 pixels (without antialiasing or smoothing), resulting in a checkerboard-like image. The fixation target was a black image of the same size with a white fixation star in the middle. The stimuli were projected onto the centre of a screen and the participants watched them through a mirror mounted on the head coil, subtending a visual angle of about ±3° by ±2°.

3.2.3 Recognition performance indices

For each subject, 4 recognition performance indices were calculated based on the behavioural data. Recollection and familiarity contributions to memory retrieval were estimated by receiver operating characteristics as described by Yonelinas (Düzel et al., 2011; Yonelinas, 1994). Therefore, a modified ROC curve was fitted to the hit and false alarm rates given by the four possible thresholds from the five ratings.

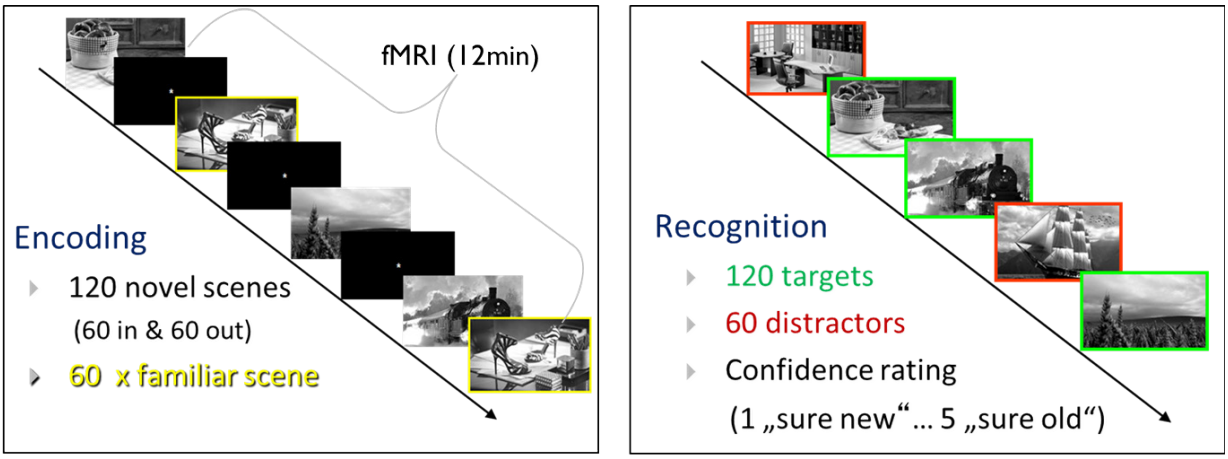

Figure 5. Visual incidental encoding task on images of scenes.
During the fMRI session subjects incidentally encoded photographs of scenes. Images were either novel or repetitions of one prefamiliarized scene (here highlighted by yellow frame) and subjects performed an indoor/outdoor discrimination task. About 90 min later, outside of the scanner, subjects performed a recognition test. They had to rate their confidence of recognizing a scene as old or new on a 5-point rating scale. Target scenes (here highlighted by green frame) were intermixed with distractors (here highlighted by red frame).

The d' of this fitted function corresponds to the familiarity estimate, the Y axis-offset to the recollection estimate.

Furthermore, the corrected hit rate was calculated as third index by subtracting the false alarm rate (response 4/5 for distractors) from the hit rate (response 4/5 for targets). A high confidence corrected hit rate was also computed as a fourth index by only counting the high confidence hits (targets with rating 5) and subtracting only the high confidence false alarms (distractors with rating 5). Measures of recollection and familiarity (estimated by ROCs) are closely related to high confidence corrected hit rate and corrected hit rate, respectively.

3.2.4 FMRI data acquisition and preprocessing

As described in 2.2, the 7T MR imaging protocol comprised the acquisition of a whole-head MPRAGE (0.6 mm^3 isotropic resolution), the functional EPI images (0.8 mm^3 isotropic resolution) and a high resolution structural T2* image (0.33 mm x 0.33 mm x 1.5 mm resolution). The fMRI session comprised 1 run (13 min). Total MRI duration was around 60 minutes.

FMRI data pre-processing and statistical modelling was done using SPM8. The pre-processing included only slice timing correction (unsmoothed data used for all ROI-based analyses), and smoothing with two different smoothing kernels: a 1.5 mm and a 2.4 mm full-width half-maximum (FWHM) Gaussian kernel. This was done to analyse activation at group level with *high specificity* (FWHM < 2 $\times$ voxel size) and *high sensitivity* (FWHM = 3 $\times$ voxel size), respectively. All models were calculated in native (= subject) space.

Encoding-related hemodynamic responses were analysed as a function of subsequent recognition memory success in the recognition memory test by sorting the stimulus onsets according to the 5 confidence rates. The onsets of the familiar and noise stimuli constituted two additional conditions. Together with the 6 movement parameters and one "error variance" condition (to take up variance due to invalid responses, i.e. failure to press a response button), this resulted in 14 conditions.

3.2.5 First-level analyses

In order to assess differences in activity due to stimulus novelty as well as activity changes related to subsequent memory, two types of contrasts were calculated. In

the “Novelty”-contrast activation for the repeatedly shown familiar image is subtracted from activation for all new images (irrespective of subsequent memory performance). For the “DM”-contrast (difference due to later memory), two positive weights were assigned to later recognized stimuli (confidence ratings 4 and 5) and three negative weights of equal value to the later forgotten items (confidence ratings 1, 2 and 3). Response category 3 “I don’t know whether the image is old or new” was classified as forgotten because this response category means that a participant does not recognize the repeated item with either familiarity or recollection. Rating 4, "may be old", on the other hand means that an item is recognized as a repetition. Excluding category 3 from the contrasts would reduce the power of the present analyses (comparing group activity maps for both a DM-contrast with and without category 3 and found the same regions being activated, but with more power for the DM-contrast which includes also the trials for response 3). It should be noted that the DM-contrast is only based on the novel items, whose memory was tested afterwards and not the familiar image (which was repeated continuously during encoding).

3.2.6 Segmentation of regions of interest

Hippocampal and entorhinal layers and subfields were manually segmented for each subject on the high resolution T2*-weighted images acquired orthogonally to the HC long axis (see 2.4 for details). In parallel, segmentation was verified and adjusted on the MPRAGEs, which had been bias-corrected and coregistered to the T2* volumes. The T1-weighted MPRAGE images provided additional information due to their different contrast, lower slice thickness and fewer susceptibility artefacts (especially in the anterior MTL including the EC). Finally, the T2* images and all the ROIs were coregistered and resliced to the individual mean functional EPI images (automatically and/or manually with SPM8). Again all ROIs were checked and (if necessary) corrected to achieve a precise overlay on the functional data. To measure laminar activity in the entorhinal cortex, the grey matter of the EC was subdivided into three equally sized portions (superficial, middle and deep; see Figure 4a for segmentation scheme of ROIs). Furthermore, the apical dendritic layer (SRLM) of the CA1 region was traced, which is visible on T2*-weighted images (Kerchner et al., 2010, 2012) and can be distinguished from the rest of CA1 (stratum pyramidale, stratum oriens, see Figure 4a).

In summary, 9 ROIs per hemisphere were segmented including the EC (with superficial, middle and deep regions), the subfields/layers of the hippocampal body (pyramidal CA1, SRLM, DG/CA2-3 and Sub) as well as the PHC and PRC.

3.2.7 Second-level analyses

3.2.7.1 Univariate analyses of group activation

First, group-level analyses (one-sample t-tests) were performed, which require smoothing and normalisation of the functional data in order to show that EC and HC regions were significantly activated across subjects and furthermore, to make the present data comparable and relatable to the previous fMRI literature. Therefore, cross-participant alignment was performed on the group-specific T1-template by use of ROI-ANTS (Avants et al., 2011) as described in the 2.3.

The resulting alignment parameters were then applied to each participant's Novelty- and DM-contrast map. One subject had to be excluded from the univariate second-level analyses, since the EC regions in particular were improperly registered to the template. Finally, the aligned contrast images of all remaining subjects (N = 19) were submitted to one-sample t-tests in SPM.

For second-level group statistics, the HC/EC template ROI (including the whole HC head and body) was used as explicit mask since the current hypotheses were specifically focused on processing of novel information within the EC-HC circuit. In order to estimate the probability of false positive clusters, the *3dClustSim* tool in AFNI (http://afni.nimh.nih.gov/afni/) was used. This program computes the cluster size threshold at chosen values for the alpha significance level and voxel-wise threshold (alpha = Prob(Cluster ≥ given size)). *3dClustSim* requires an estimate of the spatial correlation across voxels, which was determined in SPM for 1.5 mm and 2.4 mm applied smoothing kernels ($FWHM_{1.5mm}$ = 2.1 x 2.3 x 1.8 mm^3, $FWHM_{2.4mm}$ = 2.9 x 3.2 x 2.4 mm^3), respectively. For visualisation, second-level result maps were thresholded at $p_{voxel\text{-}level}$ < .005 and a cluster size of $k_{1.5mm}$ ≥ 15 voxels and $k_{2.4mm}$ ≥ 25 voxel, respectively. The type-1 error rates of the resulting clusters are listed in Table S 1 and Table S 2, where all clusters with alpha > 0.05 are highlighted (in italics).

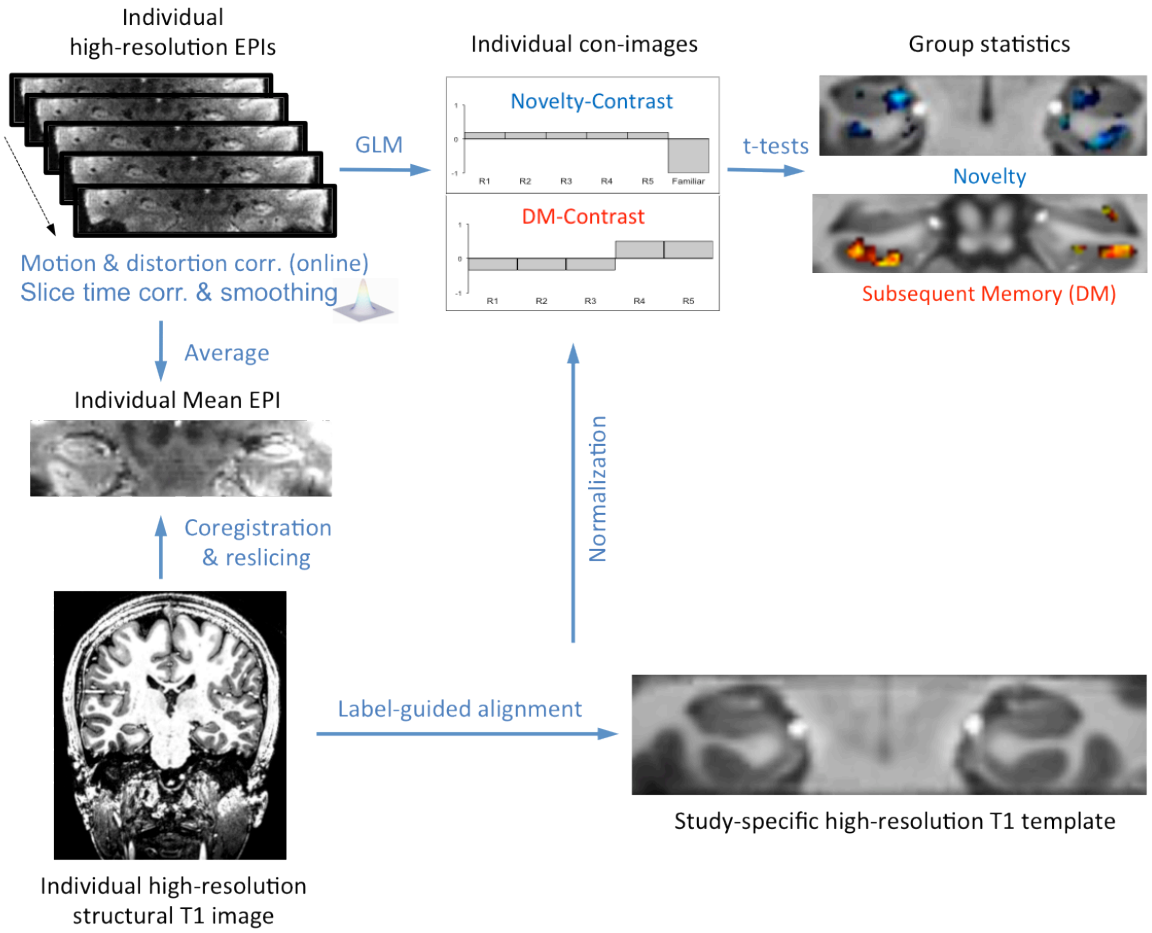

Figure 6. Processing stream for normalization-based univariate analyses.
Functional images (EPIs) were motion and distortion corrected during online reconstruction in the scanner. Preprocessing included slice time correction and smoothing with two different smoothing kernels. General linear models (GLMs) were run in native (=subject) space. For each subject, two contrasts of interest were calculated: a Novelty-contrast and a DM-contrast (due to memory). For inter-subject alignment, individual T1 images were coregistered and resliced to the mean EPI images and a group-T1 template was created with ANTS. Registration of T1 images to the template was further improved by label-guided alignment. The resulting parameters were used to normalize the individual contrast maps. Group activation for novelty and subsequent memory (DM) was assessed by second-level one-sample t-tests.

3.2.7.2 Region-specific Multivariate Bayesian decoding (MVB)

In order to test for differential activation of layers or subfields in the entorhinal cortex or hippocampus during novelty processing and successful memory encoding, a Bayesian decoding approach was used that is particularly suited to decide which region provides the best explanation of a given cognitive process.

Multivariate Bayes (MVB; see Friston et al., 2008) is a multivariate Bayesian decoding scheme in which the presence of a cognitive state is predicted from the distributed activity within a defined region of interest. In contrast to classical encoding models like the general linear model (GLM), MVB makes it possible to compare competing hypotheses about which anatomical structure hosts a

particular cognitive process (see FitzGerald et al., 2012; Morcom and Friston, 2012 for recent applications) using individual (not normalized, not smoothed) functional data. This is achieved by constructing and comparing alternative models where different data features (i.e. distributed activity in different ROIs) are used in an attempt to explain or predict a particular cognitive process, as specified by a contrast of interest. This model comparison rests on evaluating the relative marginal likelihood (or model evidence) of competing models, approximated using a (negative) free-energy bound (Friston et al., 2007; Penny et al., 2004). Thus, MVB can be used to decide whether a cognitive state (e.g. novelty or subsequent memory) is better explained in terms of activity in one region (e.g. superficial EC) than another region (e.g. deep EC). Here, using MVB in SPM8 and a sparse-coding prior, log evidences were computed for each subject-specific anatomical mask. The unsmoothed functional data were used to achieve highest anatomical precision.

For group analysis, random-effects Bayesian model selection was performed (BMS; see Stephan et al., 2009). Random-effects BMS quantifies the probability that a particular model generated the data for any randomly selected subject, relative to other models, and it is robust to the presence of outliers. The posterior distribution over models is parameterized in terms of a *Dirichlet* distribution. An intuitive way of comparing posterior model probabilities is by deriving the exceedance probability (*xp*) of each model, i.e., the probability that this model is more probable than any other model tested (Stephan et al., 2009).

3.2.7.3 Region-specific univariate comparisons of activations

Furthermore, it was tested whether hippocampal and entorhinal subregions and layers also show differential activation at the univariate level. Therefore, the number of significant voxels at a given voxel-wise threshold was extracted for each subject, contrast and region in native space for the unsmoothed raw data and the 1.5 mm smoothed data. To that end, the manually labelled ROIs were used as masks for the individual thresholded t-maps ($T > 2.33 \approx p_{voxel\text{-}level} < .01$) and determined the number of voxels surpassing this T-threshold.

It should be noted that condition × region interactions are usually considered problematic in fMRI because the scaling factor of activations (i.e., the beta coefficient in the GLM) can vary across regions due to local differences in hemodynamic coupling. Thus, the Bayesian decoding analyses (which are particularly suited for across-region comparisons) will be seen as the main basis for the current conclusions.

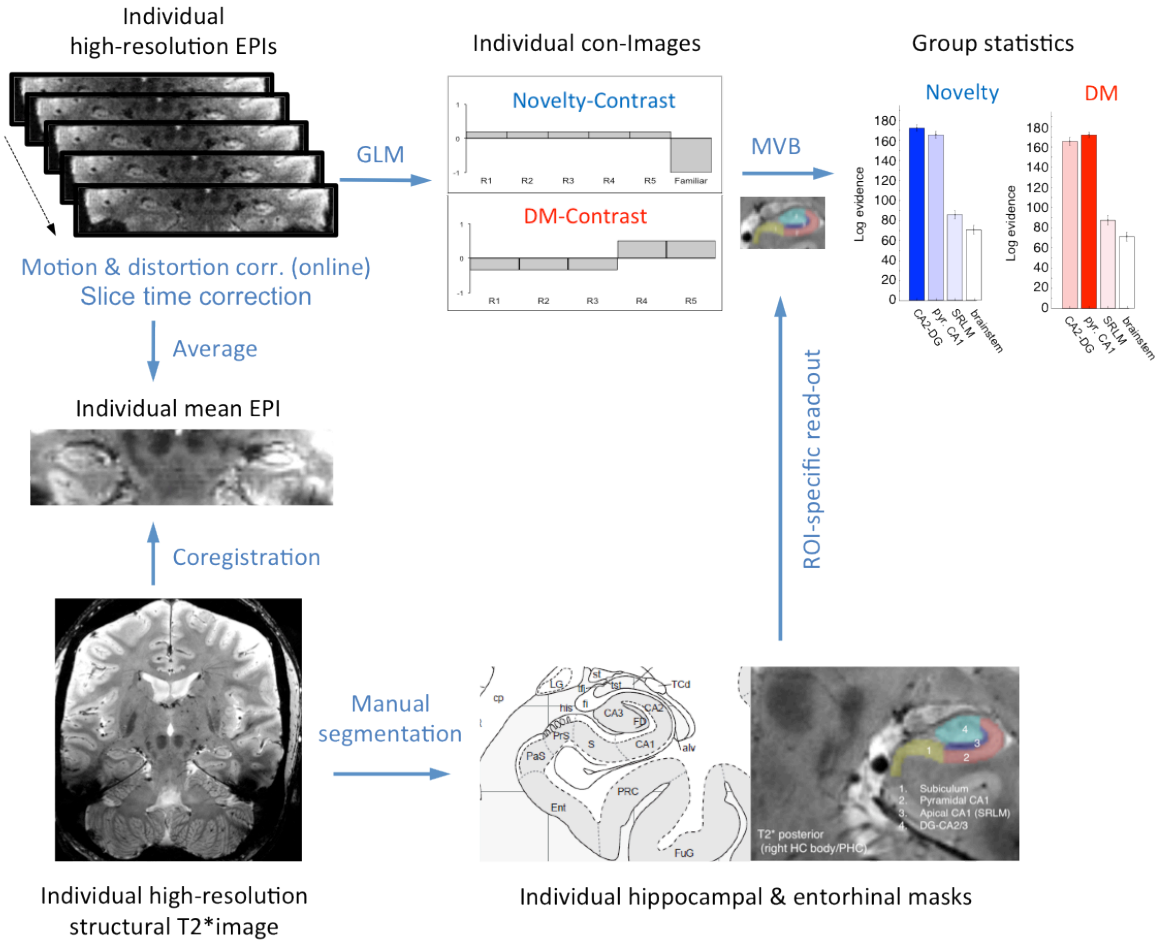

Figure 7. Processing stream for region-specific decoding analyses

Functional images (EPIs) were motion and distortion corrected online in the scanner. Preprocessing included slice time correction only. General linear models were defined in native (=subject) space. To compare novelty and subsequent memory-related activation patterns between subregions (and subjects), regions of interest were manually segmented on the individual high-resolution T2* images. These images (including the masks) were then coregistered and resliced to the mean EPI images and masks were checked and if necessary corrected. MVB decoding was used to compute log evidences for each subject-specific anatomical mask (to evaluate how well novel trials or remembered trials can be predicted from distributed activity in a subregion). For group comparison, log evidences were submitted to a random-effects Bayesian model selection.

3.2.7.4 Correlations of encoding activity with later memory performance

Bayesian model comparison showed that within the hippocampus proper/DG, subsequent memory was best explained in terms of activation in pyramidal layers of CA1. In addition, it was tested if activation strength in pyramidal layers of CA1 also correlated with later memory performance (across subjects). Therefore, the effect size (mean contrast estimate for DM) was extracted from pyramidal CA1 layers and computed correlations with memory performance (Pearson's correlation, two-tailed). First, each individual (not smoothed and not normalized; Z-transformed) first level DM-activation map was masked by the subject-specific anatomical ROI of pyramidal CA1. Then the mean contrast was calculated estimate across all voxels in the purely defined mask for each subject.

Of note, the DM-effect and the behavioural memory measures are not based on the same contrast. The DM-effect is calculated by subtracting activation for later forgotten from activation for later recognized scene images. In contrast, the behavioural measures are calculated using false alarms as references. These are responses to scenes that were never presented before (novel distractors in the recognition test), and hence could not have contributed to the DM-effect. Furthermore, the DM-effect is independent of whether the subsequent recognition was high or low confidence. The behavioural memory scores that correlated with DM-related activation, on the other hand, are related to "recollection" and restricted to high confidence ratings ("high confidence corrected hit rate") and to an ROC derived score ("recollection estimate").

3.2.7.5 Psychophysiological interaction analysis

In order to test if layer-specific activation in the EC was functionally correlated with hippocampal activation during novelty processing or successful encoding functional connectivity analyses were performed using the psychophysiological interaction (PPI) approach. This type of functional connectivity analysis identifies areas having a higher correlation with the time-course in a given seed region in one psychological context (e.g. novel trials) than in another context (e.g. familiar trials). For this analysis, individual superficial and deep EC ROIs were used as anatomical masks (seed region), and the mean time course from all voxels in the specific mask was extracted. The regressors of each subject's SPM model then comprised the seed time course from the EC region ("physiological main effect"), the task

regressor ("psychological main effect“: Novelty or DM) and the “psychophysiological interaction” vector (Friston et al., 1997) for assessing condition-dependent interregional coupling (plus the movement regressors as covariates). For the PPI analyses, the 1.5 mm smoothed EPIs were used to allow high spatial precision. Finally, cross-participants alignment of the resulting contrast-images was performed using ROI-ANTS in order to calculate a second-level group activity map.

3.3 Results

3.3.1 Univariate group activation in HC and EC subregions

In order to assess which hippocampal and entorhinal subregions were significantly activated across subjects during novelty processing and successful encoding of the novel scenes, one-sample t-tests were run after ROI-based group alignment with ANTS (Avants et al., 2011; see 2.3). Activations due to *stimulus novelty* (“Novelty”; Figure 8a) were measured by comparing all new images to the repetitions of one familiar image. Differences in activity *due to later memory* (difference due to memory, “DM”; Figure 8b) were assessed by contrasting later recognized stimuli with later forgotten items.

Functional data were smoothed with two different smoothing kernels (FWHM: 1.5 mm < 2 × voxel size and 2.4 mm = 3 × voxel size) in order to demonstrate the reliability of activation patterns across different levels of smoothing and to assess activations from the perspectives of either *higher specificity* (smoothing with 1.5 mm) or *higher sensitivity* (smoothing with 2.4 mm). A summary of activated EC/HC regions is shown in Table S 1 and Table S 2 and Figure 8, in which activation maps for the low smoothing kernel (light colours) are overlaid on the higher smoothing results maps (dark colours). For both contrasts, second-level group analysis yielded most prominent activation in medial EC and anterior HC. For novelty, strongest hippocampal activity was found in DG/CA2-3 and subiculum/presubiculum, especially in the hippocampal head. Several activity clusters were also located in CA1. With regard to successful encoding activity for the new stimuli (DM-contrast), strongest HC activity was found in the pyramidal layer of CA1 (close to the outer hippocampal border; see Figure 8b and Table S 2). Furthermore, several clusters were located in the head (medial CA1 and subiculum/presubiculum). Although some reported clusters did not survive multiple

comparison correction for the low smoothing kernel (FWHM: 1.5 mm), reliability of activation could be demonstrated by increasing sensitivity with a higher smoothing kernel (FWHM: 2.4 mm). Furthermore, there was no activation in HC or EC when testing for the inverse Novelty-contrast (familiarity-related activity; $p_{voxel\text{-}level} < .005$: no cluster > 1 voxel) or the inverse DM-contrast (higher activation for subsequently forgotten items; $p_{voxel\text{-}level} < .005$: no cluster > 4 voxels). In summary, the above univariate second-level analyses revealed significant activations in EC and specific HC subfields.

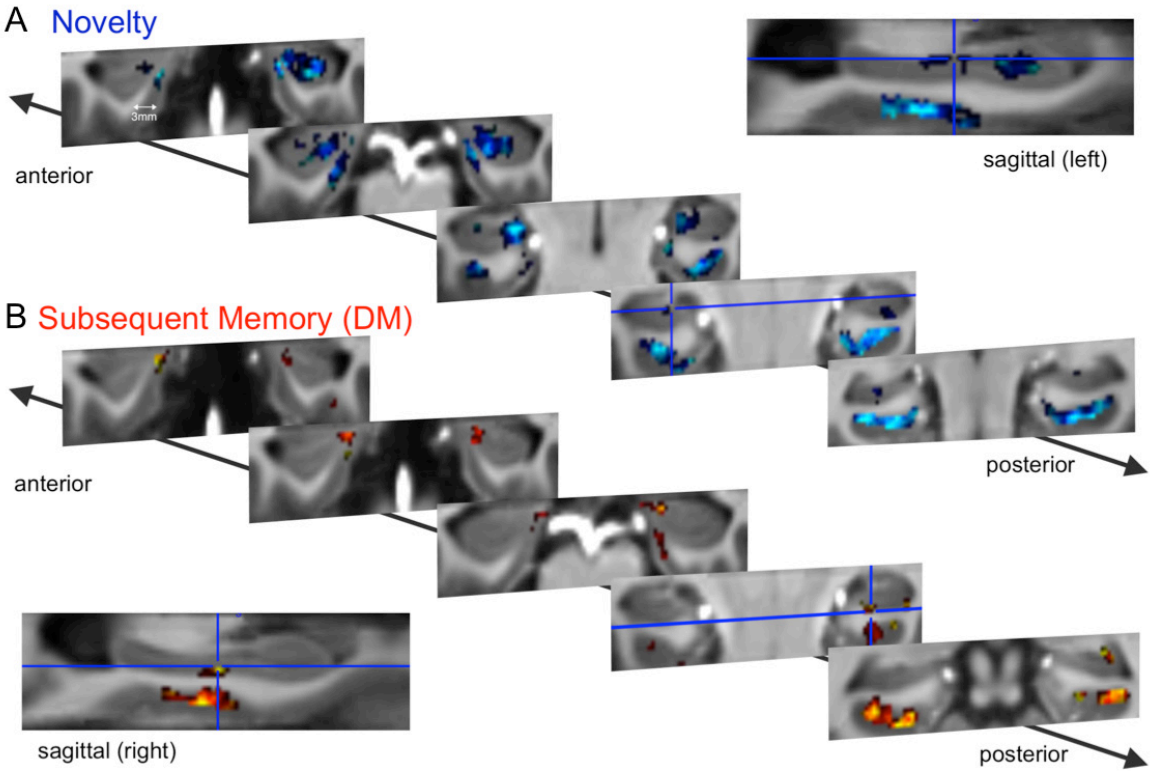

Figure 8. Novelty processing and successful memory encoding elicit a distinct activity pattern in hippocampal and parahippocampal subregions.
Group activity for (**A**) novelty and **(B)** successful encoding (difference due to memory, "DM"), overlaid on the group-specific T1-template (with same resolution as functional images: 0.8 mm^3 isotropic voxels) after ROI-based diffeomorphic registration with ANTS. Group activation is illustrated on 5 coronal sample slices for two different smoothing kernels. EPIs were initially smoothed with 1.5 mm (< 2 × voxel size, bright colours: cyan and yellow), which allows for higher anatomical precision at the cost of lower sensitivity. Furthermore, the analyses were repeated with a 2.4 mm FWHM (= 3 × voxel size, dark colours: blue and red) to increase sensitivity and demonstrate reliability of activation. For both contrasts, there was significant activation in the EC (mostly medial). In the hippocampus, novelty-related activation was most prominent in the head with peak activation in CA2/3-DG and presubiculum. For successful encoding, hippocampal activation was found in CA1 pyramidal layers (slice 4, right cluster) and subiculum (head & body) and a small cluster in CA2/3-DG (posterior body). Activation maps were thresholded at $p_{voxel\text{-}level} < .005 \approx T > 2.7$; $k_{1.5mm} \geq 15$ voxels and $k_{2.4mm} \geq 25$ voxels (N = 19). This figure is adapted from Maass et al., 2014a.

3.3.2 Region-specific Multivariate Bayesian decoding

In a second step, Multivariate Bayes (Friston et al., 2008) was used to evaluate functional differences between EC and HC layers/subregions with maximum spatial precision by using individual unsmoothed data and manually defined regions of interest.

Specifically, it was tested whether *novel trials* (vs. familiar trials) or *remembered trials* (vs. forgotten trials) can be better predicted from distributed activity in one subregion compared to another. For the second-level analysis, a random-effects Bayesian model selection (BMS; Stephan et al., 2009) was chosen. Posterior model probabilities are compared by deriving the exceedance probability (*xp*) of each model, i.e., the probability that this model is more probable than any other model tested. MVB analyses were performed on bilateral data. To test if the results were specific to EC/HC subregions and would not emerge in regions not motivated by the present hypotheses, a mask in the anterior brainstem was additionally defined for each subject (with the same number of voxels as in the individual EC ROIs). This control region was included in all subsequent MVB analyses.

First, it was tested whether novelty or subsequent memory (DM) can be better predicted from activity in superficial EC than deep EC (or vice versa). Second-level random effects analyses showed that novelty was best predicted from activity in superficial EC compared to deep EC (exceedance probability *xp*: superficial EC = 100.0%, deep EC = 0%, brainstem = 0%; see Figure 9a; with 18 of 20 subjects showing highest log evidence for superficial EC). In contrast, subsequent memory was best predicted from activity in deep EC compared to superficial EC (*xp:* superficial EC = 2.1%, deep EC = 97.8%, brainstem = 0.1%; see Figure 9b; with 15 subjects having highest log evidence for deep EC). These results demonstrate the differential engagement of separate EC subregions during novelty processing and successful memory encoding. Furthermore, the log evidences for predicting novelty and subsequent memory, respectively, from activity in the brainstem control region did not differ between both contrasts ($p > .50$) and were also much lower than the log evidences for all EC subregions (see Fig. 3). Of note, superficial and deep EC ROIs did not differ in size across subjects ($p > .19$).

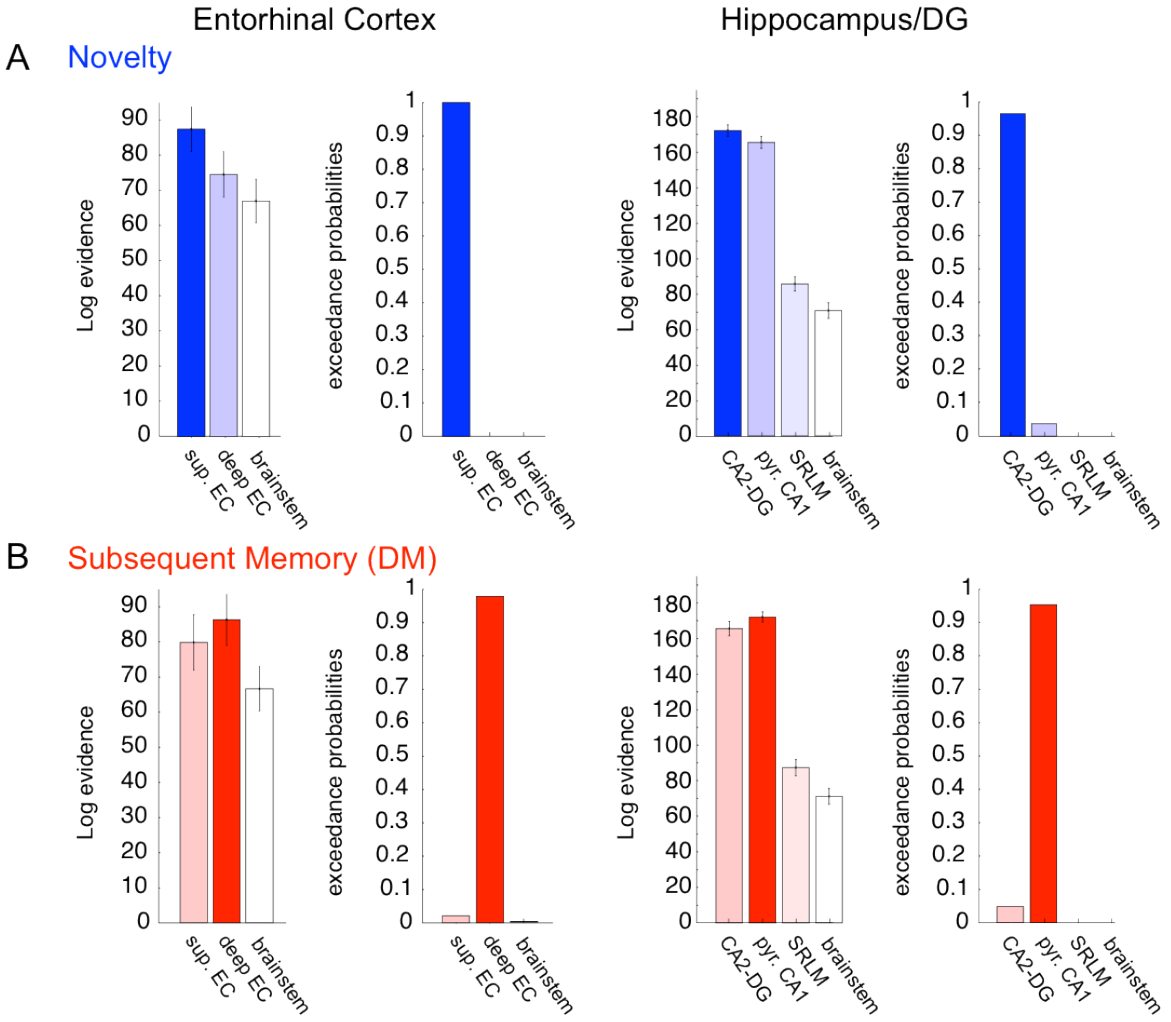

Figure 9. Bayesian model comparisons for decoding of novelty and subsequent memory in entorhinal and hippocampal layers/subregions.

Multivariate Bayes decoding (MVB) was used to test whether novelty or subsequent memory ("DM") can be better predicted from activity in one region than another. The method allows use of the individual (not normalized, not smoothed) functional data to compute the log evidences for each subject-specific anatomical mask (N = 20). The relative probability of one model (subregion) over any other model tested is expressed in terms of the exceedance probability (*xp*) based on random-effects Bayesian model selection. As control region, the anterior brainstem was included in all analyses. **A.** Novelty: Novel trials were detected with highest probability from activity in superficial ('input') subregions within the EC (*xp*: superficial EC = 100.0%, deep EC = 0%, brainstem = 0%) and from DG/CA2-3 within the hippocampus proper/dentate gyrus (*xp*: DG/CA2-3 = 96.3%, pyr. CA1 = 3.7, SRLM = 0.0 %, brainstem = 0). **B.** DM: In contrast, subsequent memory was better decoded from deep ('output') subregions within the EC (*xp*: superficial EC = 2.1%, deep EC = 97.8%, brainstem = 0.1%) and pyramidal CA1 ('output') layers within HC/DG (*xp*: DG/CA2-3 = 4.8%, pyr. CA1 = 95.2, SRLM = 0.0%, brainstem = 0.0). Please note that hippocampal analyses were restricted to the hippocampal body where subfields and CA1 apical ("SRLM") and pyramidal layers could be reliably differentiated. Error bars denote s.e.m. This figure is adapted from Maass et al., 2014a.

In a next step, it was assessed whether HC subfields or layers show differential responses to novelty and subsequent memory. Therefore, additional bilateral MVB analyses were run for the hippocampus proper and the DG (within the hippocampal body where layers and subfields could be clearly defined). Bayesian model comparison showed that novel trials were best explained in terms of DG/CA2-3 activity (*xp*: DG/CA2-3 = 96.3%, pyr. CA1 = 3.7, SRLM = 0.0 %, brainstem = 0; see Figure 9a; in 14 subjects the log evidence was highest for DG/CA2-3). In contrast, subsequent memory could be best decoded from pyramidal layers of CA1 compared to other hippocampal subregions (*xp*: DG/CA2-3 = 4.8%, pyr. CA1 = 95.2, SRLM = 0.0%, brainstem = 0.0; see Figure 9b; in 14 subjects the log evidence was highest for pyr. CA1). Please note that DG/CA2-3 and pyramidal CA1 layers did not differ in size across subjects ($p > .60$). However, the SRLM ROI was significantly smaller than the other subregions ($p < .01$) and thus contained a significantly lower number of voxels (= predictors), which might explain the low values in log evidence (compared to DG-CA2/3 and pyramidal CA1).

3.3.3 Region-specific univariate differences in activation

Multivariate Bayes decoding revealed that novel trials were best predicted by activation in superficial EC and CA2/3-DG, whereas subsequent memory of the novel images was best explained in terms of activation in deep EC and pyramidal CA1 layers. Additionally, it was analysed whether the same pattern of differential activation was also apparent at the univariate level. Therefore, ROI-based analyses were performed by using the individual (unnormalized) data and comparing the number of activated voxels in each of the ROIs (that fell above a specific voxel-wise threshold) across subjects.

These univariate analyses confirmed the findings from MVB decoding and showed that the number of activated voxels was higher in superficial EC subregions during novelty processing and vice versa in the deep EC subregions during successful encoding (Figure 10; left). These differences hold with classical statistics (i.e. paired t-tests: $Novelty_{supEC>deepEC}$: $p < .05$; $DM_{deepEC>supEC}$: $p < .01$ for both smoothing levels). With regard to HC/DG (see Figure 10; right) the same pattern of differential activation was found as revealed by multivariate decoding.

While the number of activated voxels for the Novelty-contrast was higher in CA2/3-DG than CA1 pyramidal layers, the inverse pattern was found for the DM-contrast

(successful encoding). However, these differences would be only significant for the Novelty-contrast ($Novelty_{CA2/3\text{-}DG>pyr.CA1}$: $p < .05$) but not the DM-contrast ($DM_{pyr.\ CA1>CA2/3\text{-}DG}$: $p < .15$) if paired t-tests were applied. Results are similar if a more conservative voxel-wise threshold is used ($T > 2.56 \approx p_{voxel\text{-}level} < .005$).

In addition, layer/subfield-specific peak activations for all subjects in the EC and hippocampus proper/dentate gyrus are illustrated in the Supplementary (see Figure S 2). Univariate single-subject peak activations for both contrasts are shown for the 1.5 mm smoothed data in native space (without normalization). While EC activation is illustrated on the individual coregistered (to the mean EPI) MPRAGE, peak activity in the hippocampus/dentate gyrus (hippocampal body) is overlaid on the high-resolution structural T2* image ($p_{voxel\text{-}level} < .01$, $k \geq 10$ voxels; blue cross demarcates peak activation). These analyses highlight that individual activation patterns related to novelty or subsequent memory can be remarkably confined to hippocampal subfields/layers and to superficial or deep subregions of the EC. Notably, these peak activation plots represent only a selection/cross-section of the overall activations in entorhinal and hippocampal subregions. In most subjects, several activation clusters were found bilaterally along the anterior-posterior axis. Of note region-specific differences are also apparent if 1.5 mm smoothing is applied and furthermore, that numbers of activated voxels increase in EC and HC/DG but decrease in the brainstem control region, if the images are smoothed.

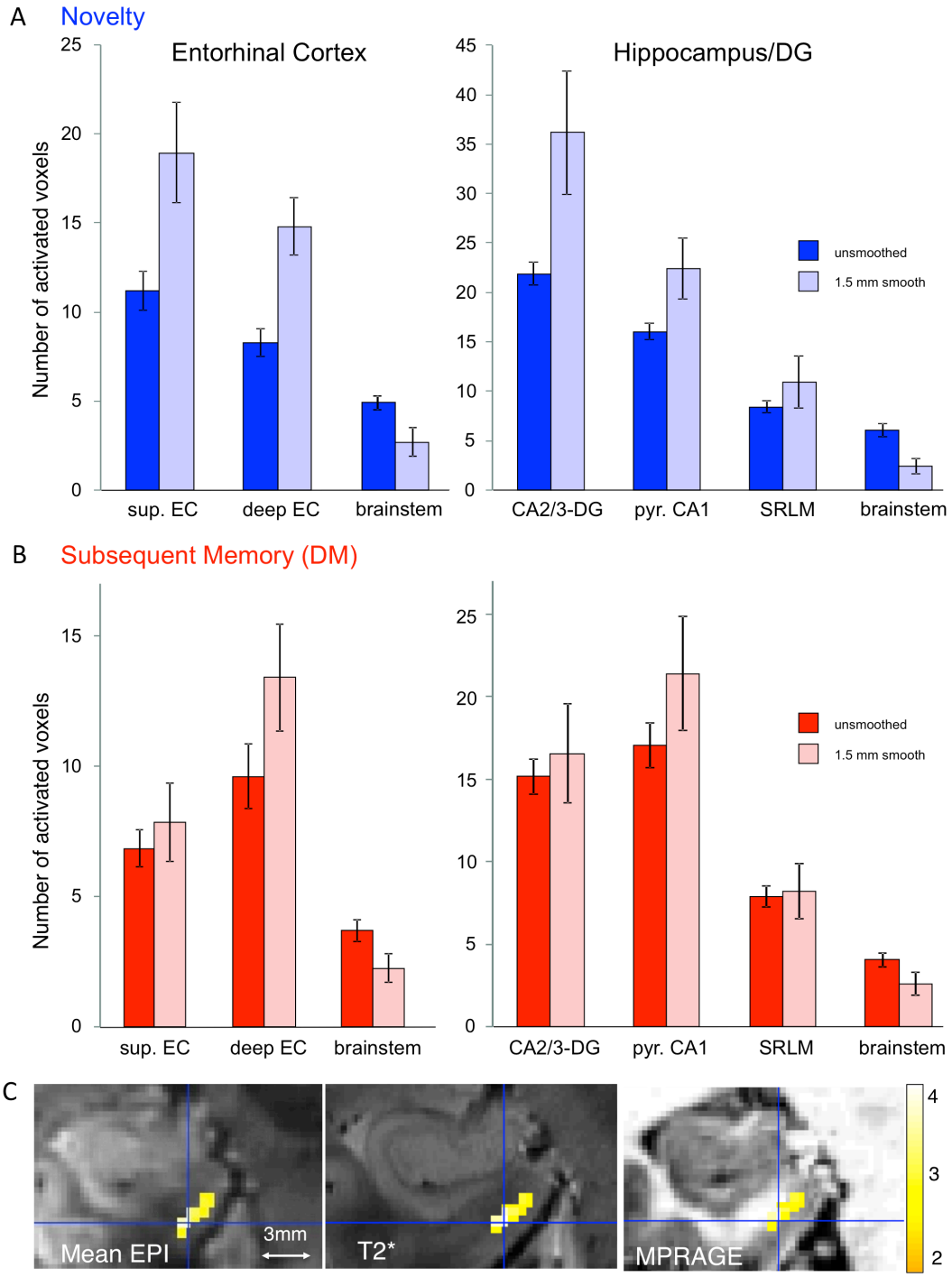

Figure 10. Univariate analyses of entorhinal and hippocampal subregion/layer-specific activation during novelty processing and successful encoding.

Averaged (across individuals) numbers of voxels activated at $p_{voxel\text{-}level} < .01$ for **A.** the Novelty- and **B.** the DM-contrast in subregions/layers of the entorhinal cortex (EC) and hippocampus proper/denate gyrus (HC/DG; hippocampal body) for the unsmoothed and the 1.5 mm smoothed (both unnormalized) data. To confirm findings from decoding analyses (see Figure 9), number of significant voxels for each subject and individual ROI were extracted. The anterior ventral brainstem (same size as EC layers and SRLM, respectively) served as control region. The same pattern of activation differences between input and output regions with respect to novelty and subsequent memory was apparent at the univariate level. Error bars denote s.e.m. **C.** Single-subject (peak) activation due to memory (successful encoding) overlaid on the individual mean EPI and the coregistered T2* and MPRAGE image (smoothing: 1.5 mm, $p_{voxel\ level} < .01$, $k \geq 10$ voxels). This demonstrates that activation can be confined to deep (vs. superficial subregions) of the EC. This figure is adapted from Maass et al., 2014a.

3.3.4 Correlations of encoding activity with later memory performance

The aforementioned ROI-specific analyses revealed that within the hippocampus proper/DG, subsequent memory could be best predicted by activation in pyramidal layers of CA1. In order to specifically test if activation strength in this region was also correlated with later memory performance across subjects, the effect size (contrast estimate from the GLM) for all voxels was extracted within the anatomically defined pyramidal CA1 ROI and computed its average across voxels. This was done at the single-subject level using the non-normalized and non-smoothed individual first-level DM-maps.

Successful encoding (DM) activity in pyramidal CA1 layers was significantly correlated with high confidence corrected hit rates (p =.014; r = 0.54; see Fig. 4a) and recollection estimates (p =.025; r = 0.50; see Fig. 4a). In other words, later recollection across subjects was predicted by activation strength in the pyramidal (output) layers of CA1. This analysis for the CA1 pyramidal layers was specifically motivated by the MVB results. However, it should be noted that there were no significant correlations with later memory performance for any other subregion. Except for a trend correlation between contrast estimates in the PHC and familiarity estimates (p = .071), all other p-values were > 0.1.

3.3.5 Layer-specific functional connectivity of the EC

The above MVB decoding results show that processing of a novel stimulus was best explained in terms of activity in superficial EC, whereas subsequent memory was predicted with highest probability from deep EC. In order to test whether novelty-related activation in superficial EC correlated with activity in DG/CA2-3 and/or SRLM, compatible with input from the EC to the HC, the context-specific coupling of this layer was examined (cf. a psychophysiological interaction analysis, PPI). For this analysis, individual superficial EC ROIs were used as seed regions. Furthermore, it was tested whether successful encoding activity (DM) in deep EC was coupled to activation in pyramidal layers of CA1 and/or subiculum. To that end, the deep EC was taken as seed for the PPI analysis based on successful encoding activity. Connectivity analyses were performed at the single-subject level in order to ensure the highest anatomical precision.

Second-level group analysis (after ROI-based registration with ANTS) of PPI results maps revealed those regions that showed significant context-specific

coupling with the seed regions across subjects. Second-level analyses yielded strongest functional connectivity of superficial EC with right anterior DG/CA2-3 (for $p_{voxel\text{-}level}$ < .005: k = 10 voxels, no other cluster > 3 voxels) during novelty processing. However, this cluster would not survive correction for multiple comparisons. For deep EC strongest functional coupling during successful memory encoding was found with pyramidal layers of right CA1 (for $p_{voxel\text{-}level}$ < .005: k = 26 voxels, alpha < 0.05; see Figure 11b). PPI (control) analyses using superficial EC ROIs as seed regions in the DM-contrast and deep EC ROIs as seed regions in the Novelty-contrast did not reveal significant connectivity with any region in the hippocampus ($p_{voxel\text{-}level}$ < .005, no cluster > 5 voxels).

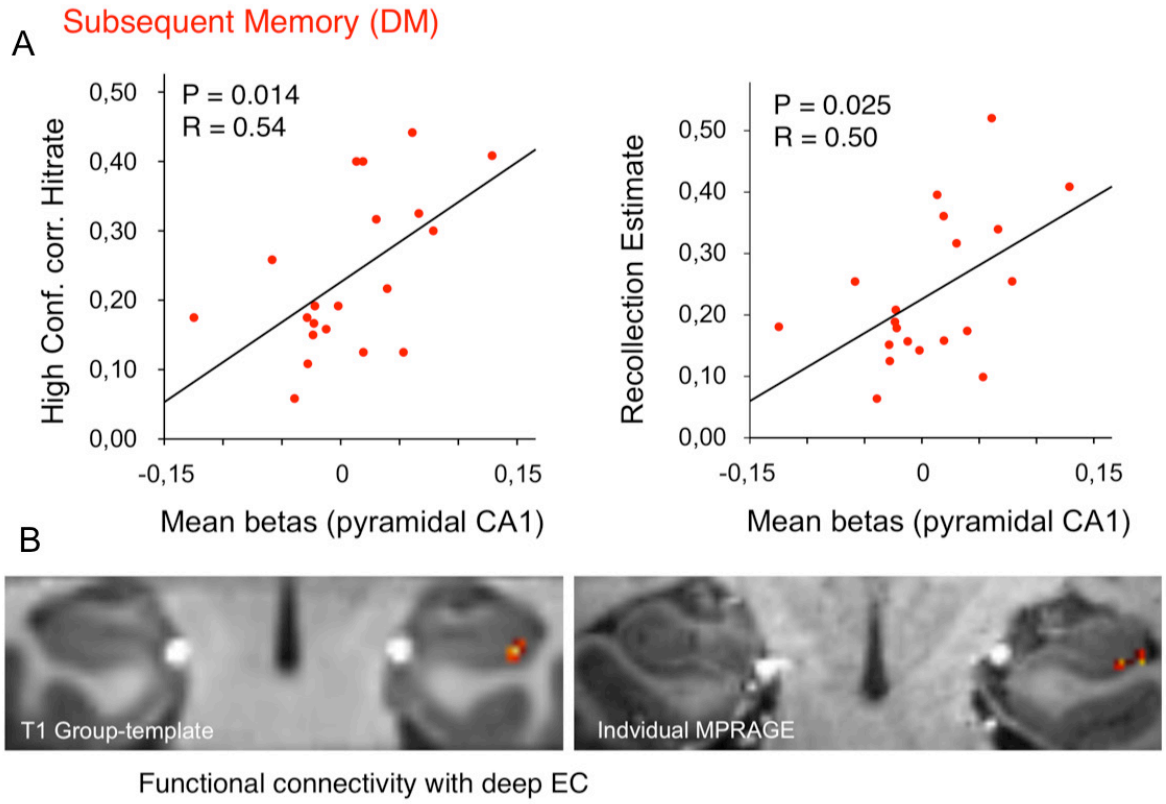

Figure 11. Successful encoding activity in pyramidal layers of CA1 predicts later memory and is correlated with activation in deep EC regions.

A. High confidence recognition and recollection estimates in the subsequent memory test were correlated with successful encoding activity strength in the pyramidal ('output') layers of CA1 across subjects (N = 20). Activation strength is defined as the mean contrast estimate (weighted betas for DM-contrast) of all voxels in our anatomically defined ROI (pyramidal CA1). Betas were extracted from the individual unnormalized and unsmoothed functional data using subject-specific anatomical masks. **B.** Functional connectivity analyses (PPI) yielded significant functional coupling of deep EC regions (seed) with pyramidal layers of CA1 during successful encoding ($p_{voxel\text{-}level}$ < .005: k = 26 voxels, alpha < 0.05, N = 19). Group results are depicted on the T1-group template after normalization with ANTS (left). In addition, results are illustrated for one sample subject on the individual MPRAGE (right). This figure is adapted from Maass et al., 2014a.

3.3.6 Comparison between BOLD characteristics of HC and EC

Finally, it was analysed if there were systematic differences between the BOLD responses in hippocampus and EC. In order to compare hemodynamic response functions (HRFs) between both regions, SPM8 ("Hemodynamics"; see Friston, 2002 for details) was used to estimate hemodynamic model parameters across subjects (N = 20). T-tests on these parameters (Feedback, Transit time, Exponent, Resting oxygen extraction and Log signal ratio) showed that, under the power which the present sample size affords, one cannot detect a significant difference in these hemodynamic parameters between regions (all $p_{corr} > .32$). This makes it unlikely that the other analyses in the present study are confounded by regional differences in the HRF.

3.4 Discussion

High-resolution fMRI at 7T was used to measure activity in subregions/layers of the entorhinal cortex and of the hippocampus during the incidental encoding of novel events. In order to compare activation between regions, a Bayesian decoding approach (Multivariate Bayes) was chosen that is particularly suited to evaluate competing hypotheses about which anatomical structure hosts a particular cognitive process (Friston et al., 2008; Morcom and Friston, 2012). Entorhinal and hippocampal in- and output regions exhibited differential activation patterns with respect to novelty processing and successful memory encoding.

Multivariate Bayes decoding revealed that novel trials were best predicted from activity in the input regions within the EC and from DG/CA2-3 within the hippocampus proper/DG (Figure 9a; see also Figure 10a for ROI-specific univariate results). Furthermore, preliminary evidence was found that activation in superficial EC is specifically correlated with activity in DG/CA2-3. These observations suggest that the input from EC to the HC is related to novelty because the superficial regions of EC are quantitatively more strongly an origin of input to the HC than being a target of output from the HC. Hence, the present data provide combined functional and anatomical evidence that perforant pathway input from EC to the hippocampus is related to novelty processing as predicted by theory (Lisman and Grace, 2005). Lesion studies in rats have indicated that the DG–CA3 network plays a key role in processing novel spatial information (Hunsaker et al.,

2008), which is in line with the present results that novelty processing most strongly engaged the DG/CA2-3 subregion (see also Olarte-Sánchez et al., 2014).

Testing subsequent recognition memory performance for the novel items enabled to determine which subfields and layers related to subsequent memory. Later remembering was better predicted by activity in deep than superficial EC (Figure 9b; see also Figure 10b for ROI-specific univariate results). Regarding the hippocampus proper and DG, subsequent memory was explained in terms of activation in pyramidal CA1 layers. Furthermore, activation strength in the pyramidal layers of CA1 was predictive for later high confidence recognition/recollection performance across subjects (Figure 11a). Finally, the functional connectivity results showed that DM-related responses in deep EC were most strongly correlated with activation of pyramidal CA1 layers (Figure 11b). The deep EC ROI very likely covered the entorhinal layers V, VI. These deep EC layers are more strongly a target of output from the HC (that mostly arises from the pyramidal layers of CA1 and subiculum) than providing input to HC. Therefore, these findings suggest that the ability to later recollect the exposure to a novel item is more related to the results of intrinsic computations within HC and EC and their output-level activity (during encoding) than the strength of activity driving input to the HC from EC. Together, the current results propose that the hippocampus receives input for novel information, but creates output only for some of the novel events, namely those events that are successfully encoded into long-term memory (for a more detailed discussion, see 6.2.1).

Multivariate Bayesian decoding within EC regions related activity in superficial (input) and deep (output) EC to novelty and subsequent memory, respectively. Previous studies in primary sensory areas have shown that draining venous blood might affect the signal of deep and superficial layers differently (draining vein effect) with a bias towards responses from superficial layers (see, e.g. Goense and Logothetis, 2006; Harel et al., 2006; Koopmans et al., 2010; Zhao et al., 2006). However, systematic differences of BOLD responses between layers cannot explain the present findings of an inverse activation pattern for the DM-contrast compared to novelty in superficial versus deep EC. Although the BOLD signal from superficial regions might contain a hemodynamic contribution from the deep regions, this only makes the inference about what is encoded by superficial regions more conservative. In other words, finding that BOLD signal from the superficial EC

encodes novelty despite a putative confounding hemodynamic influence from the deep EC speaks to the robustness of the present results.

In this study BOLD activation was differentiated between pyramidal and apical dendritic layers (SRLM) of CA1. Previous work in monkeys (Logothetis and Wandell, 2004; Goense and Logothetis, 2008; see also 1.4) has shown that the BOLD response is correlated with postsynaptic LFPs but robust BOLD responses can be also observed in correlation with LFPs even in the absence of neural spiking (Logothetis and Wandell, 2004). Therefore, it is conceivable that input to the SRLM could cause local BOLD responses that are not associated with a firing response of CA1 pyramidal neurons. Another line of research that combined optogenetic stimulation with fMRI showed that the BOLD response also correlates with neuronal firing of excitatory pyramidal neurons (Lee et al., 2010). Thus, it is also conceivable that firing output of neurons can cause local BOLD responses (either directly or through local horizontal microcircuits). Hence, taken together, it is theoretically plausible that selective BOLD responses can occur in the SRLM and the pyramidal layer of CA1. One interpretational complication to this scenario is that the stratum oriens of CA1 provides input from CA2-CA3 to the pyramidal layer of CA1 (van Strien et al., 2009). The present fMRI measures cannot distinguish to what extent the local BOLD responses associated with the DM-effect in the CA1 pyramidal layer are caused by such CA2-CA3 projections. However, the functional connectivity results show that BOLD responses in deep EC are correlated with those in the pyramidal layer of CA1 in the context of the DM-effect, supporting the possibility that DM-related activity of CA1 is indeed related to CA1 output rather than input from CA2-CA3.

4 Experiment 2 (Functional subregions of the human EC)

4.1 Introduction

The entorhinal cortex is the primary interface between the neocortex and the hippocampus. Studies in rodents and non-human primates suggest that the EC can be divided into functional subregions based on their differential anatomical connectivity with PRC vs. PHC/POR and with hippocampal subfields (i.e. subiculum and CA1) along the proximo-distal axis (for more details, see 1.2.2). While preferred connections of PRC to EC are in the anterolateral domain, those from PHC/POR are in the posteromedial domain (Suzuki and Amaral, 1994; Witter, et al., 2000a). Although the position of the EC on the cortical surface of the brain differs across species, its connectivity is strikingly preserved. This suggests that connectivity of the human EC might also differ along longitudinal and lateral-medial axes, but because anatomical tracing studies cannot be performed in humans, direct evidence for this idea is lacking. Recent structural and functional MRI studies have assumed a lateral-medial distinction in humans according to the rodent nomenclature of LEC and MEC (e.g. Reagh and Yassa, 2014). However, whether such a lateral-medial dissociation of EC connectivity exists in humans and/or whether connectivity differs along the anterior-posterior EC axis has not been assessed so far.

Numerous studies have demonstrated that networks of brain regions linked by direct and indirect anatomical connections exhibit temporally coherent, low-frequency fluctuations in BOLD fMRI data during both the resting and task states. Recent work has demonstrated that spatially contiguous but anatomically distinct brain regions can be reliably differentiated based on functional connectivity profiles measured with BOLD fMRI (for a review see Fox and Raichle, 2007). Using fMRI at 3 Tesla, human resting-state fMRI studies (Kahn et al., 2008; Libby et al., 2012) have reported reliable differences in connectivity between the PRC and PHC with the hippocampus. Whereas the PRC showed higher functional connectivity with the anterior hippocampus, the PHC showed stronger connectivity with the posterior hippocampus, a dissociation that was most evident for subiculum and CA1 subfields (Libby et al., 2012). Due to limitations in SNR and spatial resolution, these studies were unable to assess functional connectivity with the EC. This lack

of knowledge is a serious limitation for neurobiological theories of memory and navigation and for understanding the clinical impact of localized EC damage in the early stages of neurodegenerative conditions such as Alzheimer's disease.

To determine the topographical organization of intrinsic functional connectivity in the human EC and thereby identify its potential functional subdivisions, connectivity profiles of PRC and PHC were assessed at 7 Tesla. In two independent samples, correlations of activation were examined between individually anatomically defined PRC vs. PHC seeds and the EC along its anterior-posterior and lateral-medial axis. In addition, it was tested whether functionally distinct EC subregions also exhibited differential connectivity with hippocampal subfields along a transverse or longitudinal axis. Seed-to-voxel correlation analyses were performed on the residual fMRI data after extraction of task-related activity.

4.2 Methods

4.2.1 Participants

Two independent samples of young, healthy subjects underwent high-resolution fMRI scanning. Data set 1 comprises the data of Experiment 1 that included 21 subjects (see 3.2.1; one subject was scanned in both studies and excluded from data set 1). Data set 2 is based on a 7T fMRI study conducted by David Berron (unpublished data), which included 22 subjects (mean age 28 ± 3.9 yrs, 7 male). Six subjects from data set 1 and six from data set 2 were excluded due to strong dropouts in the PRC and/or EC or severe movement or distortion artefacts. Functional connectivity analyses were performed on the residuals of task data after extraction of task effects (N_1=15, N_2 =14).

4.2.2 Tasks

4.2.2.1 Data Set 1 (Encoding of novel vs. familiar images of scenes):

Subjects performed an incidental visual encoding paradigm (see 3.2.2).

4.2.2.2 Data Set 2 (Differentiation of original images and similar lures)

During the fMRI session, subjects performed an explicit mnemonic discrimination task. Stimuli were presented in short sequences consisting of 3 - 5 stimulus presentations of the same two stimuli (two similar versions of the same indoor scene). Sequences were presented in an event-related design. Each stimulus was

presented for 3 s and stimuli were separated by a presentation of a scrambled noise picture for 3.5 s to prevent an afterimage or pop out effects. Sequences were separated by a presentation of a fixation star for 4 s. Subjects had to keep the first stimulus of each sequence (target) in mind and indicate the third presentation of this exact stimulus via button press with their right index finger. Of note, connectivity analyses were performed after extraction of task-related variance in the fMRI BOLD signal.

4.2.3 7T fMRI data acquisition and preprocessing

The fMRI session comprised 1 run (13 min) with 370 EPI volumes in data set 1 (see also 0) and 4 runs (13.5 min each) with 400 EPI volumes in data set 2. Furthermore, the 7T MR imaging protocol included the acquisition of a whole-head MPRAGE (0.6 mm^3 isotropic resolution) and a high resolution structural T2* image (0.33 mm x 0.33 mm x 1.5 mm resolution) as described in 2.2 and 0. Total MRI duration was around 60 minutes for data set 1 (i.e. Experiment 1) and 100 min in data set 2, respectively.

The fMRI data pre-processing included slice timing correction and low smoothing with a 1.5 mm Gaussian kernel (FWHM < 2 x voxel size) to keep high anatomical precision. Outliers in average intensity and/or scan-to-scan motion were identified using the *ARTRepair* toolbox for SPM (Percent threshold in global intensity: 1.3, movement threshold: 0.3 mm/TR) and included as spike regressors.

To remove task effects, general linear models were run (including all task conditions and the movement parameters) and the residual images were saved for subsequent intrinsic functional connectivity analyses. Based on previous studies suggesting a linear superposition of task activity and spontaneous BOLD fluctuations, removing task-induced variance of event-related fMRI data should yield a remaining residual signal similar to “continuous” resting state data (e.g. Fox et al., 2006). Although quantitative differences between residuals derived from task data and continuous resting state data have been reported (Fair et al., 2007), in qualitative terms patterns of functionally connected regions have been shown to be remarkably consistent (Fair et al., 2007; Lacy and Stark, 2012).

4.2.4 Segmentation of regions of interest

In order to analyse PRC vs. PHC seed-to-voxel connectivity, seed regions were manually segmented on the individual high-resolution MPRAGEs (which had been bias-corrected and coregistered to the individual mean EPIs before). Furthermore, the EC and the subiculum were labelled on the T1 group template in order to analyse connectivity topography of seeds with the EC and the subiculum at group level along anterior-posterior and lateral-medial axes (individual beta-maps were registered to the template). A detailed description of the segmentation landmarks is given in 2.4.

For the purpose of the current study, PRC mask voxels that where directly neighboured to the EC/PRC border were deleted (leaving a gap of approx. 2 voxels ~ 1 mm) to avoid autocorrelations between PRC seed voxels and the target EC ROI. The subiculum was labelled in the head and body (until the colliculi disappeared) according to Wisse et al. (2012) in order to dissociate connectivity along the long axis of the HC. For division of EC and subiculum masks into anterior-posterior and lateral-medial or proximal-distal subregions, see “Second-Level Analyses” (4.2.6.1).

Subsequently, PRC and PHC masks were coregistered to the individual mean EPI images and manually adjusted to achieve a precise overlay on the functional data. To exclude voxels susceptible to signal dropout, for each ROI, voxels with mean intensity (across timepoints) < 2 SD from the mean intensity (across voxels) in an ROI were excluded (Libby et al., 2012). Thresholding led to the rejection of no more than 5% of voxels in any ROI. Additionally, areas of PRC were occasionally subject to distortion artefact, and these voxels were manually deleted from ROIs. These adjusted and thresholded ROIs were used as seed regions for the functional connectivity analyses. White matter (WM) and cerebral spinal fluid (CSF) masks were generated by automated segmentation (SPM8, “New Segment”) of the co-registered MPRAGE images and masks were thresholded (P(tissue) > .95) .

4.2.5 First-level functional connectivity analyses

Seed-to-voxel correlational analyses were performed on the native (preprocessed, unnormalized) residual fMRI data using the *conn-toolbox* (Whitfield-Gabrieli and Nieto-Castanon, 2012). First, functional connectivity patterns of PRC vs. PHC seeds with the EC were analysed. For each functional connectivity analysis, seed

regions' average time series were generated as regressors of interest. As covariates of no interest, WM and CSF time series and subjects' realignment parameters (including spike regressors) were included to account for physiological noise and movements, respectively. Functional data were band-pass filtered for frequencies of 0.01– 0.1 Hz. Bivariate correlations were computed where generated beta maps contain the Fisher-transformed correlation coefficients (z=atanh(r)). To perform group-analyses, beta-maps were registered to the group-specific T1 template and Z-standardized.

4.2.6 Second Level analyses

4.2.6.1 Univariate analyses of functional connectivity

In order to perform group analyses (one-sample and paired t-tests) individual MPRAGEs were coregistered on the group-specific T1-template using *ROI-ANTS* (e.g. Avants et al., 2011; see 2.3). The resulting transformation parameters were then applied to each participant's beta map and to the MTL masks in order to verify alignment precision (similar to the procedure in Exp.1, see also 3.2.7.1). Finally, the aligned beta images were submitted to second-level group analyses.

First, single-seed group connectivity maps were calculated by means of voxelwise one-sample t-tests to characterize the intrinsic connectivity profiles of PHC and PRC with the EC (see Figure 12). Additionally, paired t-tests were performed to determine significant differences in PRC vs. PHC connectivity (Figure 13A). Resulting *t*-maps were masked with the EC ROI and significant clusters determined by cluster-extent based thresholding ($Z > 2.3$; $p_{cluster} < .05$). In addition, the differential topographic pattern of PRC versus PHC connectivity along the x-y-z direction were visualized by 3-d plotting of connectivity preference for each voxel (see Figure 13B).

In a next step, it was directly tested for significant differences between anterior/posterior and lateral/medial EC. Therefore, the template EC ROI was divided into four equal-sized sections along the longitudinal and horizontal plane (automatically, not manually in *Matlab*) corresponding to coronal and sagittal cuts, respectively. The lateral vs. medial division was performed for each coronal slice individually in order to ensure equally-sized portions along the longitudinal axis. Mean parameter estimates were extracted from each of the four subsections for each subject (from the group-registered beta maps). The resulting PRC and PHC

connectivity estimates were submitted to a 2 x 2 x 2 repeated-measures ANOVA with seed ROI (PHC vs. PRC), longitudinal EC section (anterior vs. posterior) and horizontal EC section (lateral vs. medial) as factors. Furthermore, connectivity gradients were assessed across the longitudinal and horizontal axis by plotting slice-by-slice mean parameter estimates. As the number of transverse EC slices differed along the longitudinal axis (between 5 -11 slices), each coronal EC slice was divided into 5 equal bins and mean betas were calculated for each bin. The same approach was used to test for differential connectivity of al-EC/pm-EC and PRC/PHC seeds with the subiculum along the longitudinal or transverse axis.

4.2.6.2 Multivariate pattern classification of connectivity preference

Finally, a multivariate classifier (linear CSVMC) was used to further investigate whether the spatial patterns of voxels showing preferential connectivity with either PRC or PHC are different in the entorhinal cortex (analyses performed by D. Berron). Therefore, a linear support vector machine classifier was trained and tested on the x-y-z coordinates of all EC voxels across all subjects. The data were analysed for multivariate effects using *PyMVPA* 2.2.0 (Hanke et al., 2009). Independent data chunks were defined according to the individual subjects of each study. Each chunk consisted of the same amount of samples (EC voxels). For the purpose of evaluation of classification validity a leave-one-subject-out cross-validation was performed. In each of the validation steps a linear support vector machine (SVM, LinearCSVMC; Chang and Lin, 2011) was trained on the data of all but one subject and tested on the remaining one. Accuracy of the validation step was calculated as the proportion of the samples (voxels) that were classified correctly (either as being preferentially connected to PRC or PHC). Overall classification accuracy was defined as the mean accuracy of all validation steps (meaning mean accuracy across subjects).

Mean classifier accuracy was tested for significance using non-parametric permutation testing. Therefore, the samples (EC voxels) of the training set were relabelled 1000 times and tested on the testing set using the same leave-one-subject-out cross-validation scheme as before. This was done to generate the non-parametric null distribution. By comparing the mean accuracy of all validation steps with the generated null distribution the rank and thus the p-value could be identified (1000 permutations allow for $p < .001$) (Nichols and Holmes, 2002). This was done

separately for the data coming from each study as well as for the left and right hemisphere.

4.3 Results

4.3.1 Entorhinal connectivity topography related to PRC and PHC seeds

4.3.1.1 Seed-to-voxel connectivity of PRC vs. PHC with EC

Very high-resolution fMRI at 7T was used to characterize and compare intrinsic functional connectivity profiles of PHC and PRC seed regions with the EC. Particularly, correlations of activity over time (spontaneous changes in the BOLD signal) were investigated between individually defined PRC and PHC seed regions and the EC across subjects. Seed-to-voxel correlation analyses were performed on the native (unnormalized) residual fMRI data after extraction of task-related activity (see 4.2.3 for details). Resulting connectivity maps were normalized on a group-specific T1-template by means of ROI-ANTS (see 2.3). Group results maps were masked with a manually-defined EC ROI.

Group-level functional connectivity profiles of each seed region for data set 1 and 2 are shown in Figure 12 and Figure S 3, respectively (voxelwise one-sample t-tests, $Z > 2.3$, $p_{cluster} < .05$). While the PRC showed significant connectivity with bilateral EC clusters covering approximately the anterior two-thirds of the EC, significant functional connectivity of the PHC was found with bilateral EC clusters comprising about the posterior two thirds of the EC (see also peak coordinates of significant clusters in Table S 3). Additionally, PRC-connectivity clusters were rather located laterally, while PHC-connectivity clusters primarily covered the medial EC. Overlapping connectivity with both seeds was strongest in the transition zone between anterior-posterior and lateral-medial EC (see bright regions in Figure 12 and Figure S 3).

Paired t-tests revealed those EC regions that exhibited significant stronger connectivity with PRC than PHC seeds, and vice versa (see Table S 3). While stronger functional connectivity of the PRC was found with bilateral clusters in the anterior-lateral EC (al-EC), the PHC showed relatively stronger connectivity with bilateral clusters located in the posterior-medial EC (pm-EC). Paired t-test results are illustrated for data set 1 on Figure 13.

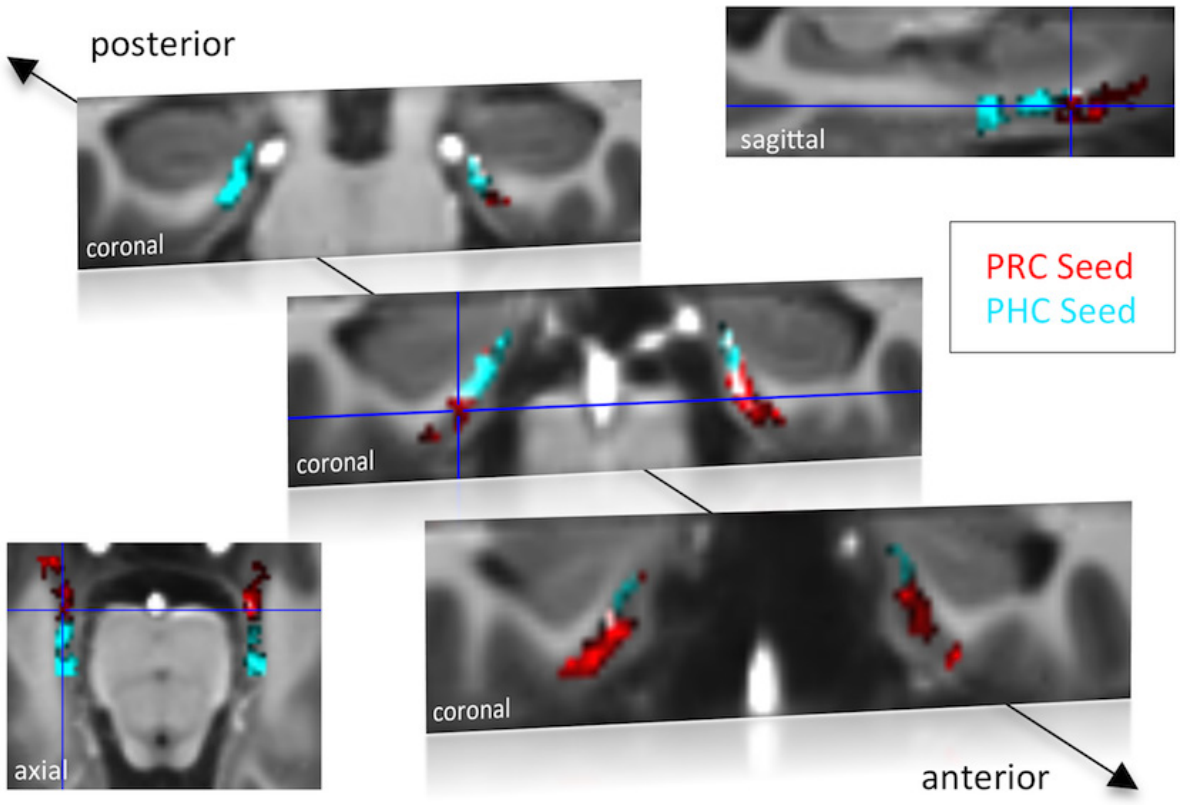

Figure 12. Functional connectivity profiles of PHC and PRC seeds with the EC.
Group results for seed-to-voxel connectivity of bilateral PRC and PHC seeds with the EC shown for data set 1 (one-sample t-test; $Z > 2.3$, $p_{cluster} < .05$, $N_1 = 15$). Bright regions denote overlapping connectivity with PRC/PHC. Single-subject beta maps were normalized on the group-specific T1-template by ROI-based alignment with ANTS and masked with a manually defined EC ROI. The T1-template has the same resolution as the high-resolution functional EPI volumes (0.8 mm x 0.8 mm x 0.8 mm). See also Supplementary Figure S 3 for results of data set 2. ROI: region of interest. This figure is taken from Maass et al., 2015.

4.3.1.2 Three-dimensional topography of entorhinal connectivity

In order to assess and visualize the 3-dimensional topography of differential EC connectivity with PRC versus PHC seeds, the connectivity preference of each voxel was plotted along the x-y-z direction (see Figure 13B and Supplementary Figure S 4A). Connectivity preference was defined on the basis of the paired t-test t-maps (red: $T_{PRC>PHC} > 0$; blue: $T_{PHC>PRC} > 0$). These plots indicated a complex 3-dimensional topography of EC connectivity with a gradient of PRC-to-PHC preference running from anterior-ventral-lateral to posterior-dorsal-medial EC. In addition, the functional connectivity preference of unilateral (left and right) PRC/PHC seeds with both the ipsi- and contralateral EC was plotted to evaluate whether connectivity patterns were symmetric across hemispheres (see Supplementary Figure S 4B for results of data set 1). These additional analyses confirmed the findings of bilateral connectivity analyses with an anterior-posterior

and lateral-medial gradient of EC connectivity for contralateral PRC and PHC seeds. These findings also suggest that the dissociation of EC connectivity cannot be simply explained by local autocorrelations of neighboured voxels.

The next analyses assessed the reliability of topographic differences in EC connectivity with PHC and PRC. If the topographic organization is reliable across participants, then it should be possible to predict the connectivity preference of specific EC voxels within any participant, simply by knowing the connectivity preferences of corresponding voxels in other participants. To test this strong prediction, a multivariate pattern classification analysis was conducted with leave-one-subject-out cross-validation. Specifically, a multivariate support vector machine classifier was trained (see 4.2.6.2) on the data from all but one subject, entering only the x-, y-, and z-coordinates of each voxel and the relative preference of PRC and PHC connectivity (based on the subject's paired t-test t-maps, analogous to the definition of preference in the previous section). The classifier was then tested on the remaining subject, and the accuracy of this validation step was calculated as the proportion of EC voxels that were classified correctly as being preferentially connected to PRC or PHC in the tested subject. The training and cross-validation steps were repeated for all combinations of participants, and a mean classification accuracy score was computed. Classification accuracy was significantly above chance across both data sets ($p < .001$). Mean classifier accuracies across all EC voxels and subjects were around 60% (data set 1: left 62%, right 60%, data set. 2: left 67%, right 57%). However, connectivity preference of voxels in the very anterior-lateral and posterior-medial EC could be predicted with more than 80% accuracy.

These analyses confirm a spatial dissociation in connectivity between EC subregions with regard to PRC vs. PHC seeds. Predicted clusters of preferential connectivity are color-coded in Figure 13C (bright regions denote high consistency of the classifier).

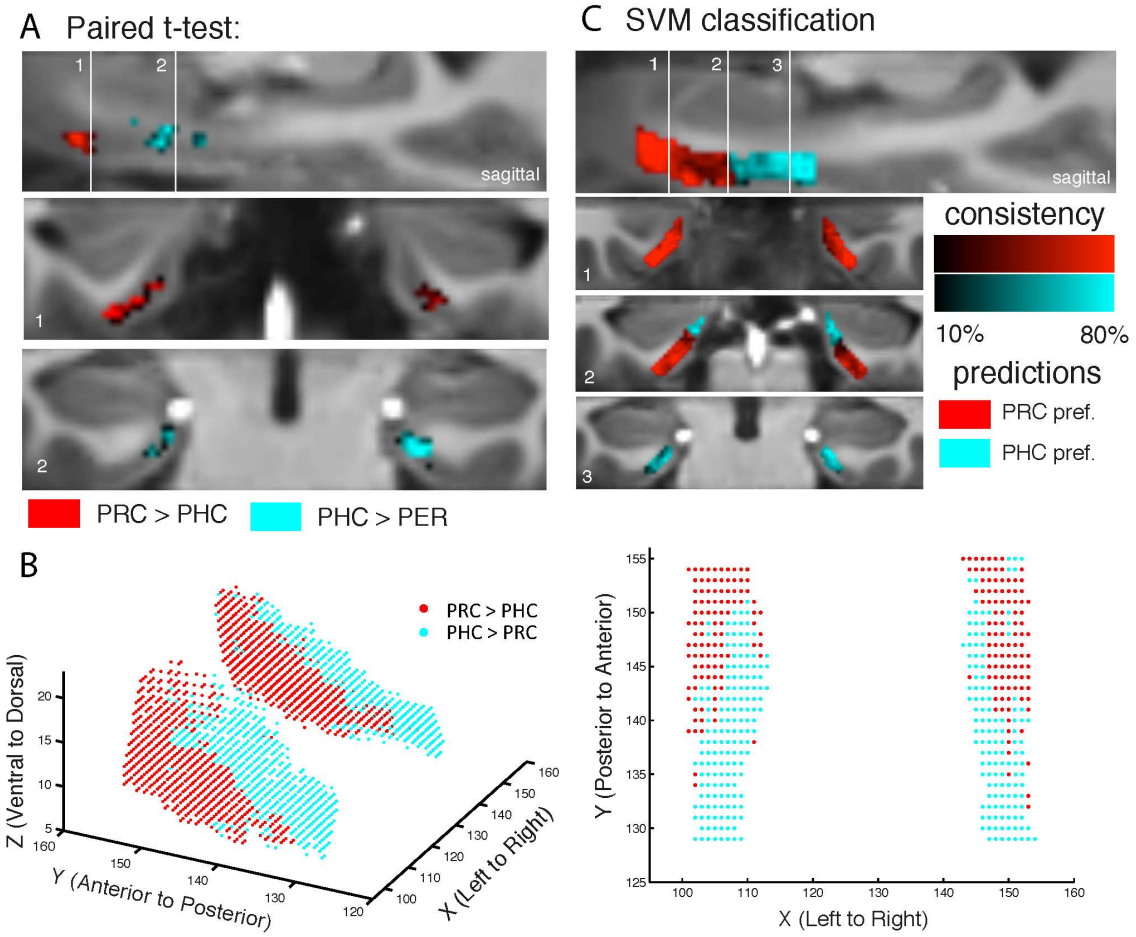

Figure 13. Differential connectivity topography of PRC vs. PHC seeds with the EC.

A. To assess differential connectivity of PRC vs. PHC with the EC, voxelwise paired-sample t-tests were performed on the normalized single-subject beta maps (resulting from seed-to-voxel connectivity analyses). Significant clusters for data set 1 are shown for two coronal sample slices (Z > 2.3. $p_{cluster}$ < .05, N_1 = 15) at the level of the anterior (1) and posterior (2) hippocampal head. **B.** To visualize the 3-dimensional geometry of connectivity, the connectivity preference with PRC vs. PHC of each EC voxel was plotted along the x-, y-, and z-axis (red: $T_{PRC >PHC}$ > 0, blue: $T_{PHC >PRC}$ > 0). **C.** Classification of PRC vs. PHC connectivity preference was tested across subjects based on the x-y-z coordinate of an EC voxel. Multivariate classification (support vector machine; leave-one-subject-out cross-validation) was significant across both data sets (p < .001; accuracies: data set 1: left: 62%, right: 60%, data set 2: left: 67%, right: 57%), which confirms a spatial dissociation of entorhinal connectivity with PRC vs. PHC. Predicted clusters are color-coded in red vs. blue, bright regions denote high consistency of the classifier. Results are shown for Exp. 1. See also Suppl. Figure S 4 for 3D plots of data set 2 and for unilateral seeds of data set 1. This figure is taken from Maass et al., 2015.

4.3.1.3 Repeated-measures ANOVAs and slice-by-slice plots

Anatomical studies in rodents have demonstrated a major lateral-medial dissociation of EC connectivity with PRC vs. PHC, while data in non-human primates suggest a dominant anterior-posterior dissociation. In order to directly test for significant differences of PRC vs. PHC intrinsic functional connectivity between the anterior vs. posterior and lateral vs. medial EC, the template EC ROI was divided equally into four portions: anterior-lateral, anterior-medial, posterior-lateral

and posterior-medial (see Figure 14A, right panel). Mean parameter estimates for PRC and PHC connectivity (mean betas) were extracted across all voxels in each section for each subject. Note that the lateral-medial split was performed for each coronal slice individually as the EC is curved along the longitudinal axis and furthermore, that this separation also corresponds to a ventral-dorsal split.

Repeated-measures ANOVAs with PRC and PHC connectivity estimates revealed significant two-way interactions of seed region x anterior-posterior EC section (data set 1: $F(1,14) = 56.0$, $p < .001$; data set 2: $F(1,13) = 95.9$, $p < .001$) and seed region x lateral-medial EC section (data set 1: $F(1,14) = 11.3$, $p = .005$; data set 2: $F(1,13) = 32.8$, $p < .001$).

Follow-up paired sample t-tests confirmed significantly greater PRC than PHC connectivity with the anterior EC (data set 1: $t(14) = 5.3$; $p < .001$; data set 2: $t(13) = 4.5$, $p = .001$) and vice versa significant higher PHC than PRC connectivity with the posterior EC (data set 1: $t(14) = 4.7$; $p < .001$; data set 2: $t(13) = 2.6$; $p = .019$). With regard to the lateral-medial dissociation, the PRC showed significant higher intrinsic functional connectivity than the PHC with the lateral EC (data set 1: $t(14) = 5.2$; $p < .001$; data set 2: $t(13) = 3.8$, $p = .002$). However, there was no significant difference in connectivity between seeds with the medial EC (all p-values > .80). Although connectivity estimates did not differ in the medial EC, the PHC showed significantly stronger connectivity with medial than lateral EC (data set 1: $t(14) = 4.4$; $p < .001$; data set 2 $t(13)= 2.6$, $p = .021$). There were no significant three-way interactions between seed, longitudinal and sagittal EC section (all p-values > .25).

To characterize the topography of PRC and PHC functional connectivity with voxels along the longitudinal (anterior to posterior) and horizontal (lateral to medial) axis of the EC, mean parameter estimates were plotted for each slice (see Figure 14B). These slice-by-slice plots further confirmed a topographical organization of EC connectivity along the longitudinal axis with decreasing PRC connectivity and increasing PHC connectivity from anterior to posterior to EC. Furthermore, lateral to medial connectivity plots demonstrated decreasing PRC and increasing PHC connectivity.

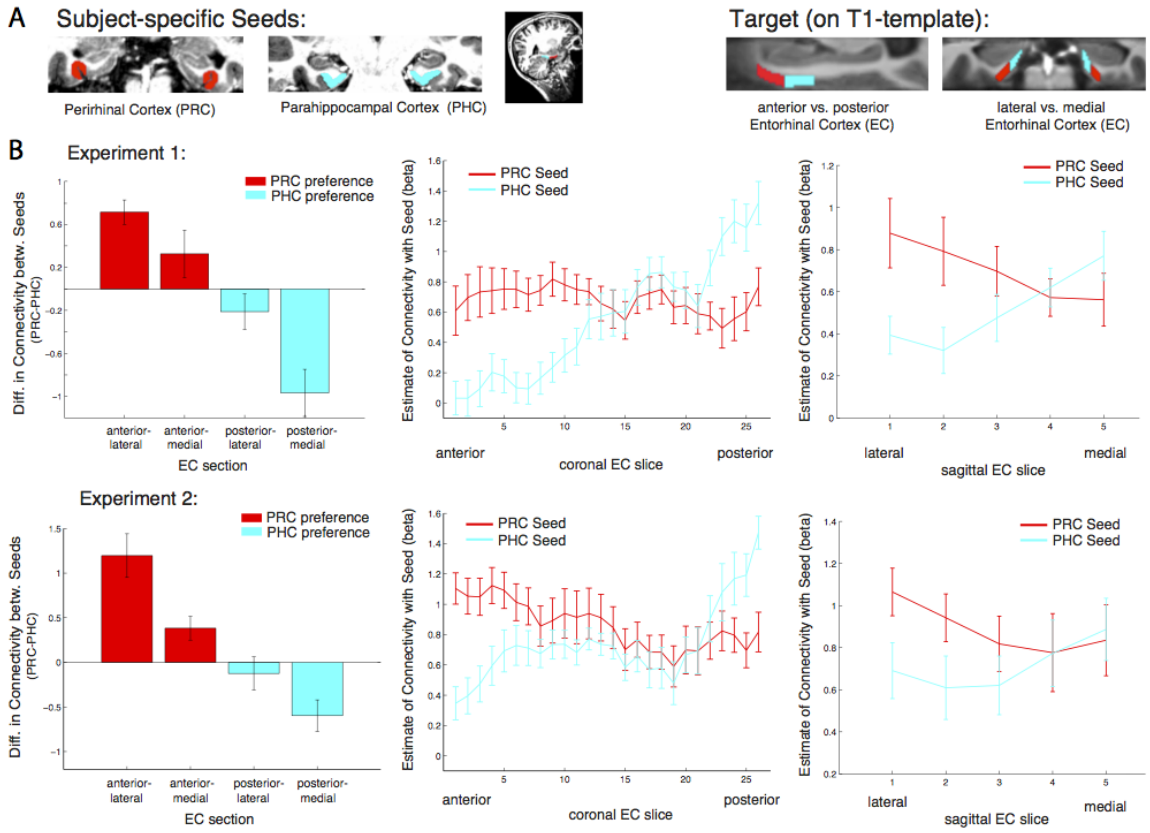

Figure 14. Anterior-posterior and lateral-medial gradients of entorhinal connectivity with PRC vs. PHC seeds.

A. To test for an anterior-posterior or lateral-medial dissociation of EC connectivity with PRC vs. PHC seeds (upper panel, left), the EC template mask was divided into four equal portions (upper panel, right) and mean parameter estimates (betas) were extracted from each subsection. **B**. Repeated-measures ANOVAs revealed significant seed (PRC vs. PHC) x anterior-posterior EC section and seed x lateral-medial EC section interactions ($p < .001$ for both data sets; $N_1 = 15$, $N_2 = 14$). Slice-by-slice plots of connectivity estimates along the longitudinal and transverse EC axis confirmed an anterior-to-posterior and lateral-to-medial dissociation with decreasing PRC-connectivity and increasing PHC-connectivity. As the number of sagittal EC slices differed from anterior to posterior, each coronal EC slice was divided into 5 equal portions (with 1 being most lateral and 5 most medial EC) and mean betas for each portion were calculated. This figure is taken from Maass et al., 2015.

4.3.2 Subicular connectivity related to al-EC/pm-EC and PRC/PHC

4.3.2.1 Repeated-measures ANOVAs and slice-by-slice plots for EC seeds

Anatomical data from rodents has demonstrated that LEC and MEC exhibit different patterns of connectivity along the proximo-distal (transverse) axis of the subiculum and CA1 (Witter et al., 2000a). A similar transverse gradient of EC projections to CA1/subiculum has been reported for anterior vs. posterior EC regions in non-human primates (Witter and Amaral, 1991). Accordingly, the next analyses examined the topographic organization of functional connectivity the EC and hippocampus. These analyses focused on connectivity with the subiculum, based on previous findings demonstrating that the topographic organization of

cortico-hippocampal functional connectivity is most prominent in the subiculum (Libby et al., 2012).

Consistent with the previous analyses for EC, the subiculum was divided (as done for the EC) into four equal portions along the longitudinal (anterior vs. posterior) and transverse (lateral vs. medial ~ proximal vs. distal) axis. Mean parameter estimates of functional connectivity with anterior-lateral and posterior-medial EC were then extracted for each subicular section and each subject. It was tested for significant interactions between seed (al-EC vs. pm-EC) connectivity with anterior vs. posterior or proximal vs. distal subiculum. Similar to the division of the EC, the proximal-distal cut was performed individually for each coronal subiculum slice.

Repeated-measures ANOVAs with EC seed connectivity estimates revealed a significant two-way interaction of seed EC subregion x proximal vs. distal subiculum (data set 1: $F(1,14) = 25.7$, $p < .001$; data set 2: $F(1,13) = 24.3$, $p < .001$). However, there was no interaction between EC seed region and longitudinal subiculum sections ($p > .26$). Follow-up t-tests confirmed that the proximal subiculum showed significantly greater connectivity with al-EC than with pm-EC (data set 1: $t(14) = 2.27$; $p = .040$; data set 2: $t(13) = 2.15$; $p = .049$) and, conversely, that distal subiculum showed significantly greater connectivity with pm-EC than with al-EC (data set 1: $t(14) = 3.06$; $p = .008$; data set 2: $t(13) = 4.24$, $p = .001$). Slice-by-slice plots confirmed that connectivity of the al-EC decreased from proximal (lateral) to distal (medial) subiculum, whereas pm-EC connectivity increased (see Figure 15A and Supplementary Figure S 5A for data of data set 1 and 2, respectively).

4.3.2.2 Repeated-measures ANOVAs and slice-by-slice plots for PRC/PHC seeds

Previous human resting-state fMRI studies at 3 Tesla (Kahn et al., 2008; Libby et al., 2012) have reported reliable differences in connectivity between the PRC and PHC with the hippocampus along the longitudinal hippocampal axis, most prominently with the subiculum (Libby et al., 2012). However, a dissociation of PRC vs. PHC connectivity along the proximo-distal axis of the subiculum, as demonstrated in rodents (Agster and Burwell, 2013; Naber et al., 1999, 2001), has not been reported so far in humans.

In order to examine whether PRC vs. PHC seeds show differential intrinsic functional connectivity with the subiculum along the transverse and/or longitudinal

axis, it was also tested for significant interactions between PRC vs. PHC connectivity with anterior vs. posterior or proximal vs. distal subiculum. Repeated-measures ANOVAs with PRC and PHC connectivity estimates revealed a significant two-way interaction of seed region x proximal vs. distal subiculum (data set 1: $F(1,14) = 20.2$, $p = .001$; data set 2: $F(1,13) = 14.4$, $p = .002$). However, the interaction between seed and anterior vs. posterior subiculum was not significant (data set 1: $F(1,14) = 2.5$, $p = .135$; data set 2: $F(1,13) = 1.4$, $p = .257$).

Follow-up t-tests confirmed significantly greater PRC than PHC connectivity with the proximal subiculum (data set 1: $t(14) = 3.7$; $p = .002$; data set 2: $t(13) = 3.9$, $p = .002$). With regard to distal subiculum there was significant higher PHC than PRC connectivity in data set 1 ($t(14) = 3.1$, $p = .009$) and a trend towards a difference in data set 2 ($t(13) = 2.0$; $p = .063$).

Slice-by-slice plots further confirmed a dissociation of PRC/PHC connectivity along the transverse hippocampal axis with decreasing PRC connectivity and increasing PHC connectivity from proximal to distal subiculum (see Figure 15B and Supplementary Figure S 5B for data set 1 and 2, respectively). Although the interaction between PRC vs. PHC seed and anterior-posterior subiculum was not significant, slice-by-slice extractions suggested that differential connectivity may be present in the most anterior and most posterior slices of subiculum. Additional analyses indeed revealed that PRC connectivity was significantly greater than PHC connectivity within the most anterior 8 slices of subiculum (data set 1: $t(14) = 2.5$; $p = .022$; data set 2: $t(13) = 3.9$, $p = .002$), while PHC connectivity was significantly higher than PRC connectivity within the most posterior 8 slices in data set 1 ($t(14) = 2.3$; $p = .035$), but not in data set 2 ($t(13) < 1$, $p > .40$).

However, it should be noted that the subiculum within the hippocampal tail (where anatomical borders are difficult to delineate) was not segmented and thus differences in the posterior subiculum might have been underestimated.

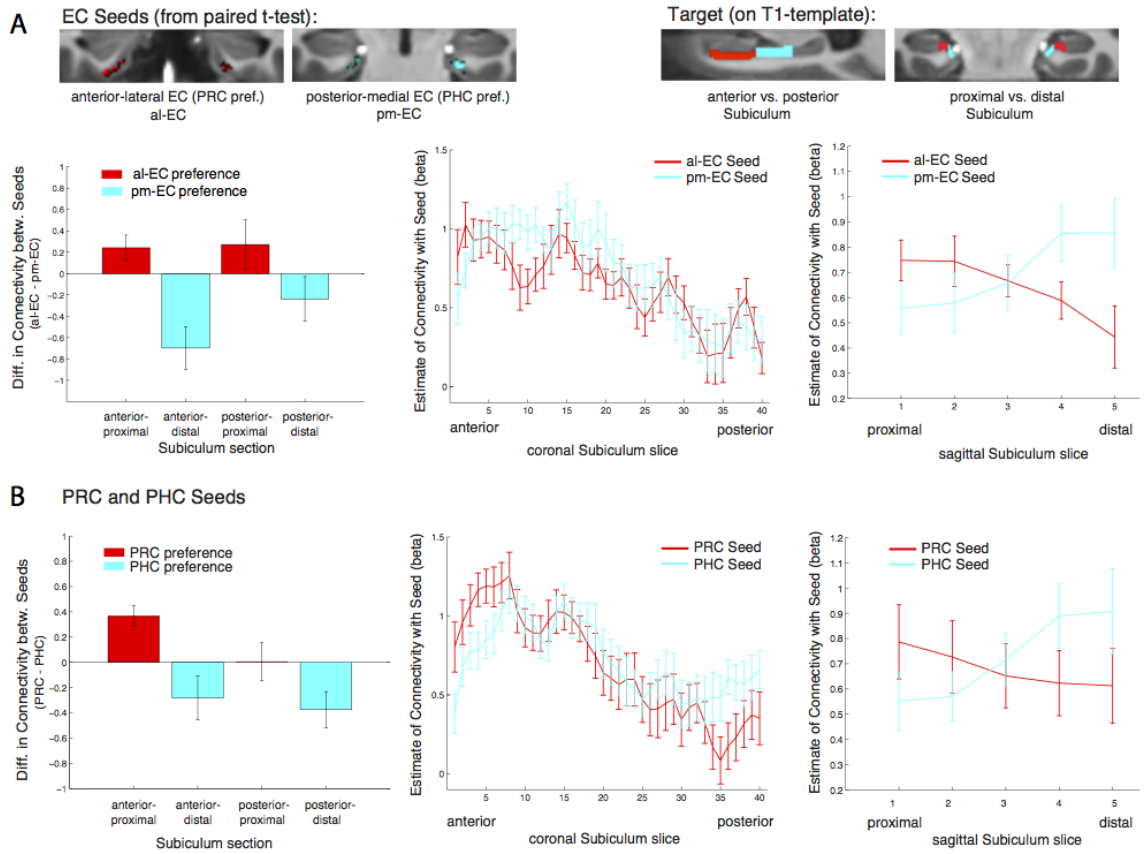

Figure 15. Functional connectivity gradients in the subiculum related to EC subregions and PRC/PHC seeds.

A. To test for differential connectivity of EC functional subdivisions with the subiculum, anterior-lateral EC (al-EC) and posterior-medial EC (pm-EC) regions that exhibited preferential connectivity with PRC vs. PHC, respectively (see paired t-tests in Fig. Figure 13A) were used as seed regions. The subiculum ROI was equally divided into four portions along the longitudinal (anterior vs. posterior) and transverse (proximal vs. distal) axis and mean betas of functional connectivity with EC seeds were extracted for each subsection. Repeated-measures ANOVAs revealed a significant seed (al-EC vs. pm-EC) x proximal-distal subiculum interaction in both datasets ($p < .001$; $N_1 = 15$, $N_2 = 14$; results shown for data set 1). Slice-by-slice plots of connectivity estimates demonstrated decreasing al-EC-connectivity and increasing pm-EC connectivity from proximal to distal subiculum but no anterior-posterior dissociation**. B.** Similarly, connectivity for PRC vs. PHC seeds with the subiculum along the longitudinal and transverse axis was evaluated. Seed (PRC vs. PHC) x proximal-distal subiculum section interactions were significant across both datasets ($p < .01$) with preferential connectivity of PRC with proximal and PHC with distal subiculum, respectively. Slice-by-slice plots of connectivity estimates along the hippocampal long axis revealed stronger PRC connectivity with the most anterior and stronger PHC connectivity with the most posterior subiculum (= 8 slices), respectively (data set 1). See also Suppl. Figure S 5 for data set 2. This figure is taken from Maass et al., 2015.

4.3.2.3 Differential subicular connectivity between EC subregions and PRC/PHC

The above analyses revealed a similar dissociation of connectivity along the proximo-distal axis of the subiculum for al-EC vs. pm-EC and PRC vs. PHC seeds. However, a dissociation along the longitudinal axis of the subiculum was only present for PRC vs. PHC seeds (evident in the very anterior and posterior subiculum) and not for al-EC vs. pm-EC. To test for differences between the

connectivity profiles of entorhinal functional subregions and PRC/PHC along the long axis of the subiculum, differences between al-EC/pm-EC and PRC/PHC connectivity estimates were calculated for anterior and posterior subiculum subsections. Repeated-measures ANOVAs revealed a significant interaction between seed regions (∆al-EC/pm-EC vs. ∆PRC/PHC) x longitudinal subiculum section (anterior vs. posterior) for data set 1 ($F(1,14) = 7.3$, $p = .017$) and a trend towards an interaction in data set 2 ($F(1,13) = 3.4$, $p = .087$). These additional analyses show that functional connectivity profiles of PRC vs. PHC and al-EC vs. pm-EC with the subiculum differ along the longitudinal hippocampal axis.

4.3.2.4 Landmarks for delineation of al-EC and pm-EC

A multivariate classification approach was used to predict al-EC and pm-EC subregions across all subjects. Based on the relative connectivity preference of an EC voxel across subjects the classifier predicts PRC or PHC connectivity preference for the left out subject. Thereby one can compute consistency maps that show the consistency of predictions for each EC voxel across all subjects. This revealed regions of high and low consistency. Based on the predictions of the classifier, a PRC-connectivity preference ("al-EC") and a PHC-connectivity preference EC ("pm-EC") mask were created. To provide these masks in a more usable manner (not on a partial volume T1-template), a whole-brain high-resolution T1-template was created based on the MPRAGEs of all participants (N = 29; voxel size: 0.6 mm^3 isotropic, AC-PC aligned). The EC masks were then aligned on the whole-brain template (linear registration) and manually corrected outer borders, if these did not fit perfectly.

Below, the approximate boundaries of al- and pm-EC subregions are further described based on coronal slices, moving from anterior to posterior on the whole brain template. These landmarks can be used for manual delineation of EC functional subregions. Notably, coronal slices on the whole-brain template are not orthogonally aligned to the hippocampal long-axis and have a different slice thickness compared to the partial-volume template on which results/figures are described. Furthermore, borders between al-EC and pm-EC differed slightly between hemispheres and thus landmarks are an intermediate approximation between sides.

At the most anterior level of the EC (when the Amygdala is visible) EC is fully covered by al-EC. Moving posteriorly, the hippocampal head (HH) starts. Around 3-4 slices (~ 2 mm) after the first appearance of the HH, pm-EC appears at the very medial/dorsal tip of the EC, touching the Amygdala. The border between pm-EC and al-EC approximately corresponds to the uncal notch, such that pm-EC covers the gyrus ambiens. Moving more posteriorly the border between pm-EC and al-EC moves progressively down (more lateral/ventral) until al-EC and pm-EC are around equal size at the level of two thirds of HH. At this level the Amygdala has fully disappeared. Going further posteriorly the border between pm-EC and al-EC moves progressively more lateral/ventral, such that pm-EC also covers parts of the ventral/lateral EC half. At the level where the uncus separates from the HC (and only the fimbria is attached to both), EC is almost fully covered by pm-EC. The EC was delineated until the collateral sulcus (or rhinal fissure) disappeared, which was one slice (0.6 mm) after disappearance of the uncus. Approximately the 4 most posterior EC slices (~ 2.4 mm) were fully covered by pm-EC.

Al-EC and pm-EC masks as well as the whole brain T1-template are available online (see Maass et al, 2015) as supplementary material in original (resolution: 0.6 mm^3 isotropic) and MNI space (resolution: 2 mm^3 isotropic).

4.4 Discussion

Functional connectivity analyses revealed the first detailed topographic parcellation of the human EC. In two independent samples, an anterior-lateral and a posterior-medial EC (al-EC and pm-EC, respectively) section exhibited distinct patterns of intrinsic functional connectivity with regions in the neocortex (PRC and PHC) and hippocampal formation (subiculum). Specifically, the al-EC region could be delineated on the basis of preferential connectivity with PRC, whereas the borders of pm-EC were derived from connectivity with PHC. Al-EC and pm-EC, in turn, were found to have preferential connectivity with proximal and distal subiculum, respectively. Moreover, subicular connectivity with al-EC and pm-EC was partially distinct from its connectivity with PRC and PHC. These results are in remarkable accordance with principles known from anatomical studies of rodents (for reviews see (van Strien et al., 2009; Witter et al., 2000a) and studies of non-human primates (see, e.g. Suzuki and Amaral, 1994; Witter and Amaral, 1991).

Previous fMRI studies at 3 Tesla have used analyses of functional connectivity to characterize topographic patterns of connectivity between the PRC, PHC, and hippocampal subfields (Lacy and Stark, 2012; Libby et al., 2012). These studies have generally found that PRC and PHC exhibit different patterns of connectivity along the longitudinal axis of the hippocampus. Unfortunately, these studies could not address the topographic organization of connectivity within the EC due to limitations in resolution and SNR. The present results demonstrate that the enhanced resolution of ultra-high field fMRI can overcome these limitations. Three-dimensional plots of entorhinal connectivity preferences revealed a gradient of decreasing PRC and increasing PHC connectivity running from anterior-lateral to posterior-medial EC. It is notable that, by training a pattern classifier on the coordinates of EC voxels that showed preferential connectivity with PRC or PHC within a subset of participants, these voxels could be reliably predicted in the remaining participant. This finding indicates that the topography of neocortical connectivity within the EC is highly conserved across participants, which, in turn, could indicate fundamental functional differences between the two EC subdivisions.

Although the EC is a major gateway for the hippocampus, PRC and PHC are also directly reciprocally connected with the hippocampus, most notably with CA1 and subiculum (Agster and Burwell, 2013; Naber et al., 1999, 2001; see 1.2.3 for details). As in rodents, common direct and indirect connectivity profiles were found along the transverse axis of the subiculum (Naber et al., 1999, 2001; O'Reilly et al., 2013; Witter, 2006; see also 6.2.5 for detailed discussion). Both al-EC and PRC showed stronger connectivity with proximal subiculum, whereas pm-EC as well as PHC showed stronger connectivity with distal subiculum. In contrast to the transverse axis, direct and indirect connectivity profiles dissociated along the longitudinal hippocampal axis. For al-EC and pm-EC, there was no evidence or trend for an anterior-posterior dissociation, compatible with the rodent anatomy (Naber et al., 1999, 2001; O'Reilly et al., 2013; Witter, 2006). On the other hand, the most anterior subiculum showed stronger direct connectivity with PRC than PHC, whereas in one data set the most posterior subiculum (in the hippocampal body) showed stronger connectivity with PHC than PRC. This finding replicated the direct connectivity profiles observed in rodents (Agster and Burwell, 2013; Naber et al., 1999, 2001). Such an anterior-posterior dissociation of hippocampal

connectivity also confirms the aforementioned findings from human resting-state fMRI studies that investigated functional connectivity profiles of PRC and PHC (rather than EC) with hippocampal subfields (Libby et al., 2012).

The results of the present study have provided a detailed description of the organization of functional connectivity within the human EC. Future studies could apply the high-resolution functional connectivity analyses to differentiate the roles of al-EC and pm-EC in memory and alterations of EC connectivity in AD and other neurodegenerative diseases (see 6.2.6 and 6.5. for a detailed discussion).

5 Experiment 3 (Vascular hippocampal plasticity after aerobic exercise in older adults)

5.1 Introduction

The hippocampus has been in the focus of research into the effects of aerobic exercise on memory because of its potential for plasticity and its role in age-related long-term memory decline (Grady, 2012; Small et al., 2011; Voss et al., 2013a; see also 1.3.2). Converging evidence from research in rodents and young/middle-aged humans indicates that a hallmark of exercise-related plasticity in the hippocampus is to increase hippocampal perfusion, specifically in DG (Pereira et al., 2007). In humans, this increase has been associated with better recall of a recently learned word list after the intervention (Pereira et al., 2007). However, whether aerobic exercise can improve hippocampal perfusion also in older humans has not been studied so far. An exercise study in old individuals has demonstrated already that exercise over a period of one year can prevent the human hippocampus from atrophy (Erickson et al., 2011). This raises the question whether the positive effects of exercise on hippocampal volume are related to vascular plasticity, that is, increased perfusion. There is also ongoing uncertainty to what extent the memory effects of exercise in old age depend on modality (verbal versus visuospatial), retrieval demands (recall versus recognition) and delay (early versus late).

Studies in mice have shown that aerobic exercise induces neurogenesis in the DG subfield of the hippocampus, which is correlated with increased perfusion in DG (Pereira et al., 2007) and is associated with improved pattern separation (Creer et al., 2010; see 1.3.4 for more details). Furthermore, hippocampal neurogenesis seems to be specifically linked to the PRC-LEC network (Vivar and Van Praag, 2013; Vivar et al., 2012). These regions convey novel object information to the hippocampus and are required for complex object discrimination and object recognition memory, which decline with age (e.g. Burke et al., 2011; Ryan et al., 2012; see also 1.3.2). If effects of aerobic exercise are specific to a PRC-LEC network linked to the hippocampus, one might expect a differential improvement in complex object-recognition tests that pose high demands on pattern separation. A comparable finding has been recently observed in young human adults, where aerobic exercise improved performance in a memory test that poses high demands

on object pattern separation (Dery et al., 2013). However, an effect of exercise on object recognition memory in older adults has not yet been demonstrated.

In this study, healthy older humans (60 to 77 years) were pseudo-randomly assigned to either an aerobic exercise group (indoor treadmill, N_T = 21) or to a control group (indoor progressive-muscle relaxation/stretching, N_C = 19). A summary of the main physiological and psychological parameters, collected in the study, is given in Table 2. Fitness levels were determined before and after each type of intervention using spiroergometry. Gadolinium contrast-based perfusion imaging (3 Tesla) was used to measure changes in regional cerebral blood flow and volume (rCBF/ rCBV). Changes in hippocampal volumes were assessed by high-resolution structural MRI at 7 Tesla. Based on previous studies suggesting a relationship of exercise-related brain changes to verbal memory in young/middle-aged adults (Pereira et al., 2007) and to spatial memory in older adults (Erickson et al., 2011), verbal (*Verbal Learning and Memory Test*, VLMT) and visuospatial (configural) object memory (*Complex Figure Test*, CF) were used as primary outcome measures of long-term memory effects. The CF Test allows assessments of free recall (both early and late) as well as recognition, the latter test posing high demands on pattern separation and hippocampal integrity. Similarly, early recall, late recall and recognition memory were also measured in the VLMT. Path analysis (structural equation modeling, SEM) was used to determine whether memory gains as a function of increased fitness were accounted for by mediation through hippocampal volume changes or were also compatible with a direct effect of perfusion on memory. To study the effects of exercise-related changes in neurotrophic and angiogenic growth factors on hippocampal plasticity and memory function, serum levels of BDNF, VEGF, IGF and PDGF were also assessed. Finally, serum cortisol levels were obtained, because cortisol is known to have a negative effect on verbal long-term memory in old age (Comijs et al., 2010) and therefore might modify potential exercise effects on verbal memory.

Table 2. Summary of main parameters assessed in the training study

Target	Method	Parameter (pre and post training)	
Fitness Level	Spiroergometry	Consumption of oxygen at Ventilatory Anaerobic threshold (**VO_2VAT**)	
Perfusion	3T Gadolinium contrast-based perfusion imaging (N=33)	**rCBF**, **rCBV** in bilateral hippocampus & gray matter [ml/100g/min]	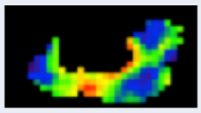
Hippocampal Structure	7T MRI (N=32) Manual segmentation on T1-weighted images	**Hippocampal Volume** [cm^3] (head, body, tail, subfields)	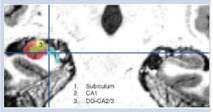
Episodic Memory	Complex Figure Test (CF) Verbal learning and Memory Test (VLMT)	**Early & Late Recall** **Recognition Memory** (CF: high demands on pattern separation)	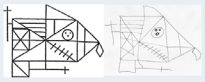 Rey Figure
Growth factors	Blood sample (ELISA)	Concentration in serum [pg/ml] **VEGF** (Vascular endothelial growth factor) **PDGF** (Platelet-derived growth factor) **BDNF** (Brain-derived neurotrophic factor)	

In a controlled 3-month intervention study with 40 healthy older adults, a variety of physiological and psychological parameters was measured before and after the intervention. Fitness levels were assed via spiroergometry (oxygen consumption at ventilatory anaerobic threshold, $VO_{2\ VAT}$). Gadolinium contrast-based perfusion imaging (3 Tesla) was used to measure changes in regional cerebral blood flow and volume (rCBF/ rCBV) in the hippocampus and grey matter. Changes in hippocampal volumes (including subregions) were assessed by high-resolution structural MRI at 7 Tesla. Hippocampus-dependent memory was tested by means of a visuospatial (configural) object and a verbal memory task. Blood samples were taken to assess changes in angiogenic and neurogenic growth factors.

5.2 Methods

5.2.1 Experimental Design

The third experiment was designed as a controlled 3-month intervention trial with 40 sedentary healthy older participants (mean age = 68.4 ± 4.3 yrs, 55% female) at the German Center for Neurodegenerative Diseases (DZNE) in Magdeburg. The project was conceived by E. Düzel and N. Müller in cooperation with the Karolinska Institute, Stockholm (M. Lövden, L. Bäckman) and the Max Planck Institute for Human Development, Berlin (U. Lindenberger). For people involved in data collection and analysis, see also subchapters below.

Table 3. Characteristics of the training and control group.

Variables	aerobic exercise group	relax/stretching group
N	21	19
Age [yrs]	68.8 (4.5)	67.9 (4.1)
Gender [% female]	52%	58%
BMI	25.0 (2.9)	25.2 (3.0)
Verbal learning (delayed recall)	9.6 (3.1)	9.7 (2.7)
Self-reported activity (MET)	2414 (1851)	2295 (1087)
MMSE	28.95 (0.92)	28.95 (0.91)

Means (SD) shown for all participants enrolled in the study (N = 40). Variables for both groups were matched at baseline. Self-reported level of exercise was assessed using the *Freiburg Questionnaire of Physical Activities*. MET: Metabolic Equivalent of Task; MMSE: *Mini-Mental State Examination*. This table is taken from Maass et al., 2014b.

After completion of the initial comprehensive cardiological examination, neuropsychological assessment, and MRI sessions, participants were pseudo-randomly assigned to either the aerobic exercise group (N_T = 21), or the control group (N_C = 19). The groups were matched on age, gender, body-mass-index (BMI), activity level (self-reported mean endurance per week), and verbal memory recall (VLMT long delay; see Table 3 for group characteristics) to prevent differences in fitness or cognitive abilities between groups at baseline. There was no drop-out during the intervention.

5.2.2 Participants' recruitment

Community-dwelling older adults (N = 400) were recruited by the DZNE via announcements in radio and local newspapers. Eligible participants needed to be between 60 and 80 years old. Exclusion criteria were; (i) a score > 13 on the *Beck Depression Inventory* BDI-II (possible depression; Beck et al., 1996; Kühner et al., 2007); (ii) a score ≤ 27 on the *Mini-Mental State Examination* (MMSE; Rovner and Folstein, 1987); (iii) low visual acuity despite correction; (iv) a history of neurological diseases or infarcts (e.g. stroke, medically treated diabetes mellitus, Parkinson disease, Alzheimer's disease); (v) joint or muscle complaints whilst walking; (vi) history of major cardiovascular disease and presently uncontrolled hypertension; (vii) self-report of regular exercise of more than 1 h of endurance-related exercise per week in the last three months; (viii) medication which interacts

with brain function; and (ix) contraindications against MRI. Through a screening interview via telephone, 62 participants were excluded for medical reasons (e.g. diabetes mellitus, stroke, brain surgery), 20 persons were excluded due to taking medication which interacts with brain functioning (e.g. specific sleeping pills) and 181 were not suitable for MRI (e.g. tinnitus, metal implants). Finally, due to time limitations 38 potentially suitable participants decided not to take part in the study.

After this initial screening, 100 participants underwent further assessment regarding their cardiovascular and mental health. Participants were invited to an initial 3 h cardiological examination (conducted by D. Ahrens and R. Braun-Dullaeus at the Clinic for Cardiology, Angiology and Pneumology, University Magdeburg) to exclude major cardiovascular risks and determine that all were physically able to participate in the fitness-intervention study, and to a 1 h psychological and neuropsychological assessment to ensure that participants were cognitively unimpaired. This cardiovascular and cognitive screening led to the exclusion of 60 individuals (previously undetected hypertension (60%), arteriosclerosis (10%), mild cognitive impairment (10%), and depression (5%)).

5.2.3 Determination of fitness level and metabolic rates

5.2.3.1 Fitness Level

For determination of aerobic fitness, oxygen consumption was assessed by graded maximal exercise testing on a recumbent cycle ergometer. Intensity was increased every 2 min by 20 W pedalling at 60 rpm until volitional exhaustion or symptom-related limitation. Blood pressure and electrocardiogram were continuously monitored by a cardiologist. Within intervals of 30 sec, oxygen uptake was measured by facemask spirometry and heart rates were recorded (Master Screen CPX, CareFusion 2.0, San Diego, USA). To avoid any cardiovascular risk, some participants did not perform up to maximal exhaustion, and thus did not exceed a respiratory exchange ratio (RER) greater than 1.1 (Mezzani et al., 2003). Therefore, $VO_{2\ VAT}$ (oxygen consumption at ventilatory anaerobic threshold) was calculated (instead of $VO_{2\ MAX}$) as a reasonably accurate predictor of changes in cardiovascular fitness (Noonan and Dean, 2000). $VO_{2\ VAT}$ was determined by the V-slope method (Beaver et al., 1986) as the first breaking point from linearity of carbon dioxide output (VCO_2) when plotted against oxygen uptake (VO_2).

5.2.3.2 Metabolic rates

Additionally, MET scores (Metabolic Equivalent of Task; 1 MET = 1 kcal/kg/h or 3.5 ml/kg/min) were calculated to assess training-related metabolic rates as well as self-reported “lifestyle-related” activity levels.

The *Freiburg Questionnaire of Physical Activities* (FFKA) was administered during the enrolment phase in order to exclude highly active participants. The FFKA accesses health-generating activities on the basis of self-assessment within the preceding month (Frey et al., 1999). In order to translate sum of activities into MET intensities, the *Aintsworth Compendium of Physical Activities* was used (Ainsworth et al., 2000). Weight-related energy rates per week were calculated with the formula MET x kg x h/week. Finally, these MET scores were used to match subjects’ activity levels across groups.

During the intervention period, the *International Physical Activity Questionnaire* (IPAQ) was administered by the end of each week to assess activities beyond intervention. The IPAQ (long version) captures 1-week retrospective estimates of physical activity including moderate work-related activities, transportation, household, leisure activities as well as time spent sitting (Booth et al., 1996). The IPAQ-MET scores were calculated by comparing the energy consumption of different activities, based on the calories burned at each activity or oxygen consumption, multiplied with turnover at rest (1 MET = 1 kcal/kg/h or 3,5 ml/kg/min).

Additionally, a training-related MET score was calculated (across all training sessions and participants) to estimate training-induced metabolic rate.

5.2.4 Measurement of cortisol and growth factors

For all subjects, fasting serum was obtained in the morning of the cardiological examination pre intervention. Post intervention, serum was obtained either in the morning of the cardiological examination (within one week after the last training/control session; N = 17) or on the last training day (N = 23). The cooled (~4°C) samples were centrifuged, aliquoted and stored at minus 80°C. These blood samples were used to determine levels of VEGF, PDGF, IGF/IGF-BPs and cortisol.

Cortisol levels were determined using IMMULITE 2000 Cortisol (Siemens Healthcare). VEGF and PDGF-CC (homodimer of PDGF-C) levels were quantified

using enzyme-linked immunosorbent assays (ELISAs) following manufacturer's instructions (R & D Systems, Minneapolis, MN; DCC00 for PDGF-CC and DVE00 for VEGF). Pre and post intervention levels of IGF-I and IGF-II were also quantitatively analyzed via ELISAs (E 20 and E 30: Mediagnost GmbH, Reutlingen / Germany). IGF-BP-3 and IGF-BP-2 levels were determined using a quantitative Western ligand blot analysis. Measurements of cortisol, VEGF and PDGF levels were performed by the Clinic for Cardiology, Angiology and Pneumology (University Magdeburg). IGF and IGF-BP levels were determined by Ligandis GbR (Gülzow-Prüzen, Germany).

For pre and post acquisition of BDNF levels, fasting blood samples were collected in the morning of the first training day and on average 1 week after the last training session. Serum and plasma concentrations of BDNF were determined by use of sandwich ELISAs (BDNF DuoSets; R&D Systems, Wiesbaden, Germany) at the Institute of Physiology (T. Brigadski and V. Lessmann, University Magdeburg).

5.2.5 Intervention

5.2.5.1 Physical exercise (training group)

The aerobic endurance training was carried out on stationary treadmills (HP Cosmos). Participants received individually optimized 30 min interval training 3 times/week for 12 weeks, plus 5-min warm up and 5-min stretching at the end of each training session. Sport scientists (U. Sobieray and A. Becke) and a medical doctor specialized in sport medicine (D. Ahrens) supervised the intervention. Training intensity was determined by target heart rate (Karvonen method; KARVONEN et al., 1957), starting at 65% and increasing by 5% in steps for 4 weeks (accomplished by adjusting pace and/or the steepness of the treadmills). The target heart rate during training was based on the maximum heart rate during $VO_{2\ VAT}$ assessment and the felt exertion (CR10 Scale; Borg, 1998) during the training sessions. Walking/running interval duration was increased from 5 min, with slow walking breaks of 2 min at the beginning of the training period, up to 30 min continuous walking/running periods at the end of the aerobic intervention.

5.2.5.2 Progressive muscle relaxation/stretching (control group)

Participants in the control group came in twice a week and received 45 min of supervised progressive muscle relaxation/stretching training (Jacobson, 1938).

Progressive muscle relaxation was chosen as control intervention to hold variables like social interactions, schedule, and motivation as similar as possible to the training group whilst not affecting cardiovascular fitness. Here, participants were asked to tense and then relax specific muscle groups with closed eyes in supine position, following the instructions of a course leader. Total duration of training per week (= 90 min) was matched between both groups.

5.2.6 Cognitive functioning

5.2.6.1 Cognitive measures

Each participant completed the MMSE (Folstein et al., 1983; Rovner and Folstein, 1987) and the BDI-II (Beck et al., 1996). Cognitive testing before and after the intervention included the following neuropsychological tests: the VLMT (Helmstaedter and Durwen, 1990), adapted German version of the *Rey Auditory Verbal Learning Test* (RAVLT), CF Test (Strauss et al., 2006), Digit Span Test (forward and backward; Wechsler, 1997) and *Multiple-Choice Word Test* (MWT-B; Lehrl, 2005). For the purpose of the current study, only results from the CF Test and the VLMT will be reported (early recall, late recall, and recognition; see Table 4). Cognitive testing was performed or supervised and the data were analysed by S. Düzel and M. Görke (DZNE, Magdeburg).

5.2.6.2 Complex Figure Test (CF Test)

The CF Test was used to assess spatial object recall (early, late) and recognition memory. The *Rey-Osterrieth Complex Figure* (ROCF; Rey, 1941) was used pre intervention, whereas the *Modified Taylor Complex Figure* (MTCF; Strauss et al., 2006) served as the post-intervention measure. The MTCF was developed as a comparable measure to the ROCF with similar accuracy scores (Hubley, 2010) and is a valid alternative for testing visual long-term memory avoiding implicit learning that can occur when the same version of the ROCF is used for repeated testing sessions (Casarotti et al., 2013). The recognition memory test of the CF requires discrimination between similarly looking complex objects and thus poses high demands on accurate memory representations and pattern separation.

The CF Test consists of 18 different geometric patterns. First, the figure has to be copied in as detailed a manner as possible (copy trial). After a 3-min (early recall) and a 30-min (late recall) delay interval, participants are asked to reproduce the

figure as accurately as possible from memory (see example trial in Table 2). The recognition trial (RT) was administered in the present study after the 30-min late recall. The RT consists of 12 single elements of the 18 scoring elements of the original figure (Rey Figure at pretest) along with 12 new elements from the alternative figure (i.e. Modified Taylor Figure at pretest) serving as lures. Participants are instructed to circle the elements that were part of the original design that had been copied and drawn. Thus, a correct response on the recognition subtest is given if the participant correctly circles an element that was part of the original figure. A correct response is also credited if an element is not circled that was not part of the studied figure. That leads to a maximum score of 24. Correlational and factor analytic studies support the validity of the CF Test as a measure of visuo-constructive ability (copy) and memory (recall and recognition). To summarize, the recognition trial requires discrimination between highly similar objects, and thereby poses high demands on pattern separation.

5.2.6.3 Verbal Learning and Memory Test (VLMT)

The VLMT assesses learning of words including early recall, an interference list after five learning trials, free recall tests directly after interference and 30 min later (late recall), and a final recognition test (Helmstaedter and Durwen, 1990). Here it was focused on early recall, late recall, and recognition memory, in line with the memory measures collected in the CF Test.

First, a list of 15 words (List A), which are semantically unrelated, was verbally presented in five trials. After each trial, participants were asked to recall as many items as possible. The number of recalled items after the first trial measures early recall performance (learning performance of new items). Subsequently, an interference list (List B) with 15 new words was presented and participants were asked to recall as many items as possible from List B. Free recall of List A was again assessed immediately after presentation of the interference list as well as after a 30 min-delay (late recall). Finally, a recognition test consisting of all items from both lists (15 from List A, 15 from List B) and 20 new items, which are semantically or phonetically related to the list items, was sequentially presented. Participants had to recognize whether a presented item belongs to List A or not (recognition test). Two different versions of word lists were used pre and post intervention.

5.2.7 3 Tesla MRI and perfusion imaging

Gadolinium contrast-based perfusion imaging at 3T (Siemens Magnetom, Verio, 32-channel head coil) was used to measure changes in rCBV and rCBF. High-resolution (partial) perfusion-weighted images were acquired to calculate quantitative perfusion maps for rCBF and rCBV. Mean perfusion values were determined for bilateral hippocampus, hippocampal subsections (head, body, tail) and hippocampal subfields (only body of the hippocampus). Additionally, general (non-hippocampal) grey-matter (GM) perfusion was calculated.

Prior to scanning, creatinine serum levels where measured in order to determine risk for renal dysfunction (see 5.1.8.1).

The 3T imaging protocol started with acquisition of a whole-head MPRAGE volume (TE = 3.47 ms, TR = 2500 ms, TI = 1100 ms, flip angle = 7°, parallel imaging with grappa factor 2, 0.8 mm^3 isotropic resolution, 06:29 min scan duration). High-resolution (partial) perfusion weighted images were acquired with slice alignment parallel to the hippocampus main axis (TR/TE = 1500/30 ms, 1.6 mm in-plane resolution, 3 mm slice thickness, 20 slices with 10% gap, number of images = 100). Total 3T imaging time was around 65 min (including acquisition of additional functional and structural volumes, which are not reported here).

Perfusion images were analysed by K. Neumann (DZNE, Magdeburg) using the software *stroketool* (Digital Image Solutions). Quantitative perfusion maps for rCBF and rCBV were calculated based on following equation: The concentration of a tracer c(t) within a volume of interest is determined by the tissue flow F_t and the arterial input c_a to this region (Ostergaard et al., 1996). *R* is the residue function and describes the fraction of injected tracer in the vasculature.

$$c(t) = F_t \cdot \int_0^t c_a(\tau) R(t-\tau)\, d\tau$$

The automatic detection algorithm of the arterial input function (AIF) searches for pixels that are completely localized in regions of arteries. The search algorithm has two criteria: only those pixels with the largest decrease in signal intensity in time course and which reach their bolus peak at the earliest point in time are summed up to a mean AIF. Hence, different regions contributed to the AIF across participants.

To measure perfusion in bilateral hippocampi, masks (defined on the 3T MPRAGEs) were co-registered to the first image of the perfusion time course with SPM8. Afterwards, co-registered masks were applied to perfusion maps (rCBF and rCBV) and a mean-perfusion value for each hippocampal subregion of interest was calculated using *MATLAB R2008a*. Additionally, hippocampal subfield perfusion was determined (in the body of the hippocampus), after subfield segmentation on the 7T high-resolution MPRAGEs and co-registration to the 3T MPRAGEs.

To investigate whether exercise-related perfusion changes were specifically linked to the hippocampus or also affected non-hippocampal grey-matter perfusion within the cortical regions that were covered by the perfusions scans, general (non-hippocampal) cortical perfusion was extracted. Here, individual GM-maps were derived by segmentation of the MPRAGE volumes. After subtracting overlap with the hippocampal masks, mean perfusion values for each “hippocampus-free” GM-mask were calculated. Note that the perfusion images only covered a partial volume including the temporal lobes, main portions of the parietal and occipital lobes and minor parts of the cerebellum. As measures of CBF and CBV may vary considerably between different GM regions (Kuppusamy et al., 1996), conclusions about whole-brain GM perfusion can only be drawn with caution.

5.2.8 7 Tesla MRI and volume measures

High-resolution structural T1-weighted images with a resolution of 0.6 mm^3 isotropic voxels (whole-head MPRAGE, see Method sections 2.2) were acquired within one week pre and post intervention using 7T MRI. To measure changes in hippocampal volume, segmentation of hippocampal regions (head, body, tail plus subfields [subiculum, CA1, and CA2-3/DG] in the hippocampal body) was performed (by A. Weber, DZNE, Magdeburg) manually on the 7T high-resolution MPRAGEs after bias-correction and intensity- adjustment (see 2.4).

To assess inter-rater reliability in segmentation, the hippocampi of 10 randomly chosen subjects (five scans pre and five scans post intervention) were segmented by a second rater. Intra-class correlation coefficients (ICCs, two-way mixed, single measure) were calculated for left hippocampus ($ICC_{left\ HC}$ = .973, ICC_{head} = .982; ICC_{body} = .906; ICC_{tail} = .944) and for right hippocampus ($ICC_{right\ HC}$ = .920, ICC_{head} = .969; ICC_{body} = .902, ICC_{tail} = .861). These inter-rater reliabilities demonstrate high- to excellent consistency for all subregions.

5.2.9 Statistical Analysis

5.2.9.1 Missing data and outlier detection

The “outlier labeling rule” (Hoaglin et al., 1986) was used to define outliers in measures of percentage change. This rule declares observations that lie more than 2.2 times the interquartile range away from the nearest quartile as outliers and is resistant to extreme values. A summary of missing cases and outliers is given in the Supplementary Table S 4.

For one subject, fitness levels could not be determined because the person wished to terminate the ergometer assessment before reaching the ventilatory threshold. Thus, complete pre and post data for fitness levels were available for 39 subjects (no outliers were detected in change in VO_{2VAT}).

Prior to contrast-based perfusion imaging at 3T, creatinine serum levels where measured in order to determine risk for renal dysfunction. For six subjects, serum creatinine levels were not within the normal range (male: 59-104 µmol/l, female: 45-84 µmol/l), indicating renal insufficiency and thus no contrast-based perfusion imaging could be performed. For one subject, the AIF and subsequently rCBV could not be reliably calculated. One outlier in changes of both hippocampal and cortical rCBF and rCBV was excluded from analyses. Complete data for both perfusion measures were available for 32 subjects.

Seven participants could not attend or complete the 7T MRI protocol due to technical problems, non-metallic implants without 7T MRI approval or indisposition (e.g. claustrophobia, nausea) during scanning. For one subject, 7T hippocampal segmentation on the post scan could not be performed due to poor data quality (i.e. large movement artefacts). Thus, hippocampal and GM volumes could be determined for 32 subjects (no outlier was detected in volume change).

One subject did not perform CF recognition testing pre intervention. Furthermore, three outliers were detected in early and late CF recall and there was one outlier in the CF recognition test. Complete pre and post data were available for 37 subjects in CF recall and 38 subjects in the CF recognition test.

One subject did not perform VLMT recognition testing post intervention. Outlier detection led to exclusion of one subject in VLMT recall and three subjects in

VLMT recognition. Complete pre and post data were available for 39 subjects in VLMT recall and 36 subjects in the VLMT recognition test.

For three subjects, IGF-BP2 levels could not be estimated due to values being below detection limits of the assays. Furthermore, one outlier was detected for change in IGF-BP2 and one outlier for IGF-BP3 levels, respectively. There were also three outliers detected for change in VEGF levels. Complete pre and post data were available for 39 subjects regarding IGF-BP3, 36 subjects regarding IGF-BP2 and 37 subjects regarding VEGF. Full data was available for PDGF, BDNF (serum and plasma), IGF-1 and IGF-2 levels.

5.2.9.2 Repeated-measures ANOVA:

Intervention effects were first examined using repeated-measures ANOVAs with *group* (aerobic exercise, stretching control) as a between-subjects factor and *time* (pre, post) as a within-subjects factor. ANOVAs were run in SPSS (*PASW Statistics* V.20). All dependent variables met criteria for normal distribution. There was no evidence that cognitive measures were bimodally distributed. Paired t-tests (two-tailed) were performed to assess changes in fitness levels from pre to post intervention. Age, gender and differences in outside temperature on the day of measurement ($\Delta T = T_{post} - T_{pre}$) were included as covariates of no interest in all analyses. The difference in temperature was included to account for possible confounding effects of (seasonal) differences in hydration status on MRI and perfusion scans (ΔT_T = -2.7 ± 2.6 K, ΔT_C = -7.0 ± 2.1 K). This was deemed necessary due to different seasonal starting points across subjects with a potential relevance of hydration status on brain structure that has been shown in previous studies (e.g. dehydration-related shrinkage of brain tissue and an associated increase in ventricular volume (Kempton et al., 2011; Streitbürger et al., 2012). Although temperature did not significantly affect brain structures in this study, significant negative correlations between changes in temperature and changes in perfusion were found (hippocampal rCBF: r = -0.38, p = .027; GM rCBF: r = -0.35, p = .047).

5.2.9.3 Correlations of changes

Correlational analyses were performed on percentage change in $VO_{2\ VAT}$, in bilateral hippocampal rCBV/rCBF, bilateral hippocampal volume (head, body, tail), and memory performance. This approach should additionally account for inter-

individual differences in hippocampal size. To assess whether exercise-related effects were specific to the hippocampus or unspecific, perfusion and volume changes for overall grey matter were additionally analysed. The correlational analyses performed were planned comparisons, motivated by findings from previous exercise studies (Dery et al., 2013; Erickson et al., 2011; Pereira et al., 2007), in order to determine the extent to which relationships among fitness change, perfusion change, and memory change are also present in old age.

For all variables of interest, data were missing occasionally (see Supplementary Table S 4). Little's chi-square test showed that data were missing completely at random (MCAR; chi-square = 134.07, df = 130, p = .386). Thus, to conduct correlational analyses including all available variables of interest, Full Information Maximum Likelihood (FIML) was used. FIML is a SEM-based missing data estimation approach that yields unbiased parameter estimates and standard errors. This method estimates a likelihood function for each individual based on the variables that are present, such that all available data are used. To test associations for significance, two models are estimated: the H_0 (unrestricted) model, in which variables (percentage change) are correlated and the H_1 (restricted or fixed) model, in which the correlations are set to zero. The difference between the two log-likelihoods is used to derive the chi-square (a value with $p < .05$ indicates significant correlations between changes). Reported correlation coefficients (r) are standardized parameter estimates: $r_{x,y} = COV_{x,y}/(SD_x*SD_y)$. All dependent variables (percentage changes) were regressed on age, gender and ΔT. Correlations were estimated in *Mplus* (Version 6.1, Muthén and Muthén, 2011). For illustrative purposes, regressions of the residuals were plotted in SPSS after controlling for effects of age, gender, and ΔT.

5.2.9.4 Structural equation modeling (SEM)

Furthermore, path analysis and structural equation modeling (SEM) was used to test different models for the associations between the measured variables. This technique uses a combination of statistical criteria and qualitative causal assumptions. Based on previous research, three different models were defined (see Figure 20) that predict how fitness-related changes in hippocampal perfusion and volume modulate memory. The consistency between the theoretical models and the empirical data was tested in *Mplus* by means of FIML. Goodness of model

fit was evaluated by the chi-squared difference test. The following fit indexes are reported: χ^2/DF, Comparative Fit Index (CFI), and the Root Mean Square Error of Approximation (RMSEA). All dependent variables (percentage changes) were regressed on age, gender, and ΔT. SEM models were built in cooperation with M. Lövden (Karolinska Institute, Stockholm).

5.3 Results

5.3.1 Effects of exercise on fitness-related variables

Physical exercise was effective in increasing aerobic fitness levels (Figure 16 and see Table 4). A repeated-measures ANOVA yielded a significant time (pre vs. post intervention) × group (training vs. control) interaction for oxygen consumption at the ventilatory anaerobic threshold ($VO_{2\ VAT}$, $F(1,34) = 6.49$; $p = .016$). Whereas the exercise group improved significantly in $VO_{2\ VAT}$ after the intervention ($\Delta VO_{2\ VAT}$ = 11.74%, $t(19) = 3.78$, $p = .001$), the relaxation/stretching group did not change in fitness levels ($\Delta VO_{2\ VAT}$ = 1.47%, $p > .80$). The improvement in fitness due to exercise was also confirmed by a significant intervention effect on the power levels that participants could achieve at VAT ($Watt_{VAT}$, $F(1,31) = 5.13$; $p = .031$). Independent two-sample t-tests between groups also reflected significant differences in overall metabolic rate across the entire intervention period, with significantly higher training-related MET values in the exercise group than the control group ($MET_T = 469$, $MET_C = 148$, $t(20.76) = 23.57$, $p < .001$).

Note that the increase in fitness levels in the training group was observed, despite the fact that self-reported “lifestyle-related” activity levels during the intervention period (e.g. domestic or work-related activities) were higher in the control compared to the training group ($MET_T = 5395$, $MET_C = 9608$, $t(22.5) = -3.18$, $p = .013$) as revealed by the IPAC (see 5.1.3.2). Furthermore, fitness levels at baseline were significantly higher in the control than in the training group as revealed by a main effect of group on $VO_{2\ VAT}$ ($F(1,33) = 6.23$; $p = .018$) and subsequent t-tests ($t(37) = 2.41$, $p = .021$). This pattern holds true, although self-reported level of exercise (assessed by the FFKA (see 5.1.3.2), which was used to match groups in terms of activity levels before intervention, did not differ.

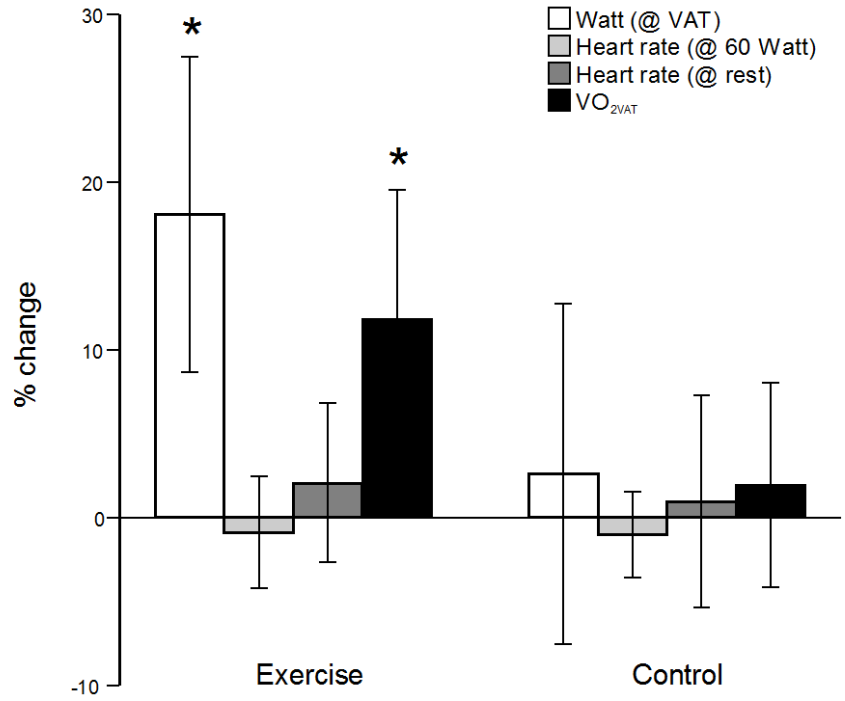

Figure 16. Changes in fitness levels after the 3-month intervention.

Bars represent percentage changes from pre to post intervention in the aerobic exercise group (N_T = 21) and the muscle relaxation/stretching control group (N_C = 19). The intervention was effective in increasing fitness levels, including oxygen consumption at the ventilatory anaerobic threshold ($VO_{2\ VAT}$) and Watt at VAT in the exercise group (paired t-test, two-tailed, all p < .01). The control group did not show any change in fitness level. Error bars denote 95% confidence intervals. This figure is taken from Maass et al., 2014b.

5.3.2 Fitness-related changes in perfusion, volume and memory

First, variables of interest were entered into repeated-measures ANOVAs with time and group as factors (see Table 4 for pre and post values). Second, correlational analyses were performed across all participants (training and control group) taking the percentage change (from pre to post intervention) in $VO_{2\ VAT}$ as an outcome measure of change in fitness (Table 5). The correlational analyses were also performed in the exercise group only and are reported in the Supplementary Table S 5. These analyses considered changes in rCBF/rCBV, memory measures (verbal and spatial object recall and recognition memory), and hippocampal volumes (head, body and tail; derived by segmentation on the 7T high-resolution MPRAGEs). To include all available data and thus account for missing cases, correlations were computed using FIML estimation. However, Pearson's correlations using pairwise deletion for missing data led to similar results.

Table 4. Group means (SD) for fitness, perfusion, volume and memory pre and post intervention.

	aerobic exercise group		relax/stretching group	
Variables	Pre (baseline)	Post (3mo)	Pre (baseline)	Post (3mo)
$VO_{2\ VAT}$	18.04 (3.55)$_{20}$	19.92 (3.33)$_{20}$	21.03 (4.16)$_{19}$	21.14 (3.87)$_{19}$
Hippocampal rCBF	104.0 (38.8)$_{16}$	97.5 (37.4)$_{16}$	102.2 (22.3)$_{16}$	101.1 (23.2)$_{16}$
Hippocampal rCBV	58.2 (29.9)$_{16}$	63.1 (51.0)$_{16}$	54.1 (20.6)$_{16}$	53.9 (24.4)$_{16}$
Grey Matter rCBF	57.9 (16.6)$_{16}$	60.1 (19.9) $_{16}$	60.9 (14.2)$_{16}$	57.0 (14.0)$_{16}$
Grey Matter rCBV	28.8 (11.7)$_{16}$	31.6 (19.5)$_{16}$	30.8 (9.8)$_{16}$	30.4(15.6)$_{16}$
HH Volume	3.24 (.64)$_{15}$	3.17 (.58) $_{15}$	3.30 (.73) $_{17}$	3.22 (.73) $_{17}$
HB Volume	2.09 (.30) $_{15}$	2.05 (.32) $_{15}$	2.08 (.37) $_{17}$	2.00 (.34) $_{17}$
HT Volume	.99 (.27) $_{15}$	.97 (.26) $_{15}$	1.03 (.26) $_{17}$	1.01 (.24) $_{17}$
CF early recall	17.3(5.6)$_{18}$	21.9 (6.4)$_{18}$	18.2 (5.6)$_{19}$	21.7 (6.0)$_{19}$
CF late recall	17.6 (5.1)$_{18}$	22.3 (6.5)$_{18}$	16.9 (6.1)$_{19}$	21.5 (6.0)$_{19}$
CF recognition	19.5 (1.7)$_{20}$	18.0 (2.1)$_{20}$	19.2 (2.0)$_{19}$	18.1 (2.3)$_{19}$
VLMT early recall	5.1 (1.7)$_{21}$	5.1 (1.3)$_{21}$	5.3 (1.6)$_{18}$	5.8(1.4)$_{18}$
VLMT late recall	9.6 (3.1)$_{21}$	8.5 (2.5)$_{21}$	10.1 (2.2)$_{18}$	9.2 (2.6)$_{18}$
VLMT recognition	11.5 (2.9)$_{20}$	8.4 (4.2)$_{20}$	12.1 (2.7)$_{16}$	10.4 (3.4)$_{16}$

$VO_{2\ VAT}$ was measured in ml/kg per min. Bilateral rCBF and rCBV were measured in ml/100g/min and ml/100g * 10, respectively. Bilateral hippocampal volumes were measured in cm^3. HH: Hippocampal Head, HB: Hippocampal Body, HT: Hippocampal Tail; CF: *Complex Figure Test*. VLMT: *Verbal Learning and Memory Test*. Subscripts indicate number of available data (see also Supplementary Table S 4 for missing data). This table is adapted from Maass et al., 2014b.

5.3.2.1 Repeated-measures ANOVA:

ANOVAs with hippocampal rCBF/rCBV, hippocampal volume, and memory did not yield any significant time × group interaction (all p-values > .10). This might be related to the aforementioned findings that the control group showed higher fitness levels at baseline and/or engaged in a more active lifestyle beyond the intervention, which may have reduced the intervention effect due to other experience-dependent effects operating to a greater extent in the control than in the exercise group. Regarding time-related changes, there was a significant main effect of time on hippocampal perfusion (rCBF: ($F(1,27) = 6.12$, $p = .020$; rCBV: ($F(1,27) = 6.61$, $p = .016$) with a significant interaction between time and age (rCBF: ($F(1,27) = 5.85$, $p = .023$; rCBV: ($F(1,27) = 6.82$, $p = .015$). More specifically, changes in perfusion were negatively correlated with age ($r_{rCBF} = -0.40$, $p = .023$; and $r_{rCBV} = -0.42$, $p = .016$, see Figure 17). Follow-up ANOVAs within each group (note that unlike t-tests, ANOVAs included age as covariate) confirmed a significant change in hippocampal rCBF and rCBV for the exercise group (CBF: $F(1,12) = 8.34$, $p = .014$; rCBV: ($F(1,12) = 5.27$, $p = .040$) but not the control group (CBF/CBV: $p > .79$). As can be seen in Figure 17 the younger individuals of the sample tended towards perfusion increases whereas the older individuals tended towards decreases. There were no significant main effects of time on recall or recognition performance neither for the VLMT (all p-values > .20) nor for the CF Test (only a trend for late recall: $p = .080$; all other p-values > .20) and no time x age interactions (all p-values > .14).

A previous exercise study in older individuals (Erickson et al., 2011) reported an improvement in spatial memory in both the training and control group (with no significant time x group interaction). In this aforementioned study analyses were performed by means of paired t-tests within each group without using age and gender as covariates (as it was done in the reported ANOVAs). If this analysis is replicated in the present sample, a significant improvement in spatial object recall is found in both groups (all p-values < .02).

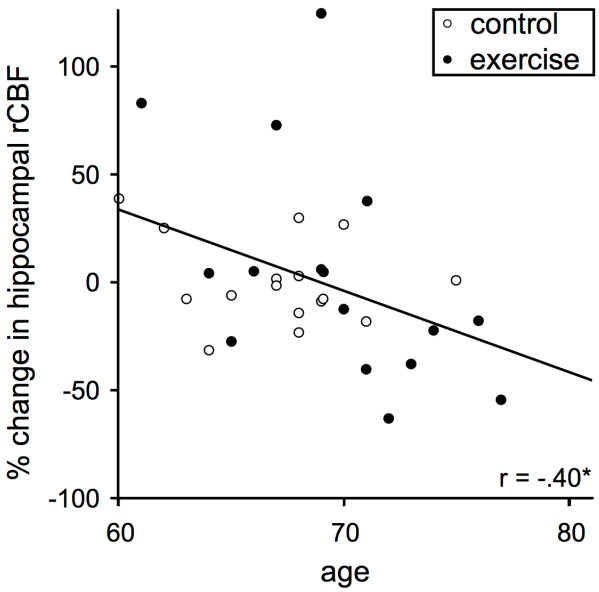

Changes in in hippocampal blood flow (rCBF) and blood volume (rCBV; not shown) over a 3-month period were negatively correlated with age (*p < .05). While the younger individuals tended towards perfusion increases as a result of exercise, older individuals tended towards decreases. Note that for this correlation plot no covariates are included. Perfusion changes refer to bilateral hippocampus. This figure is taken from Maass et al. (2014b).

Figure 17. Relationship between changes in perfusion and age.

5.3.2.2 Correlations of changes

The results of the correlational analyses are depicted in Figure 18 and Table 5. Changes in aerobic fitness levels were positively associated with changes in hippocampal rCBF (r = 0.48, p = .003; see Figure 18a) and rCBV (r = 0.35, p = .031). Fitness-related changes in perfusion were not restricted to the hippocampus, but also positively related to changes in non-hippocampal cortical rCBF (r = 0.58, p < .001) and rCBV (r = 0.39, p = .048).

Regarding hippocampal structure, significant positive correlations were found between changes in fitness level and in hippocampal head volumes (r = 0.37, p = .032; see Figure 18a), with no significant effect on body or tail volumes (all p-values > .20). These fitness-related changes in HH volume showed strong correlations with changes in hippocampal rCBF (r = 0.66, p < .001; see Figure 18a) and rCBV (r = 0.74, p < .001). This relationship was specific to the hippocampus, as whole brain GM volume was not reliably correlated with changes in fitness (p > .20).

Although HH volumes did not increase overall in the exercise group, the majority of individuals showing an increase in hippocampal perfusion from pre to post intervention also showed increased volume (see Figure 18a).

To examine whether fitness-related changes in hippocampal perfusion, volume, or both were specifically associated with spatial object memory performance,

correlational analyses were conducted on changes in early recall, late recall, and recognition in the CF Test. Additionally, verbal list learning was assessed using the VLMT, which has been used in an exercise study with young/middle-aged individuals (Pereira, 2007).

Changes in early recall and recognition memory in the CF Test were positively correlated with changes in $VO_{2\ VAT}$ (early recall: r = 0.31, *p* = .050; recognition: r = 0.39, *p* = .012; see Figure 18b), hippocampal rCBF (early recall: r = 0.42, *p* = .013; recognition: r = 0.42, *p* = .015; see Figure 18b), hippocampal rCBV (recognition: r = 0.50, p = .003) and hippocampal head volume (early recall: r = 0.34, *p* = .037; recognition: r = 0.42, *p* = .013; see Figure 18b). There were no significant correlations between changes in CF late recall and fitness, perfusion or volume (all p-values > .30). Similar to the CF Test, significant correlations were also found between changes in recognition memory in the VLMT and changes in hippocampal rCBF (r = 0.43, *p* = .017) as well as HH volume (r = 0.37, *p* = .042). For VLMT early and late recall no significant associations were found (*p* > .30).

Additionally, it was investigated whether correlations of changes in fitness, perfusion or head volume with early recall and recognition were significantly higher than correlations with late recall (using Fischer's Z-Test as described in Meng et al., 1992).This showed that correlations of changes in perfusion (rCBF/rCBV) with early recall and recognition memory were significantly higher than the corresponding correlations for late recall performance in the CF Test (*p* < .05).

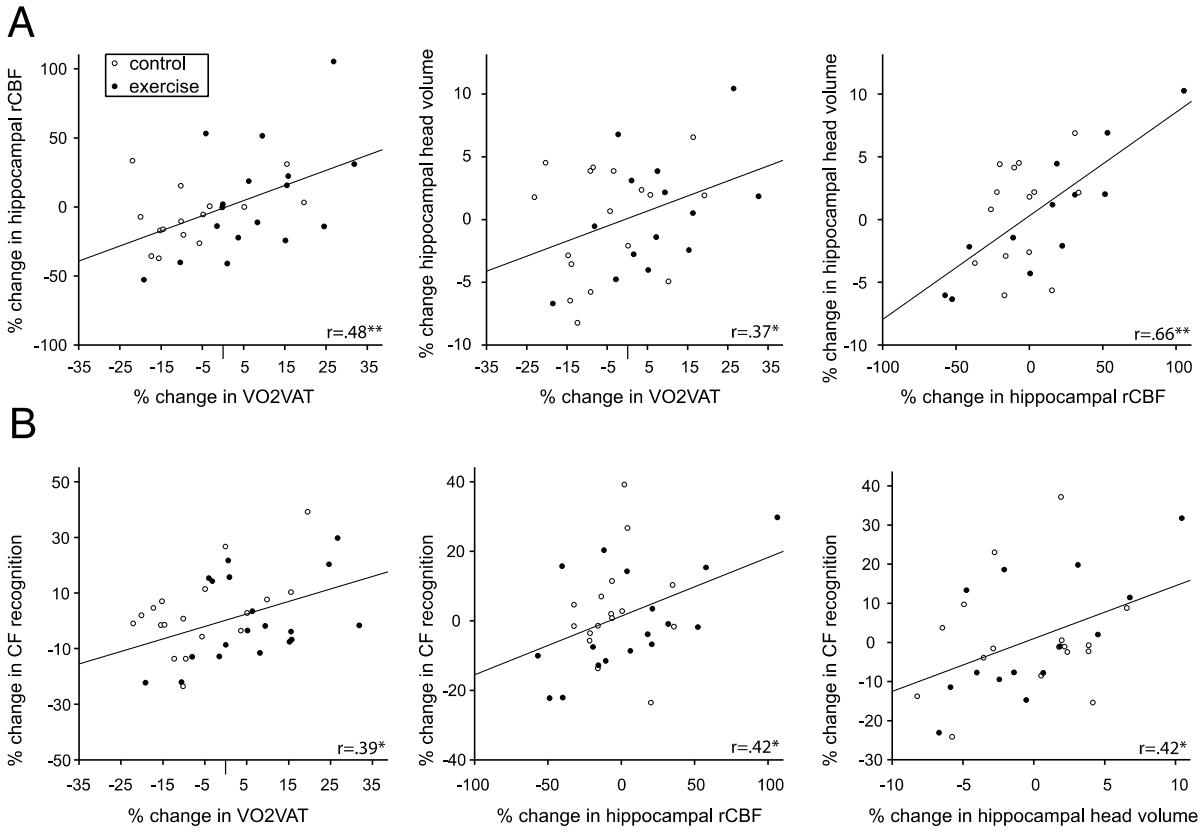

Figure 18. Relationships of changes in fitness, hippocampal perfusion and volume to memory.

A. Changes in aerobic fitness levels ($VO_{2\ VAT}$) over a 3-month period were positively correlated in hippocampal blood flow (rCBF), blood volume (rCBV; not shown) and hippocampal head volume. Changes in hippocampal perfusion and volume were closely related. **B.** Fitness-related changes in hippocampal perfusion and head volume were associated with changes in recognition memory for complex spatial objects in the CF Test. The same relationships were found for early, but not for late, CF recall (see Results section and Table 5 for details). Correlations were tested for significance ($p < .05$), using Full Information Maximum Likelihood (FIML), a missing-data estimation approach. Plots display partial residuals after controlling for age, gender, and ΔT (temperature changes from pre to post intervention). Volumes and perfusion changes refer to bilateral hippocampus. Asterisks highlight significant correlations (*$p < .05$; **$p < .01$). This figure is taken from Maass et al., 2014b.

5.3.2.3 Subfield-specific perfusion analyses

The analyses above described that fitness-induced increases in bilateral hippocampal perfusion were associated with better memory in the CF Test. Previous studies in young/middle-aged humans reported a specific effect of exercise on rCBV in the DG subfield of the hippocampus, with a potential link to neurogenesis (Pereira et al., 2007). Thus, it was further tested whether memory benefits were also coupled with perfusion in specific hippocampal subfields. Hippocampal perfusion was first determined for head, body, and tail regions. In addition, subfield-specific perfusion values were extracted within the body of the hippocampus, distinguishing between subiculum, DG/CA2-CA3, and CA1.

Subfields were segmented on the 7T high-resolution MPRAGEs and co-registered to the individual 3T MPRAGEs. In the following analyses, it was only focused on changes in rCBF as a measure of perfusion (rCBF and rCBV were strongly correlated: r = 0.69, $p < .001$).

Correlational analyses for hippocampal head, body, and tail perfusion showed a significant relation between changes in rCBF and fitness levels for all three subsections ($r_{head} = 0.52$, $r_{body} = 0.50$, $r_{tail} = 0.49$, all p-values < .005). With respect to memory performance in the CF Test, benefits in early recall were related to increased hippocampal head and body rCBF ($r_{head} = 0.45$, $p = .008$; $r_{body} = 0.36$, $p = .039$), whereas recognition memory was related to rCBF increases in hippocampal body and tail ($r_{body} = 0.43$, p = .022; $r_{tail} = 0.61$, $p < .001$), but not significantly to increases in hippocampal head ($p = .07$).

Subfield-specific analyses (in the hippocampal body) yielded significant correlations between fitness and perfusion changes in all hippocampal subfields ($r_{Sub} = 0.54$, $r_{CA1} = 0.58$, $r_{DG/CA2-3} = 0.46$, all p-values < .02). Regarding effects of perfusion on memory performance in the CF Test, there was a significant relation between changes in DG/CA2-3 perfusion and early recall ($r_{DG/CA2-3} = 0.38$, $p = .040$) as well as between CA1 perfusion changes and recognition ($r_{CA1} = 0.58$, $p = .003$). There were no other significant correlations between subfield-specific perfusion changes and performance in the CF Test (all p-values > .14). These analyses could only be performed for subjects who underwent both 7T structural MRI and 3T perfusion imaging (N = 26). Taken together, correlations among hippocampal perfusion, fitness changes and changes in CF memory (early recall and recognition) were most consistent when the entire hippocampus was taken into account.

Table 5. Correlation coefficents (r) for the relationships of changes in fitness, perfusion and volume to memory across all participants.

Fitness-related changes in perfusion and volume

Variables (% change)	*HC rCBF*	*GM rCBF*	*HC rCBV*	*GM rCBV*	*HH Vol.*	*GM Vol.*
$VO_{2\ VAT}$	**.48****	.58**	.35*	.32*	**.37***	.23

Correlations betw. changes in fitness, perfusion and HC volume with changes in memory

Variables (% change)	*CF early recall*	*CF late recall*	*CF recognition*	*VLMT early recall*	*VLMT late recall*	*VLMT recognition*
$VO_{2\ VAT}$	.31*	.09	**.39***	.23	.19	.06
Hippocampal rCBF	.42*	.01	**.42***	.13	.13	.43*
Grey Matter rCBF	.36*	-.06	.30	-.03	-.03	.24
Hippocampal rCBV	.16	-.06	.50**	-.14	.12	.33
Grey Matter rCBV	.02	-.18	.35	-.30	0	.20
Hippoc. head Vol.	.34*	.17	**.42***	-.16	.31	.37*

Correlations were tested for significance ($p < .05$), using Full Information Maximum Likelihood (FIML), a missing-data estimation approach controlling for possible confounding effects of age, gender, and ΔT. Reported correlation coefficients (r) are standardized parameter estimates. $VO_{2\ VAT}$ was measured in ml/kg per min. Bilateral rCBF and rCBV were measured in ml/100g/min and ml/100g * 10, respectively. Bilateral hippocampal volumes were measured in cm^3 (after manual segmentation). CF: Complex Figure Test. VLMT: Verbal Learning and Memory Test. Asterisks highlight significant correlations (*$p < .05$; **$p < .01$). Boldface demarcates correlations shown in Figure 18; N = 40. This table is adapted from Maass et al., 2014b.

5.3.2.4 Relationship between serum cortisol levels and verbal memory

Previous studies of verbal memory in old age have shown a negative correlation with cortisol (Comijs et al., 2010; Gerritsen et al., 2011). Therefore it was investigated whether the lack of a behavioural or physiological effect of exercise on verbal memory was related to cortisol level. Baseline serum cortisol levels were negatively correlated with early verbal recall across the entire sample (r = -0.44; *p* = .009). Changes in serum cortisol levels were negatively correlated with pretest cortisol levels, suggesting regression to the mean, with individuals who had low values at baseline showing increasing and those with high values at baseline exhibiting decreasing levels (r = -0.63; *p* < .001). Pretest levels of cortisol correlated positively with change in early verbal recall (r = 0.39; *p* = .023) compatible with the possibility that the regression to the mean phenomenon of cortisol accounted for variance in the pre to post change in early verbal recall. There was no relationship between serum cortisol levels and configural memory at baseline (early recall, late recall, or recognition memory; all p-values > .42).

5.3.2.5 Role of neurotrophic and angiogenic factors in hippocampal plasticity

Animal models have highlighted the complementary role of neurotrophic and angiogenic growth factors in mediating the downstream effects of exercise on the brain and cognition (Cotman and Berchtold, 2007; Voss et al., 2013a). In a further analysis, the effects of BDNF (plasma and serum levels), VEGF, PDGF and IGF/IGF-BPs (IGF-1, IGF-2, IGF-BP2, IGF-BP3) on fitness-related hippocampal vascular and structural plasticity were thus analysed (Maass, et al., under review). Furthermore, it was tested whether baseline levels or changes of these factors were related to age, as the potential for vascular hippocampal plasticity was reduced with increasing age.

With regard to age, there were significant negative correlations with baseline levels of IGF-2 and IGF-BP3 (IGF-2: r = -0.47, *p* = .002; IGF-BP3: r = -0.41, *p* = .009; all other p-values > .10) and a significant negative relationship between changes in IGF-2 levels and age (r = -0.39, *p* = .012; all other p-values > .01).

Assessing the relationships among changes of neurotrophic factors revealed a significant positive correlation between PDGF and VEGF changes (r = 0.56, *p* < .001), both growth factors that promote or regulate angiogenesis. In addition, changes in IGF levels were positively correlated with changes in IGF-BP3 (IGF-1: r

= .53, IGF-2: r = 0.56, $p < .001$) and negatively correlated with changes in IGF-BP2 (IGF-1: r = 0.34, $p = .043$). Furthermore, IGF-BP2 decreases were related to IGF-BP3 increases (r = -0.37, $p = .025$). There was no further significant relationship between changes of the aforementioned factors, only a positive relationship between PDGF and IGF-1 changes that was "driven" by the exercise group (r = 0.31, $p = .038$; $r_T = 0.47$, $p = .03$; $r_C = 0.11$, $p > .90$).

Repeated-measure ANOVAs with VEGF, PDGF, IGF/IGF-BPs and BDNF did not yield any significant time × group interaction (all p-values > .12). There was only a main effect of time on IGF-2 levels ($F(1,35) = 6.94$, $p = .012$) with a significant age x IGF-2 interaction ($F(1,35) = 7.52$, $p = .010$; see also correlation with age above). IGF-2 levels were significantly decreased after the 3-month intervention ($t(39) = 2.25$, $p = .03$).

There was also no significant correlation between changes in VEGF, PDGF, IGF/IGF-BPs or BDNF (after regressing out age, gender and ΔT) with changes in fitness (only trend for IGF-BP2: r = -0.32, $p = .056$; all other p-values >.10) or perfusion (all p-values > .14). The absence of any relation between changes in perfusion and VEGF changes was found although VEGF baseline levels were positively related to baseline perfusion (GM: r = 0.43, $p = .024$; HC: r = 0.37, $p = .045$). Although there was no positive relation between changes in fitness or perfusion with IGF-1 level changes, the latter was significantly positively correlated with changes in hippocampal volume (HH: r = 0.48, $p = .006$; HC: r = 0.50; $p = .004$). Interestingly, this correlation was strong in the control group but not significant in the training group (HH: $r_C = 0.65$, $p = .005$; $r_T = 0.34$, $p = .22$). A trend for a similar positive relationship with hippocampal volume changes was also found for changes in IGF-BP3 (HH: r = 0.34. p = .058), whereas IGF-BP2 changes showed a negative relationship (HH: r = -0.42, $p = .029$; HC: r = -42, $p = .022$). IGF-1 was the only growth factor, which was related to memory benefits. Specifically, changes in IGF-1 were correlated with changes in VLMT late recall performance (r = .43, $p = .005$). Aside from trend for a similar positive relation between changes in VLMT late recall performance and BDNF plasma levels (r = 0.31, p = .052) and between IGF-II changes and CF early recall (r = 0.32, p = .068), no other growth factor was positively related to memory changes (all other p-values > .06).

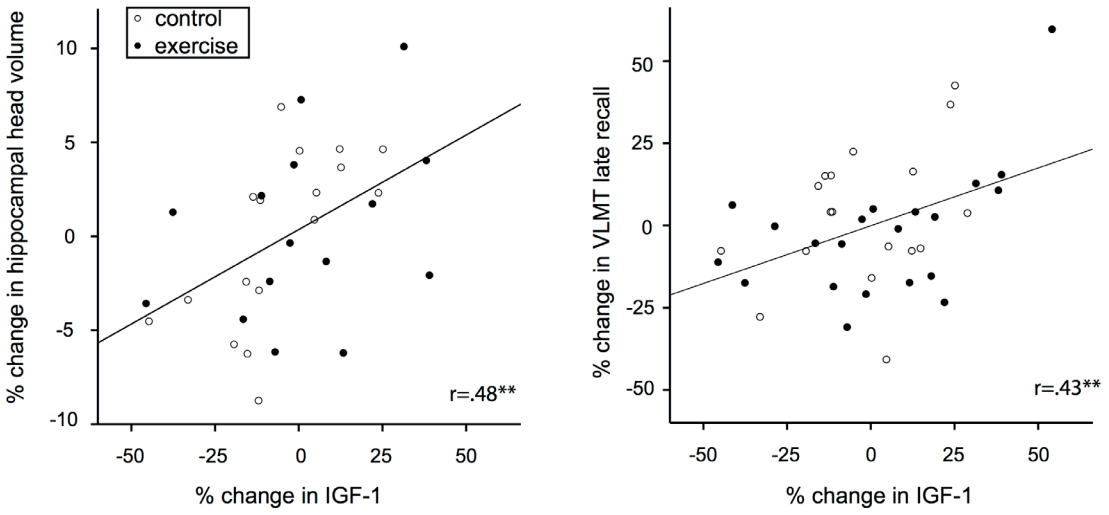

Figure 19. Relationship of changes in IGF-1 levels, hippocampal volume and verbal recall
Changes in IGF-1 over a 3-month period were positively correlated with changes in hippocampal volume (head and whole hippocampus) and changes in late recall performance in the VLMT. Plots display partial residuals after controlling for age, gender, and ΔT (temperature changes from pre to post intervention). Volumes refer to bilateral hippocampus. Asterisks highlight significant correlations (**p < .01). VLMT: *Verbal Learning and Memory Test*. (Maass, et al., under review)

5.3.3 Structural equation modeling

The correlational analyses revealed associations between fitness-related changes in hippocampal perfusion, hippocampal head volumes, and recognition memory in both the CF Test and the VLMT. Next, path analysis and SEM was used to test different models in which effects of changes in physical fitness on memory are accounted for by hippocampal volume and/or perfusion changes. In the following analyses, it was focused on rCBF as a measure of perfusion (rCBF and rCBV changes were strongly correlated: r = 0.69, p < .001).

First, Model A was defined, which is illustrated in Figure 20a. According to Model A, increases in fitness lead to higher hippocampal perfusion, leading to an increase in hippocampal head volume, which in turn results in improved recognition memory. Model A is based on the assumption that volume changes in the hippocampus are the result of different types of plasticity including vascular plasticity, synaptogenesis, and neurogenesis. Accordingly, volume changes should be the best predictor for cognitive changes. Changes in perfusion, on the other hand, should directly relate to changes in hippocampal volume (Bandettini and Wong, 1997), but not necessarily to cognition independently from hippocampal volume.

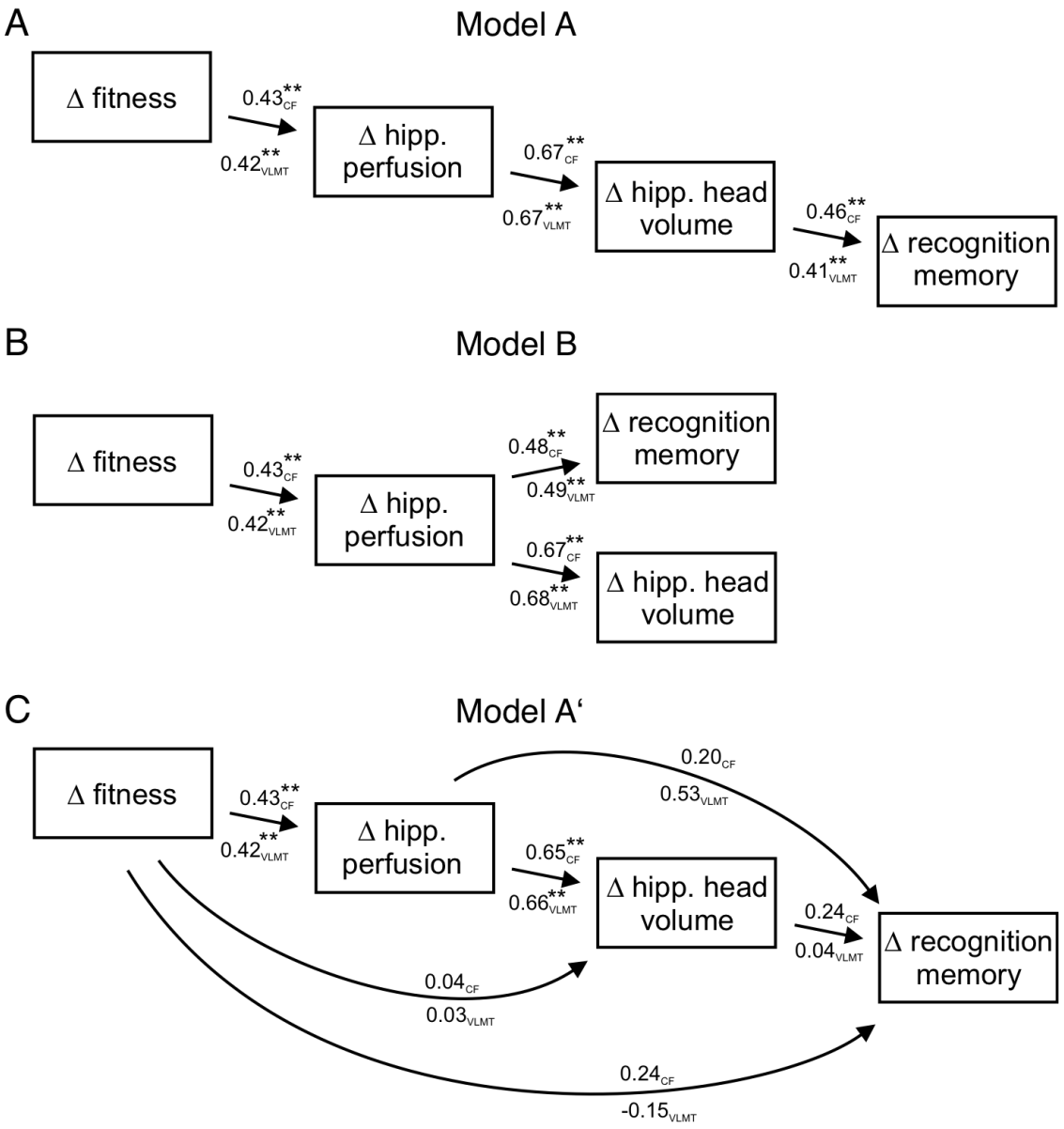

Figure 20. Estimated path models predicting the relationships of changes in fitness, hippocampal perfusion, and volume to recognition memory.

A. The initial Model A predicts that fitness-related memory improvements are modulated by hippocampal volume changes **B.** Model B predicts that memory benefits are directly linked to hippocampal perfusion. All models showed good fit to the data (CFI > 0.97, RMSEA < 0.06). Model B yielded slightly better fit than Model A, suggesting that memory changes can be well accounted for by perfusion changes, with no strong additional contribution of hippocampal volume. Note that the same model (B), in which hippocampal perfusion and volumes are replaced by non-hippocampal cortical perfusion and whole-brain grey-matter volumes did not fit the data well (CFI < .90, RMSEA > .08). **C.** Model A' enables the possibility that fitness can modulate hippocampal volume also via other mechanisms that are orthogonal to perfusion and furthermore, that fitness and perfusion changes may have also a direct influence on cognitive changes. There was no significant difference in fits for Models A and A', and thus the more parsimonious Model A is preferred over A'. Numbers are standardized path coefficients. Asterisks highlight significant paths (**p < .01). CF: *Complex Figure Test*. VLMT: *Verbal Learning and Memory Test*. This figure is adapted from Maass et al., 2014b.

The fit of the data to Model A was good (spatial object memory: $\chi^2(6) = 6.76$, CFI = .997, RMSEA = .056; verbal memory: $\chi 2(6) = 5.51$, CFI = 1, RMSEA = 0). All path coefficients in the model differed reliably from zero (see Figure 20a). Thus, a model in which fitness related-improvements in recognition memory are modulated by structural (volume) changes in the hippocampus provides a viable rendition of the observed data, with an estimated path coefficient from volume to memory of 0.46 and 0.41 for spatial object and verbal recognition memory, respectively.

Furthermore, it was examined whether adding direct paths from fitness to volume and memory and from perfusion to memory would improve the initial model (see Figure 20c). This Model A' enables the possibility that fitness can modulate hippocampal volume also via other mechanisms that are orthogonal to perfusion. Additionally, Model A' assumes that fitness and perfusion changes may have a direct influence on cognitive changes, that is effects that are not mediated by hippocampal structure or volume. Model A' did not result in statistically significant improvement in fit over Model A ($\chi^2\,\text{diff}(3)_{CF} = 4.11$ and $\chi^2\,\text{diff}(3)_{VLMT} = 2.86$, $p > .25$). Consequently, the more parsimonious Model A is favoured over Model A'. Furthermore, as highlighted in Figure 20c, neither the path from perfusion nor the path from volume to memory was reliably different from zero. This reflects the fact that perfusion is a strong mediator of volume changes in the hippocampus (and thus accounts for a large portion of the variance), both likely affecting hippocampal memory functions.

Finally, it was investigated whether a model in which memory benefits are directly linked to hippocampal perfusion would also provide a good account of our data (see Fig. Figure 20b). The alternative Model B predicts that increases in fitness lead to increases in perfusion, which result in improved recognition memory. Furthermore, this model includes a direct path from perfusion to hippocampal volume. According to this model, changes in perfusion are sufficient to account for changes in cognition, because hippocampal volume is predominantly determined by perfusion and does not reflect additional plastic processes that contribute to cognitive change. Model B yielded good fit (spatial object memory: $\chi^2(6) = 6.13$, CFI = .996, RMSEA = .023; verbal memory: $\chi^2(6) = 3.43$, CFI = 1, RMSEA = 0). Furthermore, the effect of perfusion on memory in Model B was significant (path coefficient = 0.48 and 0.49 for spatial and verbal recognition memory, respectively; see Figure 20b). Models A and B are not nested, therefore a direct statistical

comparison with a chi-square test is not possible. However, adding a direct path from volume to memory in Model B would not significantly improve the model fit (χ^2 diff(1)$_{CF}$ = 1.17 and χ^2 diff(1)$_{VLMT}$ = 0.89, p > .28). These findings suggest that there is no strong unique contribution of changes in hippocampal volume to changes in memory.

5.3.4 Analyses controlling for non-specific grey-matter changes

In order to test if the present findings could also be explained by more general, hippocampus-unspecific, changes in grey matter, SEM analyses were repeated for Model A and B after replacing hippocampal by non-hippocampal GM perfusion and hippocampal head volumes by whole-brain GM volumes. In addition, multiple regression analyses were performed (via FIML estimation), controlling for non-specific changes in GM.

Path models A and B, in which fitness related-changes in recognition memory are modulated by whole-brain structural and/or perfusion changes, did not yield acceptable fits to the data (CFI < .90, RMSEA > .08; see Hu and Bentler, 1999).

Furthermore, multiple regression analyses in which changes in CF or VLMT recognition memory were regressed on hippocampal and GM perfusion (allowing both to correlate) revealed a specific effect of hippocampal rCBF on CF recognition (r = 0.64, p = .048) and VLMT recognition (r = 0.88, p = .005) memory, respectively, with no significant correlation between non-hippocampal GM rCBF and memory (p > .15). Similarly, multiple regressions were run in which changes in cognition are explained by changes in hippocampal head and GM volumes (allowing both to correlate). Again, a significant relation between hippocampal head volumes and recognition memory in the CF Test was found (r = 0.37, p = .026) that was also marginally significant for the VLMT (r = 0.34, p = .057). However, in the same regression models whole-brain volumes and memory were not significantly related (p > .08). These results suggest that the benefits of fitness-related changes in perfusion and volume on recognition memory are mediated by the hippocampus rather than being a whole-brain effect.

5.4 Discussion

In a 3-month intervention trial with healthy old adults changes in fitness levels were positively associated with changes in hippocampal perfusion (rCBV, rCBF) and hippocampal head volumes. An increase in hippocampal rCBV has been previously reported in young/middle-aged adults (Pereira et al., 2007) and the current results indicate that the potential for exercise-induced increases in hippocampal perfusion is preserved in old age. Exercise-related improvements in perfusion among the older participants declined with age, suggesting that the capacity for vascular hippocampal plasticity may be age-dependent (for further discussion, see 6.3.1). Changes in hippocampal perfusion were closely linked to changes in hippocampal volume. An increase of hippocampal volume by 2% after 1-year exercise training and thus a reversing of age-related loss in volume has been demonstrated previously in old adults (Erickson et al., 2011). Similar to the findings from Erickson et al. (2011), the fitness-related changes in hippocampal volume observed here were restricted to the anterior hippocampus, i.e. the hippocampal head.

Hippocampal perfusion and volume changes were associated with benefits in configural object memory (early recall and recognition) and verbal memory (recognition). Delayed recall did not show any association with fitness, perfusion or volume changes (for further discussion, see 6.3.2). Path analysis was used to estimate whether the benefit of increased hippocampal perfusion for recognition memory was mediated by increased hippocampal volume or could also be accounted for by a direct influence of perfusion on memory (Figure 20). A model in which perfusion had a direct effect on memory yielded good fit to the data and was statistically parsimonious (Figure 20b). This suggests that hippocampal volume changes are predominantly determined by perfusion and do not reflect additional plastic processes that contribute to cognitive change (for further discussion, see 6.3.3).

Furthermore, there was a positive association between exercise-related changes in perfusion and early recall for configural spatial object memory, but not for verbal memory. In contrast, a previous study in young adults (Pereira et al., 2007) showed a correlation of hippocampal perfusion and early verbal recall (this study did not have a non-exercise control-group).

Such a dissociation could be related to fluctuations in serum cortisol levels as previous studies of memory in old age have shown a negative correlation between cortisol levels and verbal memory (Comijs et al., 2010). Indeed, it was also observed here that serum cortisol levels at baseline were negatively correlated with early verbal recall across the entire sample. Individuals who had high baseline levels of cortisol showed decreased levels post intervention, and this was associated with improved early verbal recall. Collectively, these data indicate that fluctuations in serum cortisol that are unrelated to the exercise intervention may have considerable impact on verbal memory and this impact may obscure the effects of (a short-lasting) exercise intervention in old age.

Finally, it was analysed whether changes in neurotrophic and angiogenic growth factors, which were measured before and after the intervention, were related to changes in hippocampal vascular or structural plasticity or memory. Animal models provide converging evidence for a key role of central and peripheral growth factors, most prominently BDNF, IGF-1, and VEGF, in mediating benefits of exercise on brain and cognition (see also 1.3.4). However, the role of these molecules in exercise-induced changes of human brain function, especially in old age, is still not clear. Previous intervention studies in healthy elderly subjects did not provide consistent evidence for an exercise-induced enhancement of these growth factors by chronic aerobic exercise (e.g. Erickson et al., 2011; Voss et al., 2013b; for reviews see Coelho et al., 2013; Vital et al., 2014). Although the 3-month training intervention performed here significantly increased fitness levels in the elderly participants, there was no effect on BDNF, VEGF, PDGF or IGF-1. Furthermore, fitness-related benefits in hippocampal perfusion and volume were also not related to changes of any of the aforementioned growth factors. The negative finding of any significant relation between the observed vascular hippocampal plasticity and the measured growth factors could suggest that increased perfusion might have benefited neural function independently of angiogenesis or neurogenesis (see 6.3.3 for detailed discussion). On the other hand, methodological limitations such as the relative small sample size or the restriction to pre and post intervention measures could have obscured any effect of growth factor on hippocampal plasticity.

6 General Discussion

6.1 Summary of findings

The findings presented in the current thesis advance our understanding of the functional organization of human long-term memory and its plasticity in old age. In the first two experiments, 7 Tesla ultra-high field functional and structural MRI was used to investigate the functional anatomy of the hippocampal-entorhinal memory network in young adults at the level of layers and subfields. Experiment 1 revealed a dissociation of novelty responses and successful encoding activation between in- and output regions of the HC-EC circuitry (Maass et al., 2014a). Moreover, Experiment 2 provided the first detailed topographic parcellation of the human EC into anterior-lateral (al-EC) and posterior-medial (pm-EC) subregions based on differential functional connectivity with PRC, PHC and the subiculum across its proximal-distal axis (Maass et al., 2015). Finally, Experiment 3 revealed the first evidence for a preserved capacity of the aged human hippocampus for functionally relevant vascular plasticity by means of very high-resolution structural MRI at 7T and Gadolinium-based perfusion imaging at 3T (Maass et al., 2014b).

The present results have not only implications for neurobiological theories of memory but also for our understanding of cognitive aging and age-related diseases as AD, as discussed in detail below (6.2). Furthermore, the current findings critically advance our understanding of the underlying mechanisms through which physical activity might enhance hippocampal plasticity and related memory functions in the aging brain (6.3). Finally, this thesis highlights the potential of 7T high-resolution imaging for studying memory function of the human MTL but also points to the challenges that high-field MRI poses (6.4).

6.2 The functional organization of the human entorhinal-hippocampal memory circuitry

6.2.1 Laminar dissociation of novelty processing and successful encoding

The current work makes the first step towards layer-specific imaging of the MTL memory circuitry in humans. High-resolution functional MRI during an incidental learning task revealed a differential engagement of hippocampal and entorhinal

input and output pathways regarding the processing of novel information and its subsequent memory. While *stimulus novelty* was relatively more related to activation of superficial EC and the DG/CA2-3 subfield of the hippocampus (i.e. input regions), *subsequent memory* in a later recognition test was best predicted by activation of pyramidal CA1 and deep EC (i.e. output regions). Moreover, activation in pyramidal CA1 predicted later recollection performance or high confidence recognition across subjects and was further correlated with activity in deep EC. These findings propose that the hippocampus receives input for novel items (signalled via superficial EC) but produces an output from CA1 preferentially for some of them (signalled via pyramidal CA1 and deep EC), namely those that are later remembered.

Increased CA1 pyramidal cell activity during novel experiences has been reported in the rodent hippocampus (see, e.g. Karlsson and Frank, 2008; Nitz and McNaughton, 2004). These findings are compatible with computational models according to which CA1 can act as a novelty detector (Hasselmo et al., 1996; Lisman and Grace, 2005; Lisman et al., 2011) by comparison of information stored in CA3/DG and direct perforant pathway inputs to CA1. However, such a comparator process in the hippocampus might be specifically critical for the detection of *associative* or *contextual novelty,* which relies on predictions and thus involves recall of previous experiences (for reviews see Kumaran and Maguire, 2007; Nyberg, 2005; Ranganath and Rainer, 2003). In contrast, generic novelty signals or *stimulus novelty* might not require CA1 and can be computed without the hippocampus. There is an extensive body of data suggesting that the PRC (and not the HC) is crucial and sufficient for discriminating familiar from novel items (e.g. Aggleton and Brown, 2005; Brown and Bashir, 2002). Regarding novelty responses for scenes (as used here), Howard et al. (2011) observed a double dissociation between hippocampal and PHC responses, with the PHC being engaged only by *scene novelty*, whereas the HC was selectively sensitive to changes in the spatial relationship between objects and their background context (i.e. associative novelty). As the hippocampus receives input from PHC and PRC about items and their spatial context, input regions of the HC-EC circuitry should be relatively more activated during the processing of novel than familiar information. In contrast, strong novelty responses in CA1 and output regions of the HC-EC circuitry might be expected for stimuli that are novel in a given context and

these mismatch signals in CA1 should facilitate long-term memory encoding. The present results are consistent with such hypotheses and indicate that CA1 is not acting as a generic novelty detector but generates novelty responses that are tightly linked to successful long-term encoding. This could be related to mismatch signals computed in CA1, for instance if after a sequence of familiar images an unpredicted novel occurs. Additionally, motivational aspects (e.g. whether an event behaviourally relevant) and salience (e.g. whether an event is emotionally arousing) might play a role as not all novel events may be of sufficient importance to enter into long-term memory (Lisman and Grace, 2005).

6.2.2 CA1 encoding activation predicts recollection

There is converging evidence that novelty encoding in the HC should primarily support the ability to later *recollect* associative information about the context and episodic details in with which a novel item was encountered, such as time and location (Eichenbaum et al., 2007; Fenker et al., 2008; Wittmann et al., 2007, but also see (Kishiyama and Yonelinas, 2003). A mere increase in *familiarity*-based recognition due to previous exposure can be preserved even after bilateral hippocampal lesions (Horner et al., 2012; Sauvage et al., 2008; Vargha-Khadem et al., 1997; Bowles et al., 2010), suggesting that familiarity per se does not critically depend on the hippocampus. Other studies suggest that familiarity also depends on the HC-EC circuitry (Smith et al., 2011; Squire et al., 2004; Wixted and Squire, 2010).

In Experiment 1, the strongest relationship of hippocampal subfield activity during encoding was found with later recollection (estimates from ROC curves) and high confidence memory scores, which were correlated with activation strength in CA1 pyramidal layers. There was no other hippocampal subfield or parahippocampal region, in which activation strength during encoding significantly correlated with later recollection. Furthermore, familiarity estimates did not show any significant correlation with hippocampal or parahippocampal activity measures (only a trending positive correlation with activation in PHC). Thus, the current findings further support the importance of the hippocampus in recollection-based recognition memory and further indicate that CA1 might be the critical subregion during episodic encoding of novel information that predicts later recollection.

6.2.3 Functional connectivity structure of the human entorhinal cortex

In addition to studying laminar activation profiles in EC and HC subfields during memory encoding, it was further assessed how hippocampal and neocortical connectivity with the EC is functionally organized in humans. While neuroanatomical studies have provided detailed knowledge about the functional organization of the EC in rodents and non-human primates (e.g. Kerr et al., 2007; Suzuki and Amaral, 1994; Witter et al., 2000a), almost nothing has been known before about the connectivity structure of the human EC. In addition to technical or methodological limitations of standard fMRI, as insufficient resolution and SNR, that challenge the study of EC subregions, the topographical framework for subdividing the EC had been missing.

Based on differential functional connectivity with PRC, PHC and subicular subregions, this work provides the first evidence that the human EC can be reliably subdivided into anterior-lateral (al-EC) and posterior-medial (pm-EC*)* subregions that may be critical nodes for cortico-hippocampal communication. Specifically, the al-EC showed stronger functional connectivity with PRC and proximal subiculum, whereas pm-EC showed higher connectivity with PHC and distal subiculum (see Figure 21 for schematic summary of findings). This topographical organization of connectivity is in remarkable accordance with anatomical principles known from rodents (PRC – LEC – proximal Sub. vs. POR – MEC – distal Sub.; see also Figure 1) and non-human primates (PRC – anterior-lateral EC – prox. Sub vs. PHC – posterior-medial EC – distal Sub.).

Further evidence for an anterolateral-posteromedial functional subdivision of the human EC comes from another high-resolution fMRI study (Navarro Schröder et al., 2015) that was conducted concurrently with the present investigations. Navarro Schröder and colleagues also examined the functional connectivity of the EC, but in contrast to the present study they differentiated EC subregions based on global network connectivity in resting state and task fMRI data (seeds were defined according to Libby et al, 2012). While al-EC exhibited stronger connectivity with regions in an anterior-temporal cortical system including medial-prefrontal and orbitofrontal cortex, the pm-EC exhibited stronger connectivity with regions in a posterior-medial system including regions in occipital and posterior-parietal cortex. Together these findings suggest that al-EC and pm-EC might be critical hubs within

two cortico-hippocampal networks that are thought to promote different types of memory, as discussed in the next chapter.

6.2.4 Implications of EC connectivity for differential memory processing

Two recent fMRI studies reported evidence for task-related activation differences between lateral and medial sections of EC in humans (Schultz et al., 2012; Reagh and Yassa, 2014). Schultz et al. (2012) found differential activation in medial and lateral sections of EC during scene and face processing in a working memory task. Reagh and Yassa (2014) reported preferential activation in the medial portion of EC during mnemonic discrimination of spatial locations and preferential activation in the lateral portion of EC during mnemonic discrimination of objects. This functional dissociation was observed by splitting the EC into equally-sized lateral and medial parts according to the rodent terminology of “LEC” and “MEC”. Notably, they also found a trend towards a dissociation between anterior and posterior EC after a similar equal division along the longitudinal axis, which is consistent with findings in monkeys (Killian et al., 2012; Suzuki and Amaral, 1994; Witter and Amaral, 1991).

The current data help to explain these findings by empirically demonstrating that al-EC and pm-EC exhibit differential functional connectivity with PRC and PHC. Numerous fMRI studies have shown that PHC is preferentially engaged in memory tasks that involve scenes or contextual information, whereas PRC is preferentially engaged in memory tasks that involve object information (see Ranganath and Ritchey, 2012 for review). This is in line with the “two streams” hypothesis which proposes that PRC processes information related to items (a “what” stream), whereas the PHC/POR processes spatial information (a “where” stream; see 1.3.1.1). Thus, it has been suggested that EC subregions that interact predominantly with PRC or PHC/POR also differentially participate in item/object and context/spatial processing. In contrast to this view, a lesion study in rodents has suggested that the MEC is also critical for non-spatial memory, in particular for recollection (see, e.g. Sauvage et al, 2010). Recent evidence for a functional dissociation between anterolateral and posteromedial EC comes also from the aforementioned study of Navarro Schröder et al. (2015). Analyses of task-related fMRI data revealed that al-EC activity was enhanced during processing of object information, whereas pm-EC activity was enhanced during processing of scenes.

In line with the studies described above, activation during the processing of scenes (novelty and subsequent memory related activation) in Experiment 1 was strongest in PHC and more medial regions of the EC. However, the current data do not allow to make strong inferences about object versus scene dissociations, as our stimulus material did only comprise images of scenes.

In summary, the current findings suggest that a simple lateral-medial distinction does not capture the functional organization of EC. Future fMRI studies (as well as structural MRI studies, e.g. Khan et al., 2014) could more effectively study the EC by using the high-consistency pm-EC and al-EC masks derived from our data (see also 4.3.2.4), or by using functional connectivity metrics to identify subject-specific EC subregions.

6.2.5 Dissociations along the longitudinal axis of the hippocampus

The current work also provides the first evidence for a proximal-distal dissociation of subicular connectivity with PRC vs. PHC, paralleling the differences of subicular connectivity with al-EC vs. pm-EC. However, in contrast to the functional EC subregions, only PRC and PHC seeds showed dissociable connectivity gradients along the longitudinal axis of the subiculum. These findings are consistent with anatomical data from rodents, in which LEC/MEC projections are diffusively organized along the entire anterior-posterior hippocampal axis, whereas direct PRC/POR projections only target a limited longitudinal extent (Agster and Burwell, 2013; Naber et al., 1999, 2001).

The existence of two parallel but topographically partly different neocortical-hippocampal circuits in humans, one that uses the EC as a gateway projecting to all subregions of the HC, and one that targets CA1 and subiculum directly, has important functional implications. While input from EC subdivisions to DG can reach CA1/subiculum indirectly after modulation or association with other cortical or subcortical inputs via the intrinsic hippocampal loop (e.g. Naber et al., 1999; Witter, 2006), CA1 and subiculum also receive a copy of the original information from PRC and PHC bypassing the DG. This organization might allow a comparison between EC gated hippocampal memory signals with direct neocortical input (e.g. Naber et al., 1999). Furthermore, the diffuse nature of LEC/MEC projections along the anterior-posterior hippocampal axis and a structured gradient of direct PRC/PHC projections could allow for both *segregation* and *integration* of

information across both processing streams. One further implication is that the topographic organization of the EC is not compatible with being a simple anatomical extension of the PRC and PHC. If that were the case, one would not have observed any dissociation from neocortical-hippocampal connectivity profiles. Evidence for a selective tuning of PRC to stimulus-type and not spatial demands (*segregatio*n), which was not present in LEC or MEC that were activated to a comparable level in spatial and non-spatial tasks (*integration*), comes from a recent study in mice (Beer et al., 2013). Thus, the current data suggest that there is intrinsic rewiring between pathways within the human EC adding support to the notion that the EC is more than a mere relay (e.g. de Curtis and Paré, 2004; Lavenex and Amaral, 2000).

Imaging studies in humans have provided extensive evidence for a functional dissociation along the longitudinal axis of the hippocampus (for a recent review see Poppenk et al., 2013) with a more prominent role of the anterior HC in motivational processing (including novelty), encoding and more global/coarse representations, and of the posterior HC in cognition, retrieval and local/detailed representations, respectively. In line with this proposed scheme, strongest activation during the encoding of novel information was found in the hippocampal head (anterior HC). However, later recollection, which relates to memory of specific details and fine-grained local representations, was best predicted by activation strength in CA1 pyramidal layers in the body (posterior part) of the HC. A similar finding has been recently made by Nakamura et al. (2015) in rodents, who showed that successful memory performance is predicted by encoding and reactivation patterns in the dorsal part of the rat hippocampus, which corresponds to the posterior hippocampus in humans. Regarding the type of stimulus being processed (object vs. scene) one might also expect differences along the long axis of the HC based on differential connectivity with PHC vs. PHC. However, in the current data (Exp.1) overall activation during scene processing was most prominent in the anterior hippocampus, which would not support such dissociation. Nevertheless, as mentioned previously, strong inferences about scene vs. object dissociations cannot be made as the stimuli used here only comprised images of scenes.

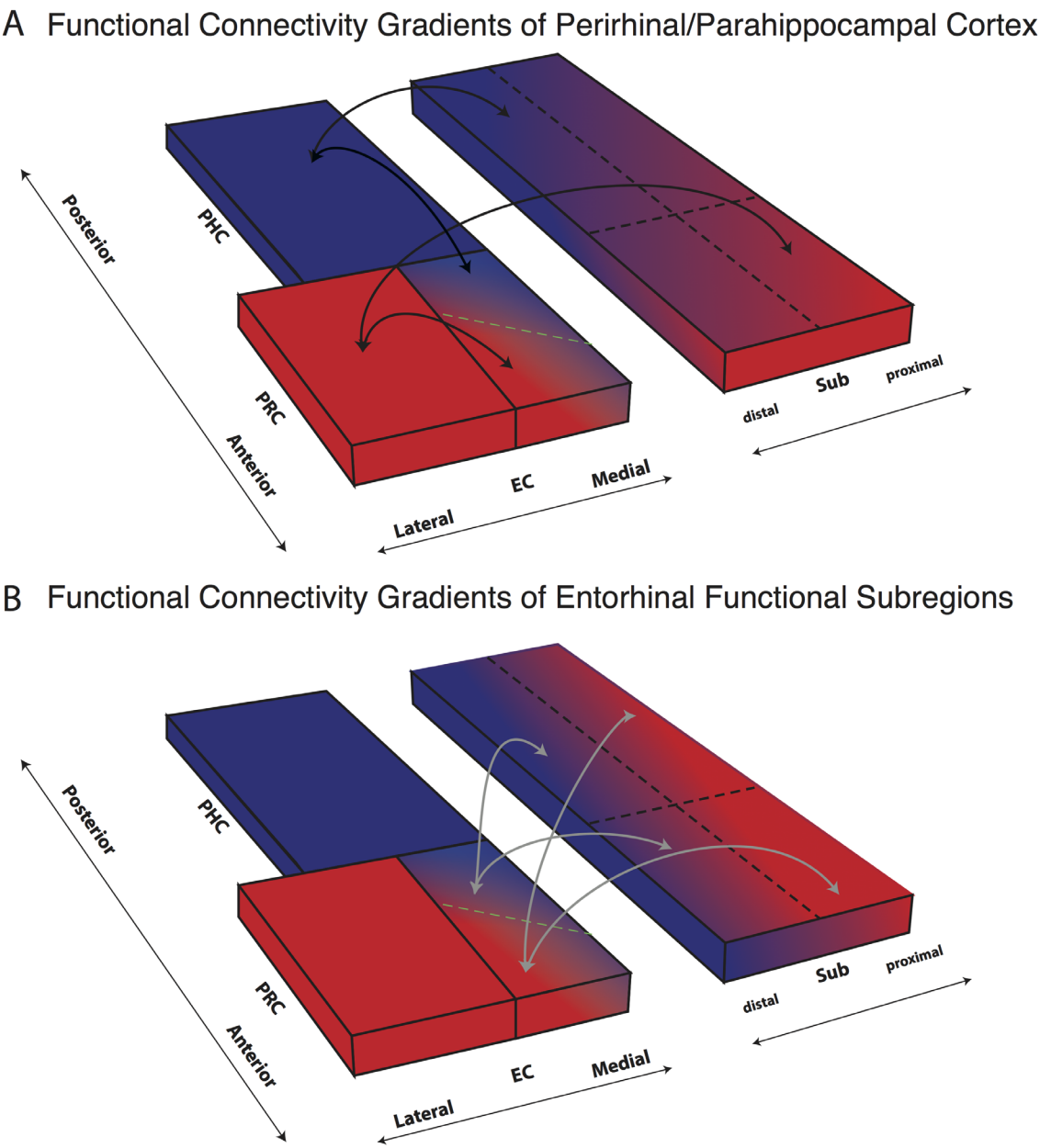

Figure 21. Schematic summary of functional connectivity gradients in the subiculum related to PRC/PHC seeds and EC subdivisions.

A. Functional connectivity analyses revealed preferential connectivity of PRC (red) with the anterior-lateral EC and PHC (blue) with the posterior-medial EC. Regarding the subiculum, PRC showed strongest connectivity with most anterior and more proximal parts, whereas PHC showed strongest connectivity with most posterior and more distal parts of the subiculum. **B.** Anterior-lateral (red) and posterior-medial (blue) EC exhibited a similar dissociation in connectivity with the subiculum along its transverse (proximal-distal) axis but there was no trend for a dissociation of entorhinal connectivity along the longitudinal axis of the subiculum. This figure is taken from Maass et al., 2015.

6.2.6 Implications for aging and disease

Neuropathological studies indicate that neurofibrillary changes associated with AD start in the transentorhinal cortex (corresponding to Stage I), subsequently extending medially into layer II of the lateral entorhinal cortex (Stage II) before proceeding to the hippocampus and temporal neocortex (Braak and Braak, 1985, 1991; Braak et al., 2006; Gómez-Isla et al., 1996). An early functional impairment – apparent as reduced regional CBV – of lateral EC portions, the adjacent transentorhinal region and PRC has been recently reported in preclinical AD patients (Khan et al., 2014).

The functional connectivity analyses performed in Experiment 2 revealed that anterior-lateral EC regions were predominately functionally connected with the PRC as part of the anterior-temporal memory system (Ranganath and Ritchey, 2012; see also Navarro Schröder et al., 2015). This proposes that very early stages of taupathology might specifically affect or alter functional connectivity between PRC, anterior-lateral EC and regions of the anterior-temporal system. This could be also associated with difficulties in complex object discrimination or impaired object recognition memory and related changes in task activation (e.g. in a task that taxes pattern separation). Braak stages I and II are generally considered as silent, preclinical stages (e.g. Delacourte et al., 2002; Price and Morris, 1999), in which standard neuropsychological tests used in clinical trials usually not indicate any memory deficits. However, these tests do not directly compare object with spatial episodic memory, which might increase their sensitivity. As neurofibrillary tangles in the MTL are common by late middle age (occurring in more than 60% of individuals aged 60 and above; see, e.g. Schultz et al., 2004), changes in PRC-anterior-lateral EC connectivity and reduced performance in object/item-specific mnemonic tasks might be similarly found in normal or “healthy” aging.

In the course of AD (and with progressing age) taupathology further propagates to more medial parts of the EC and to the hippocampus (Stage II-III), probably via transsynaptic spread along anatomically connected networks (de Calignon et al., 2012; Liu et al., 2012). The apical dendrites of hippocampal CA1 pyramidal neurons in SRLM are among the first targets of hippocampal pathology. This might

be associated with initial mild clinical symptoms (e.g. Kerchner et al., 2012) that could involve both impaired object/item and spatial/contextual memory.

In the progression of AD, when neocortical Abeta deposition begins, tau spreads outside the MTL and also affects neocortical areas. When Abeta is deposited, it is almost invariably found in the posterior cingulate and retrosplenial cortex (e.g. Buckner et al., 2005). A resulting loss of hippocampal/neocortical connectivity in this posterior memory network might lead to a more severe memory loss in AD patients that could now affect more prominently the recollection of contextual or spatial details. A decline in spatial navigation ability has been shown to occur in early AD (but not semantic dementia, see Pengas et al., 2010b). Furthermore, visual perception studies by Lee and colleagues revealed specific deficits of AD patients in spatial scene but not face discrimination (Lee et al., 2006, 2007). Evidence for a worsening of deficits in spatial memory but not item recognition from MCI to AD comes from a study by Dudas et al. (2005) that reported significant deficits of AD patients and MCI subjects in person naming, item recognition and recall of spatial location (placing), but an enhanced impairment in the placing component for the AD compared to MCI patients (Dudas et al., 2005).

To summarize, the current analyses of functional connectivity can potentially help to understand how EC degeneration in the early stages of AD impacts the functional organization of distributed cortical networks (La Joie et al., 2014; Khan et al., 2014) and could also shed light on the transsynaptic progression of AD pathology. The present work provides a foundation for the development of functional biomarkers for the early detection of Alzheimer's disease and for tracking of disease progression.

6.3 Vascular plasticity of the aged hippocampus

6.3.1 Age-dependence

Fitness benefits after a 3-month training intervention with healthy aged adults were positively associated with changes in hippocampal perfusion. This proposes that the capacity of the hippocampus for exercise-induced vascular plasticity is preserved in old age. However, among the elderly individuals, observed perfusion changes were negatively related to age. Whereas the younger individuals

(between 60 and 70 years) tended towards perfusion increases as a result of exercise, older individuals tended towards decreases.

A similar pattern has been reported by animal studies, where the exercise-related potential for neurogenesis and angiogenesis in old mice was reduced or even absent. For instance, van Praag et al. (2005) found a significant increase in DG blood vessel surface area and perimeter (no change in blood vessel number) after wheel running in young but not aged mice, with the latter showing also less increase in neurogenesis after exercise. Creer et al. (2010) observed a significant increase in DG angiogenesis (i.e. blood vessel density) and neurogenesis in adult running mice but no change in vasculature or neurogenesis in very aged runners.

It remains unclear why the potential for vascular plasticity after exercise tends to decline with progressing age. One source of variability contributing to this decline may be amyloid deposition, which can occur in around 20% of apparently healthy older adults (for reviews see Jack et al., 2010; Jagust, 2013) and may have negative impact on neural metabolism and plasticity (Bomfim et al., 2012). Another possibility is that reduced IGF-1 (Sonntag et al., 1997) and VEGF levels (Shetty et al., 2005) or stress-related increases in cortisol levels (Ekstrand et al., 2008) in old age have a negative influence on neurovascular plasticity. However, the current data did not reveal any correlation between cortisol levels and age and also no negative relationship between cortisol levels at baseline or changes in cortisol and perfusion changes (there was rather a positive relation of cortisol levels and changes in perfusion). Furthermore, VEGF baseline levels were not related to age and VEGF baseline levels or changes were also not correlated with perfusion changes. Regarding IGF-1 and IGF-BP3 baseline levels, there was a negative relationship with age. However, levels of IGF-1 or IGF-BP3 did also not predict perfusion changes.

The age-independent sources of interindividual variability that causes increases in perfusion in some individuals who show increased fitness, but not in others are also unclear. One factor that needs to be addressed in studies with larger sample sizes is that carriers of the APOE4 allele may show different benefit from exercise (Podewils et al., 2005; Raichlen and Alexander, 2014).

6.3.2 Effects on memory

A further question that was addressed in Experiment 3 is to what extent the effects of exercise on memory in old age depend on modality (verbal versus visuospatial), retrieval demands (recall versus recognition) and delay (early versus late).

There is converging evidence from animal studies that exercise can induce neurogenesis in the adult DG, which in turn is associated with improved performance in tasks that rely on pattern separation or relational binding (Creer et al., 2010; Voss et al., 2013a). Furthermore, newly born granular cells in the DG preferentially receive projections from PRC and LEC (Vivar and Van Praag, 2013), regions that critical for complex object recognition memory and object pattern separation. Performance in the same tasks seems to decline early in old age (see 1.3.2). In contrast, PHC and MEC convey information about spatial layouts and presumably aid context recall (Eichenbaum and Lipton, 2008; Eichenbaum et al., 2012; Sauvage et al., 2010). This suggests that aerobic exercise predominantly benefits discrimination of and memory for similar objects or relations between objects.

In the present study, effects of exercise and improved fitness on episodic memory were examined by two tasks, a verbal (VLMT) and a visual object memory test (CF Test), with the latter posing particularly high demands on pattern separation. Across subjects increases in fitness, HC perfusion and HH volumes were related to benefits in early recall and recognition memory for configural objects (CF Test). Similarly, there was a benefit in recognition memory for words (VLMT). Intriguingly, the VLMT recognition trial also requires discrimination between highly similar items, i.e. between semantically or phonetically related lure versus target words. Thus, also this latter verbal recognition test relies on distinct memory representations and poses high demands on DG pattern separation. Together, these findings are consistent with the exercise-induced neurogenic connectivity observed in mice. In addition, the current results suggest that exercise-related benefits in memory of older adults are not restricted to verbal or visuospatial modality. However, fitness-related changes in hippocampal plasticity did only benefit early recall and recognition memory and not late recall. One possible explanation is that tests of early recall and recognition memory more strongly depend on the DG, whereas for delayed recall, which was not affected by exercise, other medial temporal regions,

such as the parahippocampal cortex or EC, or even higher neocortical areas may play a greater role. For instance, Brickman and colleagues found that recognition memory in the *Benton Visual Retention Tes*t is specifically correlated with basal hippocampal metabolism (rCBV) in the DG (Brickman et al., 2011). In this memory test subjects are briefly shown a visual pattern and subsequently asked to identify the pattern they saw among three other novel patterns, which also poses high demands on pattern separation. In contrast, delayed retention in the *Selective Reminding Test*, a verbal memory test in which subjects are asked to freely recall words after a 15-min delay, was associated with basal perfusion in the EC. Moreover, an fMRI study in young adults on repetitive learning and recall of geometric patterns (Grön et al., 2001) revealed anterior hippocampal activity during conditions of initial learning, whereas activity during delayed recall did not reveal hippocampal responses but was characterized by a transition of neural activity to bilateral temporal cortices. This could be explained by a process of *consolidation* (Alvarez and Squire, 1994), which is the gradual establishment of long-term memories in other neocortical areas of the brain and the gradual independence from the hippocampus.

6.3.3 Underlying mechanisms

Fitness-related increases in perfusion could be mediated by exercise-induced angiogenesis, which is tightly coupled to neurogenesis (Louissaint et al., 2002; Palmer et al., 2000; Pereira et al., 2007). Supporting evidence for a link between exercise-induced increases in DG rCBV measured by Gadolinium-based perfusion imaging and neurogenesis has been provided by a previous study in mice (Pereira et al., 2007). However, angiogenic effects of increased fitness could also be uncoupled from neurogenesis and relate to plasticity of mature neurons (Licht et al., 2011).

While there were significant relationships between increases in fitness, hippocampal perfusion and hippocampal head volumes, subfield specific analyses (restricted to the body of the HC where subfields could be reliably distinguished) did not yield evidence for a specific effect on DG. In contrast, Pereira et al. (2007) did only found an exercise-induced increase in DG rCBV. Furthermore, changes in hippocampal perfusion observed here were closely linked to changes in hippocampal volume. A direct link of volumetric increases to perfusion could be

due to increased vascularization. In addition, volumetric increases could reflect subsequent cell proliferation (e.g. neurogenesis), synaptogenesis, and dendritic branching, which one would expect to be the best predictor for HC-dependent memory benefits. Nevertheless, path analyses did not support a strong additional contribution of HC volume changes to benefits in configural object or verbal recognition memory, which suggests that perfusion increases might have directly benefited neural function.

Indeed, there are a number of mechanisms through which increased perfusion could be associated with improved neuronal function. Increased hippocampal perfusion can improve the supply of oxygen and nutrients to hippocampal neurons. Furthermore, benefits of chronic or regular exercise on cognition might be related to its anti-inflammatory effects, e.g. by the reduction of inflammatory cytokines as IL1-beta or TNF-alpha that both impair growth factor signalling (for reviews see Cotman et al., 2007; Petersen and Pedersen, 2005). Moreover, exercise-induced increases in IGF-1 and VEGF– both growth factors with angiogenic actions – in cooperation with BDNF can improve hippocampus-dependent memory by modulating synaptic plasticity, synapse density and neurotransmission (aside from stimulating neurogenesis; for reviews see, e.g. Cotman et al., 2007; Fernandez and Torres-Alemán, 2012; Licht et al., 2011; Neeper et al., 1995).

Nevertheless, the current data did not support any effect of exercise or increased fitness on IGF-1, VEGF, BDNF or PDGF. Although fitness changes in the elderly participants were strongly correlated with hippocampal perfusion, which seemed to have mediated benefits in hippocampus-dependent memory, there was no relation between fitness or perfusion changes with changes in VEGF or IGF-1. This was the case although baseline VEGF levels were positively associated with perfusion levels. Correlational analyses did also not reveal any significant association between changes in serum or plasma BDNF neither with fitness or perfusion nor with hippocampal volumes.

Although fitness and perfusion benefits were not related to increases in IGF-1, hippocampal volume changes (whole HC and HH) were strongly correlated with IGF-1 changes across the entire cohort, particularly in the control group. Interestingly, these changes in IGF-1 were also positively related to late recall performance in the VLMT. This cognitive measure was also not affected by

increased fitness or fitness-related perfusion benefits, which suggest that the positive relationship between IGF-1 and late verbal recall was independent of fitness. A direct relationship between IGF-I and cognition has been derived from animal experiments which showed that administration of IGF-I can restore cognition in aging animals (Trejo et al., 2007).

A lack of exercise-induced increases in VEGF, BDNF and IGF-1 in healthy old adults has been also reported by previous exercise studies (e.g. Erickson et al., 2011; Voss et al., 2013b; for reviews see Coelho et al., 2013; Vital et al., 2014). For instance, Voss et al. (2013b) did not find any group difference in change of BDNF, VEGF or IGF-1 between the aerobic walking and non-aerobic stretching control group after 1-year training. Similar to their study, the present measures are limited to pre and post exercise time points. However, effects of exercise on growth factor levels might be fast and transient (e.g. Rojas Vega et al., 2006), in contrast to vascular and structural hippocampal changes that might occur later and be more long-lasting. Future studies should thus also consider the dynamics or time course of exercise-induced plasticity by assessing short-term and long-term measures of growth factors, perfusion, volume and memory.

6.4 The potential and challenge of 7T high-field imaging

The high SNR of MRI data collected at 7T enables to acquire BOLD fMRI data at an unprecedented level of anatomical detail. While high-resolution fMRI studies at 3T scanners have measured activation in the MTL with resolutions up to 1.5 mm^3 isotropic (Bakker et al., 2008; Bonnici et al., 2012; Duncan et al., 2012), fMRI data in the experiments presented here (Exp.1-2) have been acquired with a functional resolution of 0.8 mm^3 isotropic voxels. The present results demonstrate that the enhanced resolution of ultra-high field fMRI enables to study laminar and subfield activity patterns and revealed fine-grained topographical patterns in connectivity. Thus, ultra-high field fMRI opens up new opportunities in studying pathway-related hypotheses in the MTL that require functional resolution in the submillimetre range.

Nevertheless, the advantages that ultra-high field imaging provide are not without its additional challenges. Problems of distortion and susceptibility artefacts in echo planar imaging are caused by non-uniformities in the static magnetic field (B_0) and become more severe with higher field strengths. In particular the anterior MTL regions, such as EC and PRC, are often affected by susceptibility artefacts and

thus dropouts due to their proximity to bone and air-filled sinuses (Ojemann et al., 1997; Olman et al., 2009). These problems are not only prominent in functional but also in structural T2*-weighted imaging such as used here (see Exp.1) for subfield/layer segmentation.

An optimized 7T protocol can reduce these signal dropouts and distortions, e.g. by the use of very small voxel sizes, fast imaging techniques (e.g. parallel imaging), zoomed field-of-view, shorter echo times as well as optimized shimming and distortion correction. In the present 7T protocol, for instance, the very small functional voxel size (0.8 mm^3 isotropic) minimizes the problem of intra-voxel dephasing (at cost of SNR) and in combination with optimized image orientation, parallel imaging for fast readout (grappa factor 4) and short TE (22 ms), spatial distortions and signal loss are reduced. Moreover, an advanced distortion correction method based on a point spread function (PSF) mapping method (In and Speck, 2012; Zaitsev et al., 2004) was used here, which corrects geometric distortions in EPIs with high accuracy and quality. This distortion correction is performed during the online reconstruction.

However, susceptibly artefacts and distortions cannot be fully eliminated and have thus still affected EC and PRC subregions in the current data (see also Figure S 1). The severity of distortions was highly variable across subjects and slices. Two subjects, for instance, had to be fully excluded from the analyses in Experiment 1 due to strong artefacts in the functional data. As the PRC was most prominently affected by dropouts, additional 5 subjects were excluded from the same data set in Experiment 2 (PRC was the seed for functional connectivity analyses). Moreover, in the remaining subjects EPI slices with strong dropouts were discarded manually from the subject-specific EC and PRC ROIs (Exp.1/2). Additionally, mean signal in each PRC mask voxel was calculated in Experiment 2 and voxels with low signal automatically excluded from the PRC seed masks (see 4.2.4). Posterior PHG regions as the PHC were almost free from artefacts and dropouts. Similarly the hippocampus was only little affected by artefacts, which, if they occurred, were only found in the very anterior head.

A second issue that becomes even more important with high-resolution fMRI, which aims to resolve small subregions, is the correction of subject motion (within the functional scanning and between functional and structural scans). Head motion

can be corrected in image space, but displacements of the head also reduce the homogeneity of the magnetic field, which can lead to distortions. Moreover, motion can produce artefactual activations. In the current data, motion correction was performed during scanner online reconstruction as part of the distortion correction procedure. Motion artefacts were most obvious on the structural high-resolution T2*-weighted images (0.33 x 0.33 mm^2 in plane resolution; 12 min scan duration), particular in very anterior slices (see Supplementary Figure S 6a). T2*-weighted imaging were chosen for layer/subfield segmentation in Experiment 1 because it provides a very good contrast of the SRLM (apical CA1 layers; see Figure 4). However, as the T2*-weighted images were also highly prone to susceptibility and motion artefacts, T2-weighted structural imaging will be preferred in future studies (see Supplementary Figure S 6b).

To extract layer/subfield-specific activation from the manually defined anatomical masks, a precise overlay of structural on functional scans is of uppermost importance. EC layers were approximately 1-2 functional voxels thick and thus one millimetre movement between scans could fully displace one layer to another. A precise coregistration of structural and functional images is challenging as EPIs are usually partial images that only cover a small portion of the brain. Although our structural T2*-weighted images have the same contrast as the EPIs, they are also partial images oriented orthogonally – and not as the EPIs longitudinally – to the HC long axis, which results in a very small overlap. Coregistration of the structural and functional T2* images (if necessary at all) was automatically performed with SPM or, in case of failure, manually with SPM (via “Check Reg: Reorient image(s)”). Also challenging is the coregistration between partial T2*-weighted images (EPIs or structural) and the whole brain T1-weighted images. For alignment of the individual T1-weighted images to the EPIs “epi_reg” was used (FLIRT v6.0; Jenkinson and Smith, 2001), a program that was specifically written to register EPI images to structural images. Finally, registration was checked and in case of failure images were manually aligned with SPM (as above). Finally, overlap of anatomical masks, which were drawn on the T2* images in Experiment 1 and the T1-weighted images in Experiment 2, on the mean EPIs was examined and segmentation manually corrected in case of misalignment (note that inaccurate fit of masks could also be due to different distortions). For future studies, acquisition of a whole-head EPI would be useful as registration intermediate between the partial EPIs and the

whole brain T1-structural image (see, e.g. Limbrick-Oldfield et al., 2012 for four-step registration approach of the midbrain). Furthermore, segmentation might be even directly performed on the high-resolution EPIs if image quality and resolution is sufficient.

Finally, normalization into a standard space, which is usually done to allow group comparisons, poses similar difficulties in high-resolution imaging, specifically if hippocampal subfields are studied, which exhibit a complex anatomy and high inter-subject variability. To do so, an advanced normalization procedure (ROI-ANTS; see 2.3) was used here, which comprised a landmark-based normalization on a group-specific high-resolution template. Moreover, normalization-based group comparisons require smoothing, which "improves" inter-subject alignment by blurring residual anatomical differences and which can reduce random noise. In Experiment 1, two different smoothing kernels (FWHM: 1.5 mm < 2 $\times$ voxel size and 2.4 mm = 3 $\times$ voxel size) were applied in order to assess activations from the perspectives of either higher specificity (smoothing with 1.5 mm) or higher sensitivity (smoothing with 2.4 mm). However, for evaluating functional differences between entorhinal and hippocampal layers, regions of interest were manually defined and a novel decoding approach was chosen (Multivariate Bayes; see 3.2.7.2) that enables to use the individual (raw) functional data to achieve highest anatomical precision.

6.5 Future directions and Outlook

The present work demonstrates the feasibility of studying layer-specific memory processing by means of 7T high-resolution fMRI in young adults non-invasively across the HC-EC circuitry. This approach paves the way for studies that target pathway-specific hypotheses or neurocomputational models by incorporating anatomical directionality. While in Experiment 1 encoding-related activation of novel scenes and subsequent memory effects in hippocampal and entorhinal input and output regions were studied, subsequent experiments could use laminar imaging to directly test models of novelty detection (e.g. Kumaran and Maguire, 2007; Lisman and Grace, 2005). As CA1 is thought to be the crucial region for the detection of associative or contextual novelty generating mismatch signals when prior predictions are violated, future experiments could assess layer- and subfield-specific activation during a task designed to evoke such match-mismatch

responses (Kumaran and Maguire, 2006, 2007). In this respect, it would be also interesting to assess how SN/VTA activation is related to activity in apical CA1 layers, the potential target of DA fibres, during novelty detection and how this relates to subsequent memory (see, e.g. Duncan et al., 2014).

The present work may be also pertinent to understanding memory impairments in clinical conditions that compromise the structural integrity of the medial temporal lobes, such as AD or semantic dementia, but also memory impairments that come with “normal” aging. Cognitive aging is often associated with a reduced ability to encode novel events into long-term memory and animal models suggest that these deficits might arise from reduced pattern separation in DG due to deteriorated perforant pathway input from superficial EC layers (see, e.g. Wilson et al., 2006). Although recent 3T fMRI studies made substantial progress in studying subfield-specific activity in young and older adults during tasks that pose high demands on pattern separation (Bakker et al., 2008; Yassa et al., 2010b, 2011), these were not able to distinguish DG from CA3 or input from output layers. High-resolution studies at 7T could further disentangle how pattern separation deficits in old age are related to alterations in subfield activation or in functional connectivity between superficial EC and DG vs. CA3.

The EC is also the first site of taupathology in early stages of AD and downstream effects of EC pathology are anatomically directed (de Calignon et al., 2012; Liu et al., 2012). There is considerable clinical interest in understanding how EC degeneration in the early stages of AD impacts on functional network organization (La Joie et al., 2014; Khan et al., 2014) and also in understanding the functional consequences of transsynaptic progression of AD pathology. Intriguingly, lateral EC regions and the transition zone between EC and PRC show the earliest taupathology in AD. High-field fMRI at 7 Tesla could be used to identify early EC dysfunction by intrinsic connectivity measures that might be altered already in preclinical stages of the disease. In this respect, it would be of critical relevance to relate changes in functional connectivity or in BOLD activity to the severity of tau and amyloid deposition. Future studies that combine amyloid and tau PET imaging with high-resolution fMRI would critically advance our understanding of the neurobiological mechanisms that drive episodic memory decline in aging and dementia. Thereby, it would be also important to assess longitudinal changes in EC connectivity along different stages of the disease and if these are related to

differential impairment in item/object vs. context/scene memory (e.g. in task that tax pattern separation). In addition, future studies should also examine how entorhinal and hippocampal connectivity with posterior cingulate and retrosplenial cortices is organized in humans and how this connectivity is altered in preclinical AD, as these regions are also among the earliest sites of AD-related dysfunction (e.g. Buckner et al., 2005; Pengas et al., 2010a).

In order to use functional and structural measures derived by very high-resolution MRI as preclinical marker in aging and disease, adequate motion and distortion correction and more efficient scanning protocols are of utmost importance. Older people have a much higher tendency to move and thus motion artefacts become even more severe. In this respect, prospective motion correction is a promising method which addresses this problem by tracking the head motion and by real-time adjustment of the scanner pulse sequence such that the imaging volume follows the head motion (Maclaren et al., 2012).

The present work further highlights the potential of physical exercise as lifestyle intervention that could slow or prevent age-associated memory decline (Grady, 2012; Podewils et al., 2005; Yaffe et al., 2001). In line with previous findings in young adults, Experiment 3 revealed that a hallmark of the effects of aerobic exercise on memory is to induce vascular plasticity in the hippocampus. In this respect, animal models point towards the importance of exercise-induced angiogenesis for subsequent benefits in cognition. Although Gadolinium-based measures of perfusion, which were assessed here, are sensitive to increases in capillaries and thereby likely detect effects on angiogenesis, blood flow could also increase independent of new vessel formation. In particular, MR angiography (MRA) at high fields may reveal estimates of exercise-induced changes in vessel numbers, the radius of vessels, and their tortuosity. Encouraging results have been provided by a cross-sectional MRA study in 14 older adults that found significant reductions in vessel tortuosity and an increased number of small vessels in aerobically active subjects compared with less active subjects (Bullitt et al., 2009). Future intervention studies should incorporate MRA to assess the effects of exercise on the cerebral vasculature.

Furthermore, it remains to be established whether more long-lasting interventions, particularly when combined with cognitive stimulation such as novelty (Düzel et al.,

2010) and navigation (Lövdén et al., 2012), would lead to broader cognitive benefits that extend also to delayed free recall. Although the current findings are encouraging towards developing clinical interventions to promote healthy aging and prevent cognitive decline, it is also evident that considerable research efforts are necessary to understand the pathophysiological and genetic causes of individual variability in neurovascular plasticity. Studies with larger sample sizes should further address the impact of amyloid deposition and APOE4 status on the effects of exercise on vascular plasticity and cognition (Podewils et al., 2005; Raichlen and Alexander, 2014). Furthermore, future intervention studies should also assess more short-term effects of exercise on angiogenic and neurogenic growth factor, perfusion, structure and cognition (in addition to post exercise measure) to track the time course of neurovascular plasticity.

7 References

Adams, R.H., and Alitalo, K. (2007). Molecular regulation of angiogenesis and lymphangiogenesis. Nat. Rev. Mol. Cell Biol. *8*, 464–478.

Aggleton, J.P., and Brown, M.W. (1999). Episodic memory, amnesia, and the hippocampal-anterior thalamic axis. Behav. Brain Sci. *22*, 425–444; discussion 444–489.

Aggleton, J.P., and Brown, M.W. (2005). Contrasting hippocampal and perirhinal cortex function using immediate early gene imaging. Q. J. Exp. Psychol. B *58*, 218–233.

Agster, K.L., and Burwell, R.D. (2013). Hippocampal and subicular efferents and afferents of the perirhinal, postrhinal, and entorhinal cortices of the rat. Behav. Brain Res. *254*, 50–64.

Ainsworth, B.E., Haskell, W.L., Whitt, M.C., Irwin, M.L., Swartz, A.M., Strath, S.J., O'Brien, W.L., Bassett, D.R., Schmitz, K.H., Emplaincourt, P.O., et al. (2000). Compendium of physical activities: an update of activity codes and MET intensities. Med. Sci. Sports Exerc. *32*, S498–S504.

Alvarez, P., and Squire, L.R. (1994). Memory consolidation and the medial temporal lobe: a simple network model. Proc Natl Acad Sci U S A *91*, 7041–7045.

Augustinack, J.C., van der Kouwe, A.J.W., Blackwell, M.L., Salat, D.H., Wiggins, C.J., Frosch, M.P., Wiggins, G.C., Potthast, A., Wald, L.L., and Fischl, B.R. (2005). Detection of entorhinal layer II using 7Tesla [corrected] magnetic resonance imaging. Ann. Neurol. *57*, 489–494.

Avants, B.B., Yushkevich, P., Pluta, J., Minkoff, D., Korczykowski, M., Detre, J., and Gee, J.C. (2010). The optimal template effect in hippocampus studies of diseased populations. NeuroImage *49*, 2457–2466.

Avants, B.B., Tustison, N.J., Song, G., Cook, P.A., Klein, A., and Gee, J.C. (2011). A reproducible evaluation of ANTs similarity metric performance in brain image registration. NeuroImage *54*, 2033–2044.

Bakker, A., Kirwan, C.B., Miller, M., and Stark, C.E.L. (2008). Pattern Separation in the Human Hippocampal CA3 and Dentate Gyrus. Science *319*, 1640–1642.

Bandettini, P.A., and Wong, E.C. (1997). Magnetic resonance imaging of human brain function. Principles, practicalities, and possibilities. Neurosurg. Clin. N. Am. *8*, 345–371.

Bannerman, D.M., Rawlins, J.N.P., McHugh, S.B., Deacon, R.M.J., Yee, B.K., Bast, T., Zhang, W.-N., Pothuizen, H.H.J., and Feldon, J. (2004). Regional dissociations within the hippocampus--memory and anxiety. Neurosci. Biobehav. Rev. *28*, 273–283.

Barense, M.D., Groen, I.I.A., Lee, A.C.H., Yeung, L.-K., Brady, S.M., Gregori, M., Kapur, N., Bussey, T.J., Saksida, L.M., and Henson, R.N.A. (2012). Intact memory for irrelevant information impairs perception in amnesia. Neuron *75*, 157–167.

Bartko, S.J., Winters, B.D., Cowell, R.A., Saksida, L.M., and Bussey, T.J. (2007). Perceptual functions of perirhinal cortex in rats: zero-delay object recognition and simultaneous oddity discriminations. J. Neurosci. Off. J. Soc. Neurosci. *27*, 2548–2559.

Beaver, W.L., Wasserman, K., and Whipp, B.J. (1986). A new method for detecting anaerobic threshold by gas exchange. J. Appl. Physiol. Bethesda Md 1985 *60*, 2020–2027.

Beck AT, Steer RA, Beck GK B. (1996). Depression Inventory. 2nd edn. Manual San Antonio: The Psychological Corporation.

Beer, Z., Chwiesko, C., Kitsukawa, T., and Sauvage, M.M. (2013). Spatial and stimulus-type tuning in the LEC, MEC, POR, PrC, CA1, and CA3 during spontaneous item recognition memory. Hippocampus *23*, 1425–1438.

Bomfim, T.R., Forny-Germano, L., Sathler, L.B., Brito-Moreira, J., Houzel, J.-C., Decker, H., Silverman, M.A., Kazi, H., Melo, H.M., McClean, P.L., et al. (2012). An anti-diabetes agent protects the mouse brain from defective insulin signaling caused by Alzheimer's disease- associated Aβ oligomers. J. Clin. Invest. *122*, 1339–1353.

Bonnici, H.M., Chadwick, M.J., Kumaran, D., Hassabis, D., Weiskopf, N., and Maguire, E.A. (2012). Multi-voxel pattern analysis in human hippocampal subfields. Front. Hum. Neurosci. *6*, 290.

Bonnici, H.M., Sidhu, M., Chadwick, M.J., Duncan, J.S., and Maguire, E.A. (2013). Assessing hippocampal functional reserve in temporal lobe epilepsy: A multi-voxel pattern analysis of fMRI data. Epilepsy Res.

Booth, M.L., Owen, N., Bauman, A.E., and Gore, C.J. (1996). Retest reliability of recall measures of leisure-time physical activity in Australian adults. Int. J. Epidemiol. *25*, 153–159.

Borg, G. (1998). Borg's Perceived Exertion and Pain Scales (Human Kinetics).

Boss, B.D., Peterson, G.M., and Cowan, W.M. (1985). On the number of neurons in the dentate gyrus of the rat. Brain Res. *338*, 144–150.

Bowles, B., Crupi, C., Pigott, S., Parrent, A., Wiebe, S., Janzen, L., and Köhler, S. (2010). Double dissociation of selective recollection and familiarity impairments following two different surgical treatments for temporal-lobe epilepsy. Neuropsychologia *48*, 2640–2647.

Braak, E., and Braak, H. (1997a). Alzheimer's disease: transiently developing dendritic changes in pyramidal cells of sector CA1 of the Ammon's horn. Acta Neuropathol. (Berl.) *93*, 323–325.

Braak, H., and Braak, E. (1985). On areas of transition between entorhinal allocortex and temporal isocortex in the human brain. Normal morphology and lamina-specific pathology in Alzheimer's disease. Acta Neuropathol. (Berl.) *68*, 325–332.

Braak, H., and Braak, E. (1991). Demonstration of amyloid deposits and neurofibrillary changes in whole brain sections. Brain Pathol. Zurich Switz. *1*, 213–216.

Braak, H., and Braak, E. (1997b). Frequency of Stages of Alzheimer-Related Lesions in Different Age Categories. Neurobiol. Aging *18*, 351–357.

Braak, H., Alafuzoff, I., Arzberger, T., Kretzschmar, H., and Del Tredici, K. (2006). Staging of Alzheimer disease-associated neurofibrillary pathology using paraffin sections and immunocytochemistry. Acta Neuropathol. (Berl.) *112*, 389–404.

Brickman, A.M., Stern, Y., and Small, S.A. (2011). Hippocampal subregions differentially associate with standardized memory tests. Hippocampus *21*, 923–928.

Brown, M.W., and Aggleton, J.P. (2001). Recognition memory: what are the roles of the perirhinal cortex and hippocampus? Nat. Rev. Neurosci. *2*, 51–61.

Brown, M.W., and Bashir, Z.I. (2002). Evidence concerning how neurons of the perirhinal cortex may effect familiarity discrimination. Philos. Trans. R. Soc. Lond. B. Biol. Sci. *357*, 1083–1095.

Buckner, R.L., Snyder, A.Z., Shannon, B.J., LaRossa, G., Sachs, R., Fotenos, A.F., Sheline, Y.I., Klunk, W.E., Mathis, C.A., Morris, J.C., et al. (2005). Molecular, structural, and functional characterization of Alzheimer's disease: evidence for a relationship between default activity, amyloid, and memory. J. Neurosci. Off. J. Soc. Neurosci. *25*, 7709–7717.

Bullitt, E., Rahman, F.N., Smith, J.K., Kim, E., Zeng, D., Katz, L.M., and Marks, B.L. (2009). The Effect of Exercise on the Cerebral Vasculature of Healthy Aged Subjects as Visualized by MR Angiography. Am. J. Neuroradiol. *30*, 1857–1863.

Burdette, J.H., Laurienti, P.J., Espeland, M.A., Morgan, A., Telesford, Q., Vechlekar, C.D., Hayasaka, S., Jennings, J.M., Katula, J.A., Kraft, R.A., et al. (2010). Using network science to evaluate exercise-associated brain changes in older adults. Front. Aging Neurosci. *2*, 23.

Burke, D.M., and Mackay, D.G. (1997). Memory, language, and ageing. Philos. Trans. R. Soc. B Biol. Sci. *352*, 1845–1856.

Burke, S.N., Wallace, J.L., Hartzell, A.L., Nematollahi, S., Plange, K., and Barnes, C.A. (2011). Age-associated deficits in pattern separation functions of the perirhinal cortex: a cross-species consensus. Behav. Neurosci. *125*, 836–847.

Burwell, R.D. (2000). The parahippocampal region: corticocortical connectivity. Ann. N. Y. Acad. Sci. *911*, 25–42.

Burwell, R.D., and Amaral, D.G. (1998). Cortical afferents of the perirhinal, postrhinal, and entorhinal cortices of the rat. J. Comp. Neurol. *398*, 179–205.

Bussey, T.J., Saksida, L.M., and Murray, E.A. (2003). Impairments in visual discrimination after perirhinal cortex lesions: testing “declarative” vs. “perceptual-mnemonic” views of perirhinal cortex function. Eur. J. Neurosci. *17*, 649–660.

Buzsáki, G. (1996). The hippocampo-neocortical dialogue. Cereb. Cortex N. Y. N 1991 *6*, 81–92.

De Calignon, A., Polydoro, M., Suárez-Calvet, M., William, C., Adamowicz, D.H., Kopeikina, K.J., Pitstick, R., Sahara, N., Ashe, K.H., Carlson, G.A., et al. (2012). Propagation of tau pathology in a model of early Alzheimer’s disease. Neuron *73*, 685–697.

Canto, C.B., Wouterlood, F.G., and Witter, M.P. (2008). What does the anatomical organization of the entorhinal cortex tell us? Neural Plast. *2008*, 381243.

Carr, V.A., Rissman, J., and Wagner, A.D. (2010). Imaging the human medial temporal lobe with high-resolution fMRI. Neuron *65*, 298–308.

Casarotti, A., Papagno, C., and Zarino, B. (2013). Modified Taylor Complex Figure: Normative data from 290 adults. J. Neuropsychol.

Cashdollar, N., Malecki, U., Rugg-Gunn, F.J., Duncan, J.S., Lavie, N., and Duzel, E. (2009). Hippocampus-dependent and-independent theta-networks of active maintenance. Proc. Natl. Acad. Sci. *106*, 20493–20498.

Chaddock, L., Hillman, C.H., Buck, S.M., and Cohen, N.J. (2011). Aerobic Fitness and Executive Control of Relational Memory in Preadolescent Children: Med. Sci. Sports Exerc. *43*, 344–349.

Chang, C.-C., and Lin, C.-J. (2011). LIBSVM: A Library for Support Vector Machines. ACM Trans Intell Syst Technol *2*, 27:1–27:27.

Clelland, C.D., Choi, M., Romberg, C., Clemenson, G.D., Fragniere, A., Tyers, P., Jessberger, S., Saksida, L.M., Barker, R.A., Gage, F.H., et al. (2009). A functional role for adult hippocampal neurogenesis in spatial pattern separation. Science *325*, 210–213.

Coelho, F.G. de M., Gobbi, S., Andreatto, C.A.A., Corazza, D.I., Pedroso, R.V., and Santos-Galduróz, R.F. (2013). Physical exercise modulates peripheral levels of brain-derived neurotrophic factor (BDNF): a systematic review of experimental studies in the elderly. Arch. Gerontol. Geriatr. *56*, 10–15.

Comijs, H.C., Gerritsen, L., Penninx, B.W.J.H., Bremmer, M.A., Deeg, D.J.H., and Geerlings, M.I. (2010). The association between serum cortisol and cognitive decline in older persons. Am. J. Geriatr. Psychiatry Off. J. Am. Assoc. Geriatr. Psychiatry *18*, 42–50.

Cotman, C.W., and Berchtold, N.C. (2007). Physical activity and the maintenance of cognition: learning from animal models. Alzheimers Dement. J. Alzheimers Assoc. *3*, S30–S37.

Cotman, C.W., Berchtold, N.C., and Christie, L.-A. (2007). Exercise builds brain health: key roles of growth factor cascades and inflammation. Trends Neurosci. *30*, 464–472.

Creer, D.J., Romberg, C., Saksida, L.M., Praag, H. van, and Bussey, T.J. (2010). Running enhances spatial pattern separation in mice. Proc. Natl. Acad. Sci. *107*, 2367–2372.

De Curtis, M., and Paré, D. (2004). The rhinal cortices: a wall of inhibition between the neocortex and the hippocampus. Prog. Neurobiol. *74*, 101–110.

Delacourte, A., Sergeant, N., Champain, D., Wattez, A., Maurage, C.-A., Lebert, F., Pasquier, F., and David, J.-P. (2002). Nonoverlapping but synergetic tau and APP pathologies in sporadic Alzheimer's disease. Neurology *59*, 398–407.

Deller, T., Martinez, A., Nitsch, R., and Frotscher, M. (1996). A novel entorhinal projection to the rat dentate gyrus: direct innervation of proximal dendrites and cell bodies of granule cells and GABAergic neurons. J. Neurosci. Off. J. Soc. Neurosci. *16*, 3322–3333.

Dery, N., Pilgrim, M., Gibala, M., Gillen, J., Wojtowicz, J.M., MacQueen, G., and Becker, S. (2013). Adult hippocampal neurogenesis reduces memory interference in humans: opposing effects of aerobic exercise and depression. Front. Neurosci. *7*.

Deuker, L., Doeller, C.F., Fell, J., and Axmacher, N. (2014). Human neuroimaging studies on the hippocampal CA3 region - integrating evidence for pattern separation and completion. Front. Cell. Neurosci. *8*.

Drapeau, E., and Nora Abrous, D. (2008). Stem Cell Review Series: Role of neurogenesis in age-related memory disorders. Aging Cell *7*, 569–589.

Duncan, K., Ketz, N., Inati, S.J., and Davachi, L. (2012). Evidence for area CA1 as a match/mismatch detector: a high-resolution fMRI study of the human hippocampus. Hippocampus *22*, 389–398.

Duncan, K., Tompary, A., and Davachi, L. (2014). Associative Encoding and Retrieval Are Predicted by Functional Connectivity in Distinct Hippocampal Area CA1 Pathways. J. Neurosci. *34*, 11188–11198.

During, M.J., and Cao, L. (2006). VEGF, a mediator of the effect of experience on hippocampal neurogenesis. Curr. Alzheimer Res. *3*, 29–33.

Düzel, E., Vargha-Khadem, F., Heinze, H.J., and Mishkin, M. (2001). Brain activity evidence for recognition without recollection after early hippocampal damage. Proc. Natl. Acad. Sci. *98*, 8101–8106.

Düzel, E., Bunzeck, N., Guitart-Masip, M., and Düzel, S. (2010). NOvelty-related motivation of anticipation and exploration by dopamine (NOMAD): implications for healthy aging. Neurosci. Biobehav. Rev. *34*, 660–669.

Düzel, E., Schütze, H., Yonelinas, A.P., and Heinze, H.-J. (2011). Functional phenotyping of successful aging in long-term memory: Preserved performance in the absence of neural compensation. Hippocampus *21*, 803–814.

Eichenbaum, H., and Lipton, P.A. (2008). Towards a functional organization of the medial temporal lobe memory system: Role of the parahippocampal and medial entorhinal cortical areas. Hippocampus *18*, 1314–1324.

Eichenbaum, H., Yonelinas, A.P., and Ranganath, C. (2007). The medial temporal lobe and recognition memory. Annu. Rev. Neurosci. *30*, 123–152.

Eichenbaum, H., Sauvage, M., Fortin, N., Komorowski, R., and Lipton, P. (2012). Towards a functional organization of episodic memory in the medial temporal lobe. Neurosci. Biobehav. Rev. *36*, 1597–1608.

Ekstrand, J., Hellsten, J., and Tingström, A. (2008). Environmental enrichment, exercise and corticosterone affect endothelial cell proliferation in adult rat hippocampus and prefrontal cortex. Neurosci. Lett. *442*, 203–207.

Ekstrom, A. (2010). How and when the fMRI BOLD signal relates to underlying neural activity: The danger in dissociation. Brain Res. Rev. *62*, 233–244.

Ekstrom, A.D., Bazih, A.J., Suthana, N.A., Al-Hakim, R., Ogura, K., Zeineh, M., Burggren, A.C., and Bookheimer, S.Y. (2009). Advances in high-resolution imaging and computational unfolding of the human hippocampus. NeuroImage *47*, 42–49.

Elfman, K.W., Parks, C.M., and Yonelinas, A.P. (2008). Testing a neurocomputational model of recollection, familiarity, and source recognition. J. Exp. Psychol. Learn. Mem. Cogn. *34*, 752–768.

Erickson, K.I., Voss, M.W., Prakash, R.S., Basak, C., Szabo, A., Chaddock, L., Kim, J.S., Heo, S., Alves, H., White, S.M., et al. (2011). Exercise training increases size of hippocampus and improves memory. Proc. Natl. Acad. Sci. *108*, 3017–3022.

Erickson, K.I., Miller, D.L., and Roecklein, K.A. (2012). The Aging Hippocampus: Interactions between Exercise, Depression, and BDNF. Neurosci. Rev. J. Bringing Neurobiol. Neurol. Psychiatry *18*, 82–97.

Eriksson, P.S., Perfilieva, E., Björk-Eriksson, T., Alborn, A.-M., Nordborg, C., Peterson, D.A., and Gage, F.H. (1998). Neurogenesis in the adult human hippocampus. Nat. Med. *4*, 1313–1317.

Fagan, A.M., Mintun, M.A., Shah, A.R., Aldea, P., Roe, C.M., Mach, R.H., Marcus, D., Morris, J.C., and Holtzman, D.M. (2009). Cerebrospinal fluid tau and ptau(181) increase with cortical amyloid deposition in cognitively normal individuals: implications for future clinical trials of Alzheimer's disease. EMBO Mol. Med. *1*, 371–380.

Fair, D.A., Schlaggar, B.L., Cohen, A.L., Miezin, F.M., Dosenbach, N.U.F., Wenger, K.K., Fox, M.D., Snyder, A.Z., Raichle, M.E., and Petersen, S.E. (2007). A method for using blocked and event-related fMRI data to study "resting state" functional connectivity. NeuroImage *35*, 396–405.

Fanselow, M.S., and Dong, H.-W. (2010). Are the dorsal and ventral hippocampus functionally distinct structures? Neuron *65*, 7–19.

Feczko, E., Augustinack, J.C., Fischl, B., and Dickerson, B.C. (2009). An MRI-based method for measuring volume, thickness and surface area of entorhinal, perirhinal, and posterior parahippocampal cortex. Neurobiol. Aging *30*, 420–431.

Felleman, D.J., and Van Essen, D.C. (1991). Distributed hierarchical processing in the primate cerebral cortex. Cereb. Cortex N. Y. N 1991 *1*, 1–47.

Fenker, D.B., Frey, J.U., Schuetze, H., Heipertz, D., Heinze, H.J., and Duzel, E. (2008). Novel scenes improve recollection and recall of words. J. Cogn. Neurosci. *20*, 1250–1265.

Fernandez, A.M., and Torres-Alemán, I. (2012). The many faces of insulin-like peptide signalling in the brain. Nat. Rev. Neurosci. *13*, 225–239.

Fischl, B., Stevens, A.A., Rajendran, N., Yeo, B.T.T., Greve, D.N., Van Leemput, K., Polimeni, J.R., Kakunoori, S., Buckner, R.L., Pacheco, J., et al. (2009). Predicting the Location of Entorhinal Cortex from MRI. NeuroImage *47*, 8–17.

FitzGerald, T.H.B., Friston, K.J., and Dolan, R.J. (2012). Action-specific value signals in reward-related regions of the human brain. J. Neurosci. Off. J. Soc. Neurosci. *32*, 16417–16423a.

Fjell, A.M., Westlye, L.T., Grydeland, H., Amlien, I., Espeseth, T., Reinvang, I., Raz, N., Dale, A.M., and Walhovd, K.B. (2014). Accelerating Cortical Thinning: Unique to Dementia or Universal in Aging? Cereb. Cortex *24*, 919–934.

Folstein, M.F., Robins, L.N., and Helzer, J.E. (1983). The Mini-Mental State Examination. Arch. Gen. Psychiatry *40*, 812.

Fortin, N.J., Wright, S.P., and Eichenbaum, H. (2004). Recollection-like memory retrieval in rats is dependent on the hippocampus. Nature *431*, 188–191.

Fox, M.D., and Raichle, M.E. (2007). Spontaneous fluctuations in brain activity observed with functional magnetic resonance imaging. Nat. Rev. Neurosci. *8*, 700–711.

Fox, M.D., Snyder, A.Z., Zacks, J.M., and Raichle, M.E. (2006). Coherent spontaneous activity accounts for trial-to-trial variability in human evoked brain responses. Nat. Neurosci. *9*, 23–25.

Frey, I., Berg, A., Grathwohl, D., and Keul, J. (1999). [Freiburg Questionnaire of physical activity--development, evaluation and application]. Soz.- Präventivmedizin *44*, 55–64.

Friston, K. (2008). Neurophysiology: the brain at work. Curr. Biol. CB *18*, R418–R420.

Friston, K.J. (2002). Bayesian estimation of dynamical systems: an application to fMRI. NeuroImage *16*, 513–530.

Friston, K.., Buechel, C., Fink, G.., Morris, J., Rolls, E., and Dolan, R.. (1997). Psychophysiological and Modulatory Interactions in Neuroimaging. NeuroImage *6*, 218–229.

Friston, K., Mattout, J., Trujillo-Barreto, N., Ashburner, J., and Penny, W. (2007). Variational free energy and the Laplace approximation. NeuroImage *34*, 220–234.

Friston, K., Chu, C., Mourão-Miranda, J., Hulme, O., Rees, G., Penny, W., and Ashburner, J. (2008). Bayesian decoding of brain images. NeuroImage *39*, 181–205.

Furtak, S.C., Wei, S.-M., Agster, K.L., and Burwell, R.D. (2007). Functional neuroanatomy of the parahippocampal region in the rat: the perirhinal and postrhinal cortices. Hippocampus *17*, 709–722.

Gallagher, M., and Koh, M.T. (2011). Episodic memory on the path to Alzheimer's disease. Curr. Opin. Neurobiol. *21*, 929–934.

Gasbarri, A., Sulli, A., and Packard, M.G. (1997). The dopaminergic mesencephalic projections to the hippocampal formation in the rat. Prog. Neuropsychopharmacol. Biol. Psychiatry *21*, 1–22.

Gazzaley, A.H., Siegel, S.J., Kordower, J.H., Mufson, E.J., and Morrison, J.H. (1996). Circuit-specific alterations of N-methyl-D-aspartate receptor subunit 1 in the dentate gyrus of aged monkeys. Proc. Natl. Acad. Sci. U. S. A. *93*, 3121–3125.

Geinisman, Y., deToledo-Morrell, L., Morrell, F., Persina, I.S., and Rossi, M. (1992). Age-related loss of axospinous synapses formed by two afferent systems in the rat dentate gyrus as revealed by the unbiased stereological dissector technique. Hippocampus *2*, 437–444.

Gerritsen, L., Comijs, H.C., Deeg, D.J.H., Penninx, B.W.J.H., and Geerlings, M.I. (2011). Salivary cortisol, APOE-ε4 allele and cognitive decline in a prospective study of older persons. Neurobiol. Aging *32*, 1615–1625.

Goense, J.B.M., and Logothetis, N.K. (2006). Laminar specificity in monkey V1 using high-resolution SE-fMRI. Magn. Reson. Imaging *24*, 381–392.

Goense, J.B.M., and Logothetis, N.K. (2008). Neurophysiology of the BOLD fMRI signal in awake monkeys. Curr. Biol. CB *18*, 631–640.

Goense, J., Merkle, H., and Logothetis, N.K. (2012). High-Resolution fMRI Reveals Laminar Differences in Neurovascular Coupling between Positive and Negative BOLD Responses. Neuron *76*, 629–639.

Gómez-Isla, T., Price, J.L., McKeel, D.W., Morris, J.C., Growdon, J.H., and Hyman, B.T. (1996). Profound loss of layer II entorhinal cortex neurons occurs in very mild Alzheimer's disease. J. Neurosci. Off. J. Soc. Neurosci. *16*, 4491–4500.

Grady, C. (2012). The cognitive neuroscience of ageing. Nat. Rev. Neurosci. *13*, 491–505.

Grön, G., Bittner, D., Schmitz, B., Wunderlich, A.P., Tomczak, R., and Riepe, M.W. (2001). Hippocampal Activations during Repetitive Learning and Recall of Geometric Patterns. Learn Mem *8*, 336–345.

Guderian, S., Brigham, D., and Mishkin, M. (2011). Two processes support visual recognition memory in rhesus monkeys. Proc. Natl. Acad. Sci. U. S. A. *108*, 19425–19430.

Van Haeften, T., Jorritsma-Byham, B., and Witter, M.P. (1995). Quantitative morphological analysis of subicular terminals in the rat entorhinal cortex. Hippocampus *5*, 452–459.

Hanke, M., Halchenko, Y.O., Sederberg, P.B., Hanson, S.J., Haxby, J.V., and Pollmann, S. (2009). PyMVPA: A python toolbox for multivariate pattern analysis of fMRI data. Neuroinformatics *7*, 37–53.

Harel, N., Lin, J., Moeller, S., Ugurbil, K., and Yacoub, E. (2006). Combined imaging–histological study of cortical laminar specificity of fMRI signals. NeuroImage *29*, 879–887.

Hasselmo, M.E., Wyble, B.P., and Wallenstein, G.V. (1996). Encoding and retrieval of episodic memories: role of cholinergic and GABAergic modulation in the hippocampus. Hippocampus *6*, 693–708.

Helmstaedter, C., and Durwen, H.F. (1990). [The Verbal Learning and Retention Test. A useful and differentiated tool in evaluating verbal memory performance]. Schweiz. Arch. Für Neurol. Psychiatr. Zurich Switz. 1985 *141*, 21–30.

Hoaglin, D.C., Iglewicz, B., and Tukey, J.W. (1986). Performance of Some Resistant Rules for Outlier Labeling. J. Am. Stat. Assoc. *81*, 991.

Horner, A.J., Gadian, D.G., Fuentemilla, L., Jentschke, S., Vargha-Khadem, F., and Duzel, E. (2012). A Rapid, Hippocampus-Dependent, Item-Memory Signal that Initiates Context Memory in Humans. Curr. Biol. CB *22*, 2369–2374.

Howard, L.R., Kumaran, D., Ólafsdóttir, H.F., and Spiers, H.J. (2011). Double dissociation between hippocampal and parahippocampal responses to object-background context and scene novelty. J. Neurosci. Off. J. Soc. Neurosci. *31*, 5253–5261.

Hu, L., and Bentler, P.M. (1999). Cutoff criteria for fit indexes in covariance structure analysis: Conventional criteria versus new alternatives. Struct. Equ. Model. *6*, 1–55.

Hubley, A.M. (2010). Using the Rey-Osterrieth and modified Taylor complex figures with older adults: a preliminary examination of accuracy score comparability. Arch. Clin. Neuropsychol. Off. J. Natl. Acad. Neuropsychol. *25*, 197–203.

Huettel, S.A., Song, A.W., and McCarthy, G. (2008). Functional Magnetic Resonance Imaging, Second Edition (Sunderland, Mass: Sinauer Associates).

Hunsaker, M.R., Mooy, G.G., Swift, J.S., and Kesner, R.P. (2007). Dissociations of the medial and lateral perforant path projections into dorsal DG, CA3, and CA1 for

spatial and nonspatial (visual object) information processing. Behav. Neurosci. *121*, 742–750.

Hunsaker, M.R., Rosenberg, J.S., and Kesner, R.P. (2008). The role of the dentate gyrus, CA3a,b, and CA3c for detecting spatial and environmental novelty. Hippocampus *18*, 1064–1073.

Hyman, B.T., Phelps, C.H., Beach, T.G., Bigio, E.H., Cairns, N.J., Carrillo, M.C., Dickson, D.W., Duyckaerts, C., Frosch, M.P., Masliah, E., et al. (2012). National Institute on Aging-Alzheimer's Association guidelines for the neuropathologic assessment of Alzheimer's disease. Alzheimers Dement. J. Alzheimers Assoc. *8*, 1–13.

Hoaglin, D. C., and Iglewicz, B. (1987), Fine. Tuning Some Resistant Rules for Outlier. Labeling, Journal of American Statistical. Association., *82*, 1147-1149

In, M.-H., and Speck, O. (2012). Highly accelerated PSF-mapping for EPI distortion correction with improved fidelity. Magma N. Y. N *25*, 183–192.

Ishizuka, N., Weber, J., and Amaral, D.G. (1990). Organization of intrahippocampal projections originating from CA3 pyramidal cells in the rat. J. Comp. Neurol. *295*, 580–623.

Jacobson, E. (1938). Progressive relaxation (2nd ed.) (Oxford, England: Univ. Chicago Press).

Jagust, W. (2013). Vulnerable Neural Systems and the Borderland of Brain Aging and Neurodegeneration. Neuron *77*, 219–234.

Jenkinson, M., and Smith, S. (2001). A global optimisation method for robust affine registration of brain images. Med. Image Anal. *5*, 143–156.

La Joie, R., Landeau, B., Perrotin, A., Bejanin, A., Egret, S., Pélerin, A., Mézenge, F., Belliard, S., de La Sayette, V., Eustache, F., et al. (2014). Intrinsic connectivity identifies the hippocampus as a main crossroad between Alzheimer's and semantic dementia-targeted networks. Neuron *81*, 1417–1428.

Jones, B.F., and Witter, M.P. (2007). Cingulate cortex projections to the parahippocampal region and hippocampal formation in the rat. Hippocampus *17*, 957–976.

Jung, M.W., and McNaughton, B.L. (1993). Spatial selectivity of unit activity in the hippocampal granular layer. Hippocampus *3*, 165–182.

Kahn, I., Andrews-Hanna, J.R., Vincent, J.L., Snyder, A.Z., and Buckner, R.L. (2008). Distinct cortical anatomy linked to subregions of the medial temporal lobe revealed by intrinsic functional connectivity. J. Neurophysiol. *100*, 129–139.

Kajiwara, R., Wouterlood, F.G., Sah, A., Boekel, A.J., Baks-te Bulte, L.T.G., and Witter, M.P. (2008). Convergence of entorhinal and CA3 inputs onto pyramidal neurons and interneurons in hippocampal area CA1--an anatomical study in the rat. Hippocampus *18*, 266–280.

Karlsson, M.P., and Frank, L.M. (2008). Network dynamics underlying the formation of sparse, informative representations in the hippocampus. J. Neurosci. Off. J. Soc. Neurosci. *28*, 14271–14281.

KARVONEN, M.J., KENTALA, E., and MUSTALA, O. (1957). The effects of training on heart rate; a longitudinal study. Ann. Med. Exp. Biol. Fenn. *35*, 307–315.

Kempermann, G., Kuhn, H.G., and Gage, F.H. (1998). Experience-Induced Neurogenesis in the Senescent Dentate Gyrus. J. Neurosci. *18*, 3206–3212.

Kempton, M.J., Ettinger, U., Foster, R., Williams, S.C.R., Calvert, G.A., Hampshire, A., Zelaya, F.O., O'Gorman, R.L., McMorris, T., Owen, A.M., et al. (2011). Dehydration affects brain structure and function in healthy adolescents. Hum. Brain Mapp. *32*, 71–79.

Kerchner, G.A., Hess, C.P., Hammond-Rosenbluth, K.E., Xu, D., Rabinovici, G.D., Kelley, D.A.C., Vigneron, D.B., Nelson, S.J., and Miller, B.L. (2010). Hippocampal CA1 apical neuropil atrophy in mild Alzheimer disease visualized with 7-T MRI. Neurology *75*, 1381–1387.

Kerchner, G.A., Deutsch, G.K., Zeineh, M., Dougherty, R.F., Saranathan, M., and Rutt, B.K. (2012). Hippocampal CA1 apical neuropil atrophy and memory performance in Alzheimer's disease. NeuroImage *63*, 194–202.

Kerr, K.M., Agster, K.L., Furtak, S.C., and Burwell, R.D. (2007). Functional neuroanatomy of the parahippocampal region: The lateral and medial entorhinal areas. Hippocampus *17*, 697–708.

Khan, U.A., Liu, L., Provenzano, F.A., Berman, D.E., Profaci, C.P., Sloan, R., Mayeux, R., Duff, K.E., and Small, S.A. (2014). Molecular drivers and cortical spread of lateral entorhinal cortex dysfunction in preclinical Alzheimer's disease. Nat. Neurosci. *17*, 304–311.

Killian, N.J., Jutras, M.J., and Buffalo, E.A. (2012). A map of visual space in the primate entorhinal cortex. Nature *491*, 761–764.

Kirwan, C.B., Jones, C.K., Miller, M.I., and Stark, C.E.L. (2007). High-resolution fMRI investigation of the medial temporal lobe. Hum. Brain Mapp. *28*, 959–966.

Kishiyama, M.M., and Yonelinas, A.P. (2003). Novelty effects on recollection and familiarity in recognition memory. Mem. Cognit. *31*, 1045–1051.

Klein, A., Andersson, J., Ardekani, B.A., Ashburner, J., Avants, B., Chiang, M.-C., Christensen, G.E., Collins, D.L., Gee, J., Hellier, P., et al. (2009). Evaluation of 14 nonlinear deformation algorithms applied to human brain MRI registration. NeuroImage *46*, 786–802.

Kloosterman, F., Witter, M.P., and Van Haeften, T. (2003). Topographical and laminar organization of subicular projections to the parahippocampal region of the rat. J. Comp. Neurol. *455*, 156–171.

Knierim, J.J., Neunuebel, J.P., and Deshmukh, S.S. (2014). Functional correlates of the lateral and medial entorhinal cortex: objects, path integration and local-global reference frames. Philos. Trans. R. Soc. Lond. B. Biol. Sci. *369*, 20130369.

Kobayashi, Y., and Amaral, D.G. (2007). Macaque monkey retrosplenial cortex: III. Cortical efferents. J. Comp. Neurol. *502*, 810–833.

Koganezawa, N., Taguchi, A., Tominaga, T., Ohara, S., Tsutsui, K.-I., Witter, M.P., and Iijima, T. (2008). Significance of the deep layers of entorhinal cortex for transfer of both perirhinal and amygdala inputs to the hippocampus. Neurosci. Res. *61*, 172–181.

Köhler, C. (1985). A projection from the deep layers of the entorhinal area to the hippocampal formation in the rat brain. Neurosci. Lett. *56*, 13–19.

Koopmans, P.J., Barth, M., and Norris, D.G. (2010). Layer-specific BOLD activation in human V1. Hum. Brain Mapp. *31*, 1297–1304.

Kuhn, H.G., Dickinson-Anson, H., and Gage, F.H. (1996). Neurogenesis in the dentate gyrus of the adult rat: age-related decrease of neuronal progenitor proliferation. J. Neurosci. Off. J. Soc. Neurosci. *16*, 2027–2033.

Kühner, C., Bürger, C., Keller, F., and Hautzinger, M. (2007). [Reliability and validity of the Revised Beck Depression Inventory (BDI-II). Results from German samples]. Nervenarzt *78*, 651–656.

Kumaran, D., and Maguire, E.A. (2006). An Unexpected Sequence of Events: Mismatch Detection in the Human Hippocampus. PLoS Biol *4*, e424.

Kumaran, D., and Maguire, E.A. (2007). Which computational mechanisms operate in the hippocampus during novelty detection? Hippocampus *17*, 735–748.

Kumaran, D., and McClelland, J.L. (2012). Generalization through the recurrent interaction of episodic memories: A model of the hippocampal system. Psychol. Rev. *119*, 573–616.

Kuppusamy, K., Lin, W., Cizek, G.R., and Haacke, E.M. (1996). In vivo regional cerebral blood volume: quantitative assessment with 3D T1-weighted pre- and postcontrast MR imaging. Radiology *201*, 106–112.

Lacy, J.W., and Stark, C.E.L. (2012). Intrinsic functional connectivity of the human medial temporal lobe suggests a distinction between adjacent mtl cortices and hippocampus. Hippocampus.

Lacy, J.W., Yassa, M.A., Stark, S.M., Muftuler, L.T., and Stark, C.E.L. (2011). Distinct pattern separation related transfer functions in human CA3/dentate and CA1 revealed using high-resolution fMRI and variable mnemonic similarity. Learn. Mem. Cold Spring Harb. N *18*, 15–18.

Lavenex, P., and Amaral, D.G. (2000). Hippocampal-neocortical interaction: a hierarchy of associativity. Hippocampus *10*, 420–430.

Lee, A.C.H., Buckley, M.J., Gaffan, D., Emery, T., Hodges, J.R., and Graham, K.S. (2006). Differentiating the Roles of the Hippocampus and Perirhinal Cortex in Processes beyond Long-Term Declarative Memory: A Double Dissociation in Dementia. J. Neurosci. *26*, 5198–5203.

Lee, A.C.H., Levi, N., Davies, R.R., Hodges, J.R., and Graham, K.S. (2007). Differing profiles of face and scene discrimination deficits in semantic dementia and Alzheimer's disease. Neuropsychologia *45*, 2135–2146.

Lee, J.H., Durand, R., Gradinaru, V., Zhang, F., Goshen, I., Kim, D.-S., Fenno, L.E., Ramakrishnan, C., and Deisseroth, K. (2010). Global and local fMRI signals driven by neurons defined optogenetically by type and wiring. Nature *465*, 788–792.

Lehrl, S. (2005). Mehrfachwahl-Wortschatz-Intelligenztest: MWT-B. Balingen: Spitta.

Leutgeb, J.K., Leutgeb, S., Moser, M.-B., and Moser, E.I. (2007). Pattern separation in the dentate gyrus and CA3 of the hippocampus. Science *315*, 961–966.

Leutgeb, S., Leutgeb, J.K., Treves, A., Moser, M.-B., and Moser, E.I. (2004). Distinct ensemble codes in hippocampal areas CA3 and CA1. Science *305*, 1295–1298.

Li, S., Cullen, W.K., Anwyl, R., and Rowan, M.J. (2003). Dopamine-dependent facilitation of LTP induction in hippocampal CA1 by exposure to spatial novelty. Nat. Neurosci. *6*, 526–531.

Libby, L.A., Ekstrom, A.D., Ragland, J.D., and Ranganath, C. (2012). Differential connectivity of perirhinal and parahippocampal cortices within human hippocampal subregions revealed by high-resolution functional imaging. J. Neurosci. Off. J. Soc. Neurosci. *32*, 6550–6560.

Licht, T., Goshen, I., Avital, A., Kreisel, T., Zubedat, S., Eavri, R., Segal, M., Yirmiya, R., and Keshet, E. (2011). Reversible modulations of neuronal plasticity by VEGF. Proc. Natl. Acad. Sci. U. S. A. *108*, 5081–5086.

Limbrick-Oldfield, E.H., Brooks, J.C.W., Wise, R.J.S., Padormo, F., Hajnal, J.V., Beckmann, C.F., and Ungless, M.A. (2012). Identification and characterisation of midbrain nuclei using optimised functional magnetic resonance imaging. Neuroimage *59*, 1230–1238.

Lisman, J.E., and Grace, A.A. (2005). The Hippocampal-VTA Loop: Controlling the Entry of Information into Long-Term Memory. Neuron *46*, 703–713.

Lisman, J., Grace, A.A., and Duzel, E. (2011). A neoHebbian framework for episodic memory; role of dopamine-dependent late LTP. Trends Neurosci. *34*, 536–547.

Liu, L., Drouet, V., Wu, J.W., Witter, M.P., Small, S.A., Clelland, C., and Duff, K. (2012). Trans-Synaptic Spread of Tau Pathology In Vivo. PLoS ONE *7*, e31302.

Logothetis, N.K. (2010). Bold claims for optogenetics. Nature *468*, E3–E4; discussion E4–E5.

Logothetis, N.K., and Wandell, B.A. (2004). Interpreting the BOLD signal. Annu. Rev. Physiol. *66*, 735–769.

Louissaint, A., Rao, S., Leventhal, C., and Goldman, S.A. (2002). Coordinated interaction of neurogenesis and angiogenesis in the adult songbird brain. Neuron *34*, 945–960.

Lövdén, M., Schaefer, S., Noack, H., Bodammer, N.C., Kühn, S., Heinze, H.-J., Düzel, E., Bäckman, L., and Lindenberger, U. (2012). Spatial navigation training protects the hippocampus against age-related changes during early and late adulthood. Neurobiol. Aging *33*, 620.e9–e620.e22.

Maass, A., Schütze, H., Speck, O., Yonelinas, A., Tempelmann, C., Heinze, H.-J., Berron, D., Cardenas-Blanco, A., Brodersen, K.H., Enno Stephan, K., et al. (2014a). Laminar activity in the hippocampus and entorhinal cortex related to novelty and episodic encoding. Nat. Commun. *5*, 5547.

Maass, A., Düzel, S., Goerke, M., Becke, A., Sobieray, U., Neumann, K., Lövden, M., Lindenberger, U., Bäckman, L., Braun-Dullaeus, R., et al. (2014b). Vascular hippocampal plasticity after aerobic exercise in older adults. Mol. Psychiatry.

Maass, A., Berron, D., Libby, L., Ranganath, C., and Düzel, E. (2015). Functional subregions of the human entorhinal cortex. Elife *4*.

Maass, A., Düzel, S., Goerke, M., Becke, A., Sobieray, U., Neumann, K., Lövden, M., Lindenberger, U., Bäckman, L., Braun-Dullaeus, R., Ahrens, D., Heinze, H.–J., Müller, N.G., Brigadski, T., Lessmann, V., Sendtner, M. & Düzel, E. Relationship between peripheral IGF-1, VEGF and BDNF levels and exercise-related changes in memory, hippocampal perfusion and volumes in older adults. Under Review (Neuroimage)

Maclaren, J., Armstrong, B.S.R., Barrows, R.T., Danishad, K.A., Ernst, T., Foster, C.L., Gumus, K., Herbst, M., Kadashevich, I.Y., Kusik, T.P., et al. (2012). Measurement and Correction of Microscopic Head Motion during Magnetic Resonance Imaging of the Brain. PLoS ONE *7*.

Mai, J.K., Paxinos, G., and Voss, T. (2007). Atlas of the Human Brain, Third Edition (Amsterdam: Academic Press).

Marr, D. (1971). Simple memory: a theory for archicortex. Philos. Trans. R. Soc. Lond. B. Biol. Sci. *262*, 23–81.

McClelland, J.L., and Goddard, N.H. (1996). Considerations arising from a complementary learning systems perspective on hippocampus and neocortex. Hippocampus *6*, 654–665.

McClelland, J.L., McNaughton, B.L., and O'Reilly, R.C. (1995). Why there are complementary learning systems in the hippocampus and neocortex: Insights from the successes and failures of connectionist models of learning and memory. Psychol. Rev. *102*, 419–457.

Meng, X., Rosenthal, R., and Rubin, D.B. (1992). Comparing correlated correlation coefficients. Psychol. Bull. *111*, 172–175.

Mezzani, A., Corrà, U., Bosimini, E., Giordano, A., and Giannuzzi, P. (2003). Contribution of peak respiratory exchange ratio to peak VO2 prognostic reliability in patients with chronic heart failure and severely reduced exercise capacity. Am. Heart J. *145*, 1102–1107.

Monti, J.M., Hillman, C.H., and Cohen, N.J. (2012). Aerobic fitness enhances relational memory in preadolescent children: The FITKids randomized control trial. Hippocampus *22*, 1876–1882.

Morcom, A.M., and Friston, K.J. (2012). Decoding episodic memory in ageing: a Bayesian analysis of activity patterns predicting memory. NeuroImage *59*, 1772–1782.

Moreno H, Wu WE, Lee T, and et al (2007). IMaging the aβ-related neurotoxicity of alzheimer disease. Arch. Neurol. *64*, 1467–1477.

Mueller, S.G., Stables, L., Du, A.T., Schuff, N., Truran, D., Cashdollar, N., and Weiner, M.W. (2007). Measurement of hippocampal subfields and age-related changes with high resolution MRI at 4T. Neurobiol. Aging *28*, 719–726.

Naber, P.A., Witter, M.P., and Lopez da Silva, F.H. (1999). Perirhinal cortex input to the hippocampus in the rat: evidence for parallel pathways, both direct and indirect. A combined physiological and anatomical study. Eur. J. Neurosci. *11*, 4119–4133.

Naber, P.A., Witter, M.P., and Lopes da Silva, F.H. (2001). Evidence for a direct projection from the postrhinal cortex to the subiculum in the rat. Hippocampus *11*, 105–117.

Nakamura, N.H., Flasbeck, V., Maingret, N., Kitsukawa, T., and Sauvage, M.M. (2013). Proximodistal Segregation of Nonspatial Information in CA3: Preferential Recruitment of a Proximal CA3-Distal CA1 Network in Nonspatial Recognition Memory. J. Neurosci. *33*, 11506–11514.

Nakamura, N.H., and Sauvage, M.M. (2015). Encoding and reactivation patterns predictive of successful memory performance are topographically organized along the longitudinal axis of the hippocampus. Hippocampus.

Schröder, T.N., Haak, K.V., Jimenez, N.I.Z., Beckmann, C.F., and Doeller, C.F. (2015). Functional topography of the human entorhinal cortex. eLife Sciences *4*, e06738.

Neeper, S.A., Góauctemez-Pinilla, F., Choi, J., and Cotman, C. (1995). Exercise and brain neurotrophins. Nature *373*, 109–109.

Neeper, S.A., Gómez-Pinilla, F., Choi, J., and Cotman, C.W. (1996). Physical activity increases mRNA for brain-derived neurotrophic factor and nerve growth factor in rat brain. Brain Res. *726*, 49–56.

Nichols, T.E., and Holmes, A.P. (2002). Nonparametric permutation tests for functional neuroimaging: a primer with examples. Hum. Brain Mapp. *15*, 1–25.

Nitz, D., and McNaughton, B. (2004). Differential modulation of CA1 and dentate gyrus interneurons during exploration of novel environments. J. Neurophysiol. *91*, 863–872.

Noonan, V., and Dean, E. (2000). Submaximal exercise testing: clinical application and interpretation. Phys. Ther. *80*, 782–807.

Norman, K.A., and O'Reilly, R.C. (2003). Modeling hippocampal and neocortical contributions to recognition memory: a complementary-learning-systems approach. Psychol. Rev. *110*, 611–646.

Nyberg, L. (2005). Any novelty in hippocampal formation and memory? Curr. Opin. Neurol. *18*, 424–428.

Ogawa, S., Menon, R.S., Tank, D.W., Kim, S.G., Merkle, H., Ellermann, J.M., and Ugurbil, K. (1993). Functional brain mapping by blood oxygenation level-dependent contrast magnetic resonance imaging. A comparison of signal characteristics with a biophysical model. Biophys. J. *64*, 803–812.

Oh, H., Habeck, C., Madison, C., and Jagust, W. (2012). Covarying alterations in Aβ deposition, glucose metabolism, and gray matter volume in cognitively normal elderly. Hum. Brain Mapp. n/a – n/a.

Ojemann, J.G., Akbudak, E., Snyder, A.Z., McKinstry, R.C., Raichle, M.E., and Conturo, T.E. (1997). Anatomic Localization and Quantitative Analysis of Gradient Refocused Echo-Planar fMRI Susceptibility Artifacts. NeuroImage *6*, 156–167.

Olarte-Sánchez, C.M., Kinnavane, L., Amin, E., and Aggleton, J.P. (2014). Contrasting networks for recognition memory and recency memory revealed by immediate-early gene imaging in the rat. Behav. Neurosci. *128*, 504–522.

Olman, C.A., Davachi, L., and Inati, S. (2009). Distortion and Signal Loss in Medial Temporal Lobe. PLoS ONE *4*, e8160.

O'Reilly, K.C., Gulden Dahl, A., Ulsaker Kruge, I., and Witter, M.P. (2013). Subicular-parahippocampal projections revisited: development of a complex topography in the rat. J. Comp. Neurol. *521*, 4284–4299.

O'Reilly, R.C., Bhattacharyya, R., Howard, M.D., and Ketz, N. (2014). Complementary learning systems. Cogn. Sci. *38*, 1229–1248.

Palmer, T.D., Willhoite, A.R., and Gage, F.H. (2000). Vascular niche for adult hippocampal neurogenesis. J. Comp. Neurol. *425*, 479–494.

Park, D.C., Lautenschlager, G., Hedden, T., Davidson, N.S., Smith, A.D., and Smith, P.K. (2002). Models of visuospatial and verbal memory across the adult life span. Psychol. Aging *17*, 299–320.

Pengas, G., Hodges, J.R., Watson, P., and Nestor, P.J. (2010a). Focal posterior cingulate atrophy in incipient Alzheimer's disease. Neurobiol. Aging *31*, 25–33.

Pengas, G., Patterson, K., Arnold, R.J., Bird, C.M., Burgess, N., and Nestor, P.J. (2010b). Lost and found: bespoke memory testing for Alzheimer's disease and semantic dementia. J. Alzheimers Dis. JAD *21*, 1347–1365.

Penny, W.D., Stephan, K.E., Mechelli, A., and Friston, K.J. (2004). Comparing dynamic causal models. NeuroImage *22*, 1157–1172.

Pereira, A.C., Huddleston, D.E., Brickman, A.M., Sosunov, A.A., Hen, R., McKhann, G.M., Sloan, R., Gage, F.H., Brown, T.R., and Small, S.A. (2007). An in Vivo Correlate of Exercise-Induced Neurogenesis in the Adult Dentate Gyrus. Proc. Natl. Acad. Sci. *104*, 5638–5643.

Petersen, A.M.W., and Pedersen, B.K. (2005). The anti-inflammatory effect of exercise. J. Appl. Physiol. Bethesda Md 1985 *98*, 1154–1162.

Podewils, L.J., Guallar, E., Kuller, L.H., Fried, L.P., Lopez, O.L., Carlson, M., and Lyketsos, C.G. (2005). Physical activity, APOE genotype, and dementia risk: findings from the Cardiovascular Health Cognition Study. Am. J. Epidemiol. *161*, 639–651.

Poppenk, J., Evensmoen, H.R., Moscovitch, M., and Nadel, L. (2013). Long-axis specialization of the human hippocampus. Trends Cogn. Sci. *17*, 230–240.

Van Praag, H., Kempermann, G., and Gage, F.H. (1999). Running increases cell proliferation and neurogenesis in the adult mouse dentate gyrus. Nat. Neurosci. *2*, 266–270.

Van Praag, H., Shubert, T., Zhao, C., and Gage, F.H. (2005). Exercise enhances learning and hippocampal neurogenesis in aged mice. J. Neurosci. Off. J. Soc. Neurosci. *25*, 8680–8685.

Price, J.L., and Morris, J.C. (1999). Tangles and plaques in nondemented aging and "preclinical" Alzheimer's disease. Ann. Neurol. *45*, 358–368.

Price, J.L., Ko, A.I., Wade, M.J., Tsou, S.K., McKeel, D.W., and Morris, J.C. (2001). Neuron number in the entorhinal cortex and CA1 in preclinical Alzheimer disease. Arch. Neurol. *58*, 1395–1402.

Raichlen, D.A., and Alexander, G.E. (2014). Exercise, APOE genotype, and the evolution of the human lifespan. Trends Neurosci. *37*, 247–255.

Ranganath, C., and Rainer, G. (2003). Neural mechanisms for detecting and remembering novel events. Nat. Rev. Neurosci. *4*, 193–202.

Ranganath, C., and Ritchey, M. (2012). Two cortical systems for memory-guided behaviour. Nat. Rev. Neurosci. *13*, 713–726.

Reagh, Z.M., and Yassa, M.A. (2014). Object and spatial mnemonic interference differentially engage lateral and medial entorhinal cortex in humans. Proc. Natl. Acad. Sci. U. S. A.

Rey, A. (1941). L'examen psychologique dans les cas d'encephalopathie traumatique. Archives de Psychologie; *28*: 286–340

Rojas Vega, S., Strüder, H.K., Vera Wahrmann, B., Schmidt, A., Bloch, W., and Hollmann, W. (2006). Acute BDNF and cortisol response to low intensity exercise and following ramp incremental exercise to exhaustion in humans. Brain Res. *1121*, 59–65.

Rovner, B.W., and Folstein, M.F. (1987). Mini-mental state exam in clinical practice. Hosp. Pract. Off. Ed *22*, 99, 103, 106, 110.

Ryan, L., Cardoza, J.A., Barense, M.D., Kawa, K.H., Wallentin-Flores, J., Arnold, W.T., and Alexander, G.E. (2012). Age-related impairment in a complex object discrimination task that engages perirhinal cortex. Hippocampus *22*, 1978–1989.

Saksida, L.M., and Bussey, T.J. (2010). The representational-hierarchical view of amnesia: translation from animal to human. Neuropsychologia *48*, 2370–2384.

Sauvage, M.M., Fortin, N.J., Owens, C.B., Yonelinas, A.P., and Eichenbaum, H. (2008). Recognition memory: opposite effects of hippocampal damage on recollection and familiarity. Nat. Neurosci. *11*, 16–18.

Sauvage, M.M., Beer, Z., Ekovich, M., Ho, L., and Eichenbaum, H. (2010). The caudal medial entorhinal cortex: a selective role in recollection-based recognition memory. J. Neurosci. Off. J. Soc. Neurosci. *30*, 15695–15699.

Sauvage, M.M., Nakamura, N.H., and Beer, Z. (2013). Mapping memory function in the medial temporal lobe with the immediate-early gene Arc. Behav. Brain Res. *254*, 22–33.

Scheff, S.W., Price, D.A., Schmitt, F.A., DeKosky, S.T., and Mufson, E.J. (2007). Synaptic alterations in CA1 in mild Alzheimer disease and mild cognitive impairment. Neurology *68*, 1501–1508.

Schultz, C., Tredici, K.D., and Braak, H. (2004). Neuropathology of Alzheimer's Disease. In Alzheimer's Disease, R.W.R.M. FACP, and B.Z.R. DiplPharm, eds. (Humana Press), pp. 21–31.

Schultz, H., Sommer, T., and Peters, J. (2012). Direct evidence for domain-sensitive functional subregions in human entorhinal cortex. J. Neurosci. Off. J. Soc. Neurosci. *32*, 4716–4723.

Selkoe, D.J. (2002). Alzheimer's disease is a synaptic failure. Science *298*, 789–791.

Shetty, A.K., Hattiangady, B., and Shetty, G.A. (2005). Stem/progenitor cell proliferation factors FGF-2, IGF-1, and VEGF exhibit early decline during the course of aging in the hippocampus: role of astrocytes. Glia *51*, 173–186.

Small, S.A., Chawla, M.K., Buonocore, M., Rapp, P.R., and Barnes, C.A. (2004). Imaging correlates of brain function in monkeys and rats isolates a hippocampal subregion differentially vulnerable to aging. Proc. Natl. Acad. Sci. U. S. A. *101*, 7181–7186.

Small, S.A., Schobel, S.A., Buxton, R.B., Witter, M.P., and Barnes, C.A. (2011). A pathophysiological framework of hippocampal dysfunction in ageing and disease. Nat. Rev. Neurosci. *12*, 585–601.

Smith, C.C., and Greene, R.W. (2012). CNS dopamine transmission mediated by noradrenergic innervation. J. Neurosci. Off. J. Soc. Neurosci. *32*, 6072–6080.

Smith, C.N., Wixted, J.T., and Squire, L.R. (2011). The hippocampus supports both recollection and familiarity when memories are strong. J. Neurosci. Off. J. Soc. Neurosci. *31*, 15693–15702.

Smith, S.M., Jenkinson, M., Woolrich, M.W., Beckmann, C.F., Behrens, T.E.J., Johansen-Berg, H., Bannister, P.R., De Luca, M., Drobnjak, I., Flitney, D.E., et al. (2004). Advances in functional and structural MR image analysis and implementation as FSL. NeuroImage *23 Suppl 1*, S208–S219.

Smith, T.D., Adams, M.M., Gallagher, M., Morrison, J.H., and Rapp, P.R. (2000). Circuit-specific alterations in hippocampal synaptophysin immunoreactivity predict spatial learning impairment in aged rats. J. Neurosci. Off. J. Soc. Neurosci. *20*, 6587–6593.

Sonntag, W.E., Lynch, C.D., Cooney, P.T., and Hutchins, P.M. (1997). Decreases in cerebral microvasculature with age are associated with the decline in growth hormone and insulin-like growth factor 1. Endocrinology *138*, 3515–3520.

Sørensen, K.E., and Shipley, M.T. (1979). Projections from the subiculum to the deep layers of the ipsilateral presubicular and entorhinal cortices in the guinea pig. J. Comp. Neurol. *188*, 313–333.

Squire, L.R., and Zola-Morgan, S. (1991). The medial temporal lobe memory system. Science *253*, 1380–1386.

Squire, L.R., Stark, C.E.L., and Clark, R.E. (2004). The Medial Temporal Lobe*. Annu. Rev. Neurosci. *27*, 279–306.

Stephan, K.E., Penny, W.D., Daunizeau, J., Moran, R.J., and Friston, K.J. (2009). Bayesian Model Selection for Group Studies. NeuroImage *46*, 1004–1017.

Steward, O., and Scoville, S.A. (1976). Cells of origin of entorhinal cortical afferents to the hippocampus and fascia dentata of the rat. J. Comp. Neurol. *169*, 347–370.

Strange, B.A., Witter, M.P., Lein, E.S., and Moser, E.I. (2014). Functional organization of the hippocampal longitudinal axis. Nat. Rev. Neurosci. *15*, 655–669.

Strauss, E., Sherman, E.M.S., Spreen, O., and Spreen, O. (2006). A compendium of neuropsychological tests: administration, norms, and commentary (Oxford; New York: Oxford University Press).

Streitbürger, D.-P., Möller, H.E., Tittgemeyer, M., Hund-Georgiadis, M., Schroeter, M.L., and Mueller, K. (2012). Investigating Structural Brain Changes of Dehydration Using Voxel-Based Morphometry. PLoS ONE *7*, e44195.

Van Strien, N.M., Cappaert, N.L.M., and Witter, M.P. (2009). The anatomy of memory: an interactive overview of the parahippocampal-hippocampal network. Nat. Rev. Neurosci. *10*, 272–282.

Suzuki, W.A., and Amaral, D.G. (1994). Topographic organization of the reciprocal connections between the monkey entorhinal cortex and the perirhinal and parahippocampal cortices. J. Neurosci. *14*, 1856–1877.

Swanson, L.W., and Cowan, W.M. (1977). An autoradiographic study of the organization of the efferent connections of the hippocampal formation in the rat. J. Comp. Neurol. *172*, 49–84.

Tamamaki, N., and Nojyo, Y. (1993). Projection of the entorhinal layer II neurons in the rat as revealed by intracellular pressure-injection of neurobiotin. Hippocampus *3*, 471–480.

Taylor, K.I., and Probst, A. (2008). Anatomic localization of the transentorhinal region of the perirhinal cortex. Neurobiol. Aging *29*, 1591–1596.

Thal, D.R., Holzer, M., Rüb, U., Waldmann, G., Günzel, S., Zedlick, D., and Schober, R. (2000). Alzheimer-related tau-pathology in the perforant path target zone and in the hippocampal stratum oriens and radiatum correlates with onset and degree of dementia. Exp. Neurol. *163*, 98–110.

Theysohn, N., Qin, S., Maderwald, S., Poser, B.A., Theysohn, J.M., Ladd, M.E., Norris, D.G., Gizewski, E.R., Fernandez, G., and Tendolkar, I. (2013). Memory-related hippocampal activity can be measured robustly using FMRI at 7 tesla. J. Neuroimaging Off. J. Am. Soc. Neuroimaging *23*, 445–451.

Thomas, A., Dennis, A., Bandettini, P.A., and Johansen-Berg, H. (2012). The effects of aerobic activity on brain structure. Mov. Sci. Sport Psychol. *3*, 86.

Trejo, J.L., Carro, E., Lopez-Lopez, C., and Torres-Aleman, I. (2004). Role of serum insulin-like growth factor I in mammalian brain aging. Growth Horm. IGF Res. Off. J. Growth Horm. Res. Soc. Int. IGF Res. Soc. *14 Suppl A*, S39–S43.

Vargha-Khadem, F., Gadian, D.G., Watkins, K.E., Connelly, A., Van Paesschen, W., and Mishkin, M. (1997). Differential effects of early hippocampal pathology on episodic and semantic memory. Science *277*, 376–380.

Villeneuve, S., Madison, C., Ayakta, N., La Joie, R., Cohn-Sheehy, B.I., Vogel, J., Marks, S., Arthur-Bentil, S.K., Reed, B., DeCarli, C., et al. (2014). EXISTING THRESHOLDS FOR PIB POSITIVITY ARE TOO HIGH. Alzheimers Dement. J. Alzheimers Assoc. *10*, P4–P5.

Vital, T.M., Stein, A.M., de Melo Coelho, F.G., Arantes, F.J., Teodorov, E., and Santos-Galduróz, R.F. (2014). Physical exercise and vascular endothelial growth factor (VEGF) in elderly: A systematic review. Arch. Gerontol. Geriatr. *59*, 234–239.

Vivar, C., and Van Praag, H. (2013). Functional circuits of new neurons in the dentate gyrus. Front. Neural Circuits *7*, 15.

Vivar, C., Potter, M.C., Choi, J., Lee, J.-Y., Stringer, T.P., Callaway, E.M., Gage, F.H., Suh, H., and van Praag, H. (2012). Monosynaptic inputs to new neurons in the dentate gyrus. Nat. Commun. *3*, 1107.

Voss, M.W., Vivar, C., Kramer, A.F., and van Praag, H. (2013a). Bridging animal and human models of exercise-induced brain plasticity. Trends Cogn. Sci. *17*, 525–544.

Voss, M.W., Erickson, K.I., Prakash, R.S., Chaddock, L., Kim, J.S., Alves, H., Szabo, A., Phillips, S.M., Wójcicki, T.R., Mailey, E.L., et al. (2013b). Neurobiological markers of exercise-related brain plasticity in older adults. Brain. Behav. Immun. *28*, 90–99.

Wechsler, DA. (1997). Wechsler Adult Intelligence Scale. 3rd edn. San Antonio, TX: The Psychological Corporation.

West, M.J., Coleman, P.D., Flood, D.G., and Troncoso, J.C. (1994). Differences in the pattern of hippocampal neuronal loss in normal ageing and Alzheimer's disease. Lancet *344*, 769–772.

Whitfield-Gabrieli, S., and Nieto-Castanon, A. (2012). Conn: a functional connectivity toolbox for correlated and anticorrelated brain networks. Brain Connect. *2*, 125–141.

Wilson, I.A., Ikonen, S., Gallagher, M., Eichenbaum, H., and Tanila, H. (2005). Age-associated alterations of hippocampal place cells are subregion specific. J. Neurosci. Off. J. Soc. Neurosci. *25*, 6877–6886.

Wilson, I.A., Gallagher, M., Eichenbaum, H., and Tanila, H. (2006). Neurocognitive aging: prior memories hinder new hippocampal encoding. Trends Neurosci. *29*, 662–670.

Wisse, L.E.M., Gerritsen, L., Zwanenburg, J.J.M., Kuijf, H.J., Luijten, P.R., Biessels, G.J., and Geerlings, M.I. (2012). Subfields of the hippocampal formation at 7T MRI: In vivo volumetric assessment. NeuroImage *61*, 1043–1049.

Witter, M.P. (2006). Connections of the subiculum of the rat: topography in relation to columnar and laminar organization. Behav. Brain Res. *174*, 251–264.

Witter, M.P. (2007a). The perforant path: projections from the entorhinal cortex to the dentate gyrus. Prog. Brain Res. *163*, 43–61.

Witter, M.P. (2007b). Intrinsic and extrinsic wiring of CA3: Indications for connectional heterogeneity. Learn. Mem. *14*, 705–713.

Witter, M.P., and Amaral, D.G. (1991). Entorhinal cortex of the monkey: V. Projections to the dentate gyrus, hippocampus, and subicular complex. J. Comp. Neurol. *307*, 437–459.

Witter, M.P., Groenewegen, H.J., Lopes da Silva, F.H., and Lohman, A.H. (1989). Functional organization of the extrinsic and intrinsic circuitry of the parahippocampal region. Prog. Neurobiol. *33*, 161–253.

Witter, M.P., Wouterlood, F.G., Naber, P.A., and Van Haeften, T. (2000a). Anatomical organization of the parahippocampal-hippocampal network. Ann. N. Y. Acad. Sci. *911*, 1–24.

Witter, M.P., Naber, P.A., van Haeften, T., Machielsen, W.C., Rombouts, S.A., Barkhof, F., Scheltens, P., and Lopes da Silva, F.H. (2000b). Cortico-hippocampal communication by way of parallel parahippocampal-subicular pathways. Hippocampus *10*, 398–410.

Wittmann, B.C., Bunzeck, N., Dolan, R.J., and Düzel, E. (2007). Anticipation of novelty recruits reward system and hippocampus while promoting recollection. Neuroimage *38*, 194–202.

Wixted, J.T., and Squire, L.R. (2010). The role of the human hippocampus in familiarity-based and recollection-based recognition memory. Behav. Brain Res. *215*, 197–208.

Yaffe, K., Barnes, D., Nevitt, M., Lui, L.Y., and Covinsky, K. (2001). A prospective study of physical activity and cognitive decline in elderly women: women who walk. Arch. Intern. Med. *161*, 1703–1708.

Yassa, M.A., and Stark, C.E.L. (2008). Multiple signals of recognition memory in the medial temporal lobe. Hippocampus *18*, 945–954.

Yassa, M.A., and Stark, C.E.L. (2009). A quantitative evaluation of cross-participant registration techniques for MRI studies of the medial temporal lobe. NeuroImage *44*, 319–327.

Yassa, M.A., and Stark, C.E.L. (2011). Pattern separation in the hippocampus. Trends Neurosci. *34*, 515–525.

Yassa, M.A., Muftuler, L.T., and Stark, C.E.L. (2010a). Ultrahigh-resolution microstructural diffusion tensor imaging reveals perforant path degradation in aged humans in vivo. Proc. Natl. Acad. Sci. U. S. A. *107*, 12687–12691.

Yassa, M.A., Stark, S.M., Bakker, A., Albert, M.S., Gallagher, M., and Stark, C.E.. (2010b). High-resolution structural and functional MRI of hippocampal CA3 and dentate gyrus in patients with amnestic Mild Cognitive Impairment. Neuroimage *51*, 1242–1252.

Yassa, M.A., Lacy, J.W., Stark, S.M., Albert, M.S., Gallagher, M., and Stark, C.E.L. (2011). Pattern separation deficits associated with increased hippocampal CA3 and dentate gyrus activity in nondemented older adults. Hippocampus *21*, 968–979.

Yonelinas, A.P. (1994). Receiver-operating characteristics in recognition memory: evidence for a dual-process model. J. Exp. Psychol. Learn. Mem. Cogn. *20*, 1341–1354.

Yonelinas, A.P. (2001). Components of episodic memory: the contribution of recollection and familiarity. Philos. Trans. R. Soc. Lond. B. Biol. Sci. *356*, 1363–1374.

Yonelinas, A. P. (2002). The Nature of Recollection and Familiarity: A Review of 30 Years of Research. *Journal of Memory and Language*, *46*, 441–517.

Yonelinas, A.P., and Parks, C.M. (2007). Receiver operating characteristics (ROCs) in recognition memory: a review. Psychol. Bull. *133*, 800–832.

Yonelinas, A.P., Kroll, N.E.A., Quamme, J.R., Lazzara, M.M., Sauv|[eacute]|, M.-J., Widaman, K.F., and Knight, R.T. (2002). Effects of extensive temporal lobe damage or mild hypoxia on recollection and familiarity. Nat. Neurosci. *5*, 1236–1241.

Zaitsev, M., Hennig, J., and Speck, O. (2004). Point spread function mapping with parallel imaging techniques and high acceleration factors: fast, robust, and flexible method for echo-planar imaging distortion correction. Magn. Reson. Med. Off. J. Soc. Magn. Reson. Med. Soc. Magn. Reson. Med. *52*, 1156–1166.

Zeineh, M.M., Engel, S.A., Thompson, P.M., and Bookheimer, S.Y. (2001). Unfolding the human hippocampus with high resolution structural and functional MRI. Anat. Rec. *265*, 111–120.

Zhao, F., Wang, P., Hendrich, K., Ugurbil, K., and Kim, S.-G. (2006). Cortical layer-dependent BOLD and CBV responses measured by spin-echo and gradient-echo fMRI: Insights into hemodynamic regulation. NeuroImage *30*, 1149–1160.

8 Appendix

Supplementary Figures

Figure S 1. Sample EPI slices with and without dropouts. ii

Figure S 2. Univariate single-subject peak activation for the Novelty- and DM-contrast. iv

Figure S 3. Functional connectivity profiles of PHC/PRC seeds with the EC for data set 2..... v

Figure S 4. Differential connectivity topography of bilateral (A) and unilateral (B) PRC vs. PHC seeds with the EC for data set 2 (A) and data set 1 (B). vi

Figure S 5. Functional connectivity gradients in the subiculum related to EC subregions (A) and PRC/PHC seeds (B) for data set 2. vii

Figure S 6. Comparison of T2*- and T2-weighted high-resolution structural images and their vulnerability to artefacts. viii

Supplementary Tables

Table S 1. Novelty-related group activation after ROI-based alignment. ix

Table S 2. Subsequent memory (“DM”)-related group activity after ROI-based alignment..... x

Table S 3. Univariate group-results for seed-to-voxel connectivity of PRC and PHC seeds with the EC xi

Table S 4. Number of missing data and outliers in the training and control groups. xii

Table S 5. Correlation coefficents (r) for the relationships of changes in fitness, perfusion and volume to memory in the exercise group. xiii

8.1 Supplementary Figures

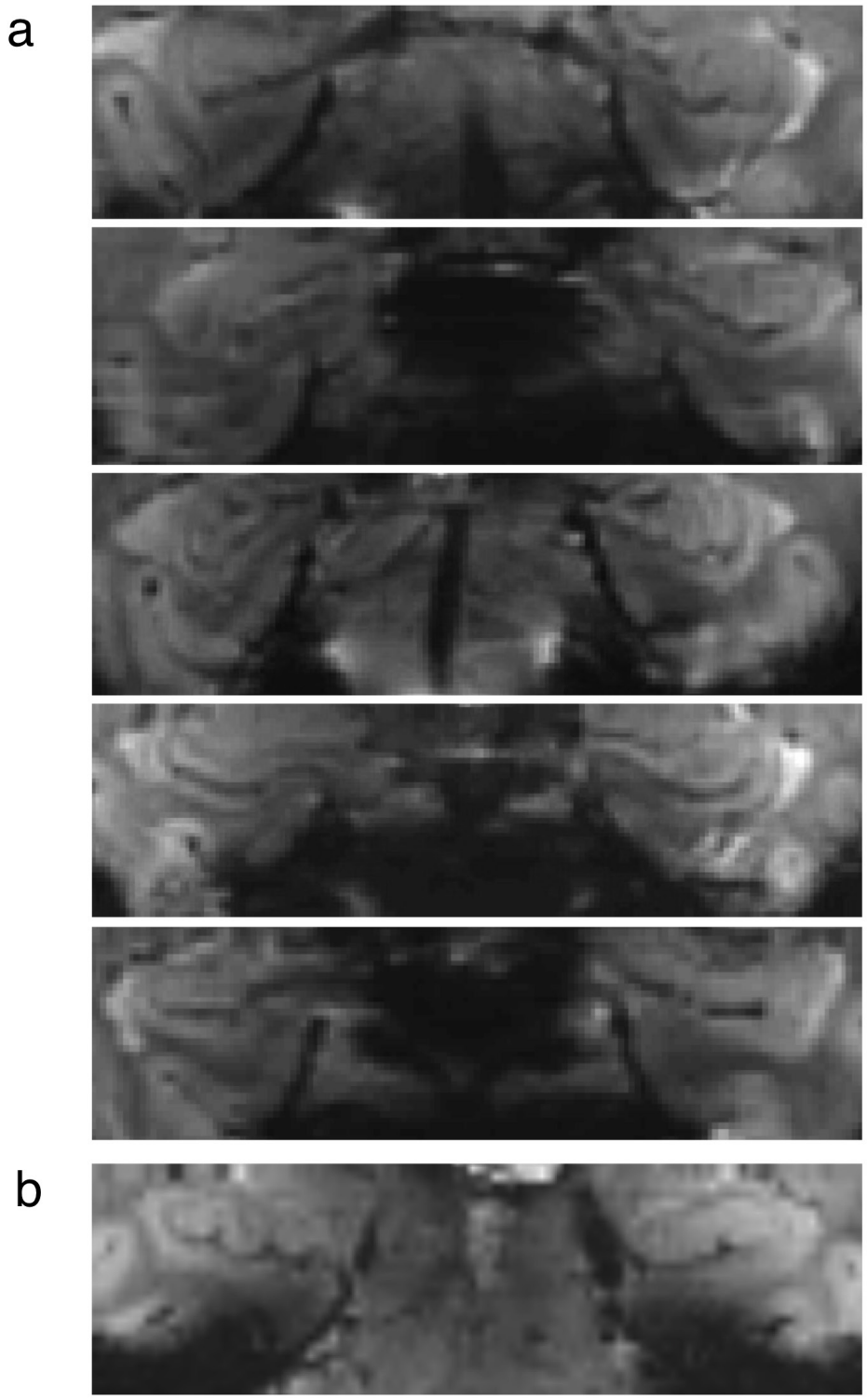

Figure S 1. Sample EPI slices with and without dropouts.

Shown are coronal sample slices from individual mean EPI volumes (average of 370 functional volumes, resolution: 0.8mm^3 isotropic) at the level of the hippocampal head. **a)** Five EPI sample slices without artefacts or dropouts in the EC that were included in the analyses. **b)** Sample EPI slice with partial dropout in the perirhinal cortex, laterally spreading into the EC (here: most prominent on the right). Dropouts occurred most frequently close to the ear canals. Overall, ca. 70% of slices covering the EC were usable for the final analysis (Left EC = 69% ± 17; Right EC = 73% ± 13).This figure is taken from Maass et al., 2014a.

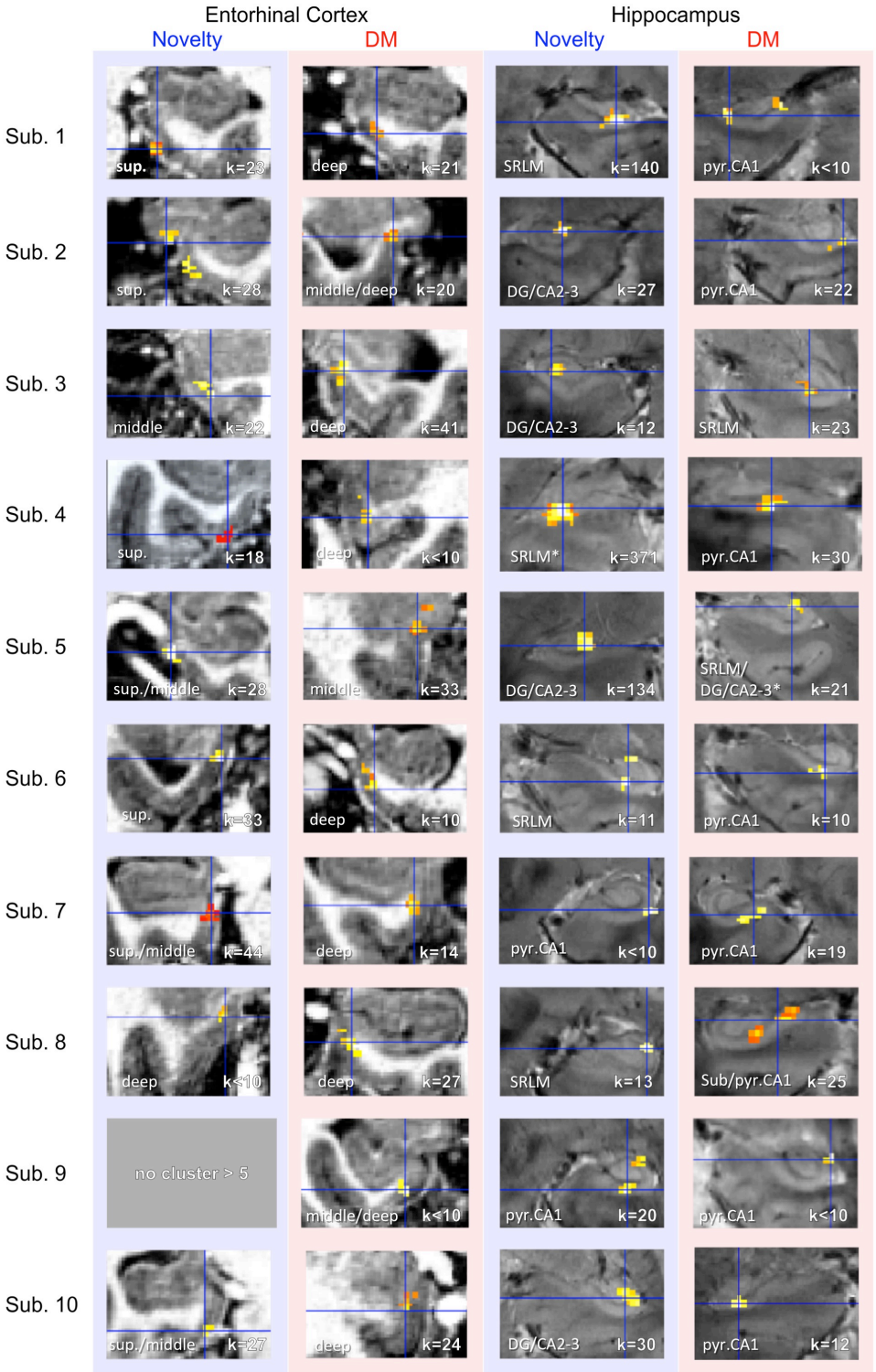
Entorhinal Cortex
Hippocampus
Novelty
DM
Novelty
DM
Sub. 1
sup. k=23
deep k=21
SRLM k=140
pyr.CA1 k<10
Sub. 2
sup. k=28
middle/deep k=20
DG/CA2-3 k=27
pyr.CA1 k=22
Sub. 3
middle k=22
deep k=41
DG/CA2-3 k=12
SRLM k=23
Sub. 4
sup. k=18
deep k<10
SRLM* k=371
pyr.CA1 k=30
Sub. 5
sup./middle k=28
middle k=33
DG/CA2-3 k=134
SRLM/ DG/CA2-3* k=21
Sub. 6
sup. k=33
deep k=10
SRLM k=11
pyr.CA1 k=10
Sub. 7
sup./middle k=44
deep k=14
pyr.CA1 k<10
pyr.CA1 k=19
Sub. 8
deep k<10
deep k=27
SRLM k=13
Sub/pyr.CA1 k=25
Sub. 9
no cluster > 5
middle/deep k<10
pyr.CA1 k=20
pyr.CA1 k<10
Sub. 10
sup./middle k=27
deep k=24
DG/CA2-3 k=30
pyr.CA1 k=12

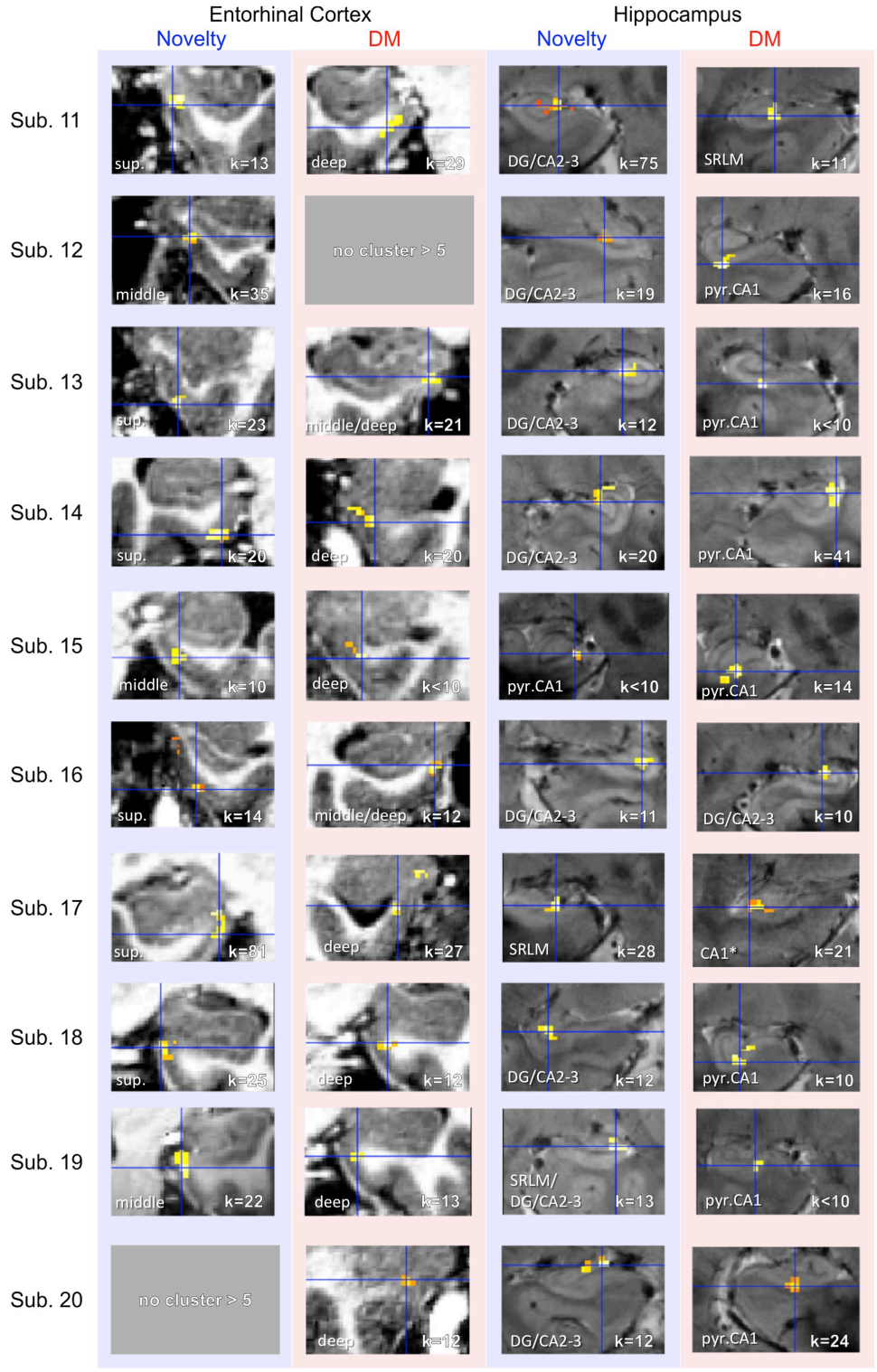

Figure S 2. Univariate single-subject peak activation for the Novelty- and DM-contrast.

Single-subject peak activations in the entorhinal cortex (EC) and hippocampus proper/dentate gyrus (HC/DG; in hippocampal body) for the Novelty- and subsequent memory (DM)-contrast overlaid on the individual coregistered MPRAGE (for EC, left panel) and T2*-image (for HC/DG, right panel). The blue cross demarcates the location of peak activation at a threshold of $p_{voxel\text{-}wise} < .01$ and $k \geq 10$ voxel (smoothing kernel 1.5 mm). For illustration purposes activation maps were masked with the individual EC or HC/DG ROIs. * demarcates cases where the location could not be clearly assigned. For most of the subjects, several (bilateral) activations were found at this threshold. If no cluster survived $k \geq 10$ voxel, the largest cluster is shown. These images serve to illustrate that individual activation patterns related to novelty or subsequent memory are remarkably confined to HC/EC subfields/layers. This figure is taken from Maass et al., 2014a.

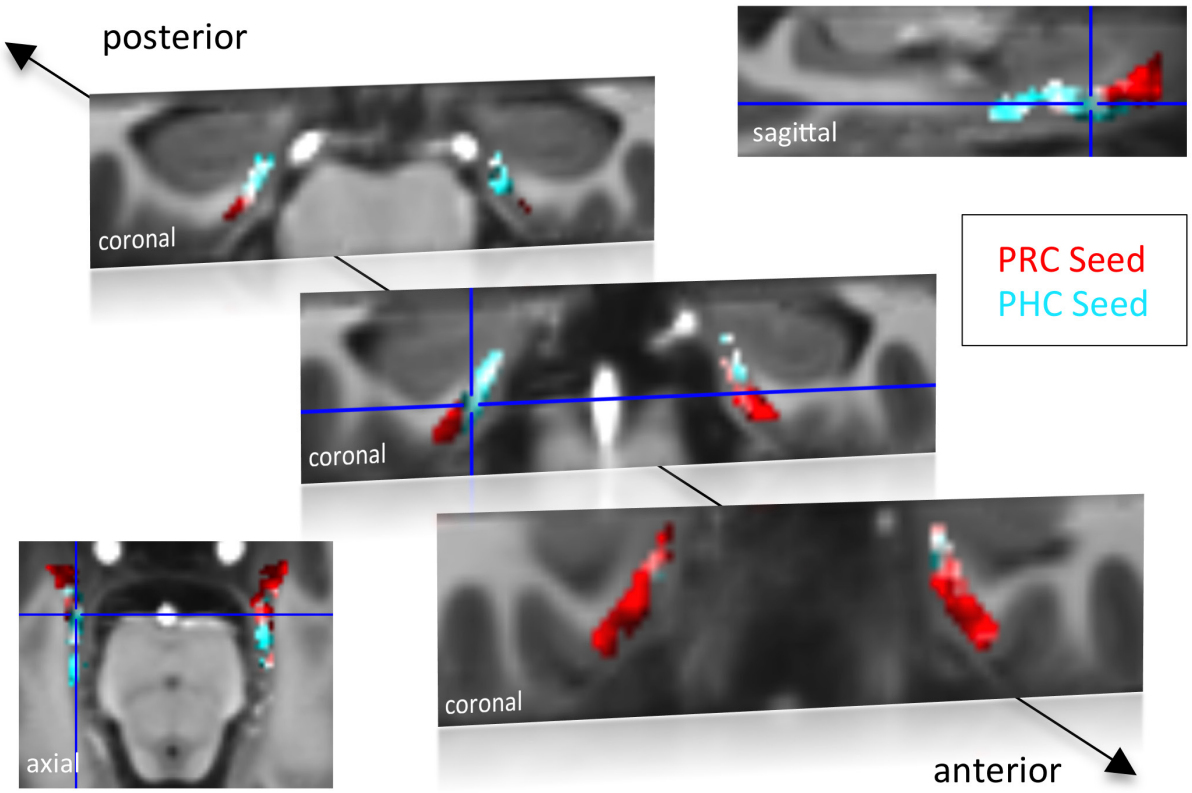

Figure S 3. Functional connectivity profiles of PHC/PRC seeds with the EC for data set 2.

Group results for seed-to-voxel connectivity of bilateral PRC and PHC seeds with the EC shown for data set 2 (one-sample t-test; $Z > 2.3$, $p_{cluster} < .05$, $N_1 = 15$). Bright regions denote overlapping connectivity with PRC/PHC. Single-subject beta maps were normalized on the group-specific T1-template by ROI-based alignment with ANTS and masked with a manually defined EC ROI. The T1-template has the same resolution as the high-resolution functional EPI volumes (0.8 mm x 0.8 mm x 0.8 mm). ROI: region of interest. This figure is taken from Maass et al., 2015.

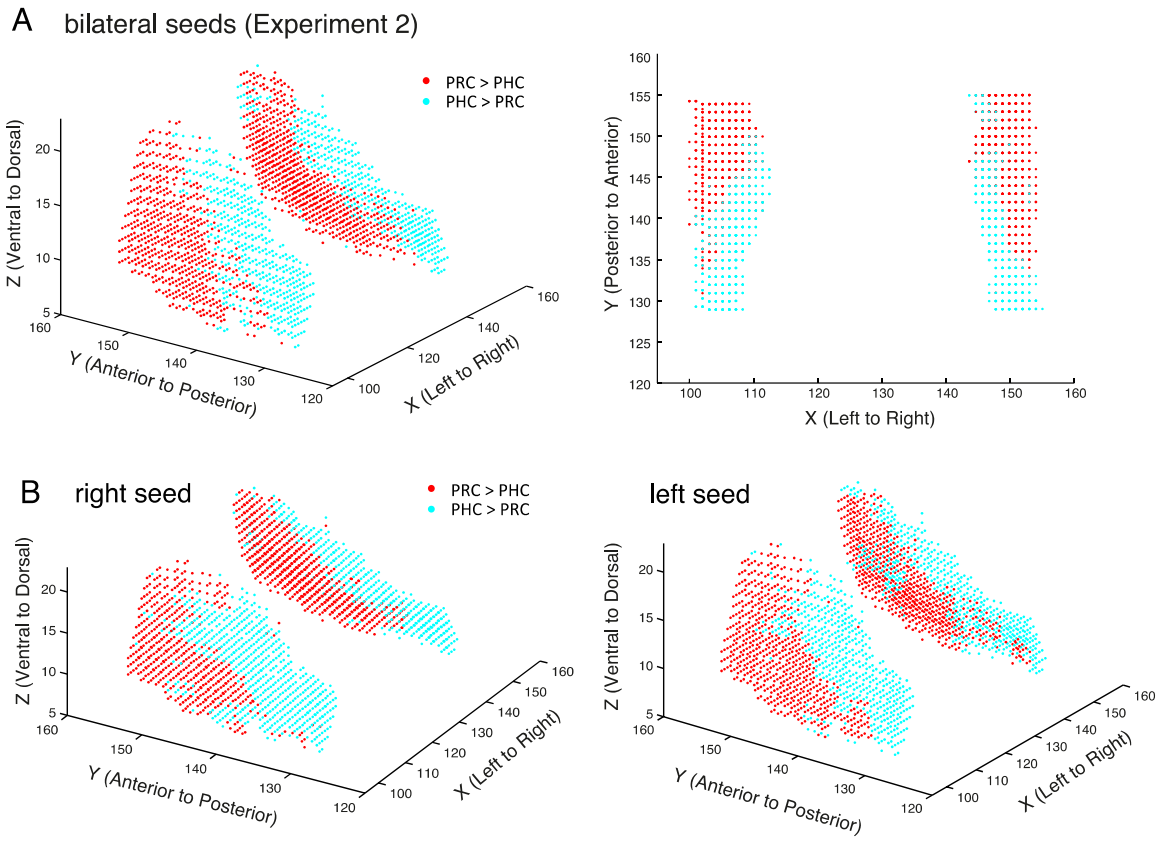

Figure S 4. Differential connectivity topography of bilateral (A) and unilateral (B) PRC vs. PHC seeds with the EC for data set 2 (A) and data set 1 (B).

A. To visualize the 3-dimensional geometry of connectivity, the connectivity preference with PRC vs. PHC of each EC voxel was plotted along the x-, y-, and z-axis (red: $T_{PRC\ >PHC} > 0$, blue: $T_{PHC\ >PRC} > 0$). These plots indicated a complex 3-dimensional topography of EC connectivity with a gradient of PRC-to-PHC preference running from anterior-ventral-lateral to posterior-dorsal-medial EC also for data set 2. **B.** In addition, the functional connectivity preference of unilateral (left and right) PRC/PHC seeds with both the ipsi- and contralateral EC was plotted to evaluate whether connectivity patterns were symmetric across hemispheres. This figure is taken from Maass et al., 2015.

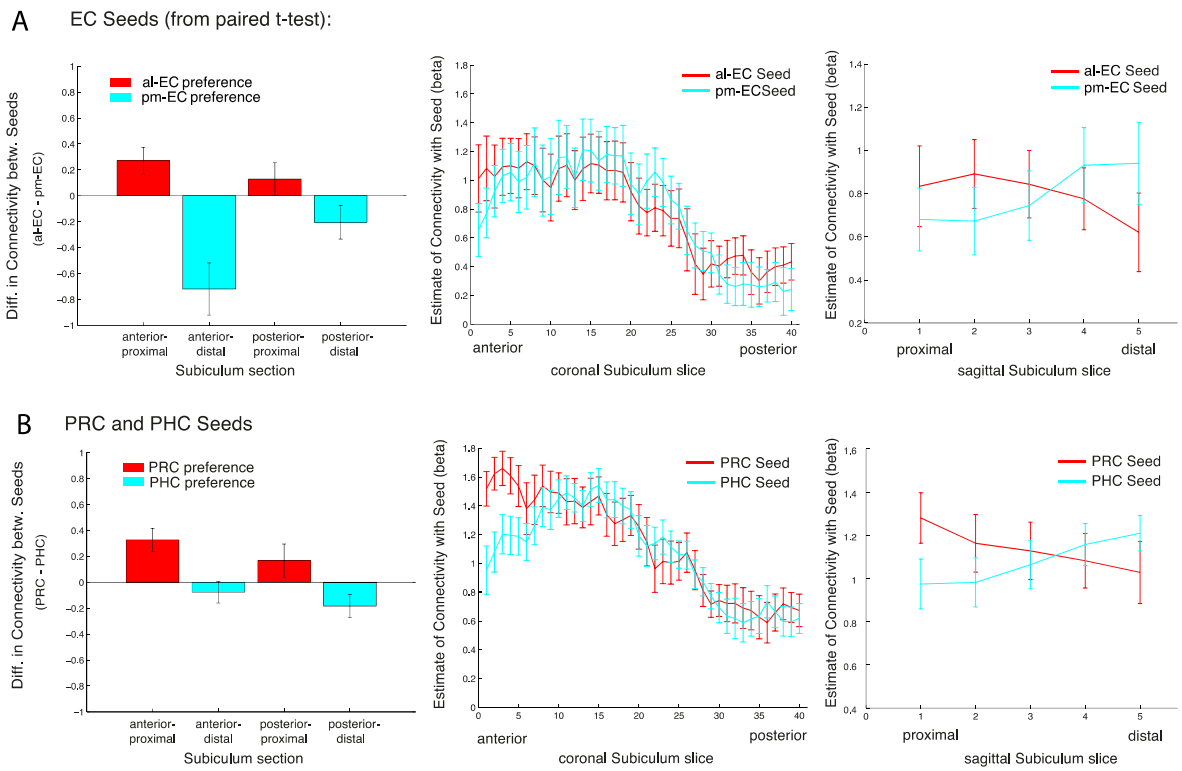

Figure S 5. Functional connectivity gradients in the subiculum related to EC subregions (A) and PRC/PHC seeds (B) for data set 2.

A. To test for differential connectivity of EC functional subdivisions with the subiculum, anterior-lateral EC (al-EC) and posterior-medial EC (pm-EC) regions that exhibited preferential connectivity with PRC vs. PHC, respectively (see paired t-tests in Fig. Figure 13A) were used as seed regions. The subiculum ROI was equally divided into four portions along the longitudinal (anterior vs. posterior) and transverse (proximal vs. distal) axis and mean betas of functional connectivity with EC seeds were extracted for each subsection. Repeated-measures ANOVAs revealed a significant seed (al-EC vs. pm-EC) x proximal-distal subiculum interaction in both datasets ($p < .001$; $N_1 = 15$, $N_2 = 14$; results shown for data set 2). Slice-by-slice plots of connectivity estimates demonstrated decreasing al-EC-connectivity and increasing pm-EC connectivity from proximal to distal subiculum but no anterior-posterior dissociation**. B.** Similarly, connectivity for PRC vs. PHC seeds with the subiculum along the longitudinal and transverse axis was evaluated. Seed (PRC vs. PHC) x proximal-distal subiculum section interactions were significant across both datasets ($p < .01$) with preferential connectivity of PRC with proximal and PHC with distal subiculum, respectively. Slice-by-slice plots of connectivity estimates along the hippocampal long axis revealed stronger PRC than PHC connectivity with the most anterior subiculum (= 8 slices) in data set 2. This figure is taken from Maass et al., 2015.

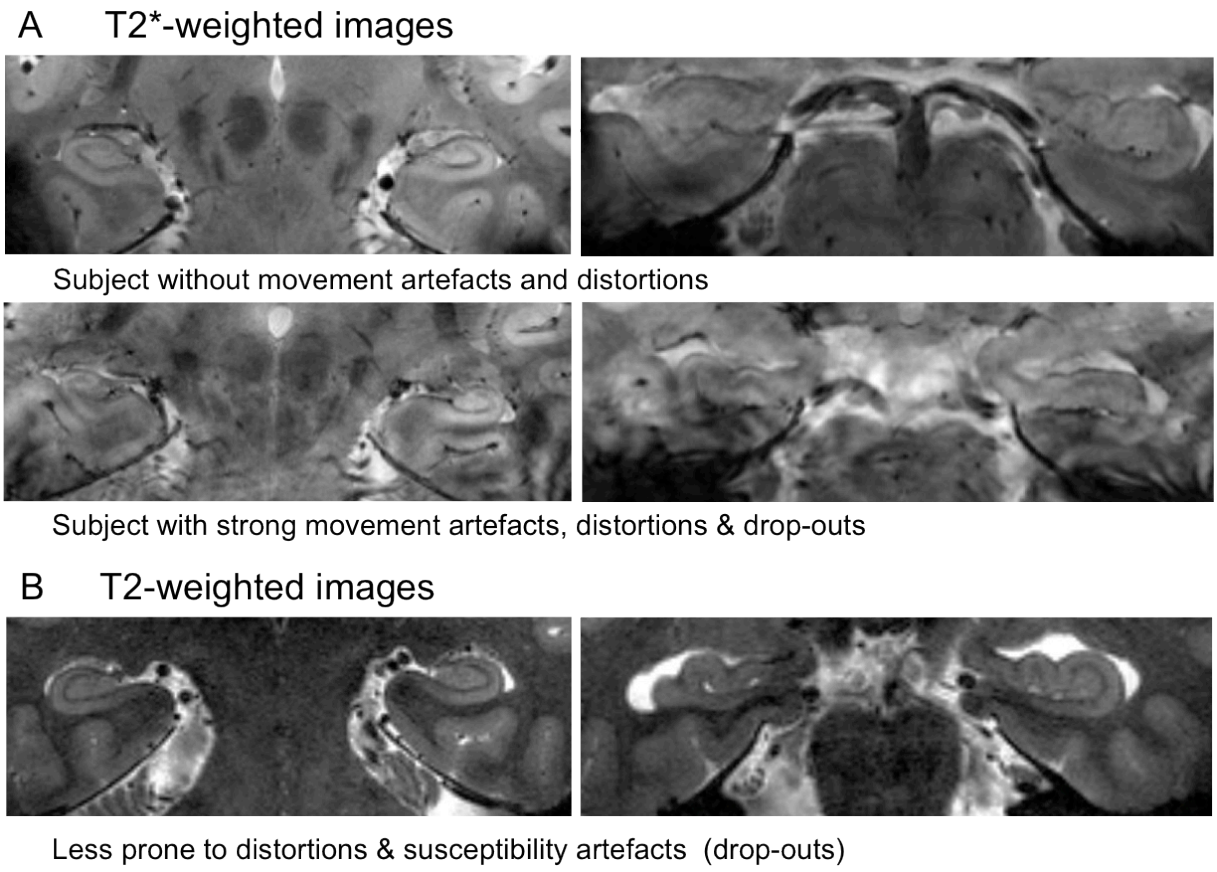

Figure S 6. Comparison of T2*- and T2-weighted high-resolution structural images and their vulnerability to artefacts.

A. In Experiment 1, very high-resolution T2*-weighted images (0.33 mm^2 in-plane resolution, 1.5 mm slice thickness) were acquired for hippocampal (and entorhinal) subfield and layer segmentation. These images provide a particularly good contrast for delineation of the apical dendritic CA1 layers. However, as visible in the lower panel of A, these images are also highly prone to motion and distortion artifacts, which makes them less suitable for volume measurements or studies with older people. **B.** For future studies, T2-weighted structural images with a littler lower in-plane resolution (0.44 mm x 0.44 mm) but also lower slice thickness (1 mm) will be favoured. These provide also a good contrast of HC subfields but, in addition, are less prone to distortions and movement artefacts. Particularly in anterior MTL regions, these images show good contrast of hippocampal head, entorhinal and perirhinal cortex due to their lower vulnerability to dropouts and distortions.

8.2 Supplementary Tables

Table S 1. Novelty-related group activation after ROI-based alignment.

Group activity for 1.5 mm smoothing

cluster size	cluster p_{uncorr}	alpha (simulated)	peak T	peak location	template x,y,z {mm}	side
688	0.000	<0.01	7.61	CA3/DG & presub./EC (posterior head, near uncus)	17.5 30.0 -21.7	R
			7.15	medial EC/presub. (head)	14.3 40.2 -28.1	R
			4.81	DG/apical CA1 (posterior head, near uncus)	22.3 38.4 -28.0	R
464	0.000	<0.01	6.34	CA3/DG & presub.	-18.6 29.2 -21.4	L
			5.33	DG/apical CA1 (head)	-23.4 33.7 -26.5	L
			5.31	EC	-14.6 39.4 -27.7	*L*
19	*0.013*	*<0.15*	*4.73*	*CA2/3-DG (head)*	*-26.6 30.2 -21.1*	*L*
16	*0.021*	*<0.25*	*4.08*	*CA1 (head)*	*27.1 32.0 -26.4*	*R*
18	*0.015*	*<0.15*	*4.05*	*CA2/3-DG (posterior body)*	*25.5 11.6 -13.7*	*R*

Group activity for 2.4 mm smoothing

cluster size	cluster p_{uncorr}	alpha (simulated)	peak T	peak location	template x,y,z {mm}	side
1339	0.000	<0.01	7.65	presub./EC (posterior head)	16.7 30.9 -26.8	R
			6.96	presub./EC (head)	14.3 39.5 -27.7	R
			5.99	DG/apical CA1 (head)	22.3 39.9 -27.0	R
1055	0.000	<0.01	6.85	DG/apical CA1 (head)	-20.2 34.4 -25.1	L
			4.61	EC	-12.2 35.2 -23.7	L
			4.47	CA2/3-DG (body)	-21.8 22.8 -18.0	L
81	0.003	<0.01	6.30	CA1 (body)	29.5 22.1 -22.9	R
48	0.018	<0.05	4.40	CA2/3-DG (body)	29.5 17.2 -16.7	R
46	0.020	<0.05	4.31	CA2/3-DG (posterior body)	23.9 12.3 -12.3	R

Functional data were smoothed with 2 different kernels to allow for higher specificity (FWHM: 1.5 mm) and higher sensitivity (FWHM: 2.4 mm), respectively. Hippocampal and entorhinal subregions showing group-level activation (at $p_{voxel\text{-}level} < .005$; $k_{1.5mm} \geq 15$ voxels and $k_{2.4mm} \geq 25$ voxels, N = 19) for the Novelty-contrast (novel > familiar). Alpha levels (type 1 error rates) were simulated with 3dClustSim (AFNI). Note that clusters that would not survive correction at low smoothing (highlighted in italics; e.g. CA2/3-DG in posterior body) become significant with higher smoothing. R = right; L = left. This table is adapted from Maass et al., 2014a.

Table S 2. Subsequent memory ("DM")-related group activity after ROI-based alignment

Group activity for 1.5 mm smoothing

cluster size	cluster p_{uncorr}	alpha (simulated)	peak T	peak location	template x,y,z {mm}	side
21	*0.007*	*<0.10*	*4.60*	*pyramidal CA1 (body)*	*31.1 22.1 -21.1*	*R*
33	0.001	<0.02	4.58	EC & Sub (head)	-14.6 41.2 -26.0	L
16	*0.017*	*<0.25*	*4.31*	*CA1/presub.(head)*	*15.1 38.1 -23.4*	*R*
17	*0.014*	*<0.20*	*4.20*	*CA2/3-DG (posterior body)*	*23.9 14.8 -12.7*	*R*

Group activity for 2.4 mm smoothing

cluster size	cluster p_{uncorr}	alpha (simulated)	peak T	peak location	template x,y,z {mm}	side
96	0.001	<0.01	5.94	CA1/presub. (head)	15.1 38.1 -23.4	R
72	0.003	<0.01	5.51	EC	-13.8 41.6 -25.3	L
25	*0.053*	*<0.20*	*4.90*	*CA2/3-DG (post. body)*	*25.5 13.7 -13.1*	*R*
44	0.014	<0.05	4.49	pyramidal CA1 (body)	31.1 22.5 -22.2	R
37	*0.022*	*<0.10*	*4.31*	*Sub/CA1 (body)*	*22.3 23.5 -21.9*	*R*
57	0.006	<0.02	4.05	EC	13.5 34.5 -26.9	R

Functional data were smoothed with 2 different kernels to allow for higher specificity and higher sensitivity, respectively. Hippocampal and entorhinal subregions showing group-level activation (at $p_{voxel\text{-}level} < .005$; $k_{1.5mm} \geq 15$ voxels and $k_{2.4mm} \geq 25$ voxels, N = 19) for the DM-contrast (difference due to memory: remembered > forgotten). Alphas were simulated with 3dClustSim (AFNI). Note that clusters that would not survive correction at low smoothing (highlighted in italics; e.g. pyramidal layers in CA1) become significant with higher smoothing. R= right; L =left. This table is adapted from Maass et al., 2014a.

Table S 3. Univariate group-results for seed-to-voxel connectivity of PRC and PHC seeds with the EC

	cluster			peak	peak coordinate (template)			
	$p_{FWE\text{-}corr}$	$p_{FDR\text{-}corr}$	size	Z-score	x	y	z	side
Data set 1								
PRC Seed	<0.001	<0.001	517	5.05	153	149	8	R
	<0.001	<0.001	273	4.82	108	146	12	L
PHC Seed	<0.001	<0.001	380	5.29	150	129	9	R
	<0.001	<0.001	510	5.05	106	138	12	L
PRC > PHC	0.038	0.022	42	4.31	151	150	8	R
	0.001	0.001	91	4.04	101	146	9	L
PHC > PRC	0.008	0.005	61	4.15	150	131	10	R
	0.001	0.002	87	3.53	108	136	11	L
Data set 2								
PRC Seed	<0.001	<0.001	777	4.82	109	152	20	L
	<0.001	<0.001	849	4.73	149	145	10	R
PHC Seed	<0.001	<0.001	669	5.31	147	137	13	R
	<0.001	<0.001	637	4.91	107	139	14	L
PRC > PHC	<0.001	<0.001	167	4.70	105	153	15	L
PHC >PRC	0.022	0.024	66	4.09	153	130	9	R
	0.047	0.026	53	3.74	108	136	18	L

Entorhinal subregions showing significant functional connectivity (one-sample t-test) or differential connectivity (paired t-test) with bilateral PRC or PHC seeds ($Z > 2.3$, $p_{cluster} < .05$, $N_{Exp\cdot1} = 15$, $N_{Exp\cdot2} = 14$). Single-subject beta maps were normalized on the group-specific T1-template and masked with a manually defined EC ROI. The EC covered 26 coronal slices on the template (y = 154: most anterior slice, y = 129: most posterior slice). This table is adapted from Maass et al., 2015.

Table S 4. Number of missing data and outliers in the training and control groups.

Variables	aerobic exercise group				relax/stretching group				Reason for missings (number of cases)
	missing prae	missing post	outlier	final	missing prae	missing post	outlier	final	
$VO_{2\ VAT}$	1	1	0	20	0	0	0	19	VO_{2VAT} not achieved because subject wished to terminate the assessment (1)
rCBF/ rCBV	4	3	1	16	3	3	0	16	No perfusion measurement due to risk for renal dysfunction (6), no AIF found (1)
Volume	5	6	0	15	2	2	0	17	No 7T MRI due to technical problems (2), implants without 7T MRI approval (2) or indisposition (1); data exclusion due to poor data quality (1)
CF recall	0	0	3	18	0	0	0	19	
CF recogn.	0	0	1	20	1	0	0	18	Missed CF recognition testing (1)
VLMT recall	0	0	0	21	0	0	1	18	
VLMT recogn.	0	0	1	20	0	1	2	16	Missed VLMT recognition testing (1)
Cortisol	1	0	0	20	0	0	0	19	Cortisol levels not in reference range: < 28 nmol/l (1)
VEGF	0	0	3	18	0	0	0	19	
PDGF	0	0	0	21	0	0	0	19	
IGF-1/ IGF-2	0	0	0	21	0	0	0	19	
IGF-BP3	0	0	1	20	0	0	0	19	
IGF-BP2	1	0	0	20	1	1	1	16	Lower limit of quantification (3)
BDNF	0	0	0	21	0	0	0	21	

Outliers were detected by the outlier labeling rule. $VO_{2\ VAT}$ was measured in ml/kg per min. Bilateral rCBF and rCBV were measured in ml/100g/min and ml/100g * 10, respectively. Bilateral hippocampal volumes were measured in cm^3 (after manual segmentation). Serum cortisol levels denote nmol/l. CF: *Complex Figure Test*. VLMT: *Verbal Learning and Memory Test*. This table is adapted from Maass et al., 2014b.

Table S 5. Correlation coefficents (r) for the relationships of changes in fitness, perfusion and volume to memory in the exercise group.

Fitness-related changes in perfusion and volume

Variables (% change)	*HC rCBF*	*GM rCBF*	*HC rCBV*	*GM rCBV*	*HH Vol.*	*GM Vol.*
$VO_{2\ VAT}$	**.54***	.63**	.42	.44	**.47**	.02

Correlations betw. changes in fitness, perfusion and HC volume with changes in memory

Variables (% change)	*CF early recall*	*CF late recall*	*CF recognition*	*VLMT early recall*	*VLMT late recall*	*VLMT recognition*
$VO_{2\ VAT}$	.62**	.33	**.41**	.31	.131	-.01
Hippocampal rCBF	.78**	.39	**.57***	.13	.08	.49
Grey Matter rCBF	.73**	.21	.49*	.06	-.10	.44
Hippocampal rCBV	.22	.23	.72**	.04	.00	.62*
Grey Matter rCBV	.05	-0.4	.56*	-.06	-.12	.55*
Hippoc. head Vol.	.50	.25	**.62***	-.05	.27	.27

Partial correlations for the exercise group only (Pearson's correlation, two-tailed) controlling for possible confounding effects of age, gender, and ΔT. $VO_{2\ VAT}$ was measured in ml/kg per min. Bilateral rCBF and rCBV were measured in ml/100g/min and ml/100g * 10, respectively. Bilateral hippocampal volumes were measured in cm^3 (after manual segmentation). CF: *Complex Figure Test*. VLMT: *Verbal Learning and Memory Test*. Asterisks highlight significant correlations (*p < .05; **p < .01). Boldface demarcates correlations shown in Fig. 18 across all participants. N_T = 21.

Curriculum Vitae

Personal Information

Name:	Anne Maaß
Birth date:	19.07.1985
Birth place:	Gardelegen, Germany
Nationality:	German

University Education

• 04/2011 – 09/2015 **PhD in Neuroscience**

Otto-von-Guericke University Magdeburg
Institute of Cognitive Neurology and Dementia Research

• 10/2008 - 03/2011 **MSc in Integrative Neuroscience**

Otto-von-Guericke University Magdeburg
English language program, final grade: 1.2

• 10/2005 – 07/2008 **BSc in Biochemistry**

University of Potsdam
Specialisation: Immunology, final grade: 1.3

School Education

• 09/1996 – 07/2005 **German Abitur**

Otto-von-Guericke-Gymnasium, Magdeburg
final grade: 1.1
Advanced courses: English, Chemistry

Magdeburg, 22.05.2015

Eigenständigkeitserklärung

Hiermit erkläre ich, dass ich die vorliegende Dissertation zu dem Thema:

„ Ultra-high resolution imaging of the functional anatomy and plasticity of the human hippocampal-entorhinal circuitry”

selbständig verfasst, nicht bereits als Dissertation verwendet habe und die benutzten Hilfsmittel und Quellen vollständig angegeben wurden.

Weiterhin erkläre ich, dass ich weder diese noch eine andere Arbeit zur Erlangung des akademischen Grades doctor rerum naturalium (*Dr. rer. nat*.) an anderen Einrichtungen eingereicht habe.

Magdeburg, den 22.05.2015